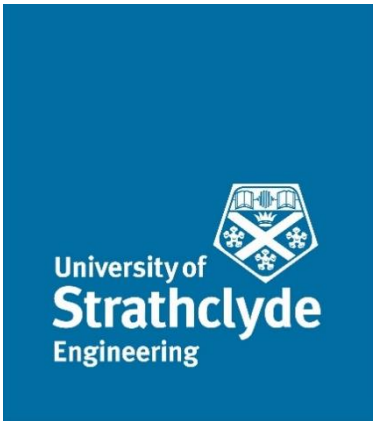

DEPARTMENT OF MECHANICAL AND AEROSPACE ENGINEERING

Towards a Unified Design-by-Analysis Solution to Pressure Vessel Nozzle-Shell Junctions under Combined Loading

by

Murat Bozkurt

A thesis presented in fulfilment of the requirements for the degree of

Doctor of Philosophy,

Glasgow, UK

March 2022

COPYRIGHT DECLARATION

This thesis is the result of the author's original research. It has been composed by the author and has not been previously submitted for examination which has led to the award of a degree.

Signed: Murat Bozkurt *Date: 05.02.2022*

To My Lovely Wife Hilda,

To My Lovely Son Muhammed Aybars,

To My Dear Mother and Father who raised me and supported me always,

and

To all people who only think about the advancement of technology for world peace and humanity.

ABSTRACT

The finite element method is the most commonly used modern approach when solving complex practical cylinder-cylinder junctions in pressure vessels. This is used when the geometrical arrangement is out with the permitted scope of the design-by-rule approaches or when detailed stress information is required as in a fatigue assessment. High-stress concentrations occur on the crotch corner for cylinder-cylinder joints, and it is possible to reach solutions for this problem by using both theoretical and numerical solutions. However, those approaches do not fully overlap nor have the same underlying assumptions. As such, an innovative high-fidelity finite element model has been developed to provide a holistic unified approach which can tackle a wide range of problems.

In this study, various detailed nozzle design challenges were investigated including single and multiple nozzle combinations, nozzle-cylinder systems with different size ratios, oblique nozzles combinations, fillet weld applications, pad reinforcements, stress linearization, external loading cases, limit loads, and cyclic loads. In addition, elastic, elastic - perfectly plastic, full plastic and fracture analysis were performed.

Stress intensity factors are obtained with the results of finite element analysis for various internal pressure and external loading conditions, and an attachment parameter and design curves are proposed. Finally, the Multiple Plastic Slope method, which is an alternative to TI and TES methods, which can be applied more practically and can make a more conservative plastic limit load estimation, has been proposed.

ACKNOWLEDGEMENTS

I would like to express my sincere gratitude to my supervisor, Prof David Nash, for his outstanding knowledge, experience, and guidance in the successful completion of my PhD process. His friend-like approach rather than a supervisor, his patience in the face of the problems encountered, the invaluable transfer of experience, the advice, and responsibilities he gave for my academic development have a great share in the conclusion of this research.

I would also like to thank Dr Asraf Uzzaman, who has followed every stage of my work since the first day of the doctoral process and has never missed his help. This study would not have been progressed so easy had it not been for the support and advice he gave during my adaptation to academic life and university, especially in my first year. I would also like to thank Visiting Professor John Wintle from TWI, who periodically followed up on my work, especially before the pandemic, and gave me advice by meeting with me one-on-one. In addition, I would like to thank Prof Dr Ali Osman Ayhan for allowing me to use the FCPAS program for the calculations I made in my fracture mechanics studies.

I would also like to thank Dr. Robert Hamilton and Dr. Haofeng Chen, who have allowed me to develop in the academic field and to do teaching assistants at certain periods. Working with them has been a great pleasure and has given me invaluable experience.

In addition to all these, I would like to thank Ibrahim Mizrak, Fatih & Zeynep Tiras, Burak Agir, Emre Dokuzparmak, Oguzhan Aydore and Muzeyyen Seckin, who have very special places in my life, and I believe our friendship that started in Glasgow will continue for a lifetime. I would also like to thank the ATAS (Association of Turkish Alumni and Students in Scotland) family, which was established for the purpose of meeting Turkish

students and alumni and continuing their cooperation, and each of its members, especially Kutlu Balci and Onder Canbulat, for their social and academic activities.

In particular, I would like to thank the Ministry of National Education of the Republic of Turkey for their financial support for 4 years within the scope of the YLSY scholarship program, Educational Counselor's Office in London, and Turkish Consulate General in Edinburgh who try to be with us in all our problems. Without the support they provide, thousands of students like me might not have had the opportunity to get to know such prestigious universities abroad, work there and develop their academic careers.

I am grateful to my beloved parents who have given me so much love, support, and encouragement throughout my life. It's an incredible feeling to feel the pride they have with me every time they look into my eyes. From now on, it will be one of my most important goals in my life to make them feel this proud and be a good son.

Finally, I would like to thank Hilda, my dear wife, for the love she has given me, the patience she has shown and the endless support that can be given to me. In a way, we have achieved this success together, with being with me at every stage of this work and the support she always gave me when I felt mentally.

RESEARCH OUTPUTS

Bozkurt, M., Nash, D., & Uzzaman, A. (2019, July). "Investigation of the stresses and interaction effects of nozzle-cylinder intersections when subject to multiple external loads". In Pressure Vessels and Piping Conference (Vol. 58943, p. V003T03A028). American Society of Mechanical Engineers. https://doi.org/10.1115/PVP2019-93306

Bozkurt, M., Nash, D., & Uzzaman, A. (2020, October). "Effect of the internal pressure and external loads on nozzles in cylindrical vessel". In IOP Conference Series: Materials Science and Engineering (Vol. 938, No. 1, p. 012007). IOP Publishing. http://doi.org/10.1088/1757-899X/938/1/012007

Bozkurt, M., Nash, D., & Uzzaman, A. (2021, July). "Calculation of Outer Crack Stress Intensity Factors for Nozzle Junctions in Cylindrical Pressure Vessels Using FCPAS". In Pressure Vessels and Piping Conference (Vol. 85321, p. V002T03A050). American Society of Mechanical Engineers. https://doi.org/10.1115/PVP2021-64385

Bozkurt, M., Nash, D., & Uzzaman, A. (2021). "A comparison of stress analysis and limit analysis approaches for single and multiple nozzle combinations in cylindrical pressure vessels". International Journal of Pressure Vessels and Piping, 104563. https://doi.org/10.1016/j.ijpvp.2021.104563

Bozkurt, M., Uzzaman, A, & Nash, D. "Mixed-mode stress intensity factors determination of inner wall elliptical corner cracks in cylindrical pressure vessels with nozzle junction". Submitted to Thin-Walled Structures.

CONTENT

LIST OF FIGURES

LIST OF TABLES

NOTATION

a	Crack depth	mm
c	Crack radius	mm
COD	Crack Opening Displacement	
d	Mean diameter of nozzle	mm
d_i	Inner diameter of nozzle	mm
d_o	Outside diameter of nozzle	mm
D	Mean diameter of shell	mm
D_i	Inner diameter of shell	mm
D_o	Outside diameter of shell	mm
D_P	Pad diameter	mm
EPFM	Elastic-Plastic Fracture Mechanics	
FCPAS	Fracture and Crack Propagation Analysis System	
FEA	Finite Element Analysis	
FEM	Finite Element Modelling	
KI	SIF due to mode-I loading	MPa·m½
KII	SIF due to mode-II loading	MPa·m½
KIII	SIF due to mode-III loading	MPa·m½
L	Length of vessel	mm
LEFM	Linear Elastic Fracture Mechanics	
M_C	Circumferential moment	kN.m
M_L	Longitudinal moment	kN.m
M_T	Torsional moment	kN.m
MPS	Multiple Plastic Slope	
n	Strain hardening exponent	
P	Tensile force	kN
Pa	Allowable pressure	MPa
P_y	First yield load	MPa, kN, kN.m,..

P_l	Limit load	MPa, kN, kN.m,..
Pint	Internal pressure	MPa
P_L	Pitch between nozzles in longitudinal direction	mm
P_p	Internal collapse pressure	MPa
P_T	Pitch between nozzles in axial direction	mm
P_φ	Gross plastic load (Burst load)	MPa
r_i	Inner radius of nozzle	mm
r_o	Outer radius of nozzle	mm
R_i	Inner radius of shell	mm
R_o	Outer radius of shell	mm
SCF	Stress Concentration Factor	
SIF	Stress Intensity Factor	
SLA	Stress Linearization Analysis	
S_{ty}	Tensile yield strength	MPa
S_{tu}	Ultimate tensile strength	MPa
t	Thickness of the nozzle	mm
T	Thickness of the shell	mm
TI	Tangent Intersection	
TES	Twice Elastic Slope	
T_P	Thickness of the pad	mm
V_L	Longitudinal force	kN
Vc	Circumferential force	kN
β	Attachment parameter	
σ_m	Membrane stress	MPa
σ_y	Yield stress	MPa
Ψ	Oblique nozzle connection angle	^{o}
γ	Shell Parameter	

CHAPTER 1. INTRODUCTION

1.1. Background

Pressure vessels are multifunctional and used in sectors such as energy production industry for fossil and nuclear energy, especially in oil, chemistry, petroleum and nuclear branches, petrochemical industry for storage and processing of crude fuel in tanks and storage at gas stations, and chemical industry for chemical reactors. are extremely important equipment. In particular, cylindrical, and spherical pressure vessels are widely used as a common structural component in many engineering design applications.

Pressure vessels can be subjected to many actions, including internal pressure and external loads applied to nozzles in a local load configuration. Detection of these loads on the system is important for the safe operation of the system. If the necessary precautions are not taken, serious damage to the structure may occur. In order to prevent failure or damage to the system, pressure vessel design codes are used to determine the vessel wall thicknesses and allowable overall design requirements to ensure safe operation requirements. The codes contain detailed formulae and rules for calculations for stress analysis and but also design by analysis approaches for use with finite element method which continue to be developed. In the main, design by rule assessments account for much of the pressure vessel design undertaken today, however, some of these approaches are now old and have restrictions and assumptions which can now be improved upon using modern finite element analysis.

All international pressure vessel codes contain rules for nozzle-shell junctions. Current methods, contained in these codes are based on experience with shell theory or limit analysis and a limited set of experimental validations. Most of these previous studies were

carried out in the 1960s in the boiler and power generation industries and were state of the art at the time. Although some updated approaches have been provided in the recent studies in the literature, there is not yet a comprehensive approach that provides a modern design-analysis solution for the industry which deals with all of the configurations required and incorporates all of the possible options for loading, reinforcement pads and also rules for the assessment of cracked structures. For this reason, both a new approach is required based on the development of a high-fidelity finite element modelling, a comprehensive series of parametric studies examining all of the options for single and combined loading and the improvement or reconstitution of existing graphs and equations have become a necessity. In addition, there are various design by analysis approaches now available including elastic analysis, limit analysis and full elastic- plastic analysis. It is also important to provide clear guidance as to how to approach the design of pressure vessels using these techniques and to show how they can be used to develop new approaches to nozzle-cylinder intersections.

1.2. Statement of the Problem

In many pressure vessel problems, the highest stresses often occur at the nozzle cylinder intersections. Determining the maximum loading conditions to be applied in any pressure vessel is of great importance in terms of taking the necessary precautions in the design and future fatigue evaluation. The conventional design sets a limit on the membrane and membrane plus bending stresses, but it is preferable to determine the boundary load and then apply an appropriate factor of safety. Finite element analysis is one of the most widely used numerical procedures and all stress values in the containers can be determined very easily with the finite element method. However, due to some method differences such as mesh techniques applied in finite element modelling, boundary

conditions, sensitivity analysis, and selection of appropriate material and element type, the results obtained from the analysis do not exactly match a hundred percent. For this reason, a high-quality model that can respond to different shapes and applications requires to be created for nozzle shell combinations with different thickness ratios. In addition, the elastic, elastic – perfectly plastic and plastic loading limit loads of this model should also be accurately determined with this model.

In addition to the finite element method, it is possible to calculate the stress values for pressure vessel nozzle connections that are subjected to various loads using classical approaches. The pressure vessel design codes developed for this purpose contain specific rules and when considering the research literature, it is noticeable that there are differences between the results obtained from the pressure vessel design codes and the results obtained by the finite element method. For this reason, it is necessary to produce solutions that respond to both finite element analysis and current international design codes with similar accuracy for nozzle-shell junctions exposed to various load configurations.

1.3. Aim and scope of this research

The aim of this study is to first construct a high-accuracy finite element model to take into account the high stress values occurring in nozzle-cylinder connections subjected to internal pressure and external loading conditions. This model can be used for external loading, determination of limit loads, connection of multiple nozzles and fracture problems. The ultimate goal is to provide more accurate results by improving some existing equations in the literature for nozzle-cylinder connection problems.

Specific objectives of this research can be listed as follow:

(i) Review the background analysis for nozzle shell junctions to the current UK, US, and EU code methods.

(ii) Understand and be able to apply classic stress analysis, finite element analysis for elastic, in-elastic, shakedown and ratchetting for such junctions.

(iii) Understand and define the loading system on such junctions – internal pressure, forces and moments and note their significance on the overall assessment

(iv) Define the bounds of applicability of each analysis technique and show how it reflects the key failure mechanisms found in pressure vessel design.

(v) Carry out the parameter study and develop relationships for the leading parameters – stress, deflection, limit loads, shakedown loads, and fracture problems.

(vi) Develop governing graphs or equations based on the outcomes of this work and provide guidance to code writers for future improvements to the rules for industry

1.4. Outline of the Thesis

Thesis consists of eight chapters.

Chapter 1 indicate the general objectives and presentation of the study.

Chapter 2 presents an extensive summary of literature studies on current international pressure vessel codes, studies on nozzle-cylinder intersections, including elastic and in-elastic analysis and their calculations, as well as fracture problems frequently seen in pressure vessels.

Chapter 3 presents studies for high-fidelity finite element modelling. In this section, the determination of geometry for a nozzle-cylinder intersection, material selection, mesh

sensitivity analysis, application of loading conditions and boundary conditions, and verification of the finite element model are included.

In Chapter 4 -5, the analysis types to be applied for the finite element models are determined. Then, elastic analysis, limit loading analysis, plastic analysis and cyclic loading analysis are performed.

Chapter 6 presents models of possible cracks on the crotch corner and welding, and calculations of the stress intensity factors in different opening modes.

Chapter 7 provides stress concentration design curves for various loading situations and introduces a new method for plastic limit load estimation.

Chapter 8 summarises the thesis and provides conclusions and suggestions for future research.

CHAPTER 2. LITERATURE REVIEW

2.1. Introductory Remarks

A brief review of the most recent literature on the design and analysis of pressure vessels, especially pertaining to cylindrical vessels, and nozzle junctions, is presented in this section. In the literature review, elastic, elastic - perfectly plastic, and plastic analysis and international design codes including their application steps are also included.

2.2. Research on Current International Pressure Vessel Codes

If pressure vessels are to be defined in the simplest way, they are containers and tanks that carry or store fluids, are exposed to internal and external pressures, and require high impermeability. The use of pressure vessels around the world has been crucial to the success and expansion of design, manufacturing, and retail point of sale in much of the engineering world. Pressure vessels have many different uses, both industrial and domestic. Estimating the explosion pressure of the vessels is of vital importance, as the explosion of these can cause serious loss of life and property. When all these are taken into consideration, it is necessary to have knowledge about the elastic and in-elastic behaviours of such structures together with finite element analysis in order to fully meet the scope in pressure vessel design. For this, in the first step, a deep understanding of the current international pressure vessel design and analysis codes that have been accepted throughout the world is required.

It is important to understand the seriousness of the situation in remembering some of the historical anecdotes that led to the emergence of pressure vessel codes. With the invention of steam engines in the late 18th century, the use of pressure vessels became very common. Following this, in the first quarter of the 19th century, thousands of boiler

explosions occurred in both America and Europe and many people lost their lives [1]. One of the most notable of these was the boiler explosion that occurred on March 10, 1905, at the Grover Shoe Factory in Brockton, Massachusetts. This accident resulted in 58 deaths and 117 injuries. For this reason, the ASME Boiler and Pressure Vessel Code (B&PVC) [2] was first conceived in 1911 to protect the safety of the public. Over the past 100 years, these standards have been developed and have survived to the present day.

There are currently 4 basic pressure vessel codes in use worldwide. These are ASME VIII DIV 2[2], PD5500 [3], EN13445 [4] and Pressure Equipment Directive (PED) [5]. Although the ASME Boiler and Pressure Vessel Code (B&PVC) was conceived in 1911, the first ASME code was issued in 1915. Various additions have been made since the inception of the code to allow for a wider variety of products to be designed after the code. In addition, reviewing the codes and making the necessary changes is a process that is still on the agenda.

On the other hand, the first code used in Britain was BS1500, issued in the 1950s. Along with BS1515, this code helped develop and create the BS5500 code. After the introduction of the European standard code EN13445 [4] in 2002, the PD5500 was created because the British Standards Institute had to withdraw the BS5500 code when the European standard was published [6].

The Pressure Equipment Directive (PED), which came into force in the EU region from 19 July 2016, is a European-level legal framework for pressure equipment presenting pressure hazards applicable to the design and manufacture of pressure equipment. The PED covers the design as per the pressure equipment directive, with pressure more than 0.5 bar gauge is termed as pressure equipment. Under the Community regime of the

Pressure Equipment Directive, pressure equipment and assemblies defined by the directive must be safe and meet essential safety requirements covering design, manufacture, and testing; meet appropriate conformity assessment procedures; and should bear the CE mark and other information.

In addition to all these, existing structures in pressure vessel applications can be exposed to external global loads and local loads including various forces and moments as well as internal pressure. A series of calculations have been proposed by the Welding Research Council to calculate local stresses due to external local loads acting on the nozzle in cylindrical shells. WRC107 [7], WRC297 [8], and WRC537 [9] are the top bulletins for these calculations. In particular, WRC107 and WRC537, which is a more exact implementation of the WRC107, offer the necessary formulas and diagrams for spherical and cylindrical pressure vessels under external loads. This approach is based on shell theory and does not take into account of the opening formed by the nozzle intersection. This is encapsulated in WRC297, which too relies on shell theory. At the junction, this method has deficiencies and cannot fully represent the geometry at the junction.

Besides all this, a cylinder/sphere model can be used for cylinder-nozzle junctions, according to a method adopted in the BS5500. The stress concentration factor thus obtained can then be applied to the nominal hoop stress in the cylindrical container. Rose [10] provides general support for the concept of using cylinder/sphere SCF values for cylinder/cylinder geometries. According to Rose, “at present there is no accurate calculation method available for nozzles in cylindrical shells, but comparisons with experimentally determined values of SCF show that the accurate calculation for spherical vessels, based on thin shell theory, can be adopted for cylindrical vessels with little error,

and is preferable to other approximate calculations for cylinders. It is probably better for small ρ (d/D) rather than large d/D".

In addition, Leckie and Penny [11] presented a large number of design curves for SCF under various parameters for nozzle joints in spherical vessels. Elastic analysis can now be done with finite element models. Surface stresses and peak stresses can be easily determined by many programs. Although the calculations and analysis are very advanced, Leckie-Penny curves remain popular because they still require great care and detailed study. So much so that even for cylinder-cylinder junctions, Leckie-Penny curves are used first and adapted to these problems.

In addition to these, in 1966 Money [12] conducted a study with experimental data obtained from the literature. In total, more than 80 test results and the effect of various basic geometric parameters (D/T, d/D, t/T etc.) on SCF were interpreted. Money then experimented with various combinations of basic sizing and found that the measured SCF values correlated best with the parameters above.

Besides, since cylinder-cylinder connection problems are handled in WRC 537, there are calculations with round attachment parameters. The calculations and parameters to be used were plotted with the results of Bijlaard's work [13] and in terms of dimensionless geometric parameters using an electronic computer. Therefore, this is considered the first step in the procedure and the applicable geometric parameters.

2.3. Research on Nozzle-Shell Junction Behaviour for in the Elastic Region

Nozzles are one of the most important components to be examined in the design and analysis of pressure vessels, as a geometric discontinuity occurs due to the opening formed in the container at the nozzle-cylinder junctions. This discontinuity creates much

higher stress concentrations in the containers under the influence of internal pressure and external local loads. Even in overload situations, the container may collapse or burst with very large plastic deformations. Considering these effects before manufacturing, design and analysis studies are carried out to avoid possible failure mechanisms. Practically, these examinations are carried out in 3 stages: elastic stress analysis, limit loading (elastic - perfect plastic) analysis and plastic strain analysis after the loads on the container and damage modes are determined. Under this subheading, some studies in the literature, mostly on elastic region analysis, are given.

In terms of engineering applications, structures such as pressure vessels, piping installations and reactors must be economical in terms of design criteria and also high security. Especially for nozzle-shell junctions exposed to internal pressure and external loads, high stresses in the connection area should be reduced as much as possible. Therefore, in pressure vessel applications, one of the most convenient and economical ways to retrofit an insulated nozzle is to use a pad or balancing/reinforcing plate. There are many studies in the literature for determination of critical stress regions and calculations. WRC107 and WRC537 are among the most widely used sources for calculating local stresses in pressure vessels.

Andrade et al. [14] examined stresses due to external loads in a study of nozzle-cylinder connections subjected to extreme loads. For this purpose, they presented a nozzle-vessel model in which reinforcement plates are not used. In this study, WRC107, WRC297 and the stress results obtained from the model subjected to external loads using the finite element method were compared. In the analysis phase, the authors used a nozzle joint finite element model without reinforcement plate and welding neglected. In addition, it can be observed that a very small diameter nozzle is modelled and the brick mesh used

prevents a perfect mesh distribution in critical areas. Despite this, the authors state that the results obtained, are safe when compared to the aforementioned Bulletins, but it does not provide a universal solution for the industry.

In other studies, Dekker et al. [15] have undertaken several finite element analyses to calculate stresses on the nozzle walls rather than stresses on the shell. The reason for this is that the local load stress calculation methods have important differences between each other. As a result of these findings, researchers formulated the 'modified improved shrink ring method' and introduced a new approach. Another purpose of this study may be that the nozzle stresses remain in the second plan in the codes. For example, in the existing codes, especially the shell design is emphasized. Similarly, Leckie-Penny did not show nozzle stresses in their codes. This is considered a weakness in terms of design and such studies are very valuable as they open new avenues for researchers.

Also, there are many specialized computer programs that provide code applications to problems with nozzle - cylinder combinations. While the approaches are generally very similar, there are some differences in results. In such a study, Chandiramani et al. [16] obtained a comparative study by comparing the solutions obtained by the finite element method with the basic calculations in Bulletin 297 and Bulletin 537. In addition, this study generally discusses the conformity of the required compensating area to the ASME code [2] at the junction of large diameter and heavy nozzles. The author states that this would not be an ideal situation for an ASME code if all the required area came from the nozzle. For this reason, the study determines the optimum shell and nozzle dimensions to achieve the lowest junction stresses.

In another study using WRC bulletins, Cheema et al. [17] performed finite element solutions for pad reinforced nozzles and compared the results with WRC107 and WRC297. The authors, who stated that the aforementioned bulletins could not respond to the geometrical limitations that occur in containers with large openings, presented a comparison method with their study. Some shortcomings were identified in the study. Since the problem in the article is taken from a pressure vessel project, they only perform analyses for a single geometry. While meshing, 8 node isoparametric shell elements are used. The authors also did not share any finite element model images. For this reason, it cannot be guaranteed that the accuracy obtained by the authors, the elements used, meshing technique, and the boundary conditions will be valid for a different geometry.

Herrmann [18], on the other hand, presents a FE analysis for elastic isotropic shells in their work. The study includes nozzle intersections and folded-plate problems. Stating that the analyses can be applied to surface and boundary loads arbitrarily, the authors has shown the accuracy of the analyses in his work with a few samples and claims that the obtained accuracy is at an excellent level. In this study, the authors modelled the nozzle-cylinder junction using shell theory. Cylinder and nozzle thicknesses were neglected. In addition, although meshing techniques are very inspiring according to the period in which the study was conducted, current technological developments and finite element analysis method can be made more refined using a variety of software platforms. For this reason, this study is invaluable in order to see the development of finite element modelling techniques and solutions for nozzle-cylinder connection problems in the last 50 years.

Furthermore, Mukhtar [19] tried to determine the stresses by using FEM for cylinder nozzle connection problems. For this, stress concentration factor expressions were obtained for both the nozzle and the cylinder. Using some models available in the

literature for validation, the authors also used the elastic FE analyses results they obtained to find the maximum stress position. This study is based on the thin shell theory and only cases where the ratio of the radius to thickness of the nozzle used is greater than 10 (Rn/Tn>10) are considered. In addition to this, SCF determination was made for only 3 parameters. (1. Rv/Tv (Vessel radius / cylinder thickness), 2. Tn/Tv (Nozzle thickness/vessel thickness), 3. Rn/Rv (Nozzle radius/Vessel radius)). In addition to this, only internal pressure loading is examined in the study. As a result, a useful database of SCF values was created for nozzle-cylinder intersections.

Moreover, Figueiredo and Neto [20], stated that the limits presented in Section III of the ASME Code are based only on shell theory and there are deficiencies in solid finite element analysis. For this purpose, they introduced an elastic stress linearization procedure for nozzle-cylinder intersection problems. The results are compared with ASME Section III limits.

In pad applications around the nozzle, the shape of the pad and the rate of material contribution is also very important. In this study, Kharat et al. [21] compared the stress results they obtained with 4 different pad applications with FEA. In the light of the obtained results, the authors suggested 2 pad types were more suitable for the design procedure. There are some shortcomings in this study as well. The authors state that reinforcement is appropriate in order not to reach the limit load, but a limit load study has not been done. In addition, there is no explanation that the maximum stresses obtained remain in the elastic region. On the other hand, material properties are not given in the study, which restricts readers from commenting on which reinforcement types can meet these stresses. Despite all this, it can be a useful study in terms of introducing different types of reinforcement plates to designers.

Xue et al. [22] run a study for cylinder-nozzle intersections with and without reinforcement plates. The aim of the study is to determine the experimental limit pressure for a constant d/D parameter. With the test results, the authors noted that pad reinforcement significantly backed and reinforced the container for the limit pressures.

In a manner similar to a previous study, the strength behaviour of the structure for pad-reinforced and non-pad cylinder-cylinder intersections was investigated by Fang et al. [23]. Vessels were produced with different diameter ratios (d/D) for this study and obtained FEA results were supported the with these experiments. By determining the plastic limit moment load affecting the nozzle, load-strain curves were obtained for each test. The study provided a broad perspective for understanding pad usefulness on the pressure vessels and nozzle junctions.

In addition, the authors have also focused on pad reinforced nozzles placed on ellipsoidal pressure vessel heads. In 1986, Chao et al. [24] tried to understand the effects of the size and thickness of the nozzles located in the ellipsoidal pressure vessel head on radial flexibility using shell theory. In 1999, a study was carried out to determine the optimum pad sizes for the nozzle connections in the ellipsoidal pressure vessel heads by Nash et al. [25]. Moreover, design curves are presented for the allowable stress calculations of the each applied forces. In 2002, Skopinsky et al. [26] was figured out stress analysis on pad-applied nozzles in different configurations on the ellipsoidal heads of pressure vessels. The geometric parameters of the connections were discussed with the numerical and experimental results.

It takes an important place in oblique nozzles for nozzle combinations in pressure vessels. As the angle between the nozzle and the shell changes, the maximum stress magnitudes

also change. For this reason, the authors have made significant studies on this subject as well. Petrovic et al. [27] completed a study on the moment effect caused by external loading on the oblique nozzle. The stress results were obtained with FEA are classified according to the maximum stress criteria. Weiß et al. [28] managed a comprehensive strength analysis for oblique nozzles in cylindrical pressure vessels. The fatigue behaviour of the nozzles was investigated in order to determine possible fatigue failure locations in nozzle connections subjected to internal pressure and axial loads. Additionally, Patel et al. [29] performed limit load analysis for multiple oblique nozzle connections. Finally, Robinson et al. [30] experimentally investigated the behaviour of oblique flush nozzles in spherical pressure vessels in the plastic region.

2.4. Research on Nozzle-Shell Junction Behaviour for in the Plastic Region

In this section, a summary of the literature review on limit load, plastic analyses, and cyclic loads for nozzle-cylinder junctions will be given.

Understanding the potential to support maximum loading conditions is an important aspect in the design and analysis of pressure vessel applications. This is especially important for thin-walled pressure vessels where stresses reaching the initial material yield point can lead to very dangerous situations. Pressure vessels can be subjected to stresses from a variety of loading conditions, including internal pressure and multiple external loads from connected piping systems. Once the yield point is exceeded, the structure can accommodate more loading until the plastic zone becomes excessive and causes the plastic to collapse. This can be difficult to determine, especially when external loads act with internal pressure. For this reason, there are many studies in the literature that examine in detail the limit value at which the system reaches the first yield point and the plastic degradation from exceeding the yield point to full collapse.

As mentioned before, bulletins such as WRC107, WRC297 and WRC537 are currently used to calculate local stresses in cylindrical and spherical pressure vessels. In addition, codes such as ASME Boiler and Pressure Vessel Code, EN 13445-3 and PD5500:2000 have put forward a series of studies and calculations in order to avoid plastic instability and to detect limit loading conditions. In addition to all these studies, there are many studies based on elastic-plastic analysis in order to calculate plastic loads in the literature.

In pressure vessels with nozzle connection, the nozzle shell connection areas are the areas where the weakest points are due to the presence of stress concentrations arising from the intersection cut. The diameter ratios d/D are important and shell theory is reliable for d/D <0.3 but has weaknesses when this rises to 1.0. It is noted that much of the literature is based on establishing the elastic stress solution with little available on limit load calculation for multiple load combinations. Sang et al. [31], attempted to obtain the results of inelastic stress analysis of a pressure vessel and nozzle connection with diameter ratios of 0.526 (d/D = 0.526). These results were solved under increasing internal pressures with the help of experimental studies and nonlinear finite element methods (FEM). The analyses were supported by experimental studies to demonstrate limit loads originating from internal pressure and to compare with the results of the FEM. In addition, a burst testing was carried out to understand and validate the limit design method. In addition, the authors stated that this method does not require the elastic analysis stress categorization procedure. They also signified that the applicability of method was much simpler than the elastic design procedure.

Besides, the ‘elastic compensation method’ used by Nadarajah et al. [32] was used for internal pressure and moment loading conditions in nozzle cylinder connections. With this method, limit and shakedown intersection diagrams can be obtained. In addition, the

mentioned method was used to determine the upper and lower limit of the nozzle cylinder junction. The main objective is to investigate a highly complex vessel problem for the nozzle-cylinder intersection under the internal pressure and the nozzle subjected to torque loading. In conclusion, it is stated that the obtained results were compared with the existing methods and better values were obtained.

In addition, Dekker and Stikvoort [33] conducted research on the stress intensities for the nozzle - cylinder connection. After reviewing the existing standards, some standards such as the PD5500, the German AD-Merkblatter [34] and the Dutch Rules for Pressure Vessel have been suggested that it is unreliable for thin-walled and relatively large nozzles. Thereupon the authors determined the purpose of the study as to provide the significant differences between the existing design codes and standards when calculating the stress intensity occurring at the nozzle-cylinder junctions. For this purpose, they compared the results using the existing design codes and finite element method. The proposed analyses have allowed for a more reliable calculation of the external loads on the nozzle. As such, in this study, a finite element approach is used to develop a suitable model and undertake a parametric limit loads study for cylinder - cylinder intersections subject to internal pressure and combinations of external loads which will lead to an improved design approach.

Additionally, Muscat et al. [35] introduced a plastic work criterion in order to enable the evaluation of plastic collapse and limit loading conditions in pressure vessels through design and analysis. The authors stated that this criterion is a suitable method to characterize gross plastic deformation.

Liu et al. [36] on the other hand, aimed to choose the breaking criteria for pressure vessels under internal pressure and to calculate the plastic collapse loads of pressure vessels with the theoretical method they proposed.

Also, Kulkarni used a finite element software and experimental data to determine the explosion pressures of domestic thin-walled LPG tanks [37]. The TES (twice-elastic slope) criterion was used as a validation method and the mean error factors were presented.

Another study using the TES method in the calculation of critical collapse loads was conducted by Balakrishnan [38]. In summary, wall thinning and ovality were investigated for pipe bends under bending moment. Finally, the effects of these parameters on the B2 stress on the existing pipe structure were investigated. B2 can be simply defined as the stress index corresponding to irregularities and uniform wall thickness in circular pipe elbows under bending moment.

Deng et al. [39], stated that the design methods of ASME Boiler and Pressure Vessel Codes should be reconsidered by addressing the decreasing safety factor values from 5.0 to 2.4 in pressure vessel design over the years. In their study, they investigated the ductile fracture stresses of the materials with some elastic-plastic stress analysis.

Furthermore, Moffat et al. [40] made an evaluation on the methods of obtaining plastic charges for some pressure vessel components. In conclusion, they stated that The CEN TC54 technique gives a more unique limit load (or plastic load) than The ASME III TES technique.

Wu [41] conducted a study of plastic load detection for nozzle cylindrical containers in their study. The plastic load values resulting from the in-plane moment at the nozzle were

compared with the experimental, finite element analysis and TES criterion. The author stated that the results were in good agreement with each other. The maximum error of the average experimental versus FE calculated limit moments was about 10%. In addition, proposed equation provides an alternative solution to determine the plastic limit moment of cylinder-nozzle connections subjected to in-plane load on nozzles.

Another study on plastic limit loading of nozzle-connected cylindrical pressure vessels was done by Prakash et al. [42] The approximate plastic limit load was obtained by TES method and examined in terms of different combined inclination angle of the nozzles. It has been stated that the obtained results give useful results in terms of design and optimization.

Lee [43] presented results for plastic load detection in 90-degree pipe bends in his study. Basically, TES and plastic limit solutions are included in the calculations. As a result, it was suggested that the in-plane closing bending mode is the most critical loading mode.

Patel et al. [44] calculated the plastic limit load by considering a 45^0 oblique nozzle. The authors conducted experimental studies to verify the stress values obtained by the finite element method. They used TES and TI methods for limit load estimation.

In the plastic limit load study performed by Li et al. [45] for lateral nozzles, the plastic load was similarly determined by TES method and the obtained results were compared with FEA and experimental results. Plastic deformation properties for the analysis model are discussed. The results showed that significant deformation properties occurred in the test vessels.

Skopinsky [46] carried out a plastic loading study for the ellipsoidal pressure vessel head – nozzle junction under internal pressure. The authors developed a new method that can

be used to determine the plastic load for this intersection. In addition, the effects of dimensionless geometric parameters on the plastic limit pressure are also discussed in the study.

As mentioned above, various calculations and limit load analyses are needed to determine the capacity that the structure can withstand before collapse. On the other hand, cyclical loadings within the elastic-plastic area should also be considered rather than single loads. Because cyclical loads may cause the structure to fail sooner than expected due to low cycle density. Examining the plastic behaviour of structures subjected to cyclic loading in pressure vessel design has been one of the issues that have been emphasized in recent years. An elastic-plastic material subjected to cyclic loading will give an elastic shakedown, plastic shakedown or ratcheting response after a certain cycle.

Zeng et al. [47] studied the plastic shakedown behaviour for a cylindrical container under cyclic loading using a water pressure loading system. In this experimentally supported study, conditions such as total strain and shakedown range, modelled stress-strain relationship under large deformation, and ratcheting behaviours were examined.

Anwar et al. [48] investigated the effect of cyclic temperature and cyclic pressure in pressure vessels. They looked into the stress distributions that occur with cyclic loads on the wall of the pressure vessel with a time dependent numerical model. From this study it was concluded that the contact surface of a cylinder subjected to cyclical pressure and temperature is always subjected to the maximum effective stress. Minimum effective stresses were detected on the outer surface. In addition, the results showed that the limit values of mean pressure and temperature were inversely proportional, and the limit values

of pressure and temperature amplitude were directly proportional. In summary the results obtained were in agreement with the study parameters and numerical findings.

Abdalla [49] determined elastic shakedown loads at nozzle intersections using a simplified technique in the study. The resulting elastic boundary loads form the Bree diagram and are compared with the elastic plastic finite element load simulations. The author says these results are in perfect correlation.

Bakry [50], on the other hand, studied internal pressure and bending cyclic loadings using hillside nozzles. According to the changing hillside angle, the cyclic loads were determined by the nonlinear superposition method and the results were discussed.

2.5. Research On Pressure Vessels Fracture Behaviour

Potential failures caused by breakage problems are an important issue in structural integrity evaluations of pressure vessels. Load carrying capacity is limited in such thin-walled structures. Buckling and compression forces due to internal pressure and external loads can cause a decrease in the limit loads in the containers and even bursting. Such problems usually start with small surface cracks and these cracks could be grown in a path until eventually the structure deteriorates. Cracks that may occur in pressurized vessels may be caused by manufacturing procedures or in various environmental effects. One of the most important problems that arises in the industry is the evaluation and consideration of the safety criteria of structures such as pressure vessels throughout their service life. For this reason, various studies have been conducted to examine the behaviour of pressure vessels and pipes containing cracks.

Studies on fracture problems in pressure vessels gained much more importance after the 1960s. Copley and Sanders [51] conducted a study in 1969 for cracks placed

longitudinally on a cylindrical vessel. This study showed an alternative way to the researchers to determine the residual strength of a broken cylindrical vessel in those years.

In 1972, Erdogan et al. [52] researched an unsymmetrical crack problem placed in a cylindrical container in a circumferential direction. In the same year, the researchers examined the fatigue and fracture conditions for cracks along the shell in cylindrical and spherical vessels [53]. In this problem, the internal pressure effect on the vessels is given with torsion. The resulting Crack Opening Displacement (COD) and Stress Intensity Factor (SIF) values were verified by bursting tests results.

In addition to all these studies, there are many additional studies in the literature related to SIF calculations and the development of these calculations. These equations are also still open to new approaches and interpretation. In 1982, Newman and Raju [54] studied internal surface cracks in cylindrical pressure vessels. In the study, stress intensity factors were determined by changing parameters such as crack length, crack depth, wall thickness at certain rates. The study includes calculations in mode - I opening mode only. Empirical equations in the study were developed with extended parameter variations. The results obtained have been confirmed by other results in the literature.

Liu et al. [55] performed linear elastic fracture analysis for a Reactor Pressure Vessel (RPV). It was assumed here that cracks may occur at the nozzle-cylinder intersections where the stress is most concentrated. As a result, calculations were made for different crack shapes and design conditions that did not endanger safety. In another study, possible elliptical cracks in the nozzle-vessel junction area were discussed by Murtaza et al. [56]. Here, the effect of pressure plus thermal stress on SIF values were investigated. After all, it was emphasized that the applications made were completely safe in terms of fracture

mechanics. On the other hand, Jin et al. [57], obtained fracture driving forces (KI, J) and T stresses in RPV corner cracks by using traditional calculation methods. Additionally, they put forward a simplified calculation process that can estimate the Weibull stress calculation occurring under this stress field and along the crack tip more effectively with the modified boundary layer model. Another study on cracks in the Reactor Pressure Vessel was done by Susmikanti [58]. In this study, J-Integral and SIF calculations were chosen as crack parameters. Also, it was stated that the 3D modelling was in accordance with the SIF calculations and some critical loading conditions that could cause breakage was specified.

Akrami et al. [59] studied the effect of buckling load on cracks in cylindrical shells. In this study, which was based on analytical and numerical evaluations, parameters such as cylinder length, crack location and intensity constitute the basic criteria. At the end of the study, the authors proposed an empirical equation to compare buckling loads in cracked and uncracked structures. Moreover, the buckling behaviour of broken cylinders was also discussed by Estekanchi and Vafai [60]. In Estekanchi's study, a program has been developed for FE modelling of cracks in different lengths and directions. Then, buckling behaviour in tensile and compression loads in these models was investigated.

Besides these, Alizadeh [61] validated his model using the extended finite element method for various parameters and investigated the use of CFRP laminates to strengthen the container in crack problems.

In this study, inclined cracks occurring on the inner surface of cylindrical pressure vessels were investigated by Subbaiah [62]. It was given point to here that the critical slope was 30 degrees and as this angle increased, the Mode-II loading became more dominant.

Furthermore, SIF calculations were made simultaneously for the presence of more than one crack with the numerical simulation

In 1996, Challanger et al. [63] stated that procedures such as BSI PD6493: 1991 [64] and ASME XI used in the fracture mechanics applications of pressure vessels in the industry do not have many examples in practice. For this reason, they compared the failure mechanisms for 8 different pressure vessels with these methods. As a result, they proved that the procedures were safe. In 1997, Liaw et al. [65] wanted to investigate the effect of material structure and mechanical properties on fracture behaviour in pressure vessels. Thereupon, the initiation and propagation of cracks were investigated by doing fatigue behaviour research on pressure vessel steels. Fatigue life analyses were compared with experimental results. Thanks to these results, crack initiation and fatigue life results that can be encountered when using different crack sizes for pressure vessel steels have been developed.

In the 2000s, Chai and Zhang [66] conducted a study on these problems by detecting that there is no calculation method in the literature on the surface crack and embedded elliptical crack interactions in cylindrical pressure vessels. SIF values were obtained for many crack variations. The result is an interpolation method that helps to estimate SIF values for specific crack depth/crack length ratios. In another study, Kiciak et al. [67] provided some computational methods for complex stress fields that cause breakage.

In 2005, Diamantoudis and Labeas [68] introduced a finite element solution for semi-elliptical cracks. The authors stated that the solutions in the literature only provide solutions for containers with equal stress distributions and there is no numerical solution for complex structures with stress distribution in different axes such as nozzle junction

areas. For this purpose, the authors proposed an alternative solution method for stress intensity factor calculations by introducing a modelling method for nozzle junction areas and cracks that may occur at the spherical end junctions of the cylinder.

In 2006, Saffih and Hariri [69] [70] examined the elliptical cracks in cylindrical structures with a thickness transition. In the first study [69], a 3-dimensional finite element model, which is also compatible with numerical solutions, was proposed. In the other study [70], a simple J integral calculation method is presented to calculate the plastic behaviour at the deepest point of the crack.

Additionally, Kirkhope [71] derived empirical equations for the KI calculation at the deepest crack location for specific crack depth / crack length ratios using the KI values of single and multiple cracks occurring in thin-walled cylinders in his study. Also, Hachi et al. [72] developed a computer code for SIF calculations of elliptical cracks in the Mode I opening state. The results obtained were compared with other methods in the literature and it was stated to have high accuracy. In 2002, Ayhan and Nied [73] conducted a study on the detailed general formulation of enriched crack tip elements for three-dimensional crack problems. The advantage of this formulation over other approaches is that the same calculation algorithm can be used for more complex crack tip areas. In another study by Ayhan [74], a three-dimensional methodology was presented for simulation of fatigue crack propagation. With this method, named Fracture and Crack Propagation Analysis System (FCPAS), mixed mode surface cracks can be easily calculated. Bozkurt et al. [75] conducted numerical and experimental studies on the mode I-III fracture sample using the finite element method and FCPAS [74]. Kurt [76] on the other hand, obtained SIF solutions for mixed-mode cracks on the interior surfaces of spherical pressure vessels, again using FEM and FCPAS.

2.6. Concluding Remarks

In summary, all these literature studies show that nozzle-vessel connection problems, elastic stress analysis, limit loading analysis, plastic load determination, fracture mechanics and international design codes have a wide research area in many subjects. The application of the finite element method has prepared the environment to carry out this research more easily and accurately in the theoretical sense. However, studies have shown that even in similar problem solutions in complex structures, application differences can occur. For this reason, it is very important for designers to gather elastic, elastic –perfectly plastic, plastic, shakedown, and fracture analyses under a single study so that the failure mechanisms can be handled with a large study. For this purpose, in the following sections, first of all, a high-fidelity nozzle-cylinder finite element model will be created and then the analysis types mentioned will be applied on this model, respectively.

CHAPTER 3. DEVELOPMENT of a HIGH-FIDELITY FINITE ELEMENT MODEL

3.1. Introductory Remarks

A high-fidelity finite element model has been developed in this section that will apply to all geometries used by industry and will provide a universal approximation to local loads for nozzle-cylinder joints, as well as account for the maximum stresses around the crotch corner of nozzle-cylinder junctions subjected to combined loads. For this purpose, geometry, material selection, mesh sensitivity analysis and loading conditions were determined, and then verification studies were carried out for the finite element model created.

3.2. Statement of the Problem

In the case of pressure vessel problems, the highest stresses often occur in the nozzle cylinder intersection regions. Accurate determination of these stress values is of great importance in terms of taking necessary precautions in design and future fatigue assessment. Finite element analysis is one of the most commonly used numerical procedures. Although all stress values on the vessels with finite element method can be determined very easily, because of the differences in the method applied, the results are not completely aligned. The aim of this study is to create a high-fidelity model which can respond to different shapes and applications for nozzle shell combinations with different thickness ratios. At this time, the scope of this problem is for a linear elastic solution establishing maximum stress values around the crotch corner which shall be taken as basis for the model.

3.3. Geometry

When creating the finite element model, the problem of an open-ended cylinder-nozzle intersection is considered. The ratio of inner nozzle diameter (d) to inner shell diameter (D) is accepted as 0.5 as a starting value and the analyses are repeated by enlarging the cylinder diameter. In addition, two different boundary conditions are examined throughout the study in order to examine the stress distributions around the crotch corner in more detail. Firstly, as shown in the **Figure 3. 1**, whilst the model is restricted by one side, by means of boundary conditions, on the other hand axial movement will be allowed on the other side.

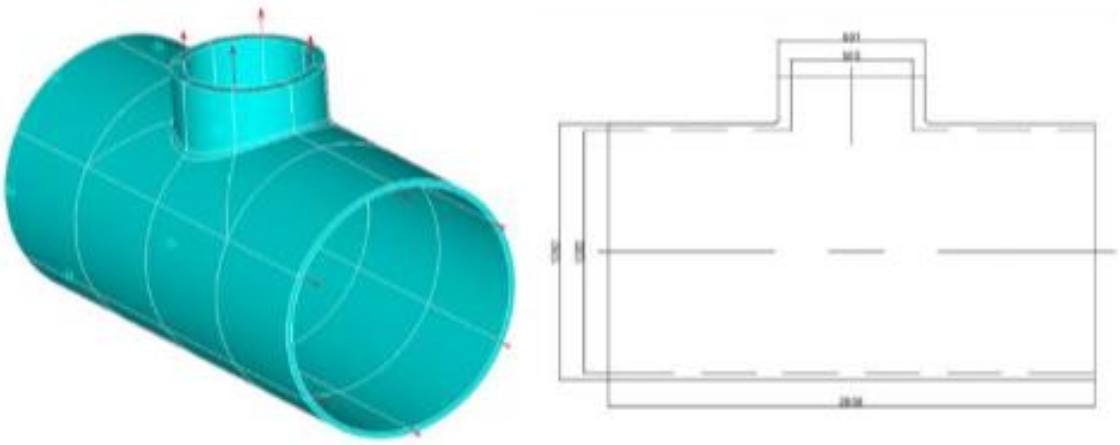

Figure 3. 1 Model of the nozzle - cylinder junctions (no saddle)

In addition, since the whole model will be under the influence of internal pressure, an open-ended cylinder is used and thrust force is observed at both ends. On the other hand, the vessel is placed on 2 saddles (**Figure 3. 2**) . For this reason, the movement will be released at the both ends of the cylinder.

Saddles, by the way, are completely restricted to movement in all directions from the bottom surface area. Moreover, internal, and external radius (welding) applications,

which are among the most effective applications for the optimization of stress values, are also examined under a subsection.

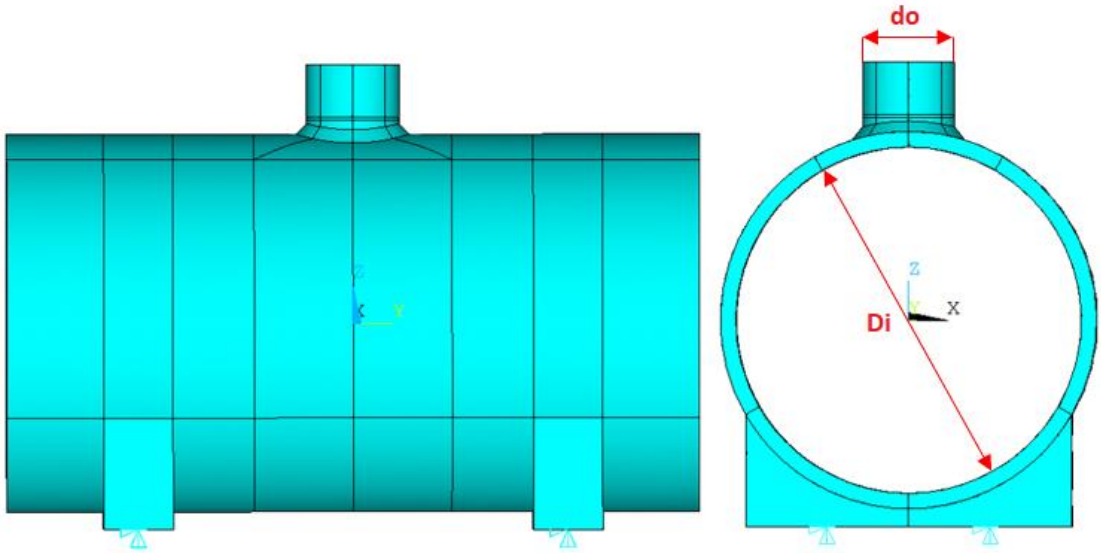

Figure 3. 2 Model of the nozzle - cylinder junctions (with saddle)

3.4. Material Selection and Properties

In this study, the use of high-quality carbon steel is considered suitable to produce boilers and pressure vessels, which ideally comply with the high standards set by the oil, gas, and petrochemical industry. For this purpose, SA-516 Grade 70 Carbon steel was chosen as the shell material, and ASTM A266 Grade 2 Carbon Steel was chosen as the nozzle candidate material [77] [78].

The material properties for the nozzle and shell are given in **Table 3. 1** in detail. For the saddle applications, a 210GPa Young's Modulus value is appropriate, and the weld material was assumed to have the same properties as the nozzle material.

Table 3. 1 Material Properties for Nozzle and Shell

Material Name	Young's Modulus	Poisson's ratio	Yield Strength	Ultimate Tensile Strength
Shell - SA-516 Grade 70 Carbon steel pressure vessel plates [77]	200GPa	0.3	260MPa	485-620MPa
Nozzle - ASTM A266 Grade 2 Carbon Steel [78]	190GPa	0.29	290MPa	570MPa

However, the tensile properties of welds are normally overmatched to the parent material. The yield strength values shown in the table are the minimum values to be considered. It is noted, however, that higher yield strength values can be obtained in practical applications. The values shown in the table are used directly in the analyses.

3.5. Element Type and Mesh Sensitivity

Figure 3. 3 shows details of a typical finite element mesh of the cylinder-nozzle interaction noting the inside diameter of nozzle(di) is always the half of vessel inside diameter(Di). For a model with an inner diameter of 500mm, the element size was 30mm, and for the remaining cases it was 50mm. Furthermore, the element type was chosen as SOLID186 which is a higher order 3-D quadratic formulation with 20-node solid element.

The choice of element type when undertaking finite element analysis is important as this is determined the ability of the model to represent the stress distribution. ANSYS SOLID186 [79], a higher-order 3-D solid element with 20-nodes that exhibits quadratic displacement behaviour is employed in **Figure 3. 4**. The element is defined by 20 nodes having three degrees of freedom per node and supports plasticity, and other phenomenon and is suitable for the present application.

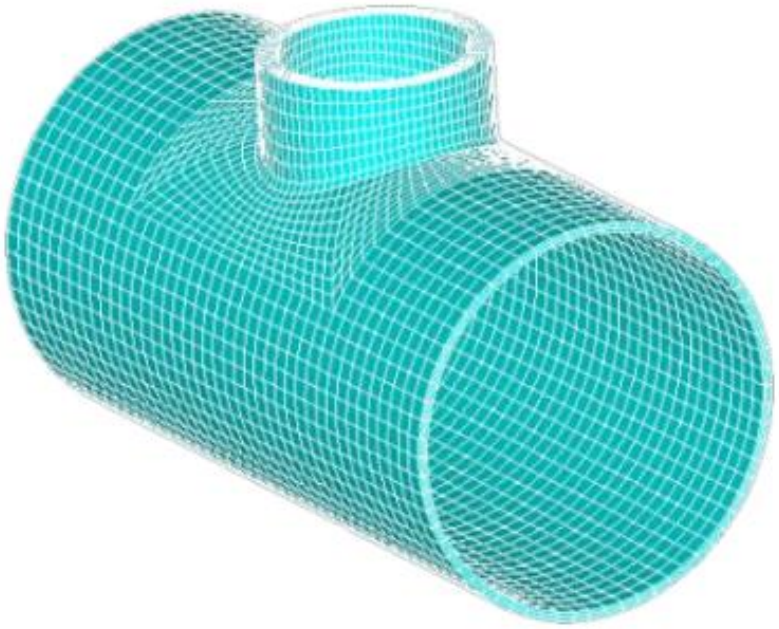

Figure 3. 3 Perspective view of the meshed model

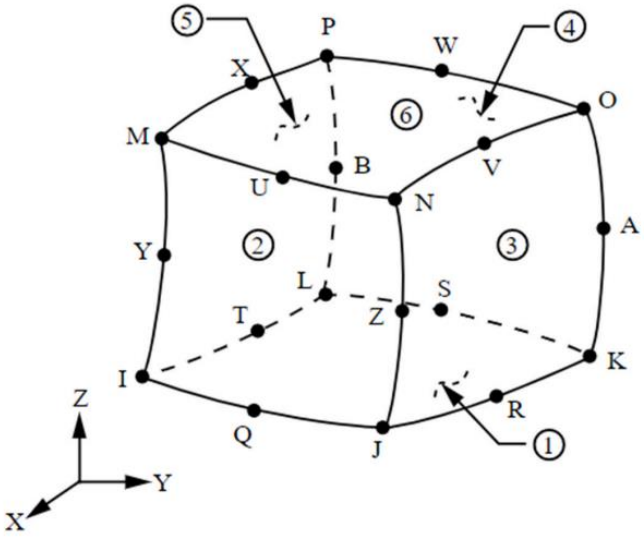

Figure 3. 4 SOLID186 homogeneous structural solid geometry

As the maximum stress variation in the analysis is the region of the nozzle-shell combination, a mesh sensitivity analysis is needed for this region. For this reason, the effect of the number of elements extending along the thickness of the nozzle to the stress values was examined. The nozzle thickness (t) is divided into 1, 2, 4, 6, 8 and 10 elements

in each analysis. The distributions of the elements for using 2 and 4 elements along the nozzle are shown in **Figure 3. 5**, and **Figure 3. 6**.

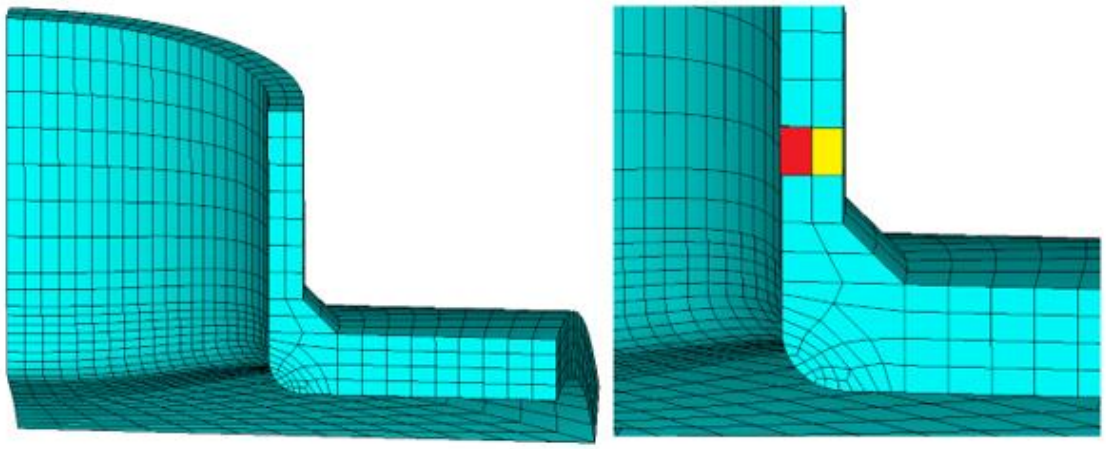

Figure 3. 5 Applying 2 elements throughout the nozzle thickness

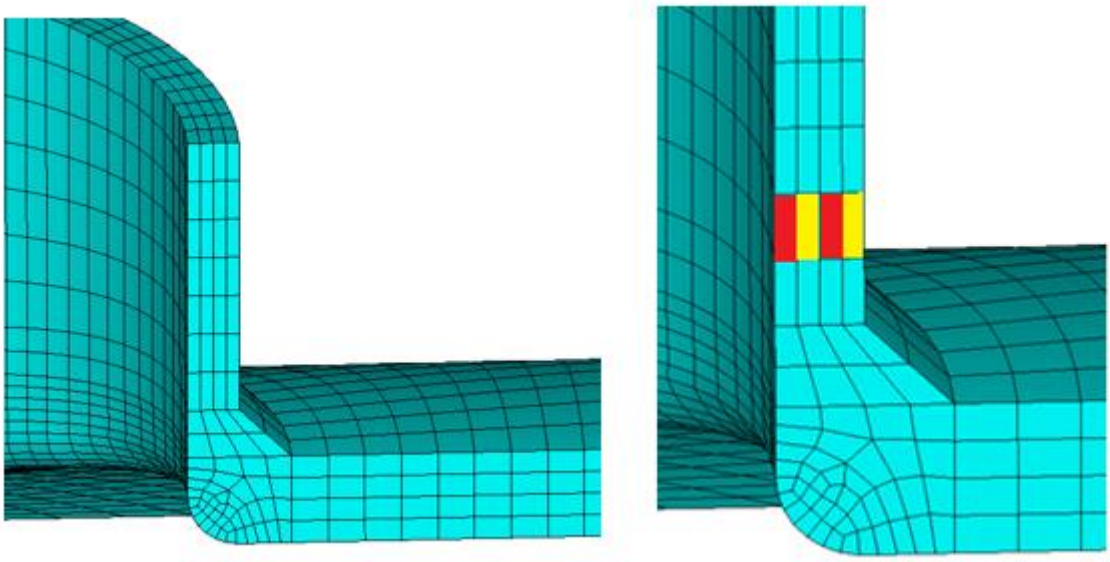

Figure 3. 6 Applying 4 elements throughout the nozzle thickness

As a result of the mesh sensitivity analysis carried out, there are no significant differences in their stress distributions and values. The maximum difference between the stress values occurred when 2 elements were used throughout the nozzle. This difference is less than 1%. The results are shown in the **Figure 3. 7**.

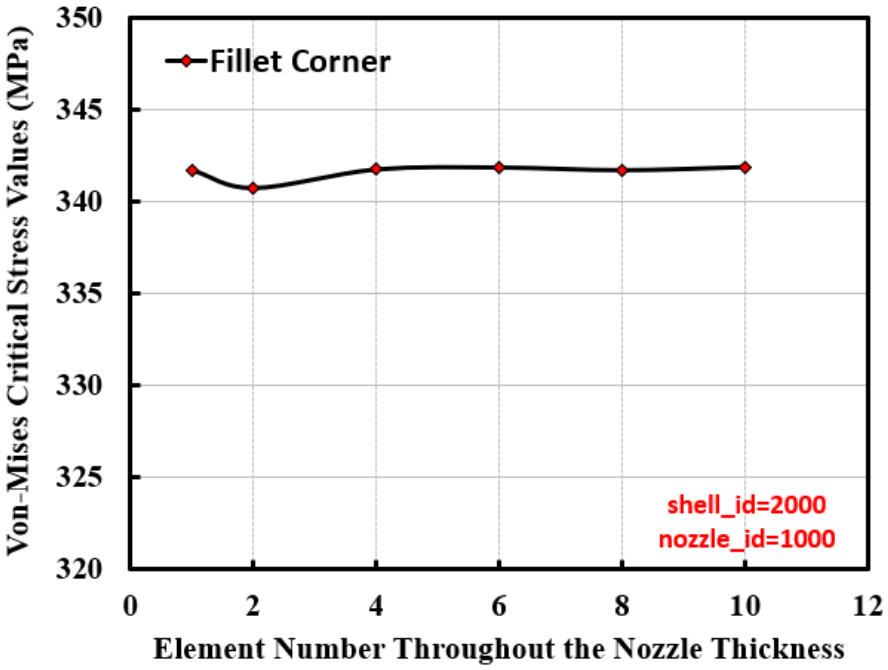

Figure 3. 7 Variation of stress values according to element numbers

Although the results are very close, it seems that mesh distributions are more reasonable when 4 and 6 elements are used. For this reason, it was decided to use 6 elements throughout the nozzle thickness to meet a common point for all studies.

3.6. Verification of the Finite Element Model

1. First, verification work will be done for the nozzle cylinder finite element model under internal pressure. While performing the verification study, the study of Chandiramani [16] is taken as a basis and the stress results of zero percentage contribution (no reinforcement) to area from the shell are used. In addition to the use of a hand calculation method, the stress values obtained by the finite element method are used in these processes. While these results are obtained, the value of internal pressure is taken as 8.5 MPa as indicated in the study. The thrust forces on the nozzle and cylinder with the effect of the internal pressure are also calculated by **Equation 3. 1** and **Equation 3. 2**

using the equivalent pressure approach for the end-cap loading. Allowable and FEA stress results are given in the below.

$$P_{shell} = \frac{P_{int} * D_i^2}{(D_o^2 - D_i^2)}$$ ***Equation 3. 1***

$$P_{nozzle} = \frac{P_{int} * d_i^2}{(d_o^2 - d_i^2)}$$ ***Equation 3. 2***

As can be seen from the **Figure 3. 8**, the results obtained are very close to the current study and the model is therefore verified with these results. In the following steps, parametric studies are carried out and studies are performed to reduce the maximum Von Mises stress values on the crotch corner.

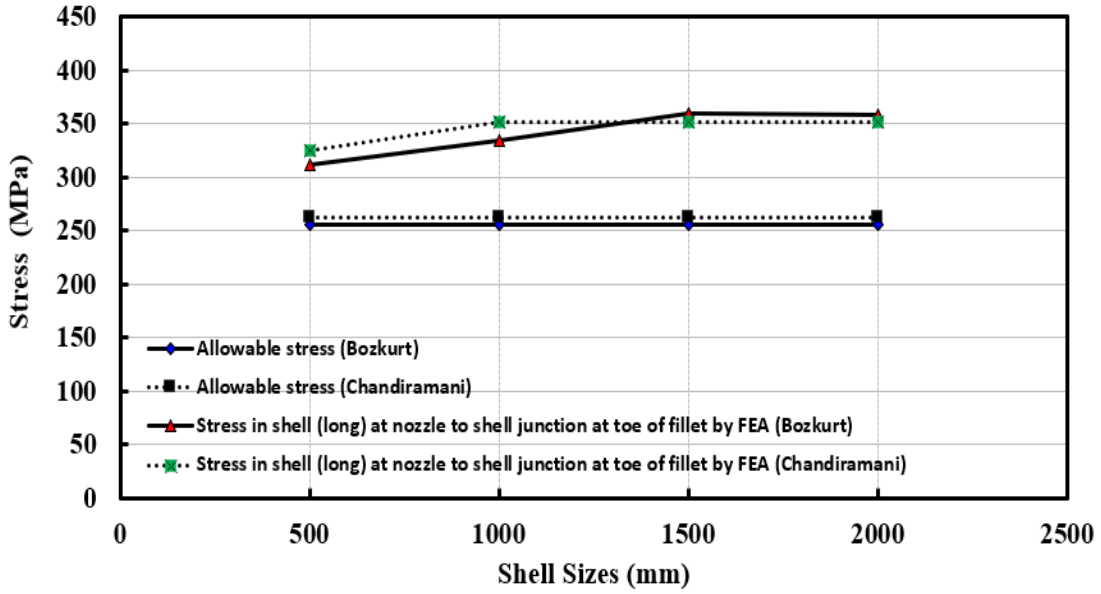

Figure 3. 8 Stresses (MPa) vs Shell sizes (mm) from shell

2. Another validation study is done for the external loading condition. These loads are applied from the nozzle centre and analyses are made for tensile load, longitudinal moment, and circumferential moment situations. The obtained FEA results

are compared with WRC 537 [9]. The results of this comparison are shown in the **Figure 3. *9*** and **Figure 3. 10**.

When **Figure 3. 9** is examined, it can be seen that the results obtained with the FEA, and WRC 537 calculations overlap perfectly. When **Figure 3. 10** is examined, the maximum difference emerges in the circumferential moment (M_C) application. FEA results here are about 5% less than WRC 537. In longitudinal moment (M_L) application, this difference is much less.

In this part, various modelling techniques, mesh sensitivity analyses and validation studies are carried out to obtain a high-accuracy finite element model. The generated finite element model is validated for both internal pressure and external loading conditions.

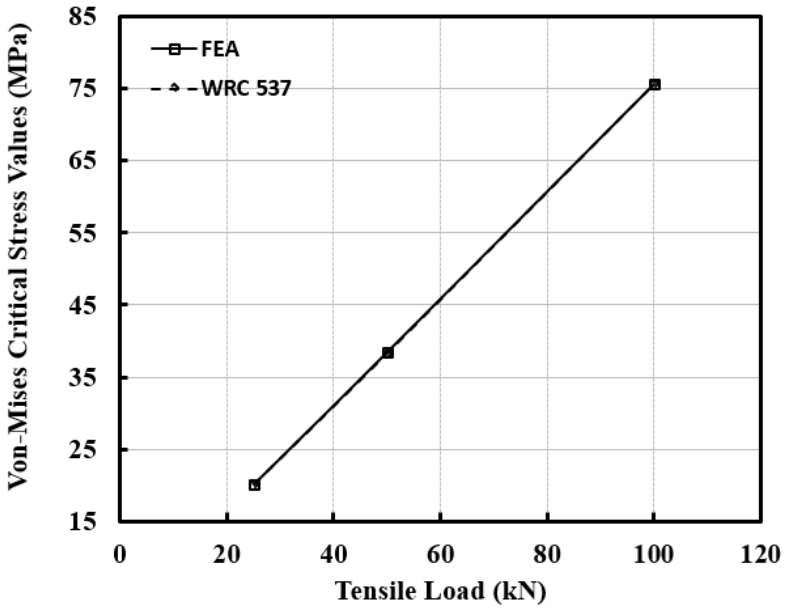

Figure 3. 9 Maximum stress values for a nozzle – cylinder junction under tensile loads

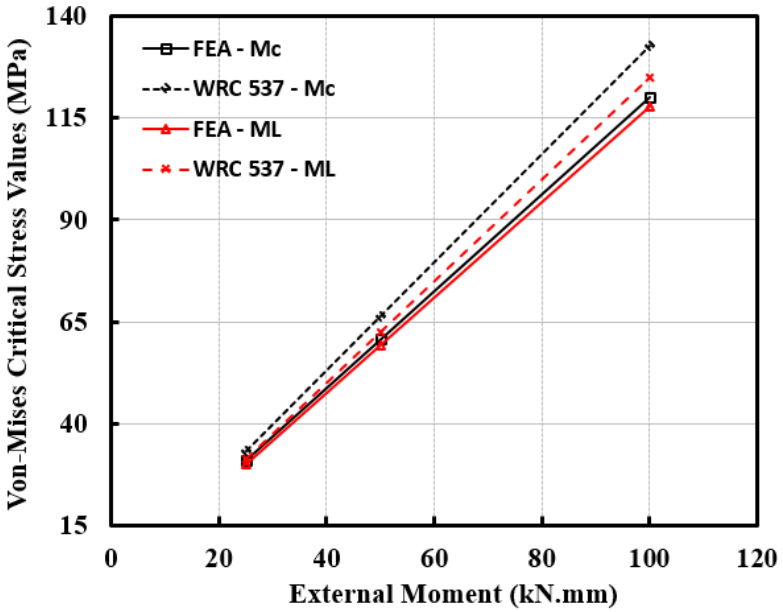

Figure 3. 10 Maximum stress values for a nozzle – cylinder junction under external moments

There are model validation analyses within the fracture analysis section of this thesis, but since the mesh technique will be different in models with cracks, this part will be examined in Chapter 6 to ensure the integrity of the topic. In addition, the created model is parameterized with the help of the written finite element macros. In this way, automatic modelling can be done by entering only geometry dimensions such as nozzle diameter, vessel thickness etc. into the macro.

In summary, a high precision finite element model that can respond to many different geometries and loading conditions has been created in this section and is now used to address a number of problems and approaches in subsequent chapters.

CHAPTER 4. FINITE ELEMENT ANALYSIS INVESTIGATION

PART 1 - ELASTIC ANALYSIS

4.1. Introductory Remarks

This chapter investigates the finite element analyses in the elastic region for nozzle connections in pressure vessel problems with parametric studies and discusses the results. Single and multiple nozzle connection problems, oblique nozzles, stress analysis, and stress linearization approach are the main research subjects.

4.2. Elastic Stress Analysis

The finite element method is the most commonly used approach when solving complex practical cylinder-cylinder junctions in pressure vessels when a design-by-analysis assessment is being undertaken. This approach is also used when the geometrical arrangement is out with the permitted scope of the design-by-rule approaches, for example d/D ratio exceeded or when oblique or hillside nozzles are employed, or when detailed stress information is required as in a fatigue assessment. High-stress concentrations occur on the crotch corner for cylinder-cylinder joints, and it is possible to reach solutions for this problem by using both theoretical and numerical solutions. However, those approaches do not fully overlap or converge to a unique solution for all methods nor have the same underlying assumptions. As such, an innovative high-fidelity finite element model should be developed to provide a holistic unified approach which can tackle a wide range of problems. In this study, various detailed nozzle design challenges were investigated including single and multiple nozzle combinations, nozzle-cylinder systems with different size ratios, fillet weld applications, and external loading cases were analysed. The results obtained are compared with well-respected calculation

methods such as WRC Bulletin 537 [9], and a new approach is presented for the analysis of cylinder-cylinder combinations.

To give more details, the priority here is to first examine the effect of sharp corner, inner fillet, and welding applications on maximum stress values for cylinder-nozzle intersections in stress analysis. In this way, it will be determined which method gives better results in order to reduce the maximum stress in critical loading situations. For this reason, the internal fillet application and its effects are introduced first. Then, the effect of changing the inner fillet and outer fillet (welding) sizes is examined. When these analyses are completed, external loading analyses is performed for a suitable nozzle-cylinder model. Verifications are made with WRC Bulletin 537, which has a very common use in external upload analysis. Then, stress analysis with multiple nozzle combinations, the effect of oblique nozzles and nozzle angle on maximum stress values is examined. In the last stage, the elastic analysis part is completed with pad reinforcement analysis, which is an effective maximum stress reduction method.

4.2.1. Investigation of the Inner Fillet Applying Effects

Firstly, it is well known in industry that the use of a weld as a stress reducer can be highly effective. In addition, the presence of a radius crotch corner can also provide a stress reducing effect. However, there is little in the literature as to how effective or to what extent the stress reducing effect actually is and to what extent the combined effect of these features can have on the overall system. As noted therefore, the ultimate target is to decrease the maximum critical stress values on the crotch corner by applying an inner fillet throughout the nozzle-cylinder intersection. This is commonly undertaken in industry. The representative image for the inner fillet application is shown in **Figure 4. 1**. The greater the nozzle opening in pressure vessels, the greater the maximum stress that

will occur at the crotch corner. At this stage, analyses are first performed for a constant internal pressure and di/Di (nozzle inner diameter / vessel inner diameter). The aim here is to observe how the size of the structure and the change in wall thickness (t/T) affect the maximum stress under the same pressure values. For this reason, the analyses are repeated by changing the t/T values for 3 different Di values (500mm, 1000mm and 2000mm). In total, 69 analyses were made for this comparison.

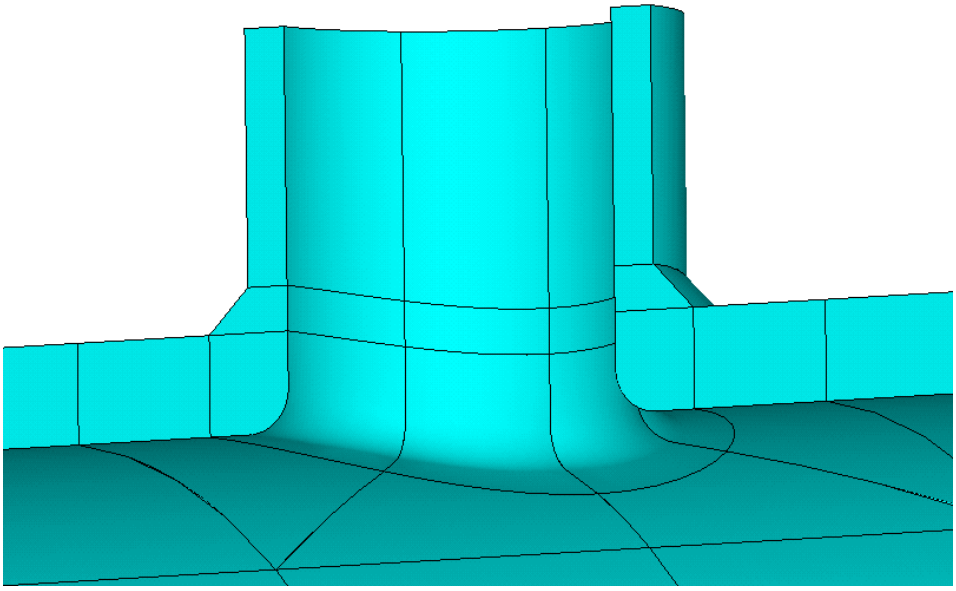

Figure 4. 1 Inner fillet application

At the end of the analyses, results were compared for models with sharp corner, outside welding fillet and inner fillet. A representative image of each of the models is shown in **Figure 4. 2**

There is sharp corners representation in **Figure 4. 2**. **a.** This means that the nozzle is directly penetrated through the vessel. An inner fillet is not applied to the crotch corner and the welding (outer fillet) is neglected. In **Figure 4. 2. b**, only the outer fillet is modelled, the inner fillet is not applied in the crotch corner. In **Figure 4. 2. c** both outer and inner fillet are applied to the crotch corner. It is possible to say that most industries

use option a and do not benefit from option b and c. The purpose of this comparison is to determine whether options b and c have a role in reducing the maximum stresses and a gain that will benefit the industry.

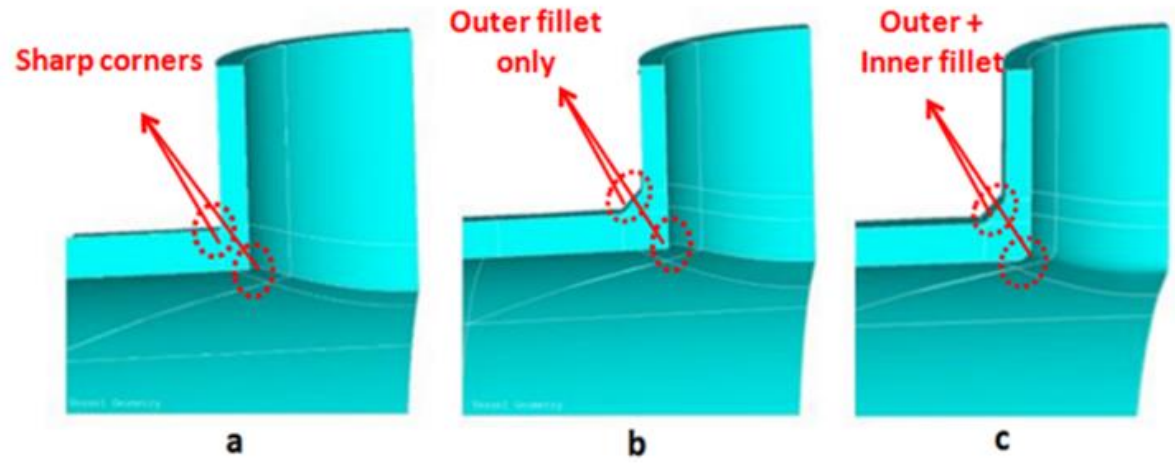

Figure 4. 2 a =no fillet, b =only outer fillet (welding), c =inner and outer fillet together.

The most challenging part in the modelling phase was the inner fillet application. Because in APDL models, it is possible to get a lot of fluctuation and topology errors while modelling non-linear oval tube structures in APDL. This may prevent proper meshing in the finite element application. Therefore, attention should be paid to this step-in order to get the stress analysis results correctly.

In all analyses, SA-516 Grade 70 Carbon Steel Pressure Vessel Plates [77] and ASTM A266 Grade 2 Carbon Steel materials [78] are used for shell and nozzle respectively. Six elements were applied throughout the nozzle thickness. The obtained maximum stress values and comparisons are given in the **Figure 4. 3**, **Figure 4. 4**, and **Figure 4. 5**.

In the analysis here, the pure elastic model is adopted without considering the yield. Values of stresses are for showing performance trend only. For this reason, very high stress values are obtained.

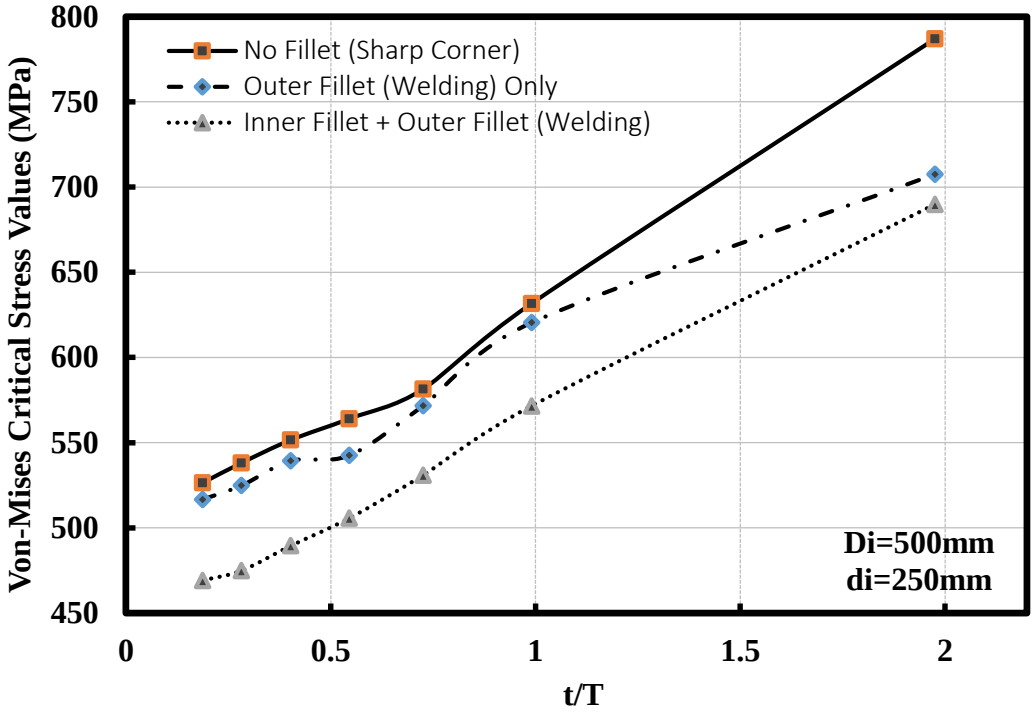

Figure 4. 3 Maximum stress values for the vessels with 500 mm inner diameter

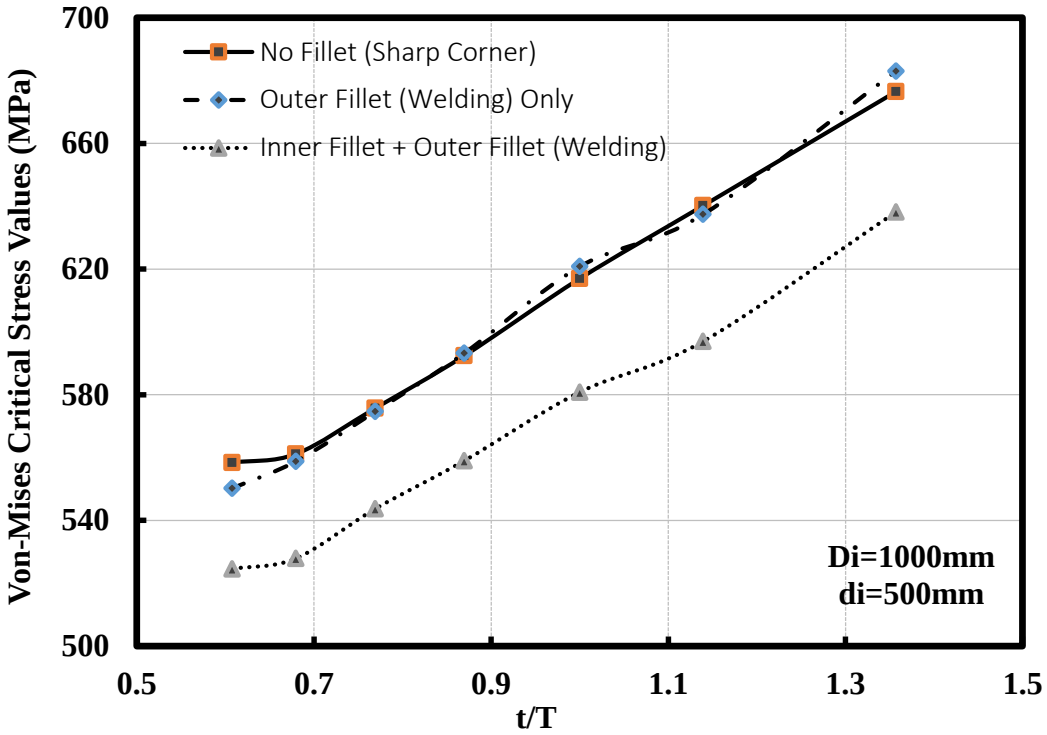

Figure 4. 4 Maximum stress values for the vessels with 1000 mm inner diameter

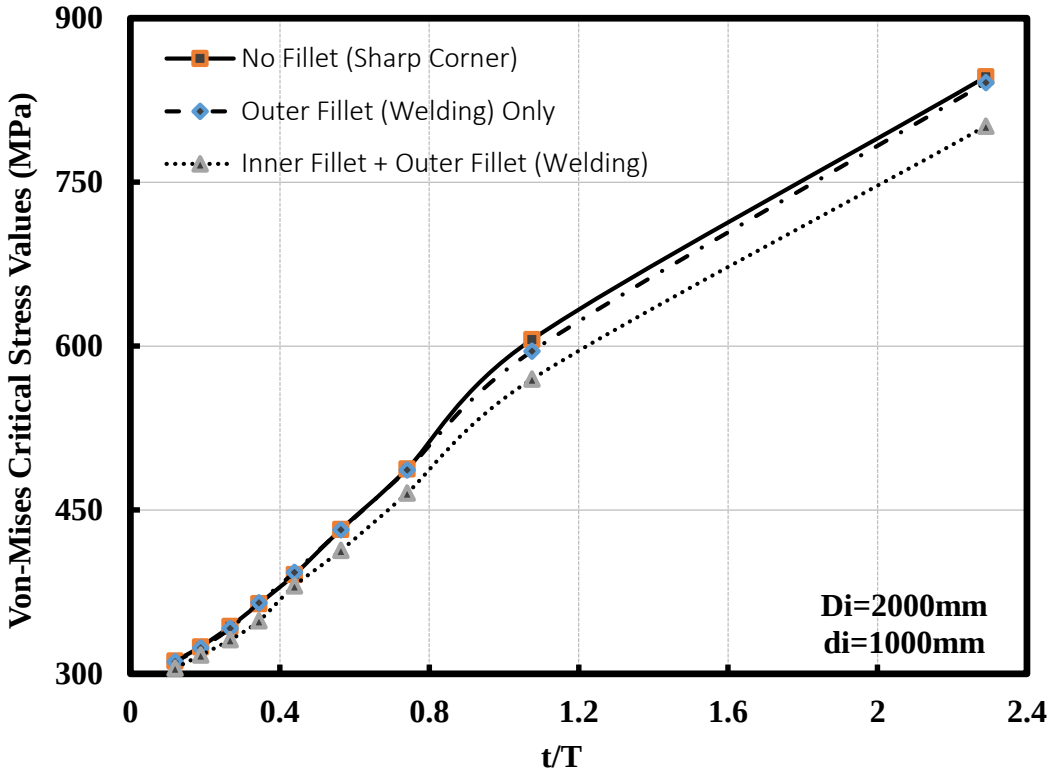

Figure 4. 5 Maximum stress values for the vessels with 2000 mm inner diameter

In the analysis carried out, the vessel dimensions were doubled each time (di/Di=0.5) from 500mm to 1000mm and from 1000mm to 2000mm. The aim here is to assess the effect of vessel flexibility. When the graphs are examined, the outside fillet weld connection for a vessel with 500 mm inner diameter provides a 4% reduction in average at maximum critical stress values for each nozzle shell thickness ratio. However, when the vessel size is increased, the differences are 1.5% in average for vessels with 1000 mm inner diameter and the differences are less than 1% for vessels with 2000 mm. Looking at the cases where the outer fillet weld and the inner fillet are applied at the same time, a reduction of about 10% for a 500 mm vessel and 5 percent for the other cases are obtained at the maximum stress values. The stress distribution for a vessel with an inner diameter of 500mm, the location of the maximum stress, and the inner and outer fillets are shown in a representative picture in **Figure 4. 6**.

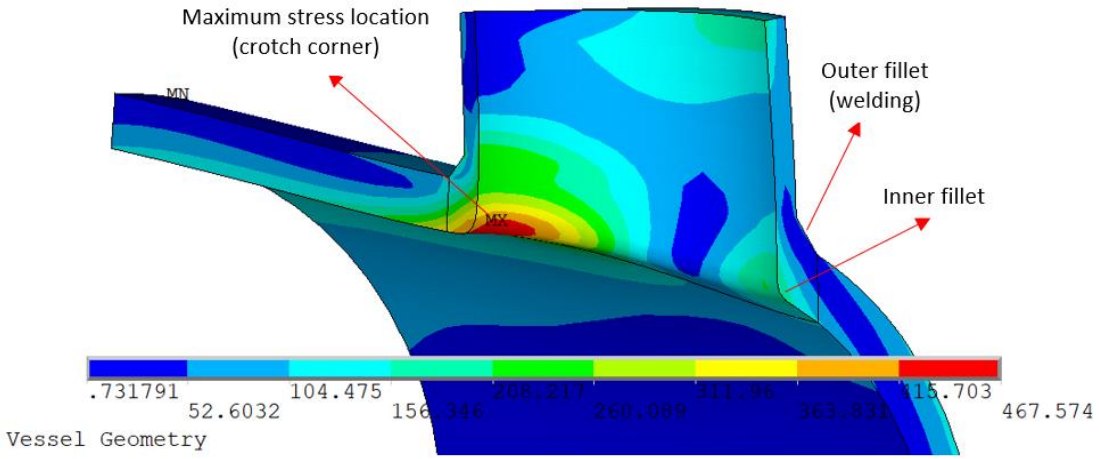

Figure 4. 6 Stress distributions for nozzle cylinder intersections under internal pressure

As such, it is obvious that the effect of the inner fillet application is more significant in reducing maximum stress values. In the analysis undertaken, the weld geometry and inner fillet dimensions were kept constant. It is therefore worth considering optimizing the junction by changing both the weld and fillet dimensions separately for any given case. Using this approach, the most reasonable parameters can be obtained for fillet applications at the nozzle-vessel intersections.

Also, as mentioned, di/Di did not change even though analyses were made for 3 different Di values. In addition, vessel and nozzle lengths were increased with the increase in vessel diameter. In this way, these graphs show us the result that the inner fillet and weld application is much more effective as the vessel gets smaller, regardless of other results. These data will lead to a useful approach to increase vessel strength, especially for small-scale pressure vessel designers and manufacturers.

4.2.2. Investigation of the Changing Outer Welding Fillet Dimension Effects

In order to investigate the effect of outside fillet weld dimensions, the maximum stress values obtained were compared for the cylinder with an inner diameter of 2000 mm and the nozzle of 1000 mm inner diameter (di/Di = 0.5). The reason for choosing a vessel

with an inner diameter of 2000mm is that, as can be seen in the **Figure 4. 5**, the maximum stress results obtained are very close to the sharp corner results. A clear difference was seen in the vessel with an inner diameter of 500mm (see **Figure 4. 3**). It will be better understood in this 2000mm inner diameter whether the change of the welding size significantly affects the stress distributions. 5mm, 10mm, 15 mm, 30 mm, and 45 mm width - length sizes are used as outer welding dimensions. The weld geometry with 15 mm leg length is given in the **Figure 4. 7**.

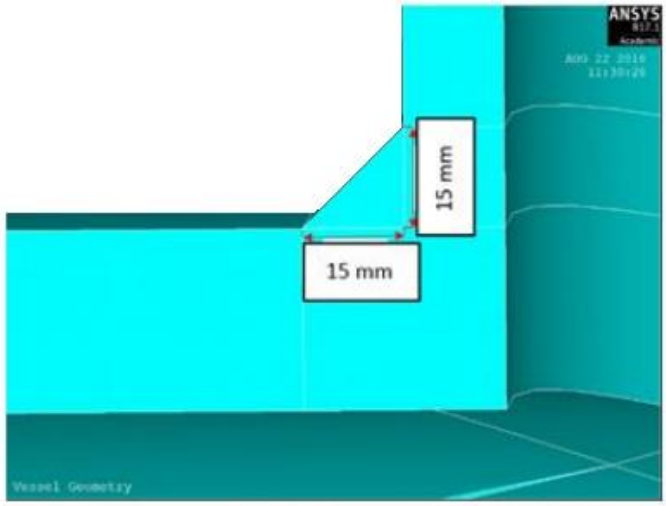

Figure 4. 7 Outside fillet weld dimensions

Analyses were undertaken for 7 different thickness ratios (t/T) and for 5 different welding width. The results can be seen in the **Figure 4. 8**. As can be seen in the graph, only the variation of the fillet weld dimensions is not a factor that influenced considerably the stress values. As can be seen in the graph, the welding size increased for each case. In all cases, the stress values on the crotch corner were very close to each other and the difference between these values was less than 1 percent. At the maximum point, this difference (between 5mm width = and 45mm width) is approximately 2%. Due to this reason, the same operation was applied in the inner fillet formed around the crotch corner.

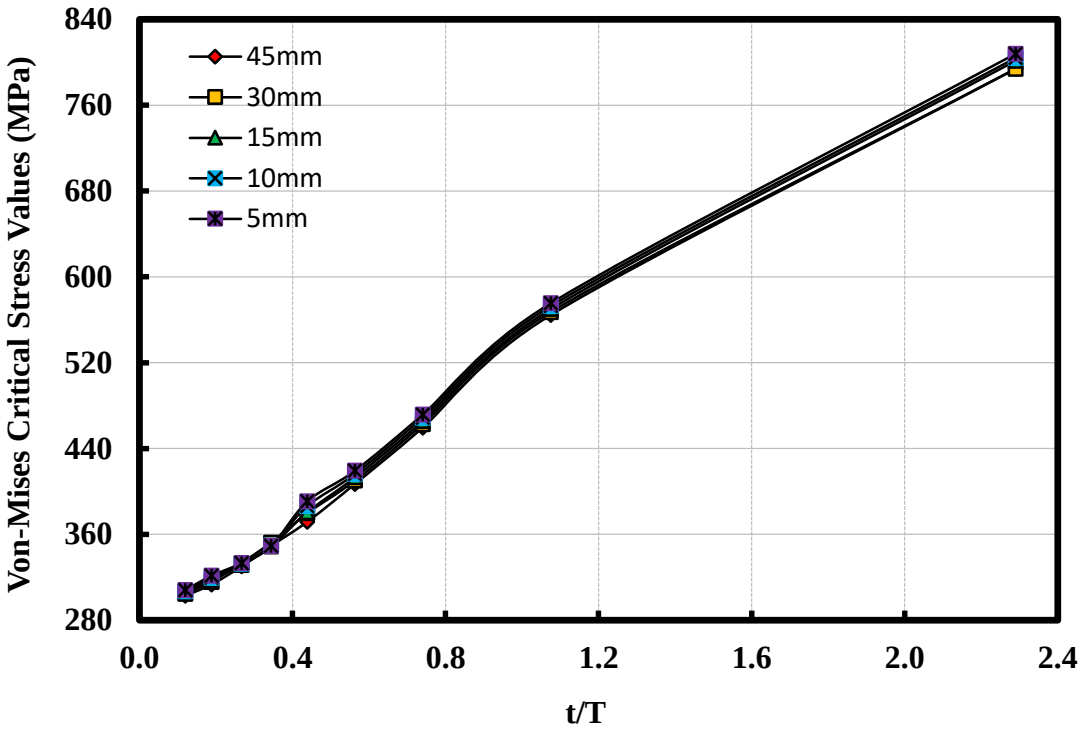

Figure 4. 8 Maximum stress values when changing outside fillet weld sizes

4.2.3. Investigation of the Changing Inner Fillet Dimension Effects

It was stated previously that the changes in weld profile dimensions did not have a significant effect. As a result of the analysis obtained, it is proposed that the formation of the inner fillet may have more significant effects. In each successive analysis, the radius of the inner fillet was increased by 5 mm and the effects were compared. The representation of the inner fillets applied for 2 different radii is given in the **Figure 4. 9**.

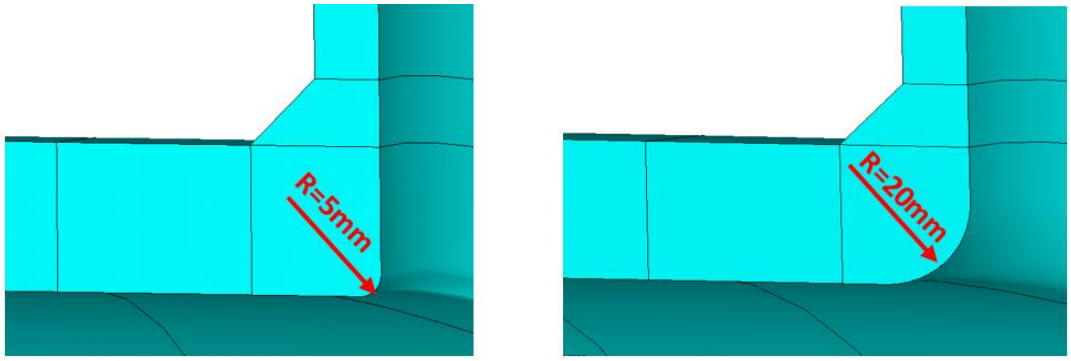

Figure 4. 9 Inner fillet application for different radii

If the model with a sharp corner is compared with a model with 5 mm internal fillet, when the thickness ratio between nozzle and shell is 0.97, a 11.8% decrease is observed in the maximum stress values on the crotch corner. This ratio is the highest value obtained in the comparative analysis. In other values, an average difference of 9 percent was observed. Stress values continue to decrease when the fillet is applied greater than 5 mm. The resulting maximum Von-Mises stress results are shown in **Figure 4. 10** with a graph.

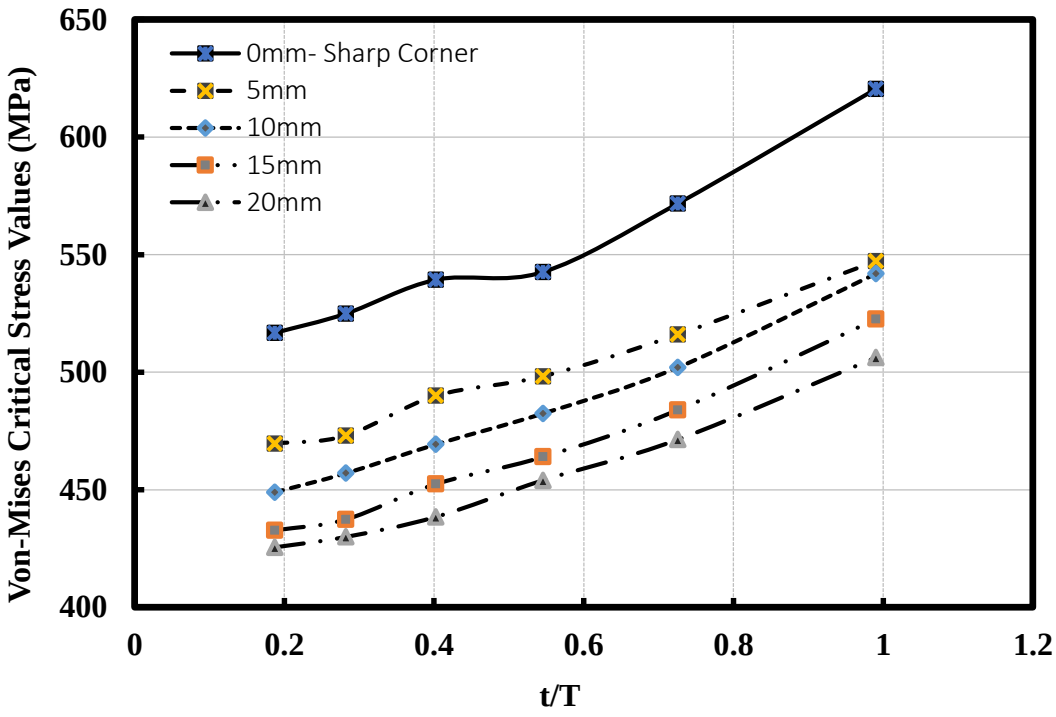

Figure 4. 10 Maximum stress values when changing inner fillet dimensions

Consequently, this difference continues albeit at a diminishing rate. Finally, when the model having a sharp junction and a model with a 20 mm inner fillet are compared, the average stress is reduced by 18% in the maximum point. In the view of such information, it is evident that the influence of internal fillet is more productive than welding to diminish stress values on cylinder- cylinder intersected cases.

4.2.4. Multiple External Loads Applications

Pressure vessels are primarily subjected to operating pressures. In addition, they must withstand other loads exerted by attachments such as nozzles and connected pipes etc. Such loads are called local loads because the stresses caused by such loads are limited to the small surrounding area. Also, it was observed that the maximum stress was dominant in the crotch corner in the inner nozzle-cylinder connections under the effect of internal pressure. It is necessary to determine this situation within the local loads. Because the direction of the load will change, the maximum stress location is expected to change.

For this study, the maximum stress values of the model under various loads will is considered for a single geometry configuration. It is shown in the **Figure 4. 11**.

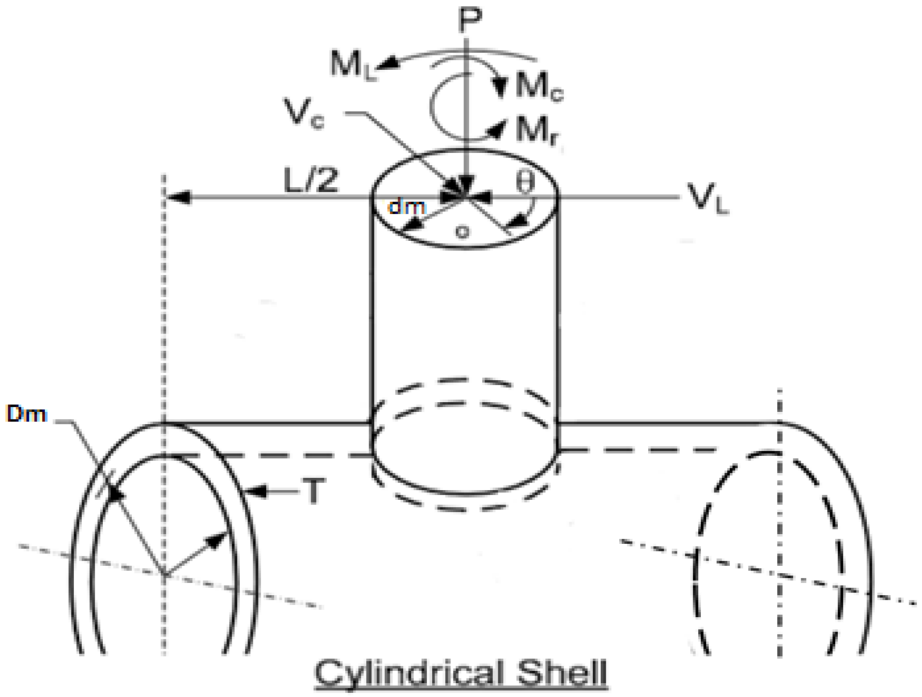

Figure 4. 11 Multiple external loading conditions

Table 4. 1 Applying loads combinations and magnitudes for each case

		Loading Magnitudes					
Analysis Number		***1st***	***2nd***	***3rd***	***4th***	***5th***	***6th***
1st case	P_{int} (MPa)	0.5	0.5	0.5	0.5	0.5	0.5
	M_T (kNm)	1	5	10	25	50	100
	M_C (kNm)	-	-	-	-	-	-
	M_L (kNm)	-	-	-	-	-	-
2nd case	P_{int} (MPa)	0.5	0.5	0.5	0.5	0.5	0.5
	M_T (kNm)	-	-	-	-	-	-
	M_C (kNm)	1	5	10	25	50	100
	M_L (kNm)	-	-	-	-	-	-
3rd case	P_{int} (MPa)	0.5	0.5	0.5	0.5	0.5	0.5
	M_T (kNm)	-	-	-	-	-	-
	M_C (kNm)	-	-	-	-	-	-
	M_L (kNm)	1	5	10	25	50	100
4th case	P_{int} (MPa)	0.5	0.5	0.5	0.5	0.5	0.5
	M_T (kNm)	-	-	-	-	-	-
	M_C (kNm)	1	5	10	25	50	100
	M_L (kNm)	1	5	10	25	50	100
5th case	P_{int} (MPa)	0.5	0.5	0.5	0.5	0.5	0.5
	M_T (kNm)	1	5	10	25	50	100
	M_C (kNm)	1	5	10	25	50	100
	M_L (kNm)	1	5	10	25	50	100

While performing local external loading analysis, di/Di will be taken as 0.5 again in order to be consistent with previous internal pressure analysis. In addition, since it is seen that 15 mm inner radius and 15 mm weld width are sufficient in terms of geometry and maximum stress values, these measures will be used again. Again, if Figure 4.3 - 4.5 is examined, the same ratios are chosen here as the lowest stress value for internal pressure is obtained at t/T = 0.24 in this geometry.

Analyses were carried out in 5 stages while examining the external loads. These load combinations and magnitudes are given in the **Table 4. 1**. In total, 6 analyses were performed for each case.

In order to apply the external loading conditions, link elements are located between the nozzle centre and the nozzle edges. An applied form of link elements is shown in **Figure 4. 12**. As a result of the use of these elements, centrally applied loading conditions can be simply added.

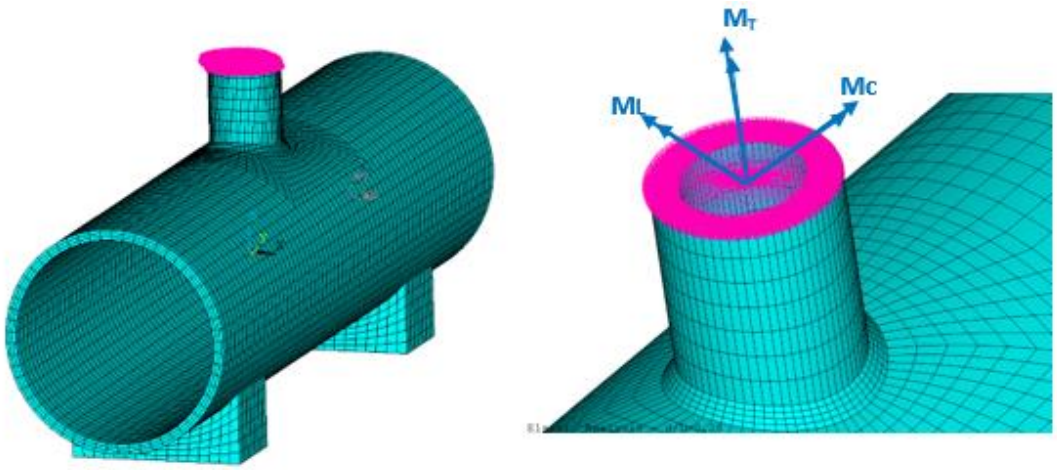

Figure 4. 12 Link elements applications

The stress values obtained as a result of the study are plotted in the **Figure 4. 16**. When the results obtained are considered, only the circumferential moment with the internal pressure and the only longitudinal moment effect have the nearly same stress results. In other cases, as the overload condition that affects the nozzle increases, the stress values also increase significantly as expected.

In addition to these, the stress distributions of the 1st case, 2nd case and 3rd case at maximum loading conditions (100kN) are shown in the **Figure 4. 13**, **Figure 4. 14**, and **Figure 4. 15**. As can be seen from the figures, the maximum stress magnitudes shift according to the local loads even they are same values (100kN each). Furthermore, the

maximum stress area seen in the crotch corner in case of residual internal pressure now tends to slide outward with the effect of local loads.

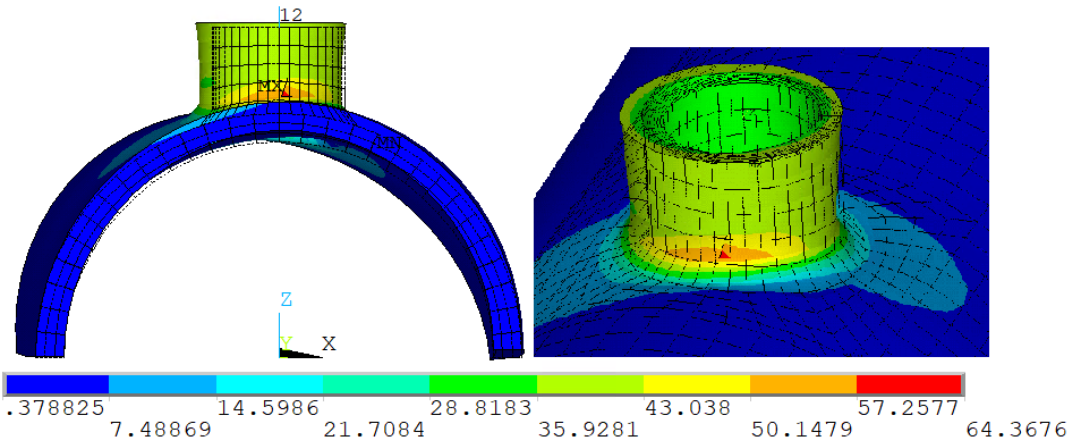

Figure 4. 13 1st case stress distribution (100kN.m torsional moment)

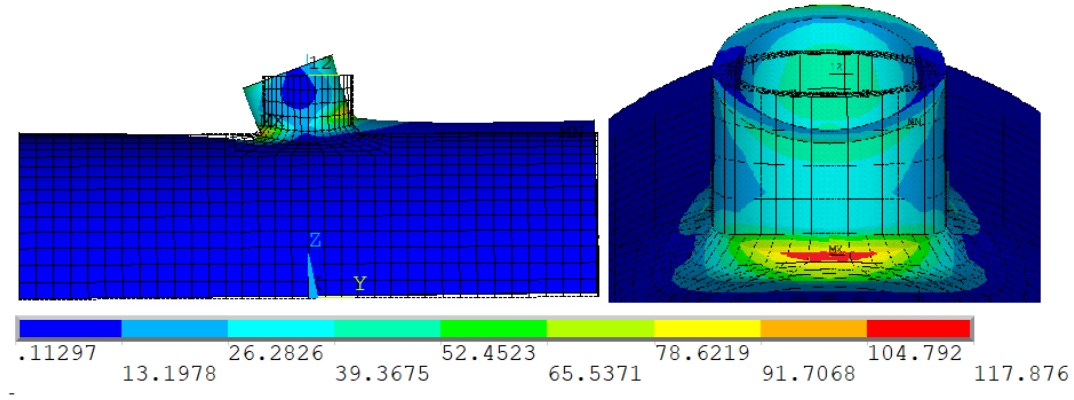

Figure 4. 14 2nd case stress distribution (100kN.m circumferential moment)

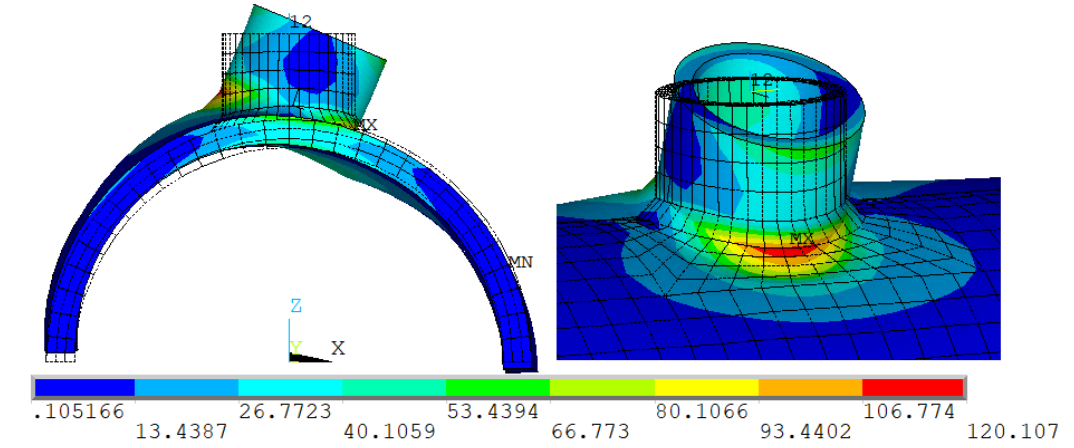

Figure 4. 15 3rd case stress distribution (100kN.m longitudinal moment)

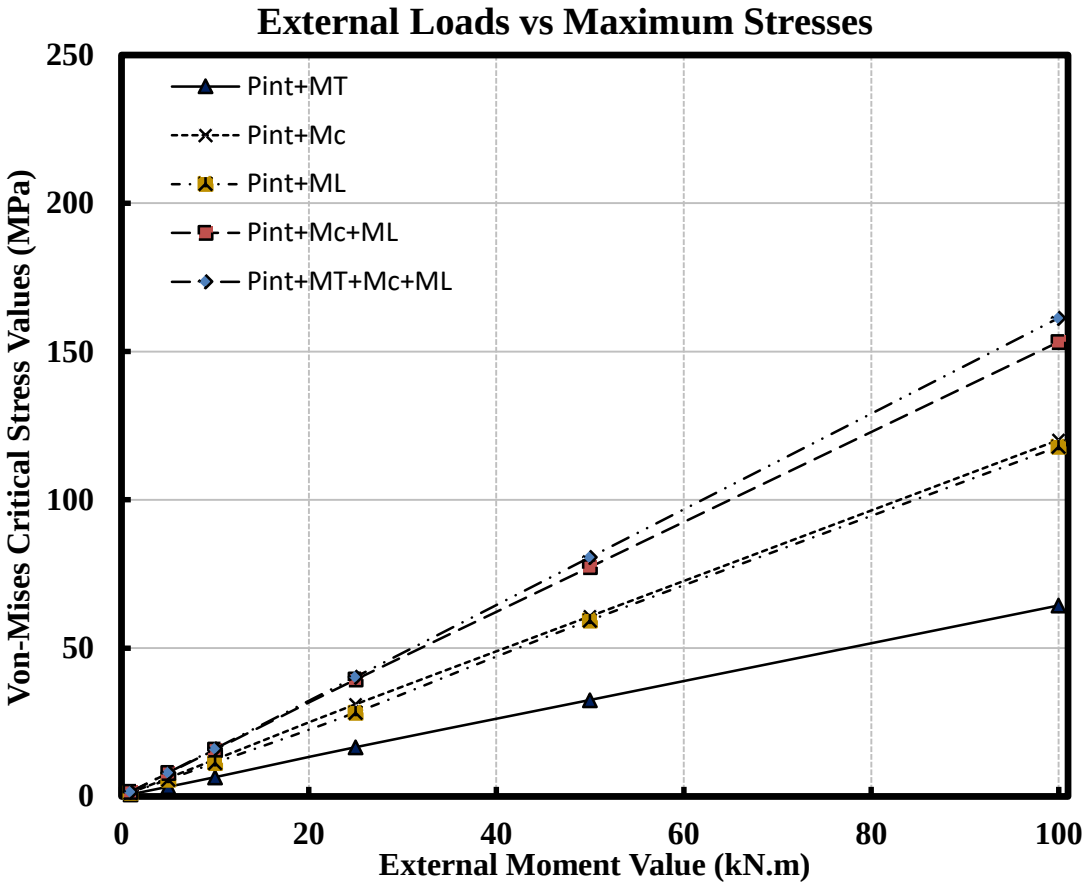

Figure 4. 16 Maximum stress values under various external loads

In addition to these analyses, the maximum stress values occurred in the models due to the tensile stress, longitudinal, and circumferential moment effect of were compared with the calculations in the WRC 537 bulletin.

WRC 537 has discussed in detail the calculations of stress due to radial load, circumferential moment, and longitudinal moment. Accordingly, the parameters must be determined before starting the calculations. In this study, since the cylinder-cylinder connection problems are handled, calculations will be made with round attachment parameters. The calculations and parameters to be used are given below.

The results of Bijlaard's work have been plotted in terms of non-dimensional geometric parameters by use of an electronic computer. Hence, the first step in this procedure is to evaluate the applicable geometric parameters γ and β.

The shell parameter γ is given by the ratio of the shell mid-radius to shell thickness thus:

$$\gamma = \frac{R_m}{T} \qquad \textbf{Equation 4. 1}$$

For cylindrical shells, either round or rectangular attachments may be considered. For a round attachment the parameter β is evaluated using the expression:

$$\beta = \frac{0.875 r_o}{R_m} \qquad \textbf{Equation 4. 2}$$

4.2.4.1. Calculation Procedure of Stresses According to WRC537

4.2.4.1.1. Stresses resulting from radial load, P

- **Circumferential Stresses (σ_φ)**

  a) STEP 1. Using the applicable values of β and γ calculated in **Equation 4. 1** and **Equation 4. 2**, enter **Figure A. 13** and read off the dimensionless membrane force $\left[\frac{N_\varphi}{P/R_m}\right]$

  b) STEP 2. By the same procedure used in STEP 1, enter **Figure A. 10** or **Figure A. 12** and find the dimensionless bending moment $\left[M_\varphi/P\right]$.

  c) STEP 3. Using applicable values of *P*, R_m, and *T*, find the circumferential membrane stress $\left[\frac{N_\varphi}{T}\right]$ by:

$$\frac{N_\varphi}{T} = \left(\frac{N_\varphi}{P/R_m}\right)\left(\frac{P}{R_m T}\right)$$ **Equation 4. 3**

d) STEP 4. By a procedure similar to that used in STEP 3, find the circumferential bending stress $\left(\frac{6M_\varphi}{T^2}\right)$ thus:

$$\frac{6M_\varphi}{T^2} = \left(\frac{M_\varphi}{P}\right)\left(\frac{6P}{T^2}\right)$$ **Equation 4. 4**

e) STEP 5. Combine the circumferential membrane and bending stresses by use of the general stress equation, together with the proper choice of sign;

$$\sigma_\varphi = K_n \frac{N_\varphi}{T} \pm K_b \frac{6M_\varphi}{T^2}$$ **Equation 4. 5**

- **Longitudinal Stresses (σ_x)**

Follow the 5 steps outlined in Circumferential Stresses except that $\left(\frac{N_x}{P/R_m}\right)$ is obtained using **Figure A. 14** ; and $\left(\frac{M_x}{P}\right)$, using **Figure A. 11** or **Figure A. 12**. It follows that:

$$\frac{N_x}{T} = \left(\frac{N_x}{P/R_m}\right)\left(\frac{P}{R_m T}\right)$$ **Equation 4. 6**

$$\frac{6M_x}{T^2} = \left(\frac{M_x}{P}\right)\left(\frac{6P}{T^2}\right)$$ **Equation 4. 7**

$$\frac{6M_x}{T^2} = \left(\frac{M_x}{P}\right)\left(\frac{6P}{T^2}\right)$$ **Equation 4. 8**

4.2.4.1.2. Stresses resulting from circumferential moment, M_c

- **Circumferential Stresses (σ_ϕ)**

a) STEP 1. Using the applicable values of β and γ calculated in **Equation 4. 1** and **Equation 4. 2**, enter **Figure A. 3** and read off the dimensionless membrane force $\left(\frac{N_\phi}{M_c/R_m^2\beta}\right)$

b) STEP 2. By the same procedure used in STEP 1, enter **Figure A. 1** and find the dimensionless bending moment $\left(\frac{M_\phi}{M_c/R_m\beta}\right)$

c) STEP 3. Using applicable values of M_c, R_m, β, and T, find the circumferential membrane stress $\left(\frac{N_\phi}{T}\right)$ by

$$\frac{N_\phi}{T} = \left(\frac{N_\phi}{M_c/R_m^2\beta}\right)\left(\frac{M_c}{R_m^2\beta T}\right) \qquad \textbf{Equation 4. 9}$$

d) STEP 4. By a procedure similar to that used in STEP 3, find the circumferential bending stress $\left(\frac{6M_\phi}{T^2}\right)$ thus:

$$\frac{6M_\phi}{T^2} = \left(\frac{M_\phi}{M_c/R_m\beta}\right)\left(\frac{6M_c}{R_m\beta T^2}\right) \qquad \textbf{Equation 4. 10}$$

e) STEP 5. Combine the circumferential membrane and bending stresses by use of the general stress equation, together with the proper choice of sign:

$$\sigma_\phi = K_n\frac{N_\phi}{T} \pm K_b\frac{6M_\phi}{T^2} \qquad \textbf{Equation 4. 11}$$

- **Longitudinal Stresses (σ_c)**

Follow the 5 steps outlined in circumferential stresses except that $\left(\frac{N_x}{M_c/R_b^2\beta}\right)$ is obtained using **Figure A. 4**; and $\left(\frac{M_x}{M_c/R_m\beta}\right)$, using **Figure A. 2** It follows that:

$$\frac{N_x}{T} = \left(\frac{N_x}{M_c/R_m^2\beta}\right)\left(\frac{M_c}{R_m^2\beta T}\right) \quad \textbf{Equation 4. 12}$$

$$\frac{6M_x}{T^2} = \left(\frac{M_x}{M_c/R_m\beta}\right)\left(\frac{6M_c}{R_m\beta T^2}\right) \quad \textbf{Equation 4. 13}$$

$$\sigma_x = K_n\frac{N_x}{T} \pm K_b\frac{6M_x}{T^2} \quad \textbf{Equation 4. 14}$$

4.2.4.1.3. Stresses resulting from longitudinal moment, M_L

- **Circumferential Stresses (σ_ϕ)**

Follow the 5 steps outlined in circumferential stresses in section 4.2.4.1.2. except that $\left(\frac{N_\phi}{M_L/R_m^2\beta}\right)$ is obtained using **Figure A. 9**; and $\left(\frac{M_\phi}{M_L/R_m\beta}\right)$, using **Figure A. 5** or **Figure A. 6**. It follows that:

$$\frac{N_\phi}{T} = \left(\frac{N_\phi}{M_L/R_m^2\beta}\right)\left(\frac{M_L}{R_m^2\beta T}\right) \quad \textbf{Equation 4. 15}$$

$$\frac{6M_\phi}{T^2} = \left(\frac{M_\phi}{M_L/R_m\beta}\right)\left(\frac{6M_L}{R_m\beta T^2}\right) \quad \textbf{Equation 4. 16}$$

- **Longitudinal Stresses (σ_x)**

Follow the 5 steps outlined in circumferential stresses in section 4.2.4.1.2. except that $\left(\frac{N_x}{M_L/R_m^2\beta}\right)$ is obtained using Figure 4B; and $\left(\frac{M_x}{M_L/R_m\beta}\right)$, using **Figure A. 7** or **Figure A. 8**. It follows that:

$$\frac{N_x}{T} = \left(\frac{N_x}{M_L/R_m^2\beta}\right)\left(\frac{M_L}{R_m^2\beta T}\right) \qquad \textbf{Equation 4. 17}$$

$$\frac{6M_x}{T^2} = \left(\frac{M_x}{M_L/R_m\beta}\right)\left(\frac{6M_L}{R_m\beta T^2}\right) \qquad \textbf{Equation 4. 18}$$

4.2.4.2. Comparison of the FEA and WRC537 Calculations for External Loading Applications

As shown in **Figure 4. 16** in external loading analysis, 5 different cases were examined, and the results were shown. In addition to these analyses, in this section, the calculations in the WRC537 bulletin are compared with the maximum stress values that occur in the models due to the tensile stress, longitudinal and circumferential moment effects. These comparison results can be seen in **Table 4. 2**, **Table 4. 3**, and **Table 4. 4**. These results are only used for the values of 25kN, 50kN, and 100kN since the moment effect is evident especially in the cases of 10kN and overload loading.

Table 4. 2 Comparison of maximum stress results for model under tensile loading

	Magnitude		**Maximum Stress Values (Von Mises)**	
Load type	P_{int} (MPa)	M_T (kN.m)	FEA (MPa)	WRC537 (MPa)
Torsional Moment	0.5	25	16.55	18.05
	0.5	50	32.49	35.93
	0.5	100	63.34	69.48

Table 4. 3 Comparison of maximum stress results for model under circumferential moment loading

	Magnitude		Maximum Stress Values (Von Mises)	
Load type	P_{int} (MPa)	M_C (kN.m)	FEA (MPa)	WRC537 (MPa)
Circumferential Moment	0.5	25	31.06	33.20
	0.5	50	60.7	66.4
	0.5	100	120.1	132.8

Table 4. 4 Comparison of maximum stress results for model under longitudinal moment loading

	Magnitude		Maximum Stress Values (Von Mises)	
Load type	P_{int} (MPa)	M_L (kN.m)	FEA (MPa)	WRC537 (MPa)
Longitudinal Moment	0.5	25	30.05	31.21
	0.5	50	59.32	62.42
	0.5	100	117.87	124.85

As can be seen in the Tables, the results are comparable, especially in cases where the model is subject to tensile loading only. For the models where the longitudinal and circumferential moment is applied, the differences are around 5percent and FEA results were lower than WRC537 calculations. The close results obtained once again demonstrate the correctness of the model. Whilst this gives confidence that WRC537 is conservative for the moment cases, it is over predicting the maximum stress which can have an influence when using these stresses for fatigue life evaluation.

In summary, in this section, the nozzle in vessel is exposed to external local loads. In total, 5 different external loading situations were examined. One of the most important points in these analyses is the displacement of the maximum stress field according to the load direction, as can be seen in the **Figure 4. 13 -15**. In other words, while the maximum stress zone is in the crotch corner region under internal pressure, it has shifted to the welding area under external loads. Another issue is that local loads of the same magnitude change the maximum stress depending on the direction (Mc was always higher).

In mixed loading situations, it is understood that the more load is placed on the system at the same time, the more the stress will increase, only the stress field will shift to the side of the dominant load.

4.2.5. Pressure Vessel with Two Nozzle Intersections

In some practical applications, it is required to have nozzles closely located in combination. If the nozzles are excessively close to each other, with a small ligament, this arrangement can cause the stress to increase significantly. The ligament distance between the nozzles should not exceed a certain ratio to prevent large stresses that may occur. If the nozzles need to be closer to each other than the calculated pitch, it may be necessary to apply additional reinforcement plates to the vessel. If two adjacent nozzles with the same diameter are to be considered, the minimum pitch P between them is determined by **Equation 4. *19***.

$$P = d + A\sqrt{DT} \qquad \textbf{Equation 4. 19}$$

Also, pitch is determined as P_L and P_T for longitudinal and axial directions respectively between nozzles. These positions are shown in **Figure 4. 17**.

Here, the stress distribution for two nozzles with longitudinal, radial and both longitudinal and radial distances without reinforcement plates are examined. The results are obtained and interpreted for the stresses occurring in the crotch corner within the two nozzles arrangement. In this case, only internal pressure is considered. Also, crotch corner fillet radius and welding fillet radius are not changed to be consistent with previous analyses, and they are 5mm and 15mm, respectively.

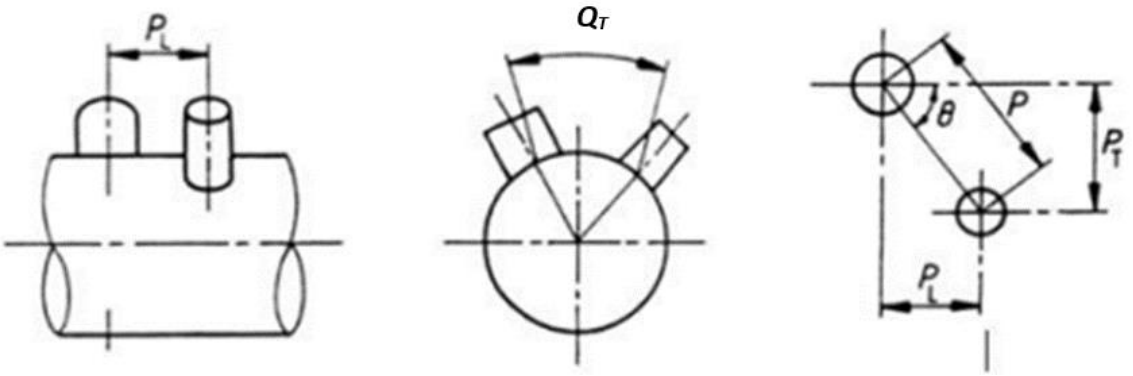

Figure 4. 17 Dimensions of the longitudinal and axial distance [13]

4.2.5.1. Investigation of the Cylindrical Vessel with 2 Longitudinal Located Nozzles

Von-Mises stress results have been obtained for 3 different distances magnitude for 2 nozzles placed in longitudinal direction on the cylindrical shell. In these analyses, the nozzles are positioned symmetrically to the midpoint of the cylindrical vessel and the spacing of the nozzle centres are defined 200mm, 300mm, and 400mm, respectively. A representative image showing the distance between the nozzles is shown in **Figure 4. 18**. In these analyses, similarly to the single nozzle model, only the inner pressure was applied to the shell and the shell was constrained to move from one side and was exposed to thrust from the other side. Furthermore, the nozzles were also under the influence of thrust with internal pressure. To distinguish the nozzles from each other, the first nozzle is closer to the side that the thrust force affects and the further away nozzle from the axial thrust side is called the 2nd nozzle. The results of the analysis for each of the 2 nozzles are given in the following **Figure 4. 19** and **Figure 4. 20**.

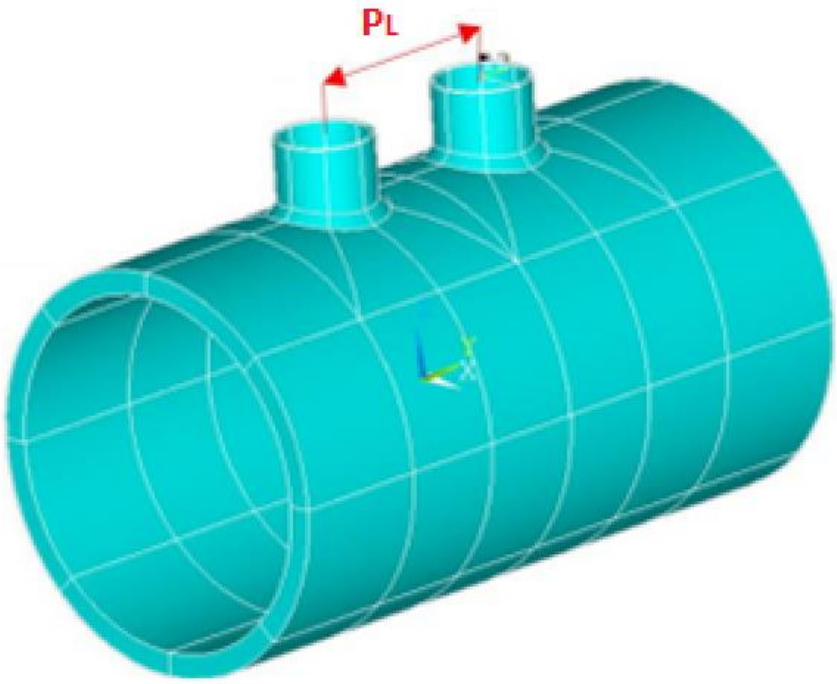

Figure 4. 18 Longitudinal placed nozzles

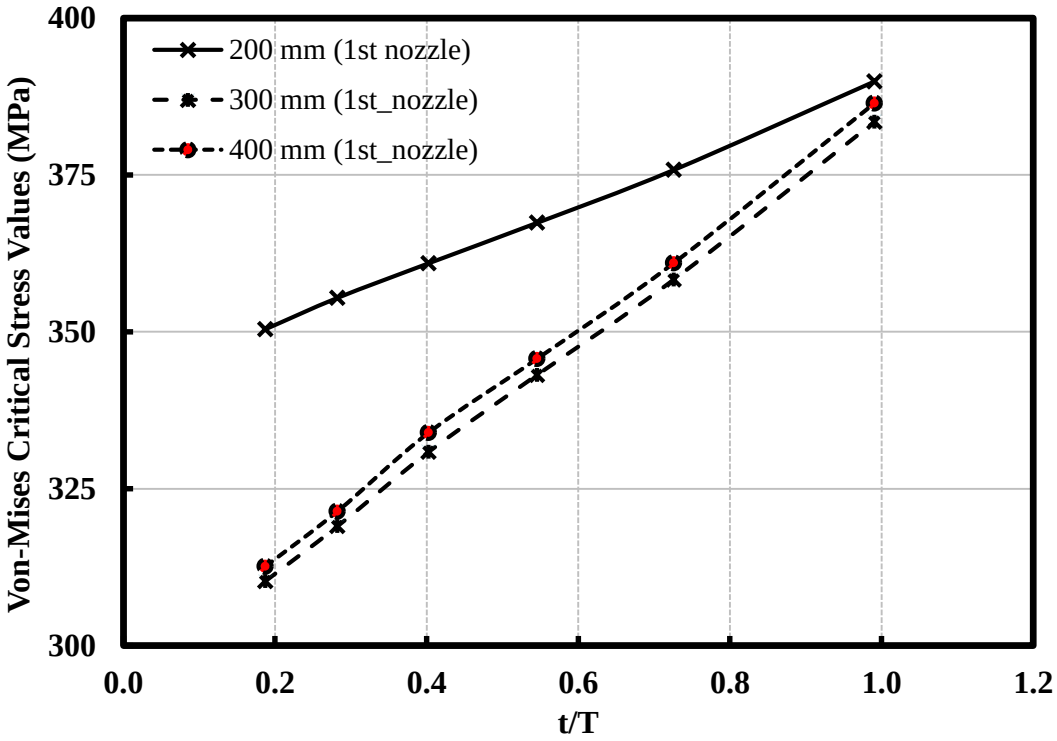

Figure 4. 19 Maximum stress values on 1st nozzle crotch corner

As can be seen from the Figures, the maximum stress point is at the junction area of the first nozzle. Especially when the distance between the nozzles reaches 300mm and

400mm, the results are very close to each other, and the differences are around 1%. On the other hand, the difference between the stress values reached up to 12% in the case of 200 mm pitch. The reason for this is that the stress increases considerably when the nozzles are very close to each other due to the influence of the die-out of the first on the second. In fact, in these 3 cases, additional reinforcement plate is required when the minimum pitches are calculated. However, it is obvious that the stress values are very high for the nozzles with a distance of 200mm.

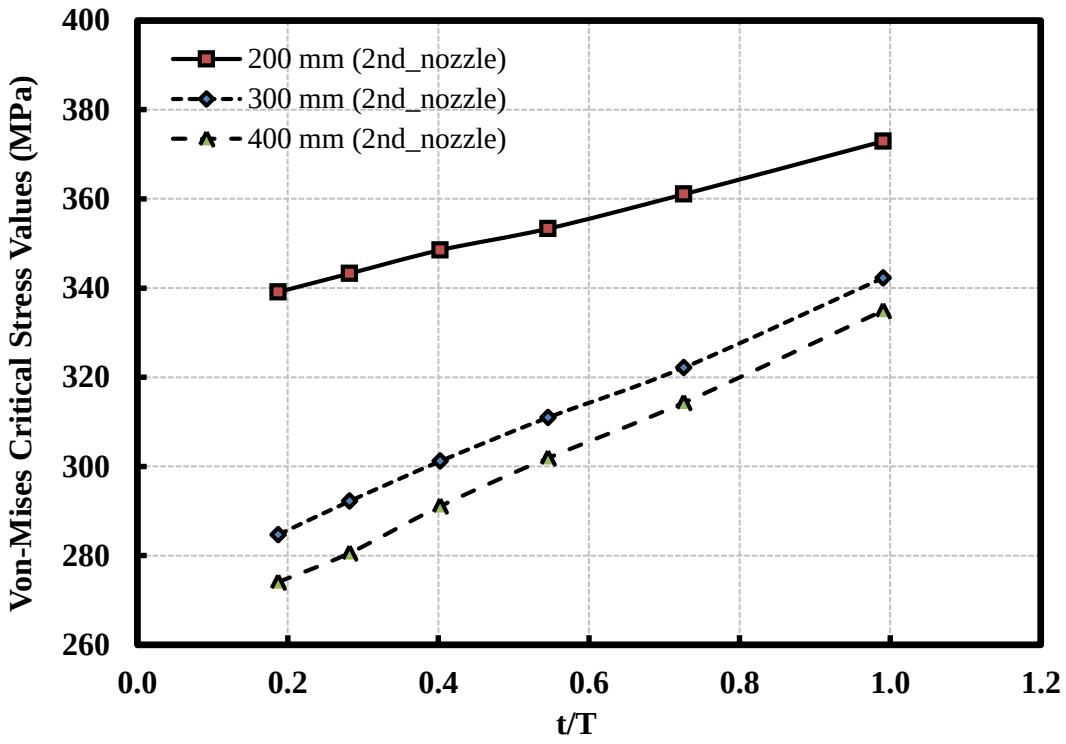

Figure 4. 20 Maximum stress values on 2nd nozzle crotch corner

4.2.5.2. Varying the distance from nozzle centre to the end of the vessel

Previously, the focus for the analysis was only on the distance between nozzles. On the other hand, as the distance between the nozzles increases, the distance between the nozzle centre and the end of the container decreases. As such, the distance between the nozzles was increased, and therefore the distance between the nozzle centre and the end of the vessel was decreased. Thus, the distance between the nozzle centre and the end of the

vessel should be kept constant by adding the material to the end of the vessel and the new cases should be re-examined under these conditions as shown in **Figure 4. 21**.

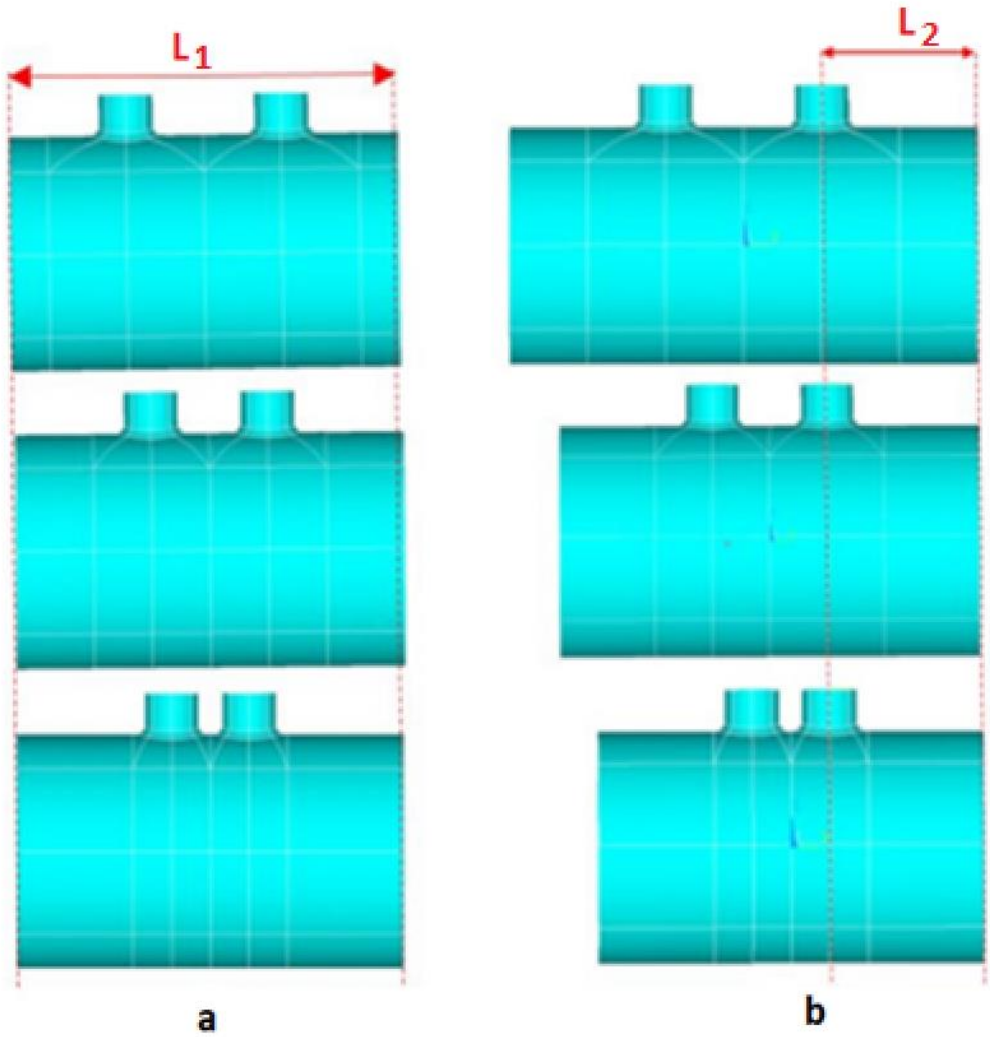

Figure 4. 21 a) the cases that lengths of vessels are same, b) the cases that distances between centre of the nozzles and end

For the three cases shown in part b of **Figure 4. 21** above, the analysis for 6 different thickness ratios was performed. Results for 1st and 2nd nozzles separately shown in **Figure 4. 22**, and **Figure 4. 23** below.

When the values in the graphs are analysed, those for the 1st nozzle, closer to the side the thrust force affects have almost the same magnitude, the differences between the values being less than 1%. That is, the addition of material to the end of the vessel has not

contributed physically to the stress values on the nozzles. Considering the 2nd nozzle, which is the nozzle close to the side where the boundary conditions are applied are examined, it is observed that the difference between the stress values reaches up to 5% when the distance between the nozzles reaches 400 mm. As noted, the pressure vessel was restricted to the movement from one side and the thrust was applied from the other side. In the light of this, along with the last change, the 2nd nozzle has been located 400mm further away from the thrust applied. In other words, the positioning of the nozzles far away from the applied force can be said to be an approach which reduces the stress values – which is common with industry practices and the use of a die-out distance.

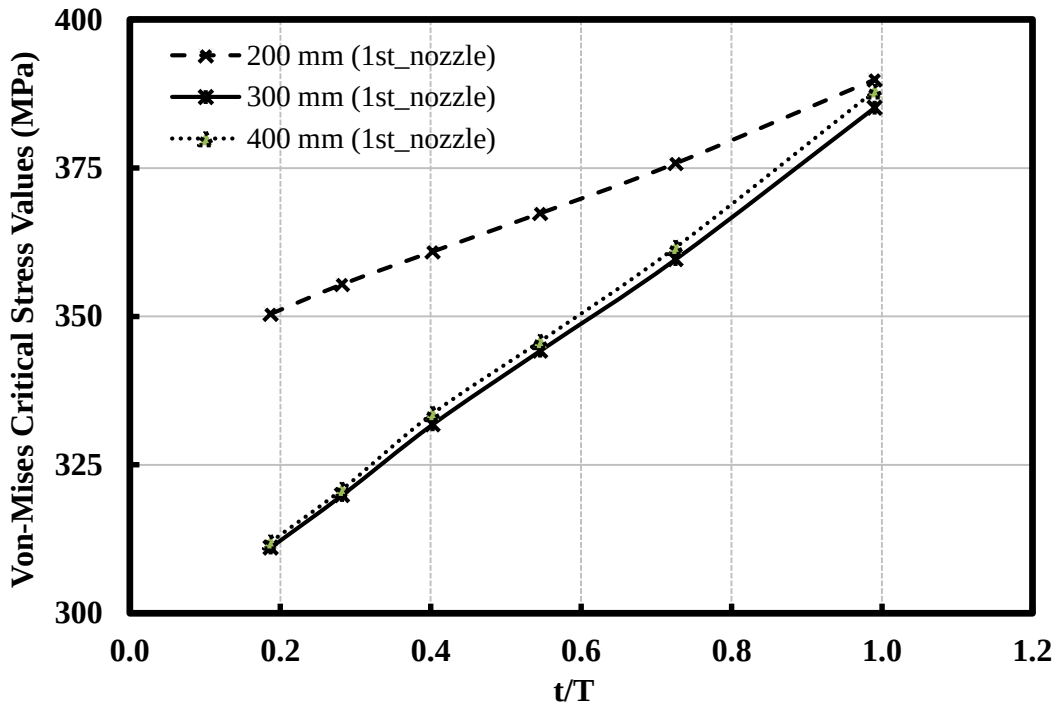

Figure 4. 22 Analysis results for 1st nozzles

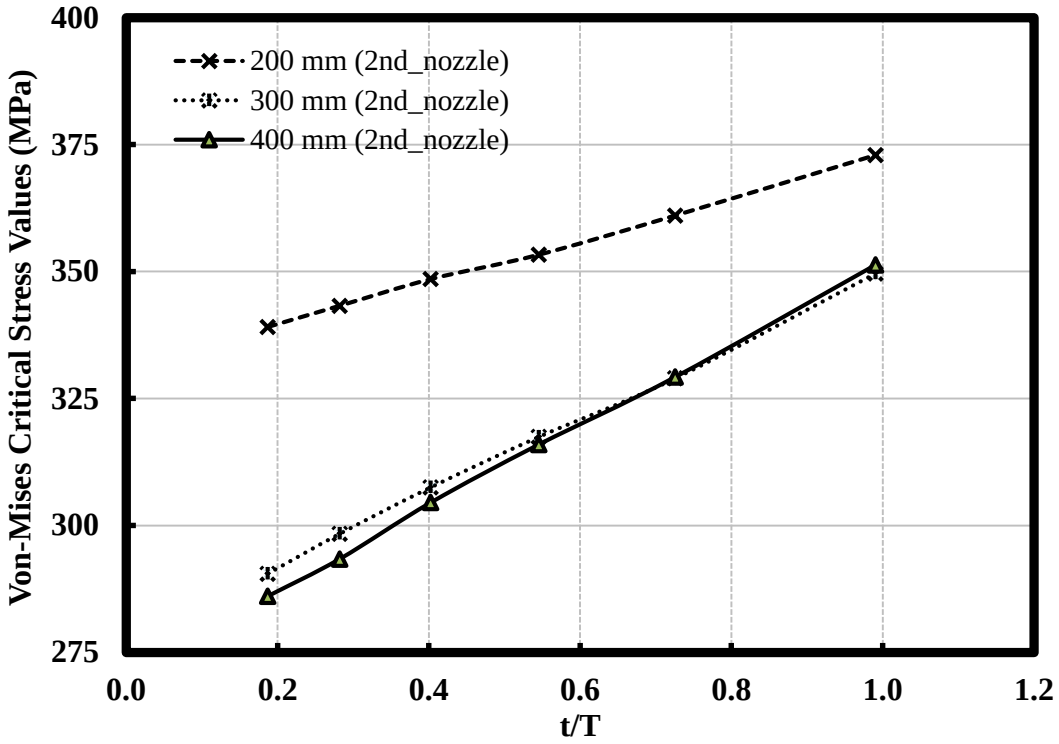

Figure 4. 23 Analysis results for 2nd nozzles

4.2.5.3. Investigation of the Cylindrical Vessel with 2 Radial Located Nozzles

This study examines four different cases for pairs of radially located nozzles. Firstly, the Von-Mises stresses are examined for two nozzles positioned in the same plane but offset at 90 degrees. Subsequent studies are carried out with the offset angle between the nozzles at 60 degrees. In the final two cases, a length of 250 mm longitudinal offset is included on the nozzles positioned (Q_T) at 90 and 60 degrees. These situations are compared with each other separately. The representative image for positioning of the nozzles is given in **Figure 4. 24**. P_L represents the longitudinal distance and P_T represents the angular distance between nozzles.

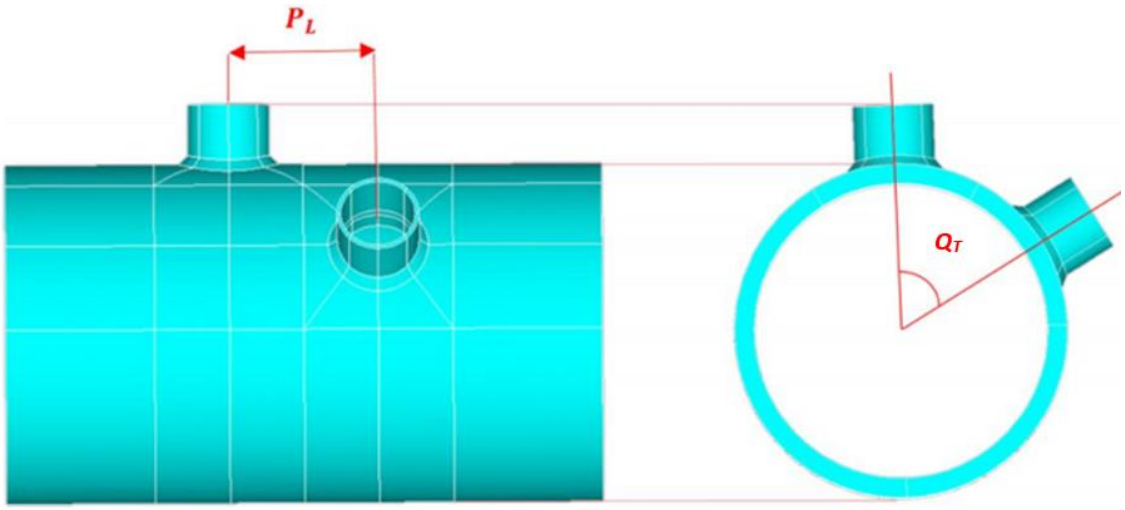

Figure 4. 24 The symbolic image for positioning of the nozzles

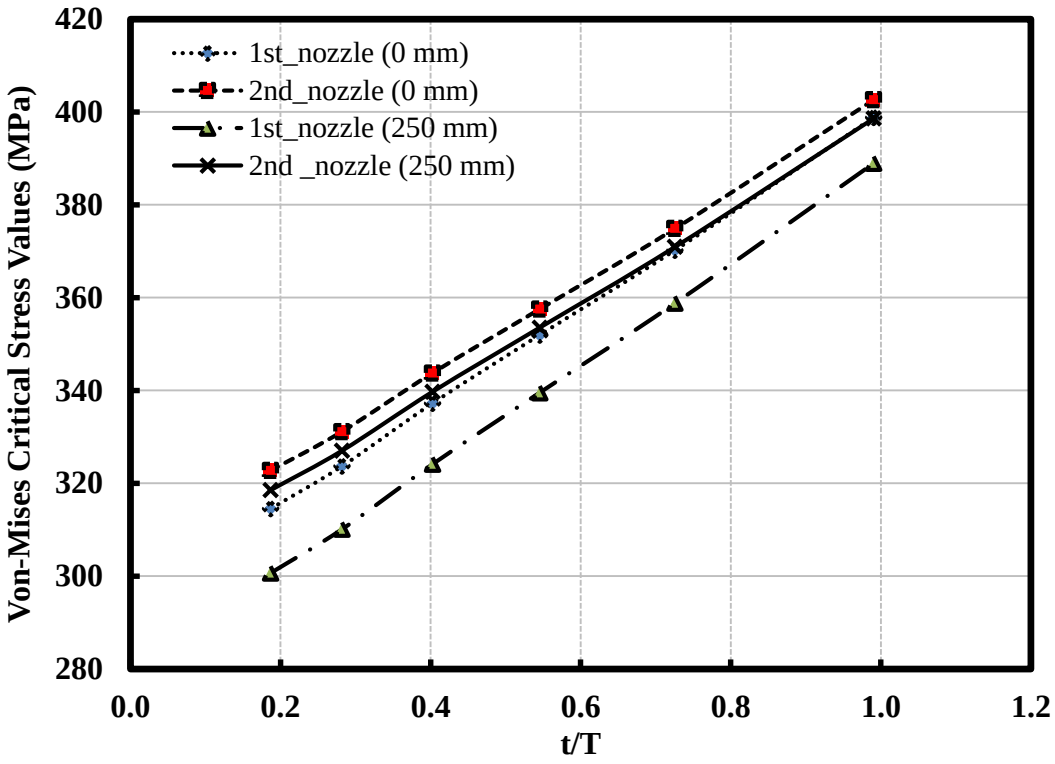

Figure 4. 25 Von-Mises stress values for 90-degree radial distance

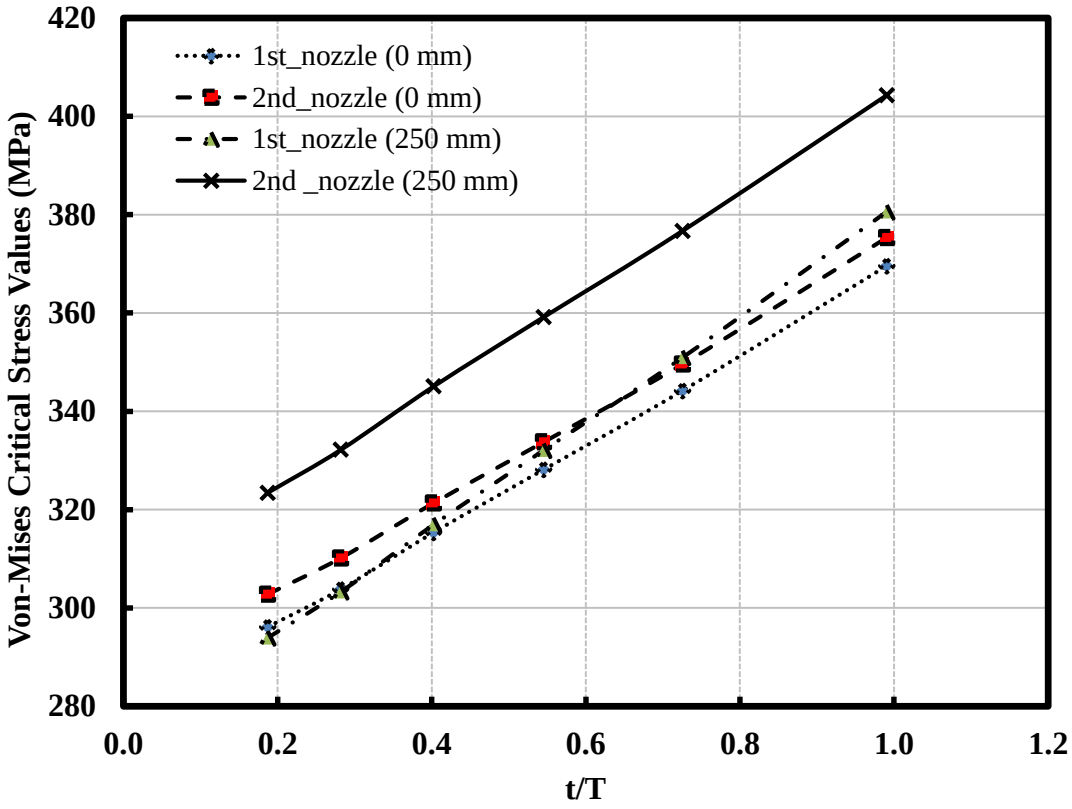

Figure 4. 26 Von-Mises stress values for 60-degree radial distance

The nozzles placed at 90 degrees are examined in two configurations. The distance between the nozzles in the first arrangement, P_L, is 0. In the second case, there is a 90-degree radial gap between the nozzles and an offset distance of 250 mm. In addition, the models are loaded by internal pressure and axial thrust driven by internal pressure. The results are presented in **Figure 4. 25**.

When the results are examined, it was observed that the stress values were lower in both radial and longitudinal nozzles. It is obvious from this that, as the area of ligament material between the nozzles increases, the stress values are observed to have decreased. In addition, in all studies, it is seen that the stress values decrease when the radial distance is reduced by 30 degrees. Also, in the model has P_T is 90 degrees, the maximum tensile stress was observed at the 1st nozzle near the corner positioned at the top of the shell. Conversely, when P_T was 60 degrees, the maximum stress was observed at the 2nd offset

nozzle. The internal pressure effect is much more pronounced when the 2nd nozzle deflection angle decreases from 90 degrees to 60 degrees. A summary of the total stress values can be seen in **Figure 4. 26**.

4.2.6. Investigation of the Pad Reinforcement for Oblique and Standard Nozzles

Due to practical requirements, pressure vessels often have nozzle connections of various shapes, sizes, and positions. Oblique nozzle is one of them and it is penetrated containers at various angles according to the design conditions. Besides, high stresses occur especially in the opening area due to effect of various loading conditions in pressure vessels with nozzles. It is very important to detect these stresses and to detect any damage before that may occur. Therefore, in pressure vessel applications, one of the most feasible and economical ways of reinforcing an isolated nozzle is to use a pad or compensating plate. Where a pad is used, the extra material is considered to as effective as provided by a thick vessel plate, so a good fit in the vessel shell is required. Considering this information, in this study, welded pad reinforcement will be applied to the nozzle cylinder intersections in the cylindrical pressure vessels. In addition, the effect of internal pressure, oblique nozzle angle and pad contribution on maximum stresses in the pressure vessel will be examined under various parameters.

In summary, the purpose of this study is to investigate the effect of pad reinforcement on nozzle problems placed in a vertical or at a certain angle in a cylindrical container. In line with this objective, critical paths will be determined on the system and stress linearization along these paths will be calculated with FEA.

4.2.6.1. Finite Element Modelling Description

In this section, the nozzle-cylinder connection will be modelled using the ANSYS program. The main variable in the model will be the oblique nozzle connection angle (Ψ), and pad thickness. For finite element modelling 3 different materials were used as can be seen in the **Figure 4. 27**. SA-516 Grade 70 Carbon steel pressure vessel plate with a Young's modulus value of 200GPa was chosen for the shell material. For the nozzle material, ASTM A266 Grade 2 Carbon Steel, which has a Young's modulus value of 190GPa, was used. Since the saddles are not in the critical region to be examined, no specific material selection has been made and the Young's modulus was defined as 290GPa.

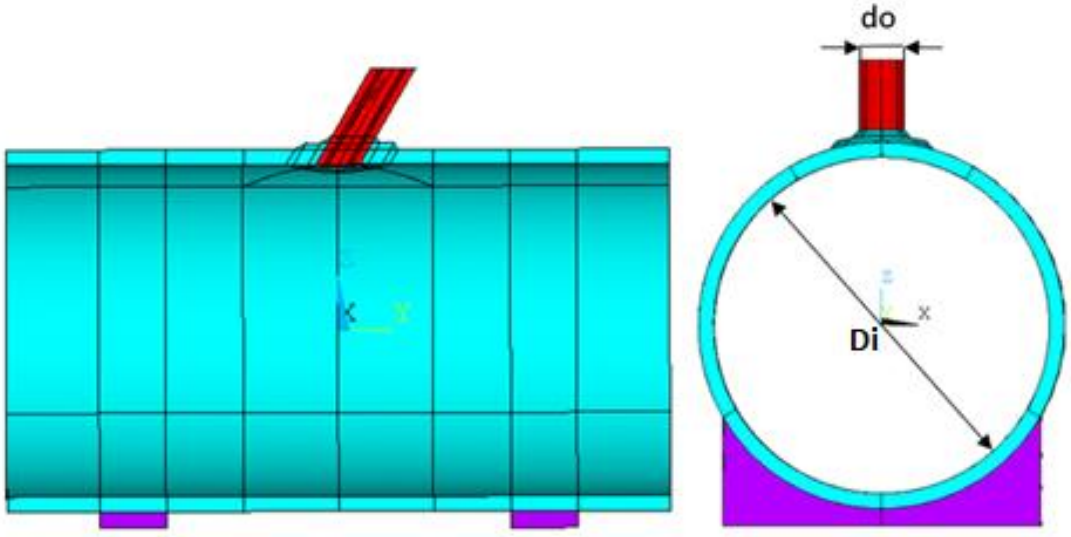

Figure 4. 27 Cylindrical shell - oblique nozzle connections

In these analyses, the nozzle inner diameter is always 1-fourth of the shell inner diameter. The system is only under internal pressure. From the saddle subfields, the model has fixed supported. By the way, shell is free to move from both ends. For cylindrical nozzles lying in a plane, higher stresses may occur in the lateral cross section. For this reason, the

oblique nozzle angle (Ψ) should not exceed 50^0 [3]. In the light of this information, analysis will be performed such that the angle (Ψ) between the nozzle and the cylindrical container will be maximum 45^0. A representative representation of the oblique nozzle angle is given in the **Figure 4. 28**.

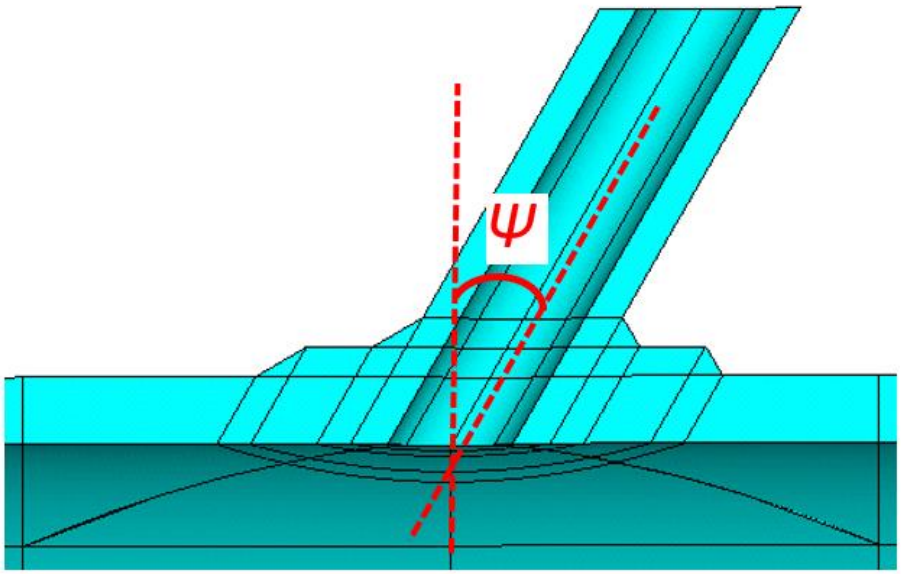

Figure 4. 28 Oblique nozzle angle (Ψ) display

4.2.6.2. Stress Linearization Analysis (SLA)

In this section, stress distributions for some locations in oblique nozzles connections will be examined. For these analysis, 6 critical paths were identified as shown in **Figure 4. 29**. The path number 1 represents the intersection of the nozzle with the shell top point and will show the distribution of stress from the nozzle outer wall to the inner wall. The path number 2 represents the intersection point of the top of the pad and the nozzle. The path number 3 is from a weld top point and nozzle combination to nozzle inner wall. The path number 4 is the joining line between the shell and the nozzle and stress change from shell inner wall to outer wall is examined. The path number 5 was determined as a path between Shell and the weld origin starting point in a similar approach to path number 4.

Von-Mises stress distributions will be obtained in all analysis. In all cases, Membrane and Total stress values will be plotted comparatively.

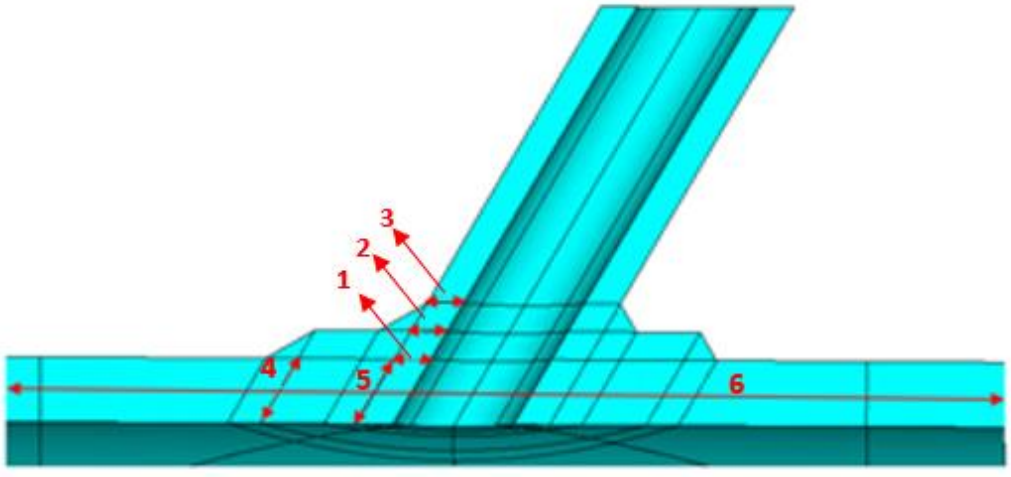

Figure 4. 29 Determined paths to be analysed for oblique nozzle

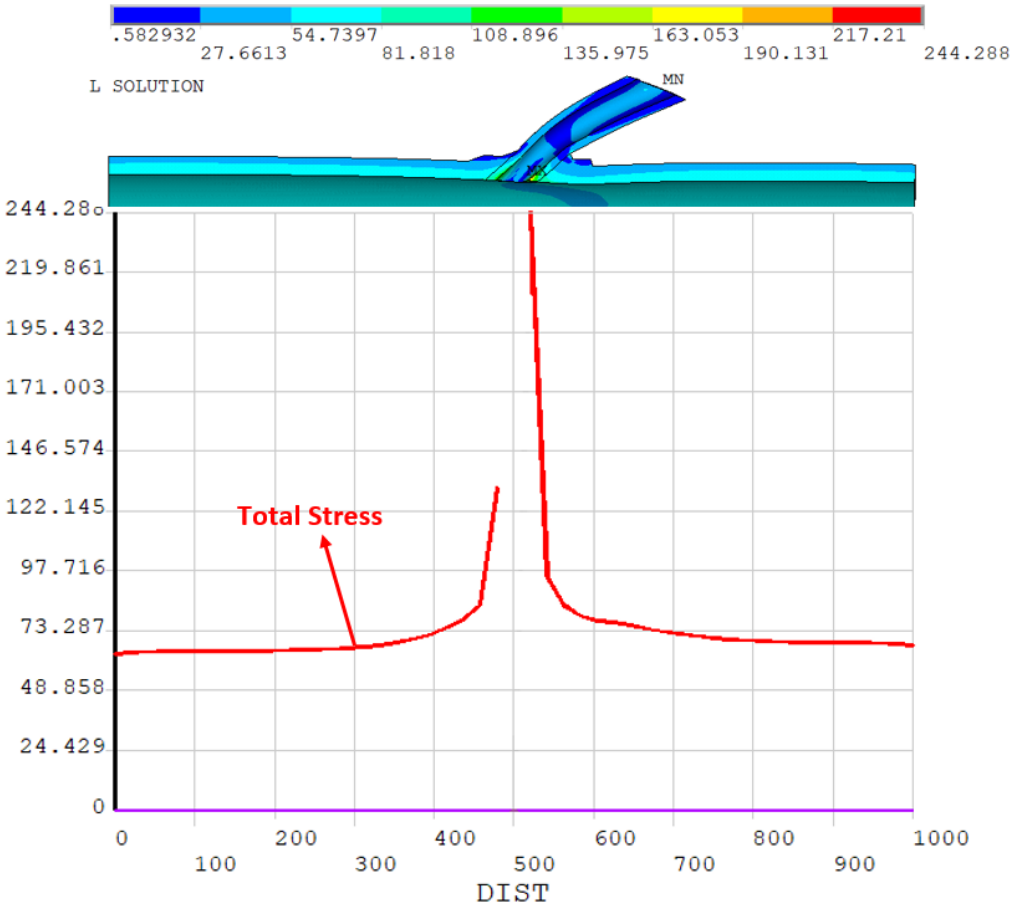

Figure 4. 30 FEA Stress distribution and a Stress linearization representation

In addition, analyses will take place in 3 states for oblique nozzles. First, the oblique nozzle angle change and then the pad contribution effect for a specific nozzle angle will be figured out. Finally pad diameter changing will be investigated. In the **Figure 4. 30**, a representative FEA solution and stress linearization graph are plotted for a pad reinforced nozzle-cylinder intersection with an oblique nozzle angle of 45 degrees.

In the following steps, the effect of pad contribution will be investigated first. For this, the pad thickness will be increased regularly for a low inclined oblique nozzle. Then, the effect of pad diameter on stress values will be investigated. Then, the effects of changing the oblique nozzle angle on the strain linearization for a constant pad contribution will be discussed.

4.2.6.2.1. Changing Pad Contribution

In this section, the effect of pad contribution on stress linearization will be studied. The paths to be investigated are the same as in the previous section. Similarly, an internal pressure of 5MPa was applied to the inner wall of the system. di/Di and t/T ratios are again similar the previous analyses. Furthermore, the nozzle angle is determined as 15 degrees. The analyses will be examined in 4 stages, these are 0% (no pad), 25%, 50% and 75% pad additions. (% pad contribution = Tp/T * 100)

The paths to be examined in the nozzles are selected as pad bottom (1), pad top (2) and welding top (3). Due to the absence of a pad contribution in the case of 0% contribution, paths 1 and 2 were eliminated automatically. For the connection between graphics to be consistent, 0% pad contribution status will be ignored in path number 3.

When **Figure 4. 31 - Figure 4. 36** are examined, it can be observed that the membrane and total stress values of the nozzle decrease as the pad contribution increases. Among

these 3 paths, the closest path to the maximum stress zone is the path number 1. When paths 1 and 3 are examined among themselves, membrane stress values of path number 3 are 50% less than path number 1 at the minimum point. In path number 1, the membrane stress difference between 25% additive and 50% additive is 2.7%, while the difference between 50% pad contribution and 75% pad contribution is 0.6%. These differences are greater in paths 2 and 3. The reason for this is that as the pad contribution increases, the 2 and 3 paths are located at points farther from the critical area.

When the 4th and 5th paths are examined in **Figure 4. 37** and **Figure 4. 40**, stress changes can be easily observed throughout the shell thickness. 0% pad contributions have also been examined in these graphs. As can be seen from the graphics, the pad contribution reduced the stress 6% at the minimum point.

In path number 6, the stress values on the side where the nozzle is inclined are on average 0.5% higher. As seen in the total stress graph in **Figure 4. 41** and **Figure 4. 42**, the stress values are almost linearly constant until the pad starts, while the tension in the area under the pad decreases and peaks at the crotch corner.

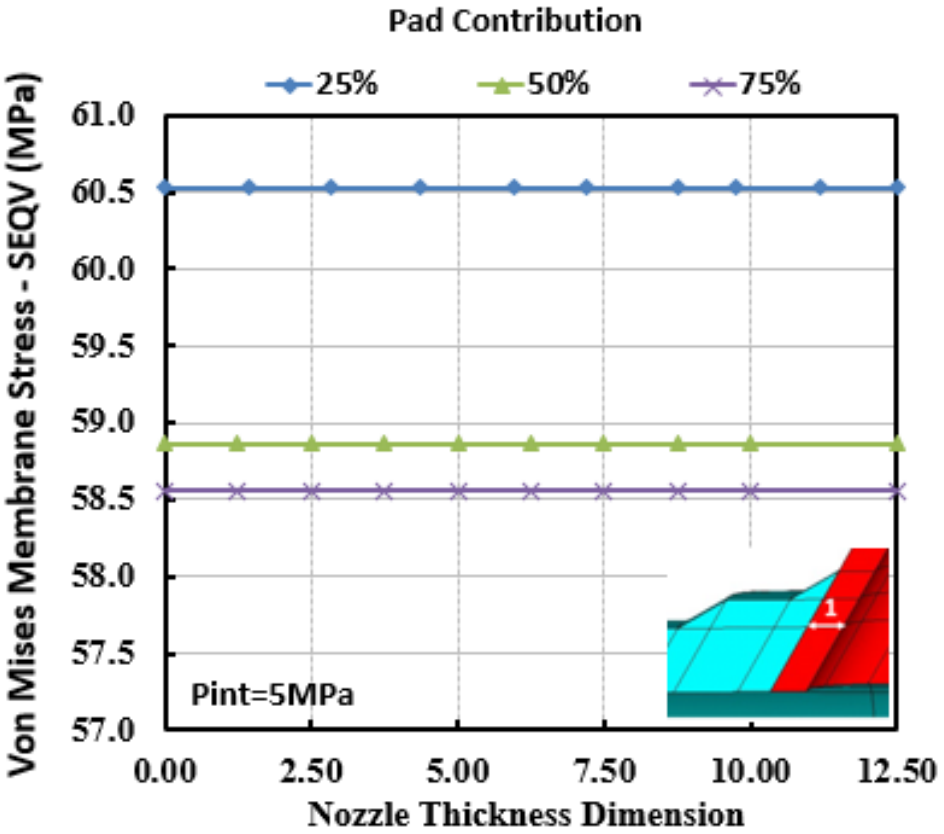

Figure 4. 31 Von-Mises SLA results with changing pad contribution (Path 1) - membrane stress

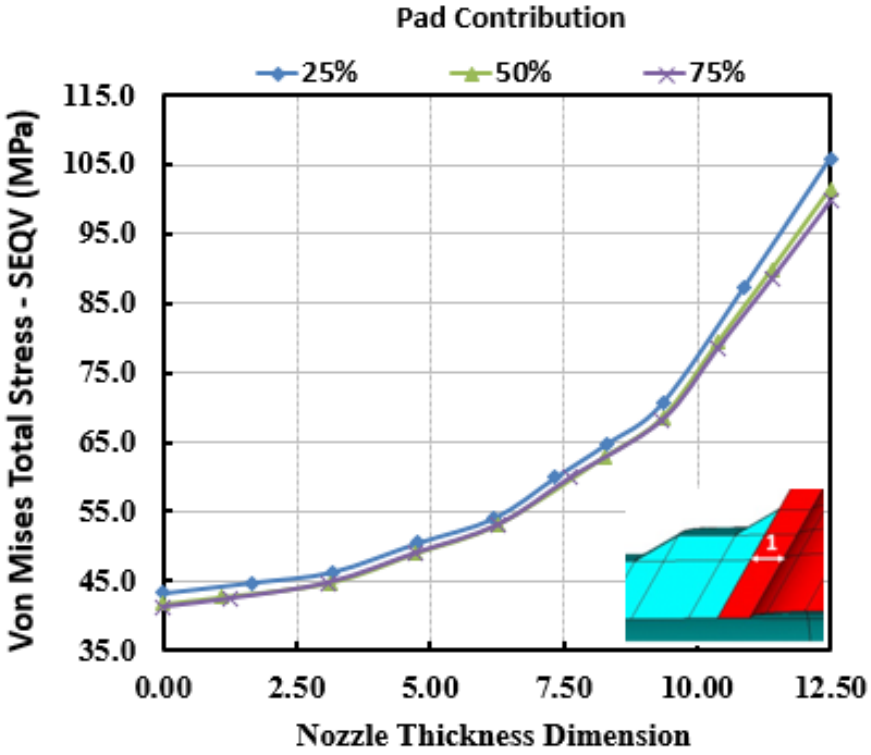

Figure 4. 32 Von-Mises SLA results with changing pad contribution (Path 1) - Total Stress

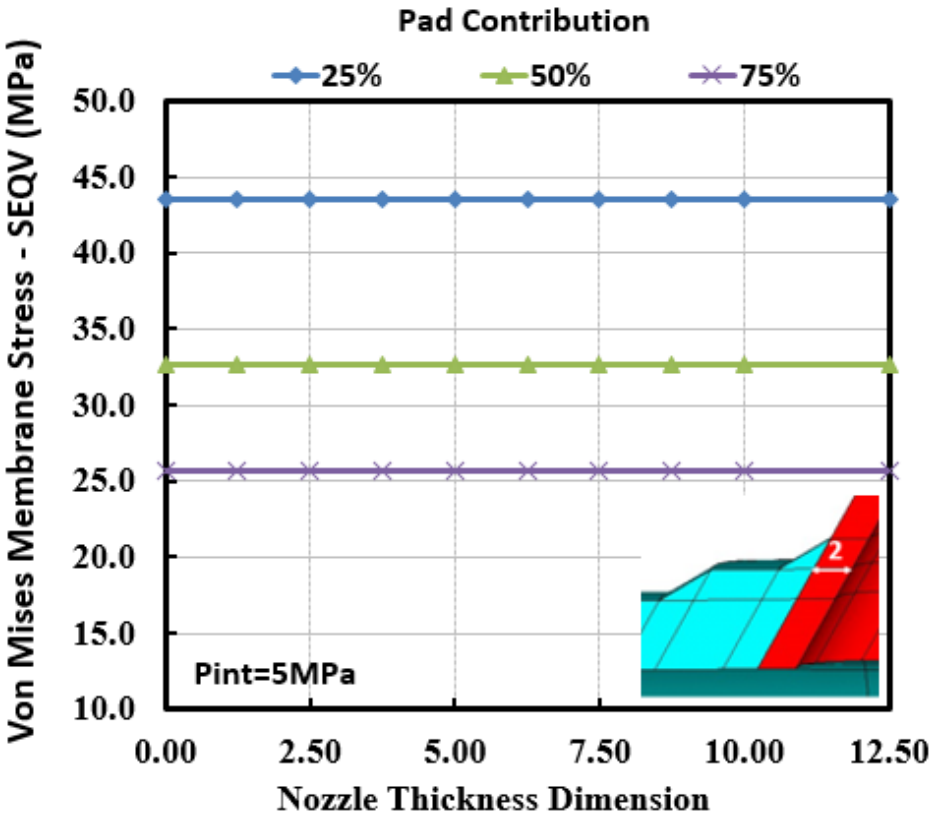

Figure 4. 33 Von-Mises SLA results with changing pad contribution (Path 2) - membrane stress

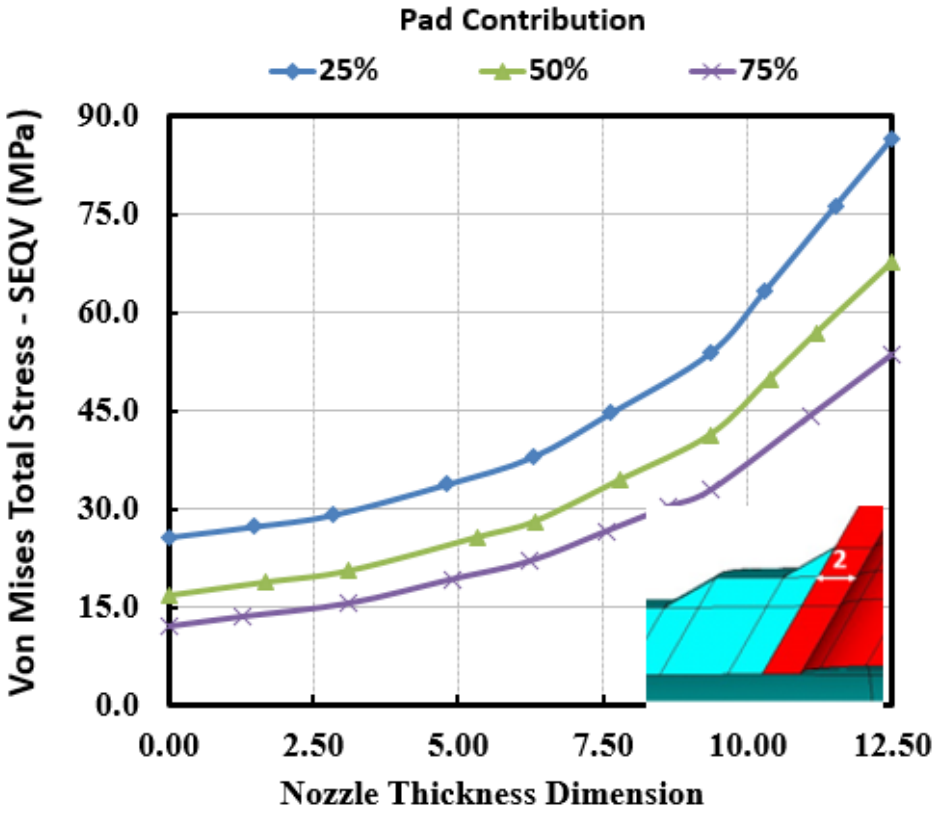

Figure 4. 34 Von-Mises SLA results with changing pad contribution (Path 2) - Total Stress

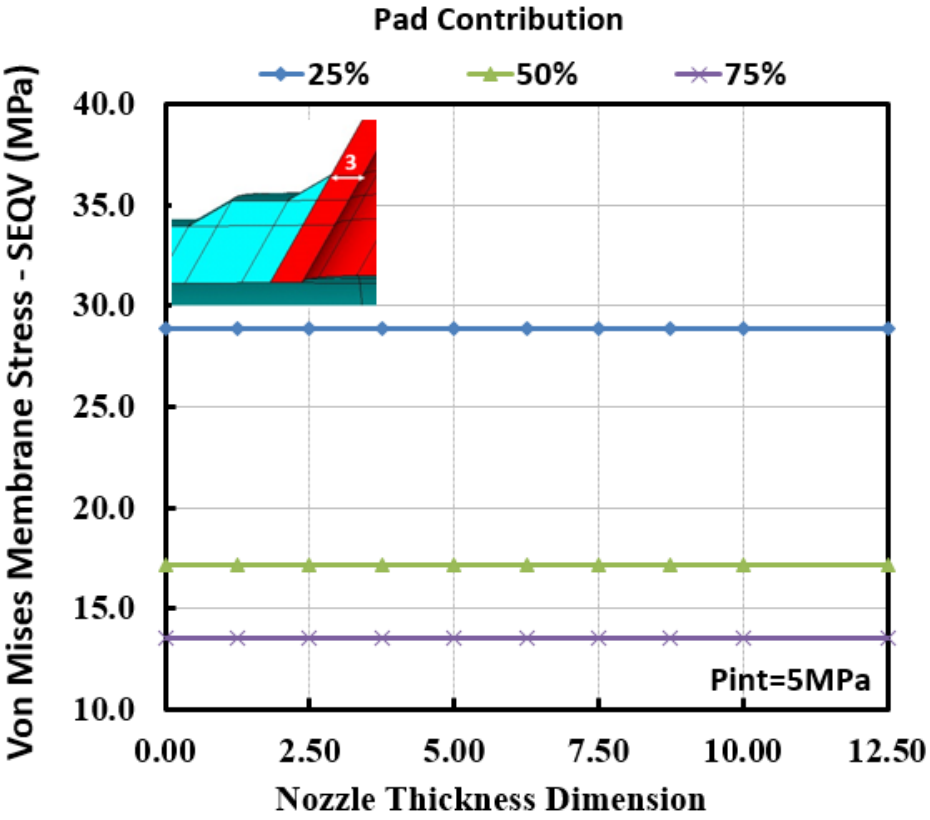

Figure 4. 35 Von-Mises SLA results with changing pad contribution (Path 3) - membrane stress

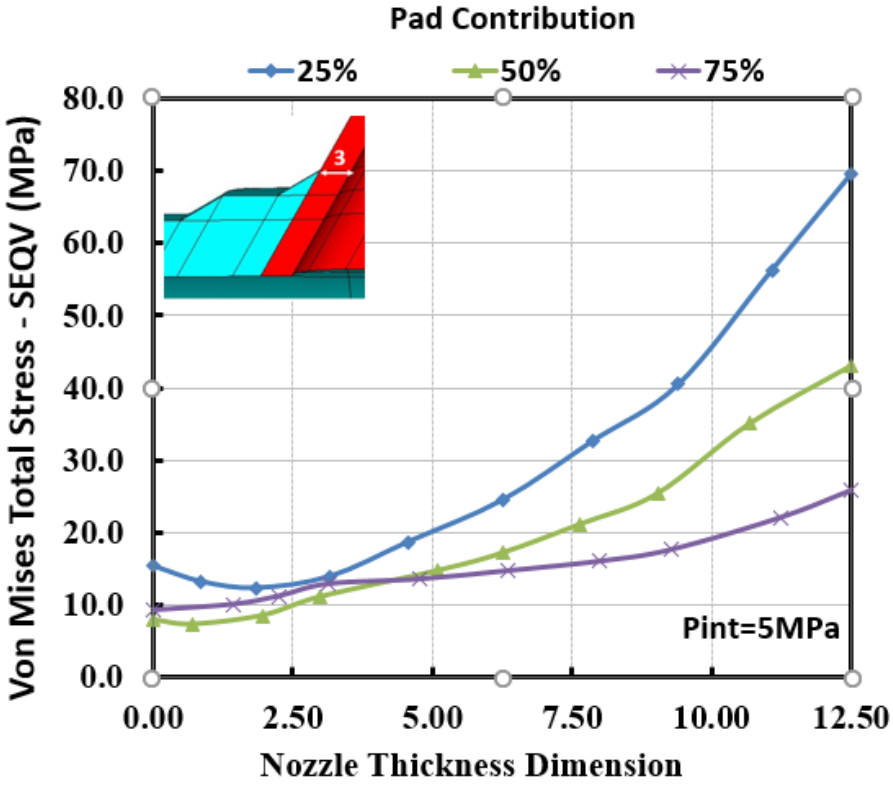

Figure 4. 36 Von-Mises SLA results with changing pad contribution (Path 3) - Total Stress

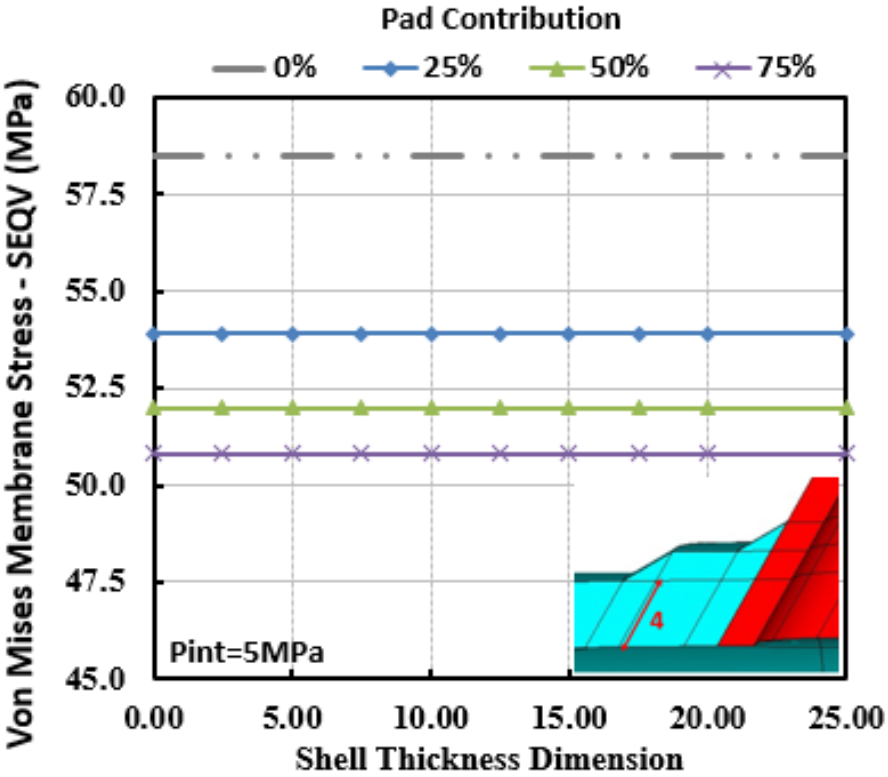

Figure 4. 37 Von-Mises SLA results with changing pad contribution (Path 4) - membrane stress

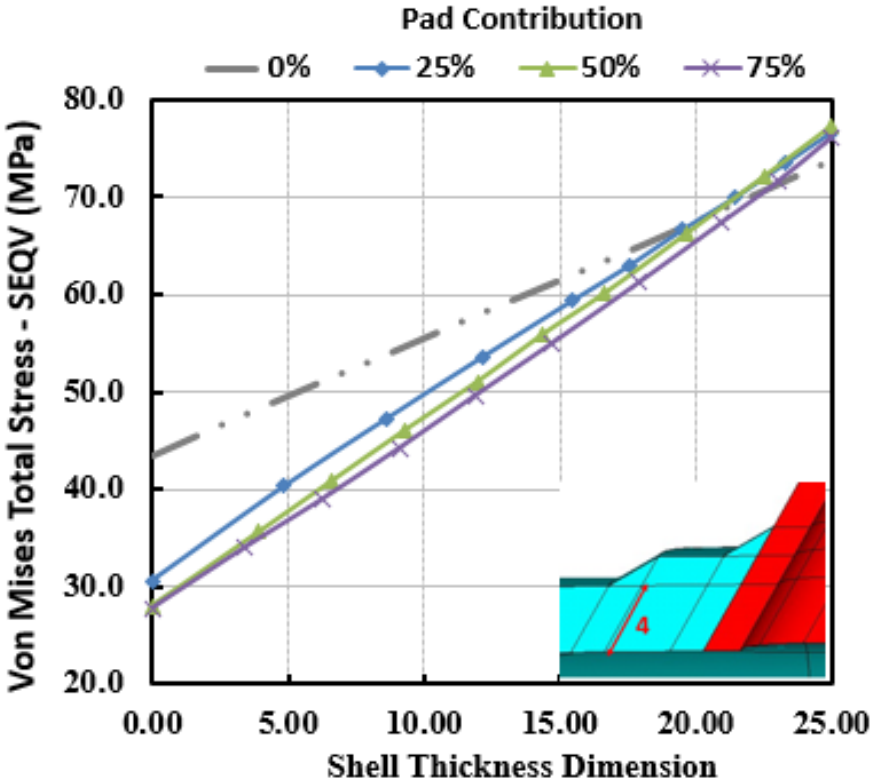

Figure 4. 38 Von-Mises SLA results with changing pad contribution (Path 4) - Total Stress

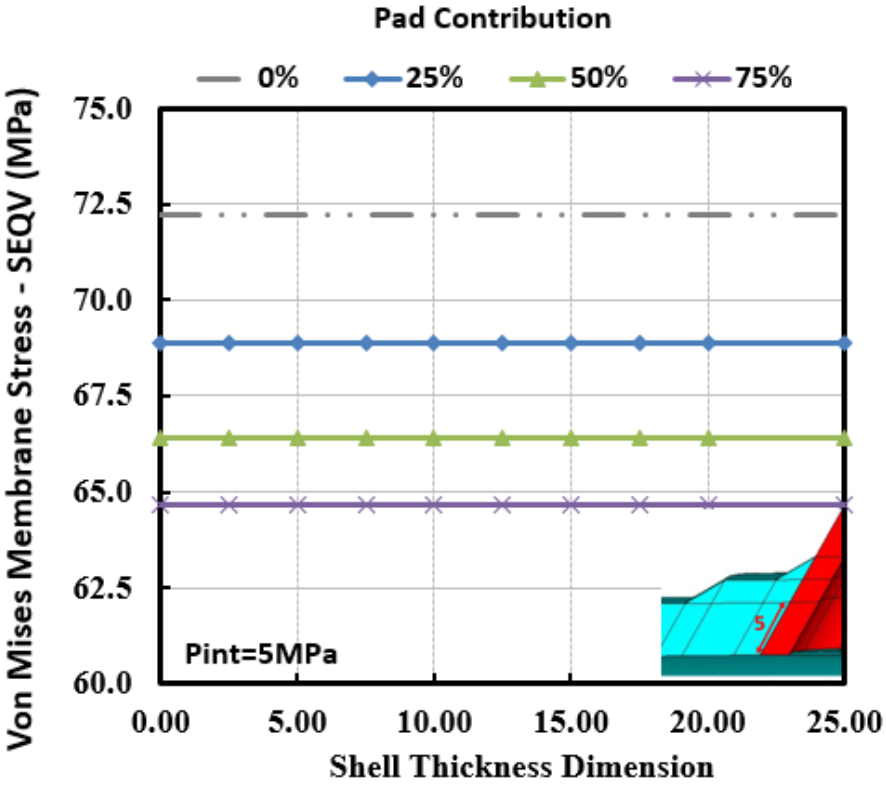

Figure 4. 39 Von-Mises SLA results with changing pad contribution (Path 5) - membrane stress

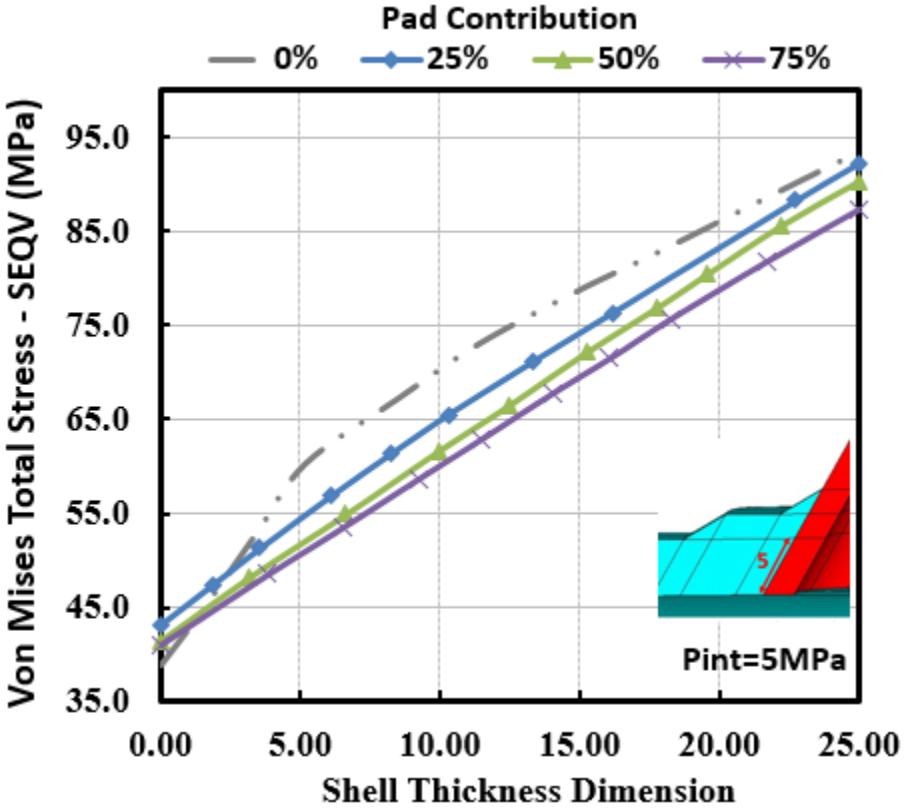

Figure 4. 40 Von-Mises SLA results with changing pad contribution (Path 5) - Total Stress

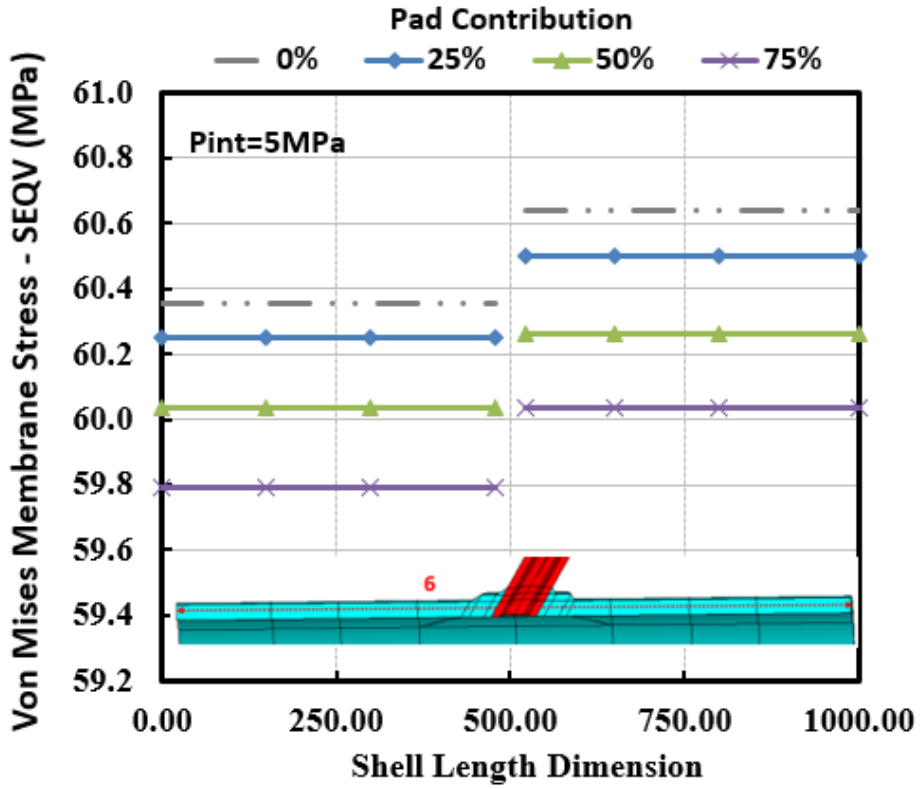

Figure 4. 41 Von-Mises SLA results with changing pad contribution (Path 6) - membrane stress

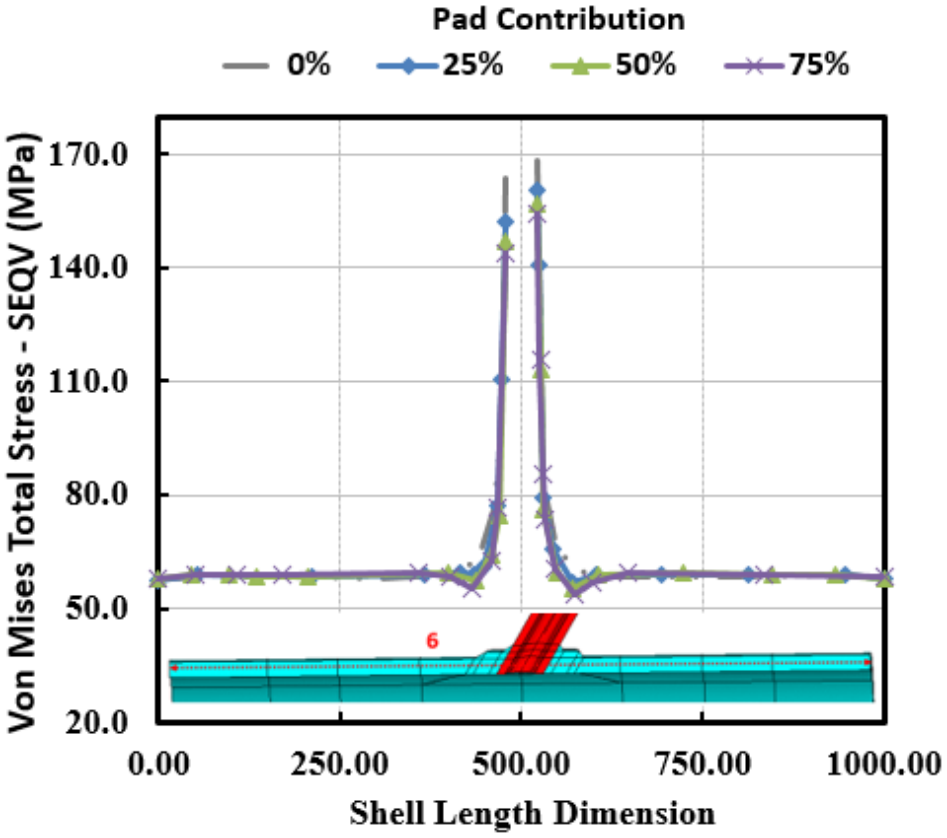

Figure 4. 42 Von-Mises SLA results with changing pad contribution (Path 6) - Total Stress

4.2.6.2.2. Changing Pad Diameter

In this section, the relationship between stress linearization and pad diameter magnitudes is examined. Unlike the others, the welding effect was ignored in the analyses. Since the pad diameter effect is examined, the pad contribution around the nozzle should be equal in terms of stress distribution. For this reason, the nozzle angle should be 0 degrees, that is, a vertical nozzle should be used. In all cases, di/Di = 0.16 and T/t = 0.9. 50% pad additive was applied to the shell. Nozzle sizes are fixed and the only variable in each analysis is the pad diameter. This variable is shown as D_p/di in the graphs. For these analyses, 4 critical paths around the pad were determined. These are the thickness of the nozzle along the bottom of the pad, the thickness of the nozzle along the pad top, the border line of the nozzle and shell under the pad, and the shell thickness of the pad end point. These are named as paths 1, 2, 3, and 4 respectively and shown in the **Figure 4. 43**.

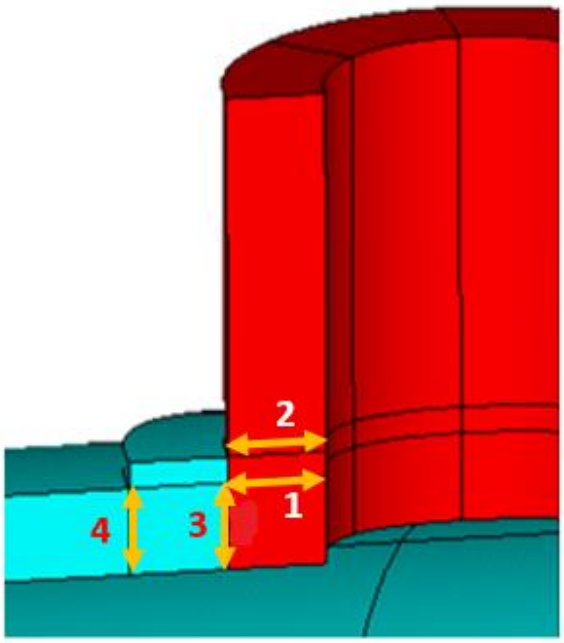

Figure 4. 43 Determined paths to be analysed for vertical nozzle

When the paths selected on the nozzle are examined, the membrane stresses obtained in the path numbered 1 are approximately 40% more than the path number 2. In addition, as the pad diameter increased, there was a decrease in the stress values.

When the paths along the shell are examined, approximately 20% more stress occurs on the path close to the nozzle. Again, as with the nozzle, the tension values decreased as the pad diameter increased.

In both nozzle and shell membrane stresses, the stress differences in paths numbered 1, 2 and 3 are less than 1.5%. Only on path number 4 the difference is around 6%. This happens because it moves away from the critical maximum stress zone. In total stresses, in all cases, very close to each other and approximately 1% difference were obtained. The most important point is that the stress values along the Shell show an almost linear increase, while the stress increase in the nozzle region is parabolic.

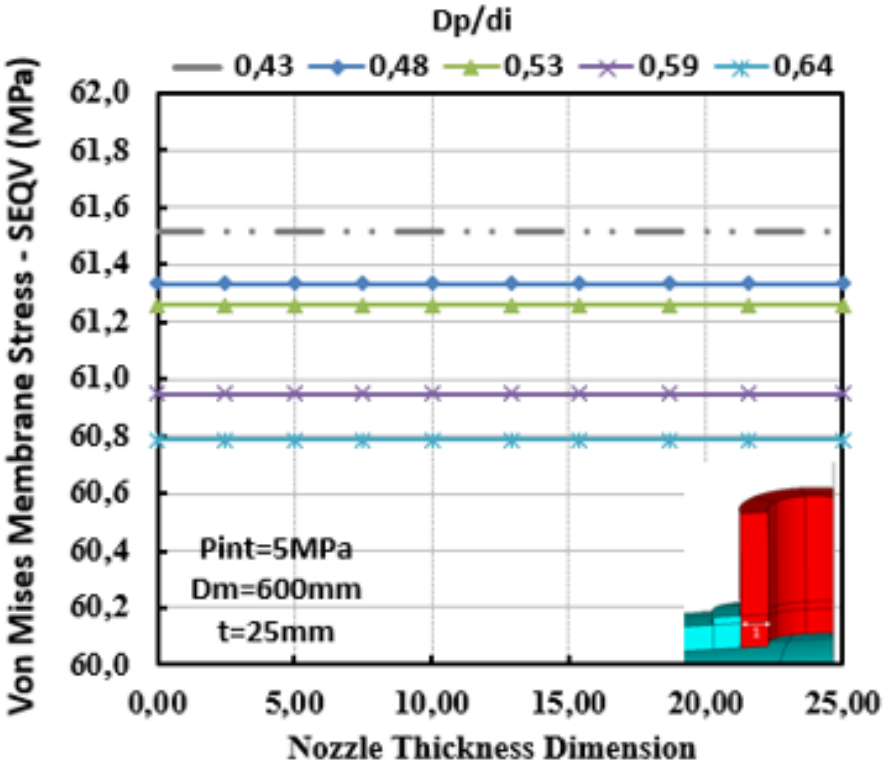

Figure 4. 44 Von-Mises SLA results with changing Dp/di (Path 1) – Membrane Stress

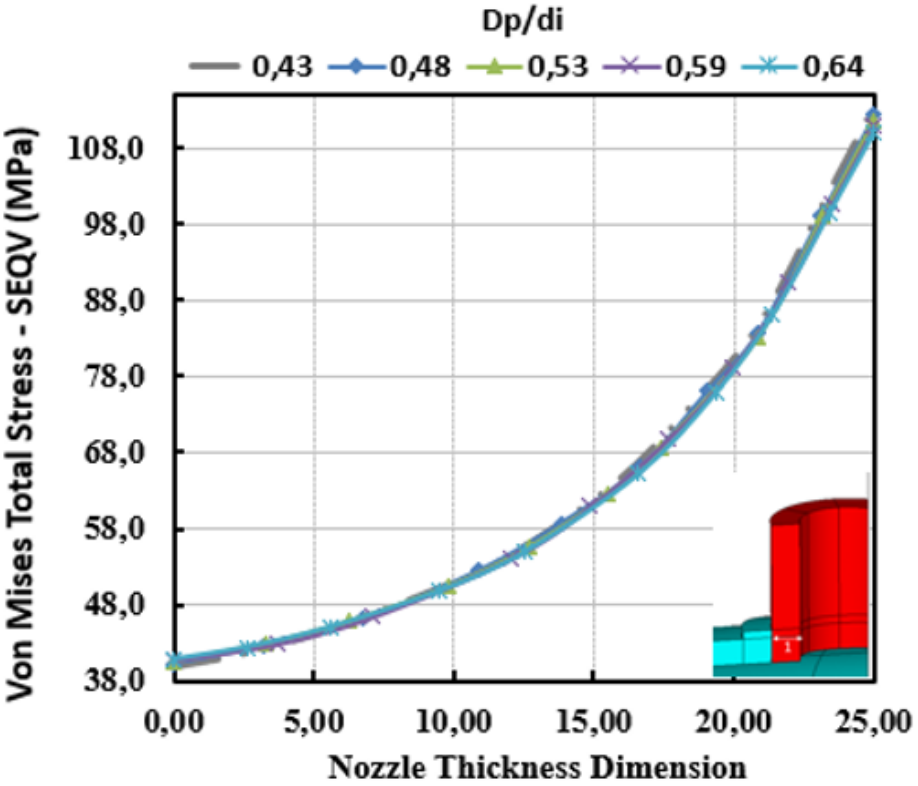

Figure 4. 45 Von-Mises SLA results with changing Dp/di (Path 1) - Total Stress

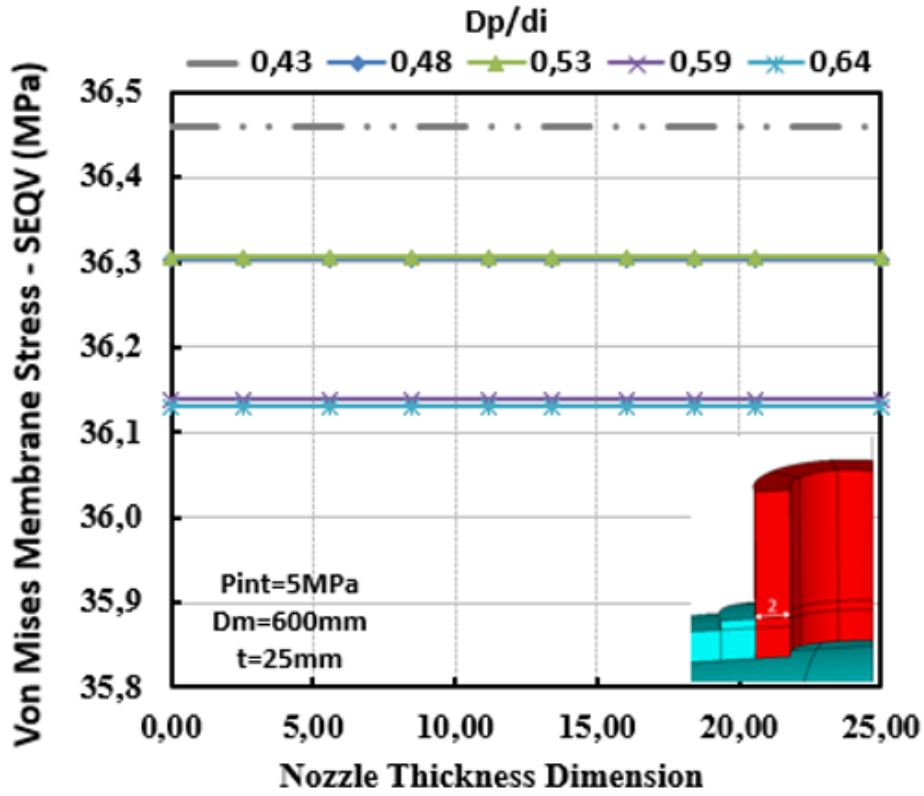

Figure 4. 46 Von-Mises SLA results with changing Dp/di (Path 2) – Membrane Stress

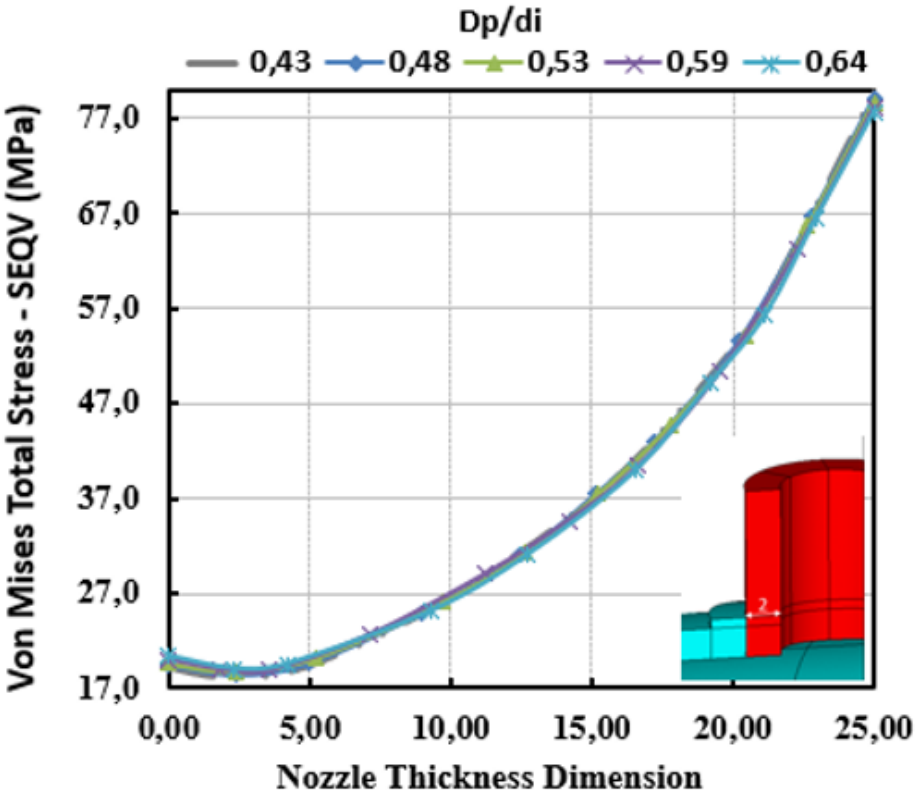

Figure 4. 47 Von-Mises SLA results with changing Dp/di (Path 2) - Total Stress

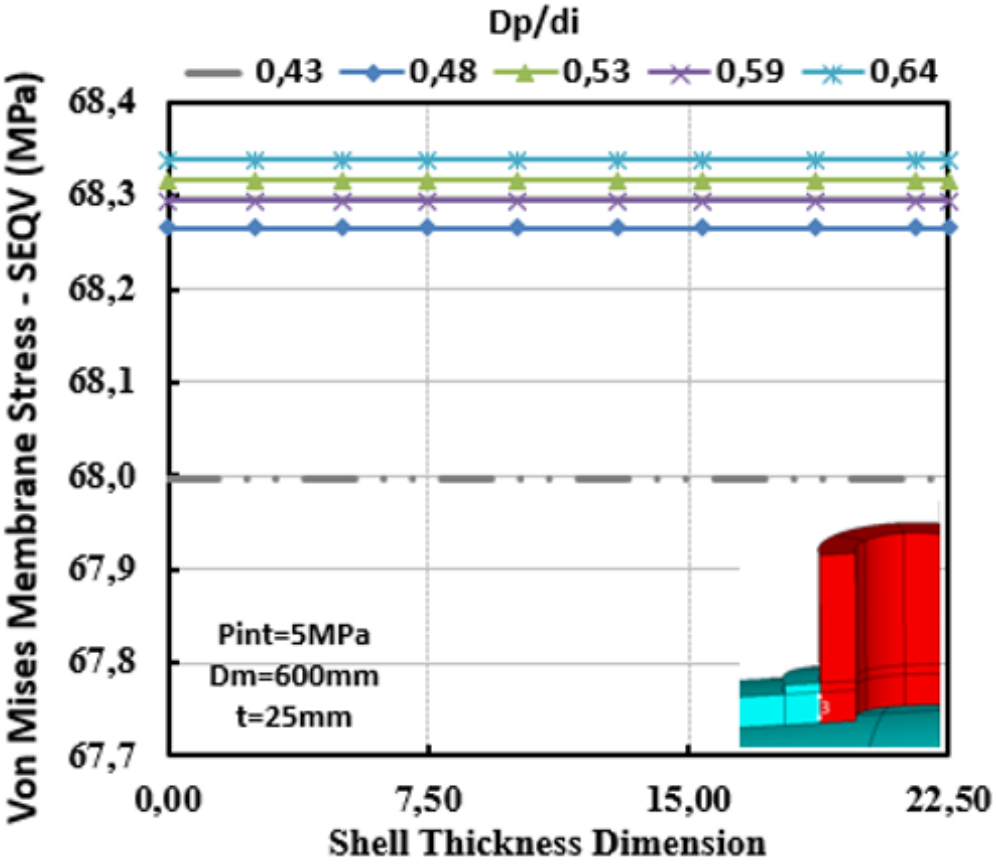

Figure 4. 48 Von-Mises SLA results with changing Dp/di (Path 3) – Membrane Stress

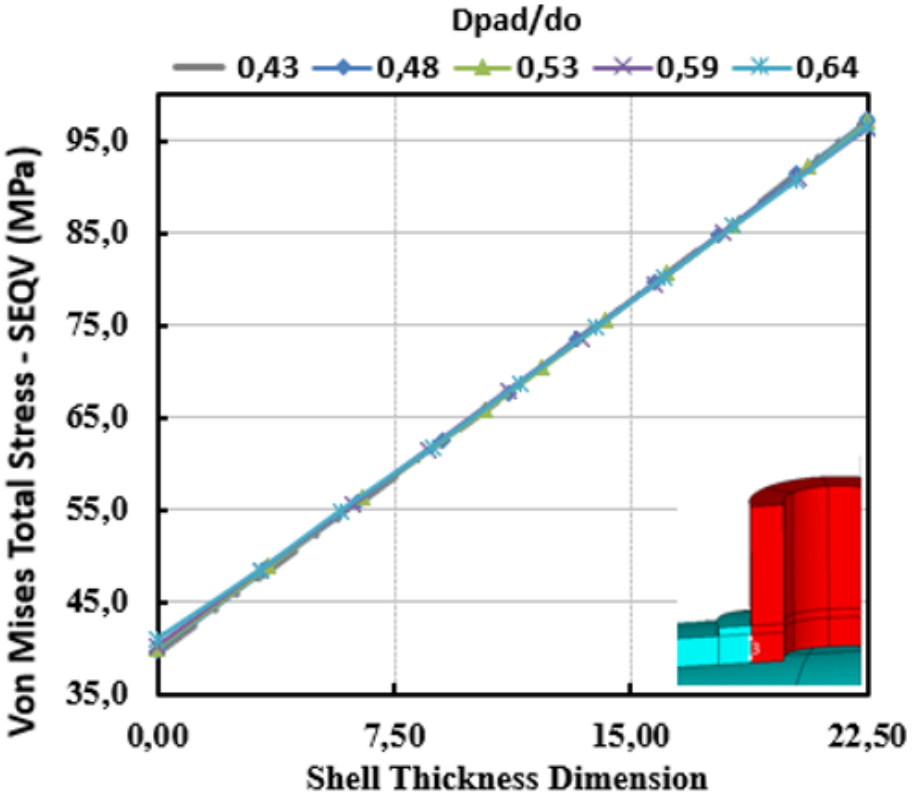

Figure 4. 49 Von-Mises SLA results with changing Dp/di (Path 3) - Total Stress

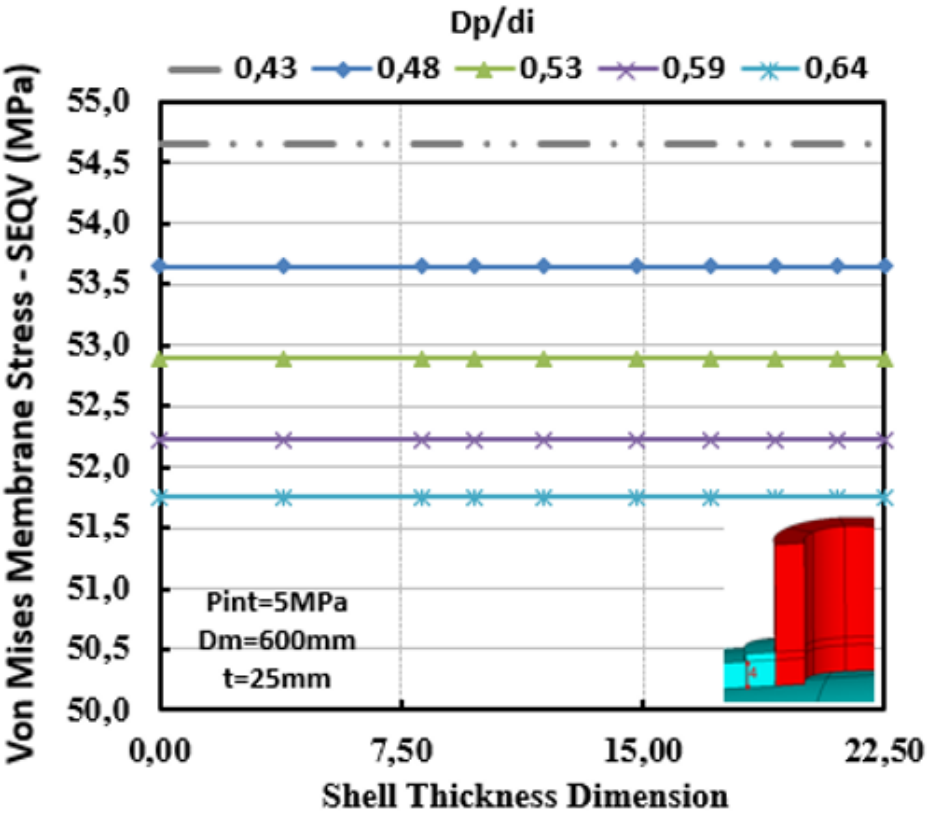

Figure 4. 50 Von-Mises SLA results with changing Dp/di (Path 4) – Membrane Stress

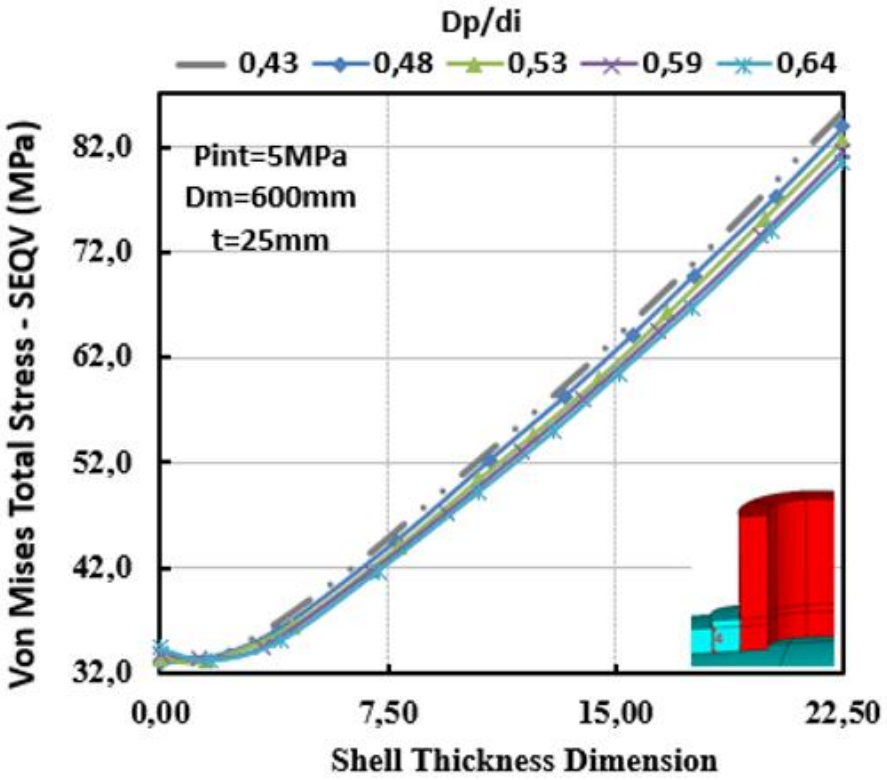

Figure 4. 51 Von-Mises SLA results with changing Dp/di (Path 4) - Total Stress

4.2.6.2.3. Changing Oblique Nozzle Angle (Ψ)

In this section, a cylindrical pressure vessel with a single nozzle under constant 5MPa pressure will be examined for stress variations for the 6 critical paths mentioned. In these analyses, Di = 500mm, T=25mm, di=Di/12 and t=12.5. There is a 50 percent pad contribution in all issues ($T_p/T = 0.5$). The only variable in the analysis is the nozzle angle. SLA analyses were repeated for 0 degrees (vertical nozzle), 15degrees, 30degrees and 45degrees nozzle angle. The obtained Von-Mises Membrane and Total stress values are given in the figures below.

When the **Figure 4. 52** - **Figure 4. 57** were examined, the stress linearization changes along the nozzle thickness are examined in 3 different locations. These can be briefly called pad bottom (1), pad top (2) and welding top (3). In nozzle joint problems, the tension values in the opening zone are maximum. That is why, stress values tend to increase as approaches the crotch corner. When the graphics are checked out within

themselves, both membrane and total stress values increase as the nozzle angle increases. In addition, the highest stress values were obtained in path number 1. However, when the nozzle angles of 0 degrees and 45 degrees are compared in membrane stress plots, the differences are approximately 14% for path number 1 (**Figure 4. 52**), 34% for path number 2 (**Figure 4. 54**), and 45% for path number 3 (**Figure 4. 56**). Total stress values increase from the nozzle outer wall to the inner wall in all graphics.

Paths 4 and 5 represent the closest and farthest shell thickness to the nozzle under the pad. The stress distribution is from the outer wall of the shell to the inner wall. The distribution of total stress values on path number 4 is very close to each other and the difference is less than 6% at the maximum point. On path number 5, the stress is maximum at the 45-degree nozzle at the initial starting point, and the difference to 0 degrees is close to 20 percent. The stress values are very close to each other at the point closest to the crotch corner and the maximum difference is less than 4%. The results are shown in the **Figure 4. 58** - **Figure 4. 61**.

Finally, stress values were obtained along top of the shell is from beginning and end point of the shell (path number 6). The reason for the gap in the graphics is the nozzle opening and opening dimension is outer diameter of the nozzle. Membrane stress as shown in the Figure is 60.3MPa and constant for a vertical nozzle with an angle of 0 degrees. On the other hand, as the nozzle angle increases, this uniformity is lost on both sides of this opening. The most important point is that the stresses are higher where the nozzle bends. Although the difference in stress values is much less than 1 percent here, it is important for stress distribution studies. In the total stress graph in **Figure 4. 62 and Figure 4. 63** while the stress distribution moves steadily along the shell, the stress reaches the peak point as it goes on the nozzle.

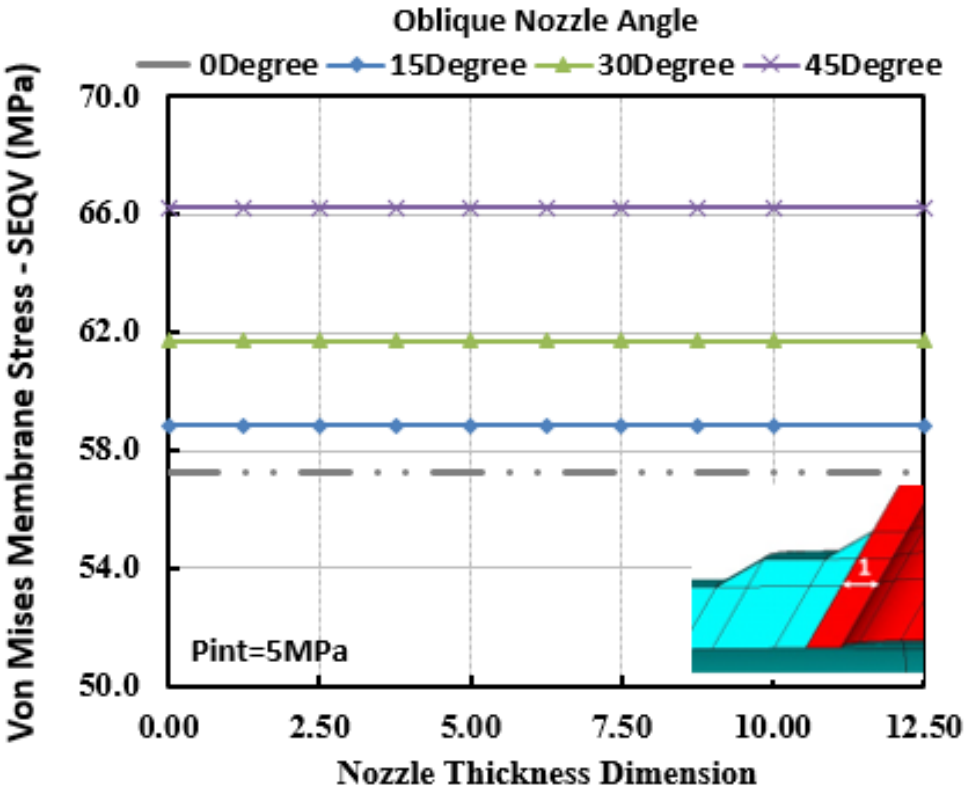

Figure 4. 52 Von-Mises SLA results with changing nozzle angle (Path 1) - membrane stress

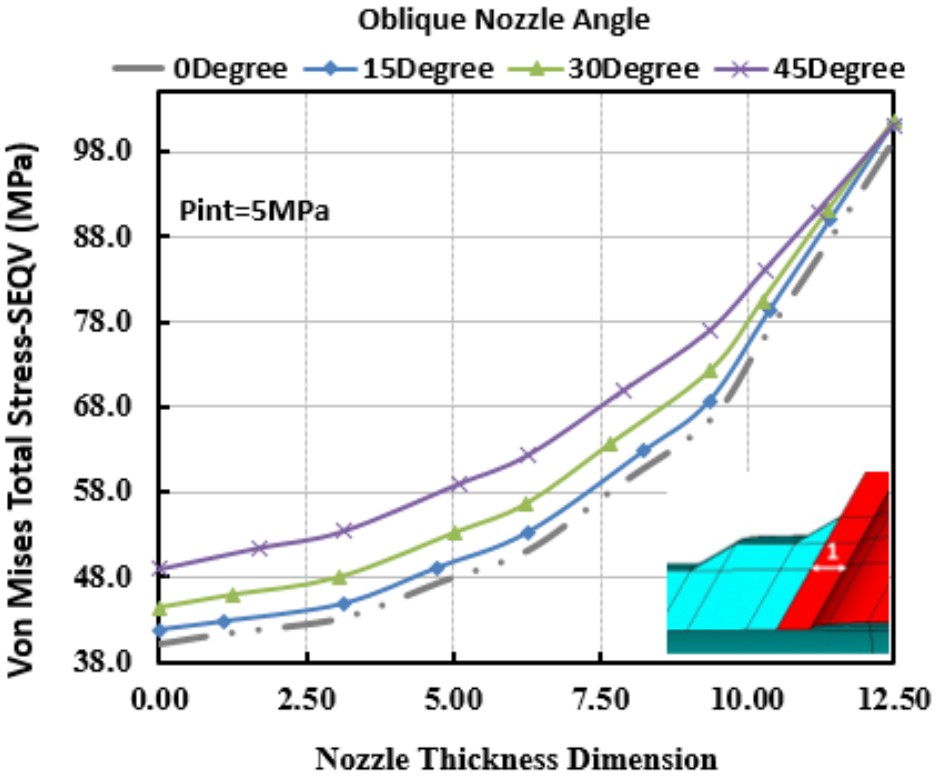

Figure 4. 53 Von-Mises SLA results with changing nozzle angle (Path 1) – Total stress

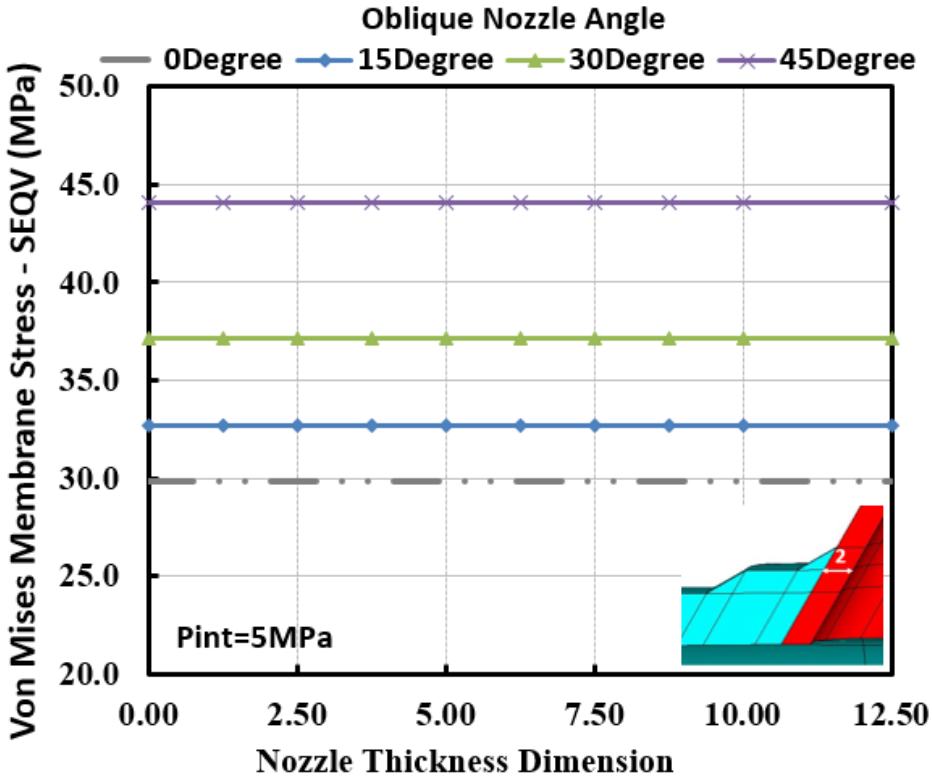

Figure 4. 54 Von-Mises SLA results with changing nozzle angle (Path 2) - membrane stress

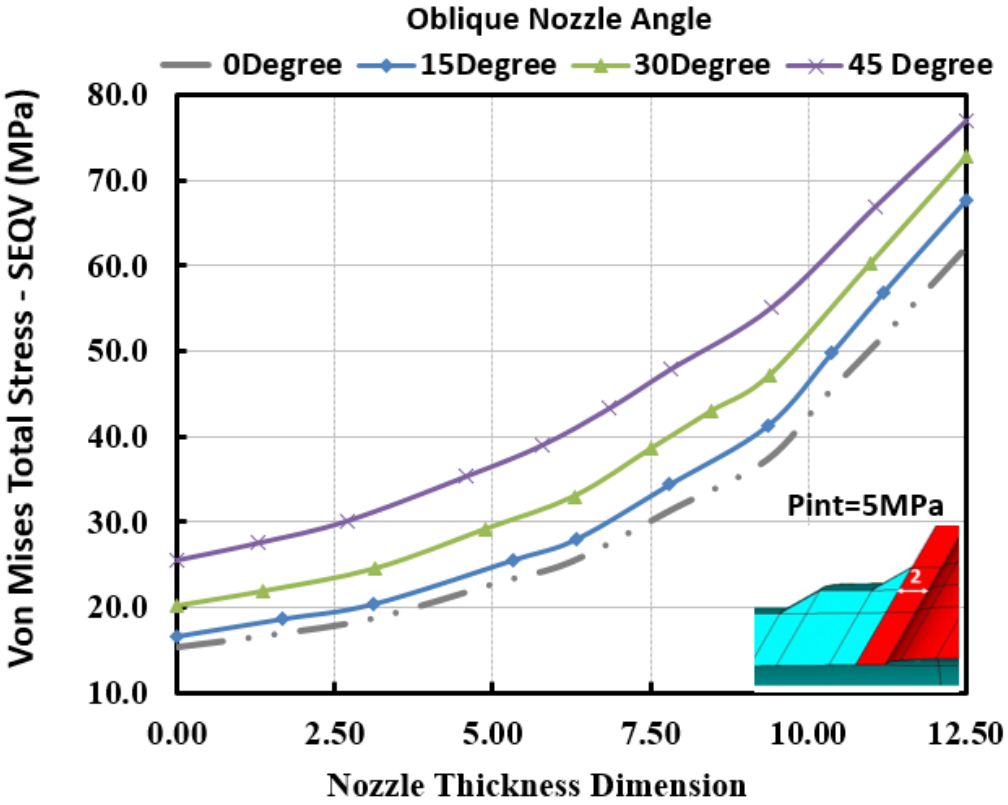

Figure 4. 55 Von-Mises SLA results with changing nozzle angle (Path 2) – Total stress

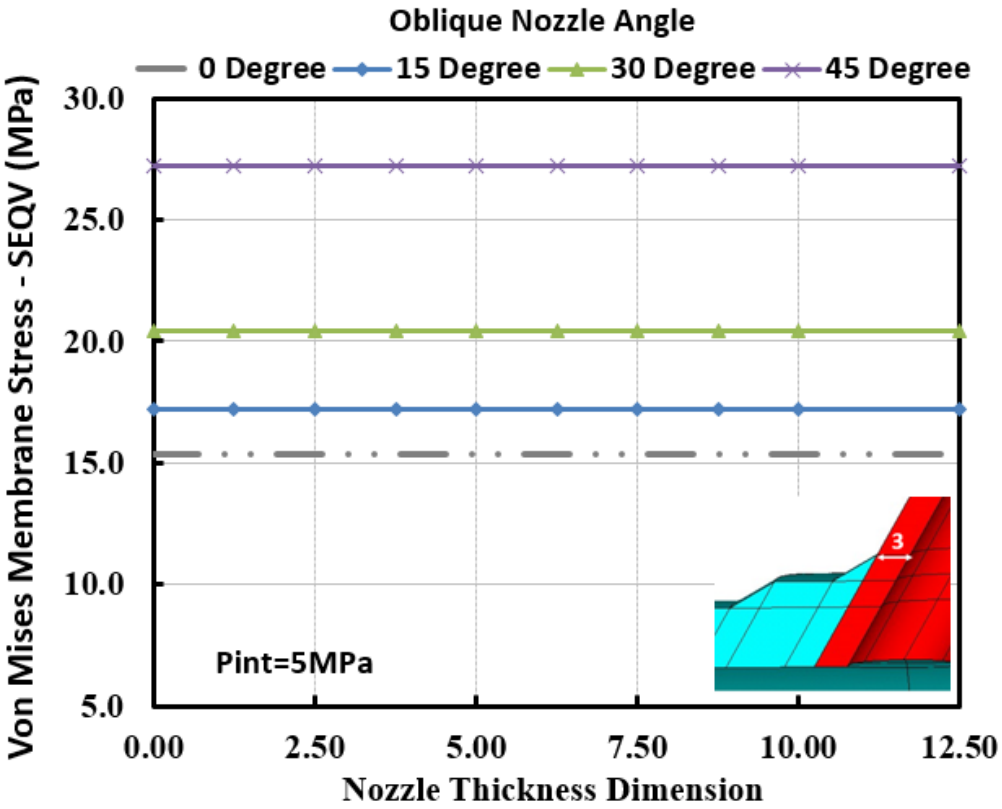

Figure 4. 56 Von-Mises SLA results with changing nozzle angle (Path 3) – membrane stress

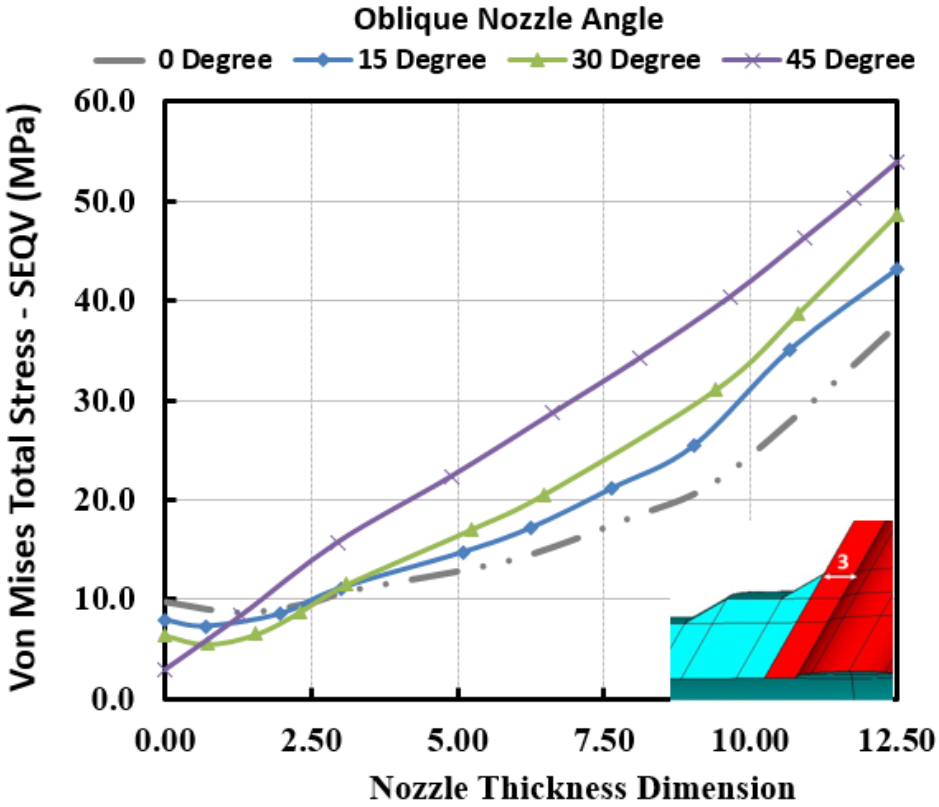

Figure 4. 57 Von-Mises SLA results with changing nozzle angle (Path 3) – Total stress

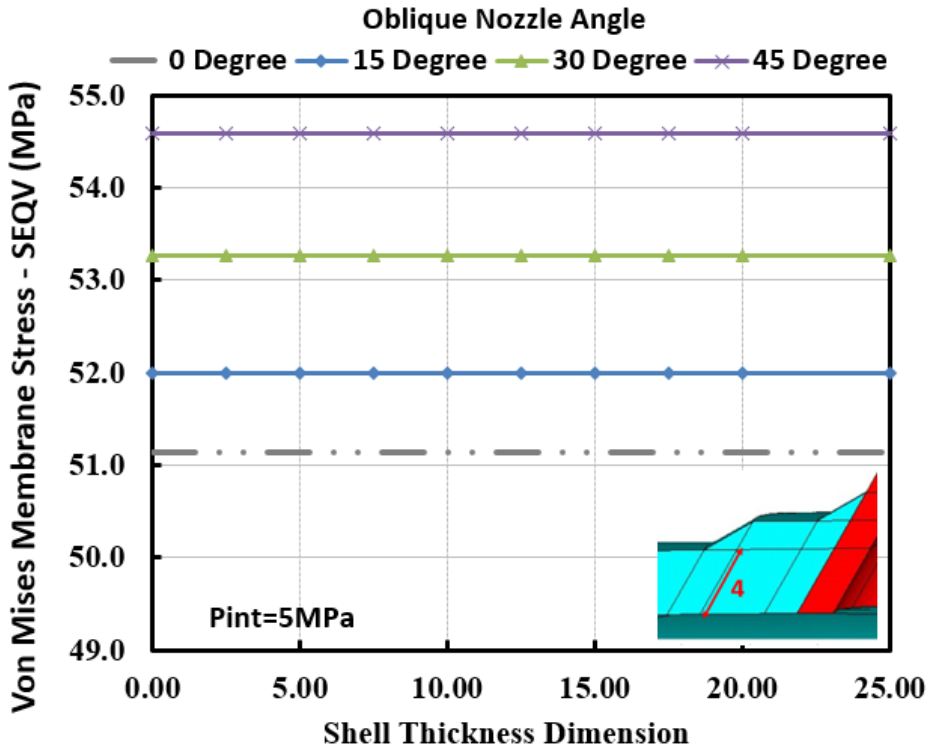

Figure 4. 58 Von-Mises SLA results with changing nozzle angle (Path 4) – membrane stress

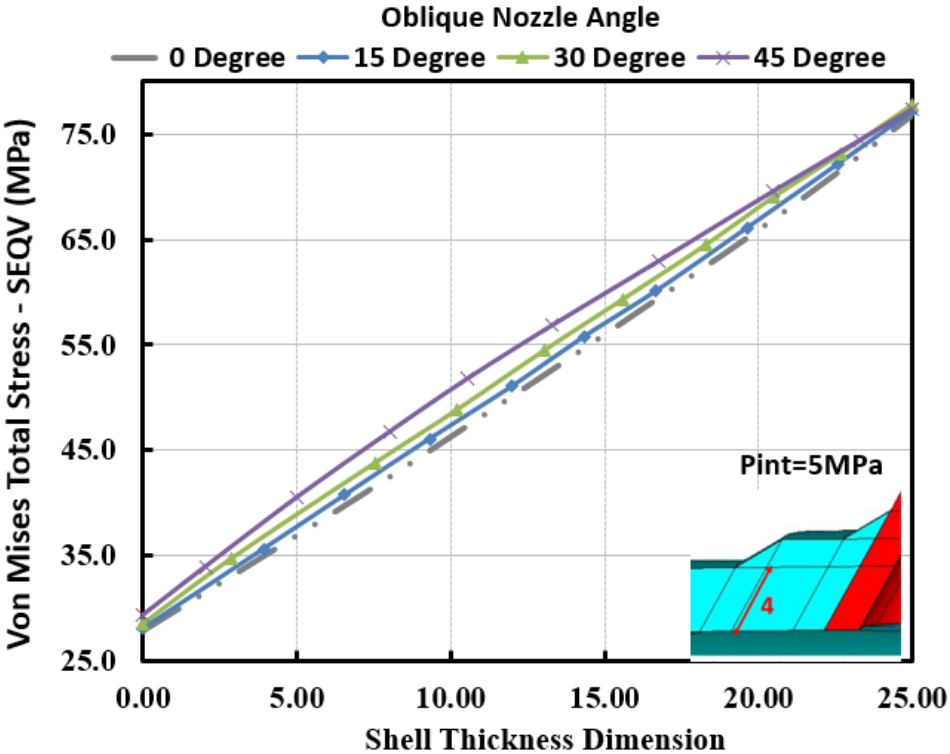

Figure 4. 59 Von-Mises SLA results with changing nozzle angle (Path 4) – Total stress

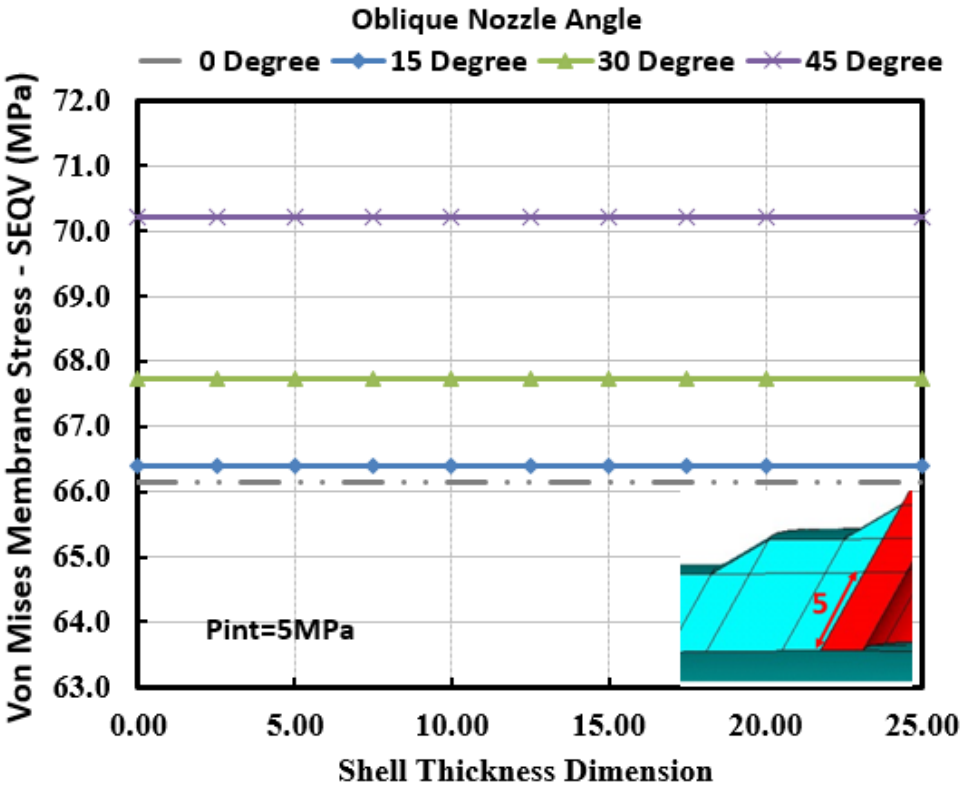

Figure 4. 60 Von-Mises SLA results with changing nozzle angle (Path 5) – membrane stress

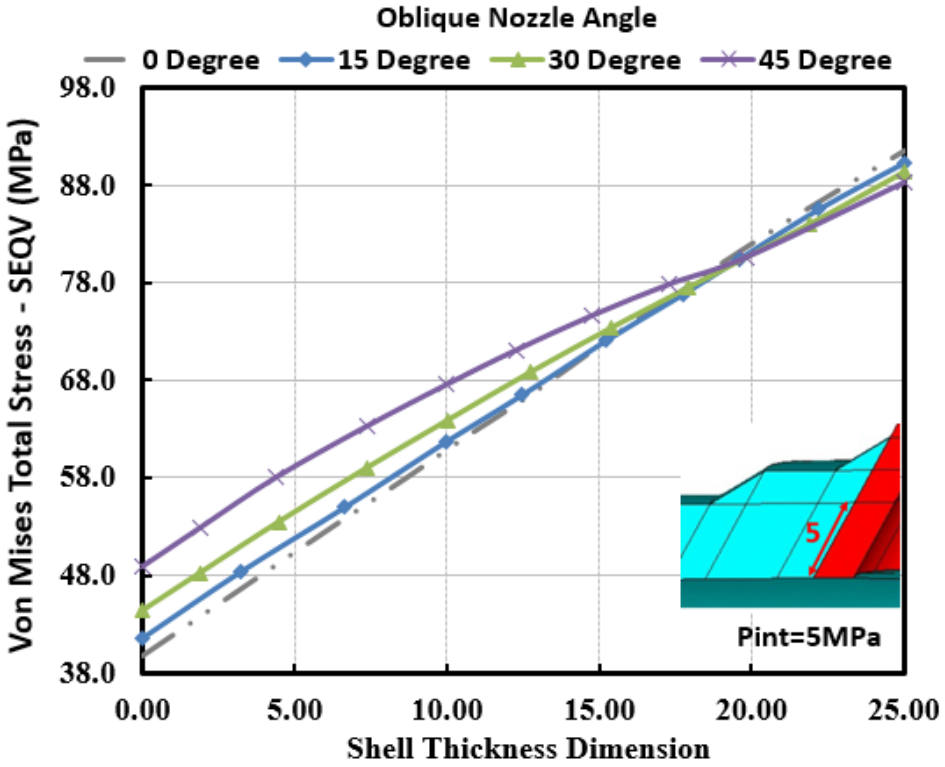

Figure 4. 61 Von-Mises SLA results with changing nozzle angle (Path 5) – Total stress

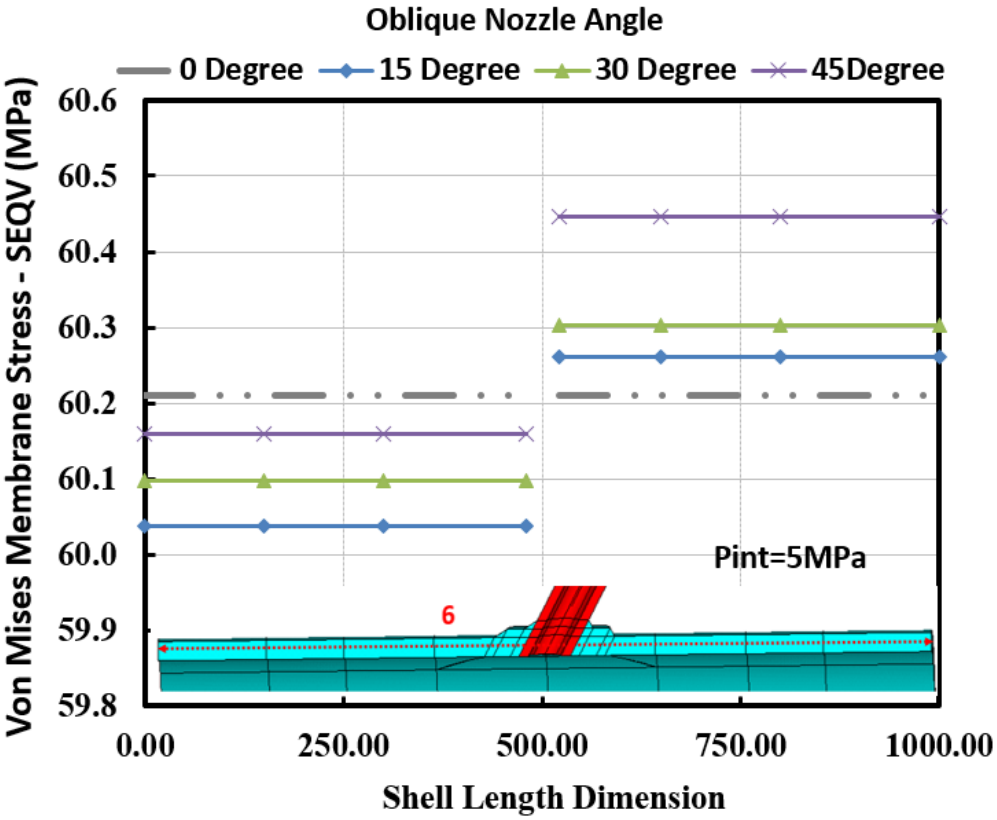

Figure 4. 62 Von-Mises SLA results with changing nozzle angle (Path 6) – membrane stress

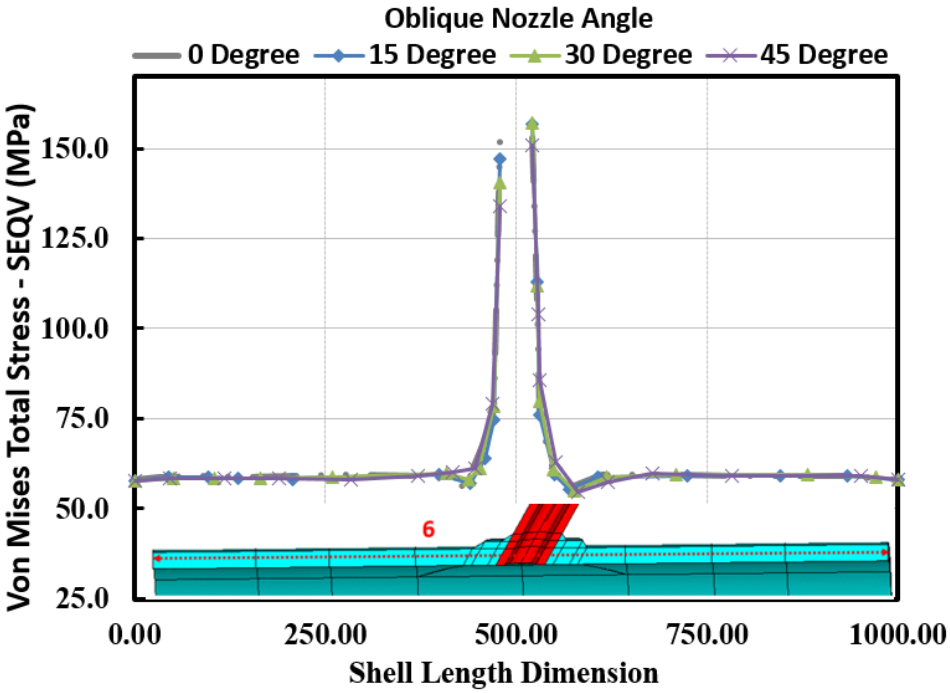

Figure 4. 63 Von-Mises SLA results with changing nozzle angle (Path 6) – Total stress

4.3. Concluding remarks

In conclusion, Stress linearization was used to define constant and linear thickness FEA (Finite Element Analysis) stress distributions and membrane and membrane + bending stress distributions in Pressure Vessel Design by Analysis in this section. The basis of this method is to correlate and determine the stress occurring along a path with the concept of limit load. As a result of this work, a comprehensive stress linearization study was carried out for a nozzle-cylinder combination that was subjected only to internal pressure. Also, stress distribution at critical locations determined on the nozzle and shell was investigated. According to the results, the tension is maximum in the paths chosen close to the opening zone in both the shell and the nozzle. Moreover, especially the increase in pad contribution significantly reduced the stresses obtained on the same paths. On the other hand, since the stress distribution on both sides of the sloping was not equal in oblique nozzles, the differences in stress magnitudes could be easily detected by this method. Finally, this study provides researchers an alternative stress analysis for critical locations in the intersection area in the design and analysis of cylinder nozzle connections.

CHAPTER 5. FINITE ELEMENT ANALYSIS INVESTIGATION PART 2 - INELASTIC ANALYSIS

5.1. Introductory Remarks

This section investigates finite element analyses in inelastic region for nozzle connections in pressure vessel problems with parametric studies and discusses the results. Elastic - Perfectly Plastic (Limit Load) Analysis, Full Elastic Plastic Analysis, and Cyclic Loading Analysis are the main research subjects.

5.2. Elastic – Perfectly Plastic (Limit Load) Analysis

In pressure vessel problems, detection of limit loads is of great importance to prevent permanent damage. The traditional design methods determine elastic membrane and bending stresses and ensure these are kept away from some recognised limit to avoid the failure mechanism on gross plastic deformation. However, an alternative to this approach is to find the limit load for the system – that is, the load just before full plasticity is reached. A suitable safety factor for the system load is then applied and the pressure vessel can be deemed safe. In this study, limit load values for internal pressure and externally applied loads are examined under various parameters and configurations. The same geometric arrangement is used as per previous chapters with the nozzle free to move in all directions. Boundary conditions are applied only under saddle and the saddle base is fully fixed. The load action variables are internal pressure, external moment, and tensile force. It is important to determine the maximum internal pressure and external load values in cylinder-cylinder connection problems to prevent plastic collapse of the system.

As a benchmark example for a circular cylinder, it is worth considering Perfect Plasticity and Tresca criteria for thick - walled open cylinders without any nozzle connection

Figure 5. 1, and as such, first yield and limit load values can be calculated using the following equations. For vessels with nozzle connection, the results will be calculated with elastic-perfectly plastic analysis.

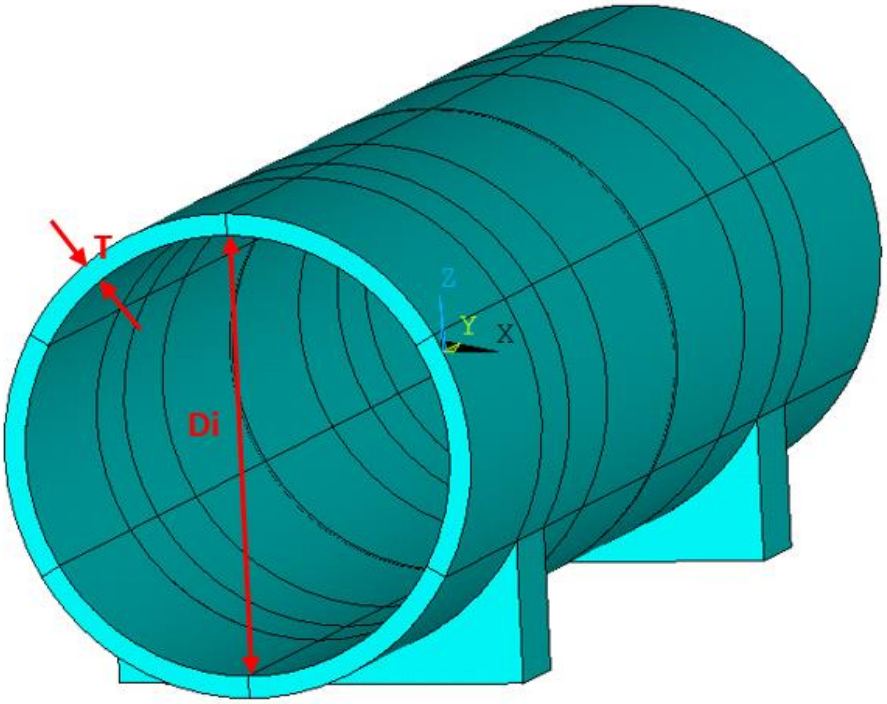

Figure 5. 1 Cylindrical vessel without nozzle connections – Perfect Cylinder

$$First\ yield: p_y = \frac{\sigma_y}{2}\left(1 - \left(\frac{r_i}{r_o}\right)^2\right)$$ **Equation 5. 1**

$$Limit\ load: p_l = \sigma_y ln\left(\frac{r_i}{r_o}\right)$$ **Equation 5. 2**

In the calculations made, the limit loads of only a perfect cylinder (Di = 500mm) subjected to internal pressure and vessel with a nozzle (Di = 500mm, di = 125mm, t = 15mm) were taken into consideration. Analyses were repeated for 4 different shell thicknesses (T). Perfect cylinder and nozzle connected cylinder are represented in **Figure 5. 1** and **Figure 5. 2** respectively.

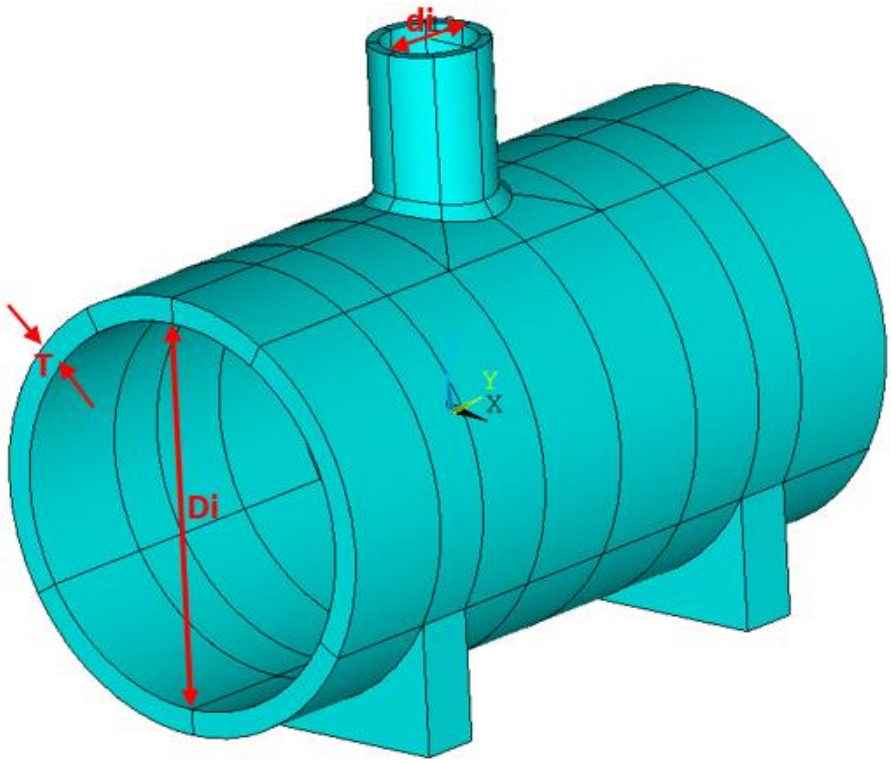

Figure 5. 2 Cylindrical vessel with nozzle connection

The results obtained are shown in the **Table 5. 1**. As it can be used from the results in the Table, as the wall thickness increases, the resistance of the vessel against the internal pressure increases, so the limit pressure values increase in both cases. Although the nozzle size remains constant, when T = 10mm, the difference between the two cases is 2.4%, while at T = 25mm, this difference has increased to 6.2%.

Table 5. 1 The effect of shell thickness change on limit load in nozzle and without-nozzle vessels

	(Perfect Cylinder – No Nozzle Junctions)	(Cylinder with a Nozzle)	
T(mm)	**Limit Pressure (MPa)**	**Limit Pressure (MPa)**	**Differences**
10	10.2	9.9	2.4%
15	15.1	14.4	5.2%
20	20.3	19.2	5.9%
25	24.8	23.3	6.2%

However, the wall thickness is not the only parameter that affects the vessel strength. Nozzle opening variation can also change the maximum stress and ultimately the limit

loading conditions. For this reason, a comparison study should be made by changing the nozzle opening with the inner diameter (di) parameter.

In these comparison analyses, Di = 500mm, T = 15mm and t = 15mm. Only the nozzle inner diameter (di) will be changed. Limit analysis results for 3 different nozzle inner diameters are given in the **Table 5. 2**.

Table 5. 2 The effect of nozzle inner diameter changes on limit load in nozzle and without-nozzle vessels

	(Perfect Cylinder – No Nozzle Junctions)	(Cylinder with a Nozzle)	
di(mm)	**Limit Pressure (MPa)**	**Limit Pressure (MPa)**	**Differences**
75	15.149	15.06	0.588%
100	15.149	15	0.984%
125	15.149	14.4	4.945%

In such analyses, it is expected that as the nozzle opening increases, the stress values on the crotch corner increase further and therefore the limit loads are also reduced. It is observed that the difference between the two cases becomes more pronounced as the nozzle opening increases. It is noted that the limit load values make a significant difference in the nozzle-cylinder crotch corner. For this reason, the effects of nozzle diameter variation, nozzle and shell thickness changes and external force magnitude on limit loads are examined in detail.

5.2.1. Effect of Changing Nozzle Diameter

In this study, the variation of the limit pressure values according to the nozzle size will be considered. In the analyses to be realized, the main shell inner diameter (D_i) is 500mm, the main shell outer diameter (D_o) is 530mm and the nozzle thickness (t) is fixed as 15mm. The only variable is the nozzle inner diameter (di), and analyses are performed for 6

different nozzle sizes. The limit pressure values obtained for t/T = 1.0 are shown in the **Figure 5. 3**.

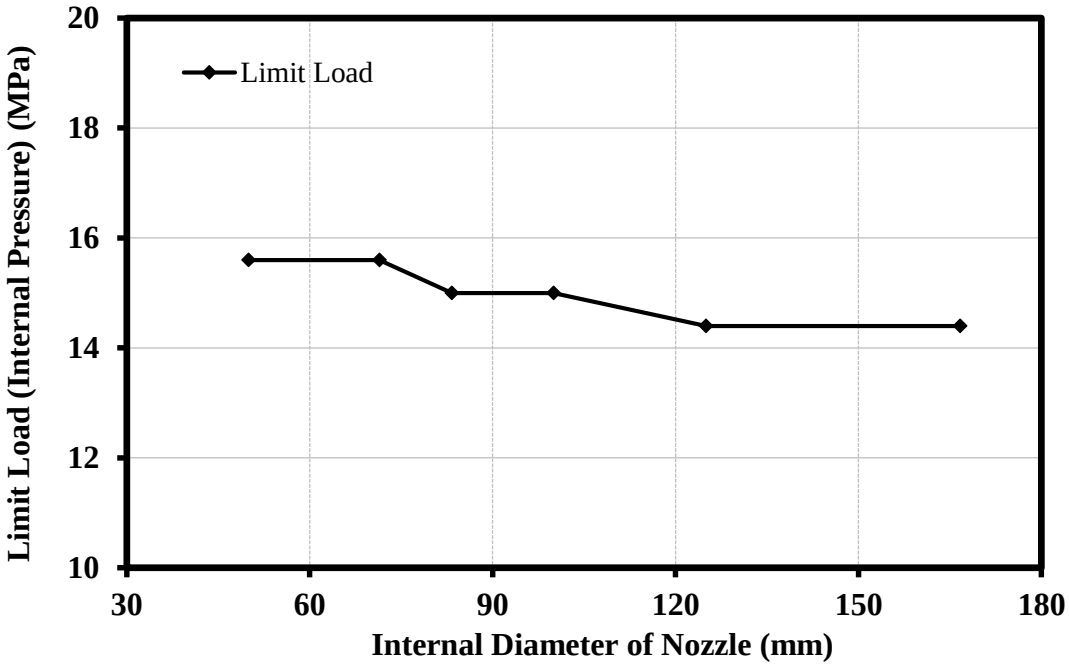

Figure 5. 3 Limit loads for changing nozzle diameter

As can be seen in **Figure 5. 3**, as the nozzle diameter increases, the maximum internal pressure that the system can bear decreases. The reason why the limit pressure magnitude decreases as the nozzle diameter increases, is that the opening in the main shell increases and reduces the available material to support the load.

5.2.2. Effect of Changing Nozzle and Shell Thicknesses

Here, the nozzle and shell inner diameters are kept constant. The thicknesses start from 5mm and is increased in 5mm increments and the analyses repeated. The load acting on the system is internal pressure only and limit internal pressure is established as seen in **Figure 5. 4**.

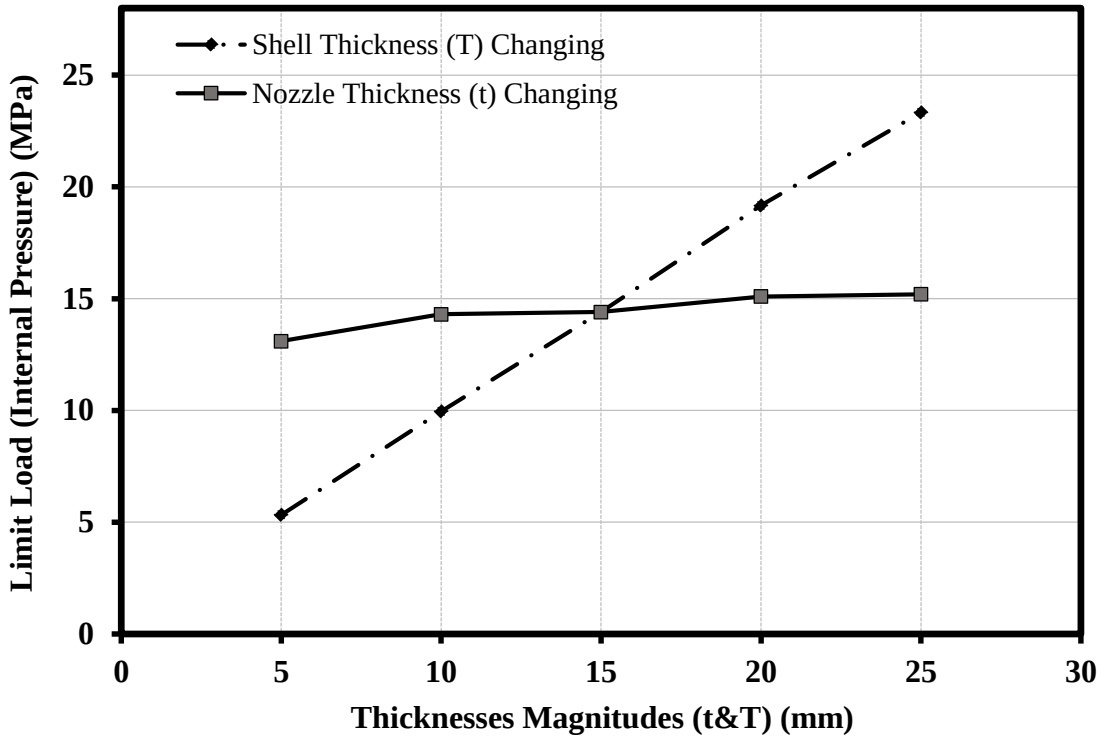

Figure 5. 4 Limit loads for changing thickness magnitudes for nozzle and shell

In both cases, as the wall thickness increases, the vessel becomes stiffer in supporting the internal pressure and larger loads are needed to develop plasticity in the system.

While a 20mm thickness increase in the nozzle increases the limiting internal pressure by about 14%, this rate is close to 80% greater for the shell. These results show that the effect of thickness change on the limiting internal pressure is about 5 times higher for the nozzle than the shell – that is the nozzle carries the load more effectively than the nozzle in this case.

5.2.3. Effect of Varying External Loads

Here, the limit external loads are investigated whilst maintaining constant internal pressure values. The external loads investigated comprise the axial(P), longitudinal (V_L) and circumferential forces(V_C). The loading conditions is shown in **Figure 5. 5**. Internal

pressure magnitudes are increased by 5MPa in each analysis. The results obtained from the analysis are shown in detail in **Figure 5. 6**.

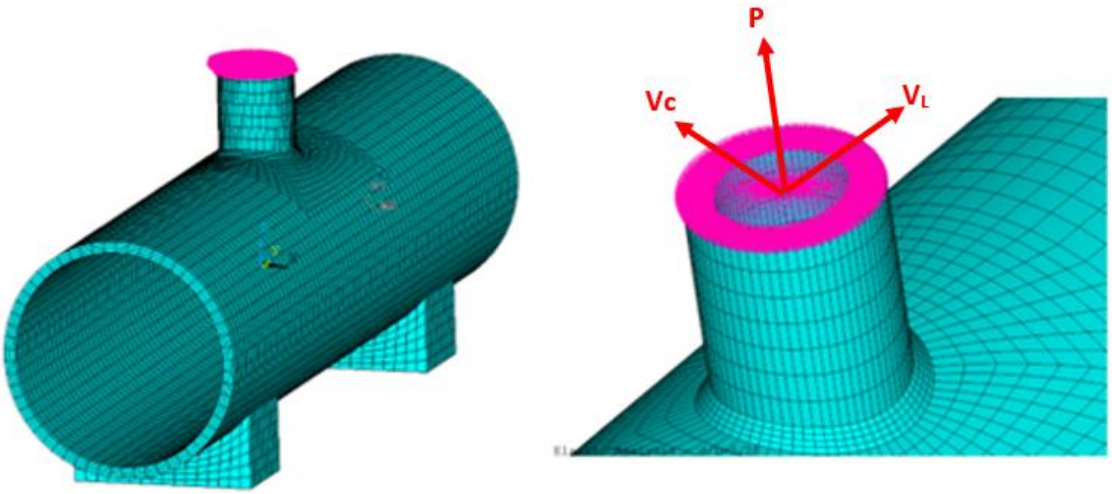

Figure 5. 5 Load conventions for the model

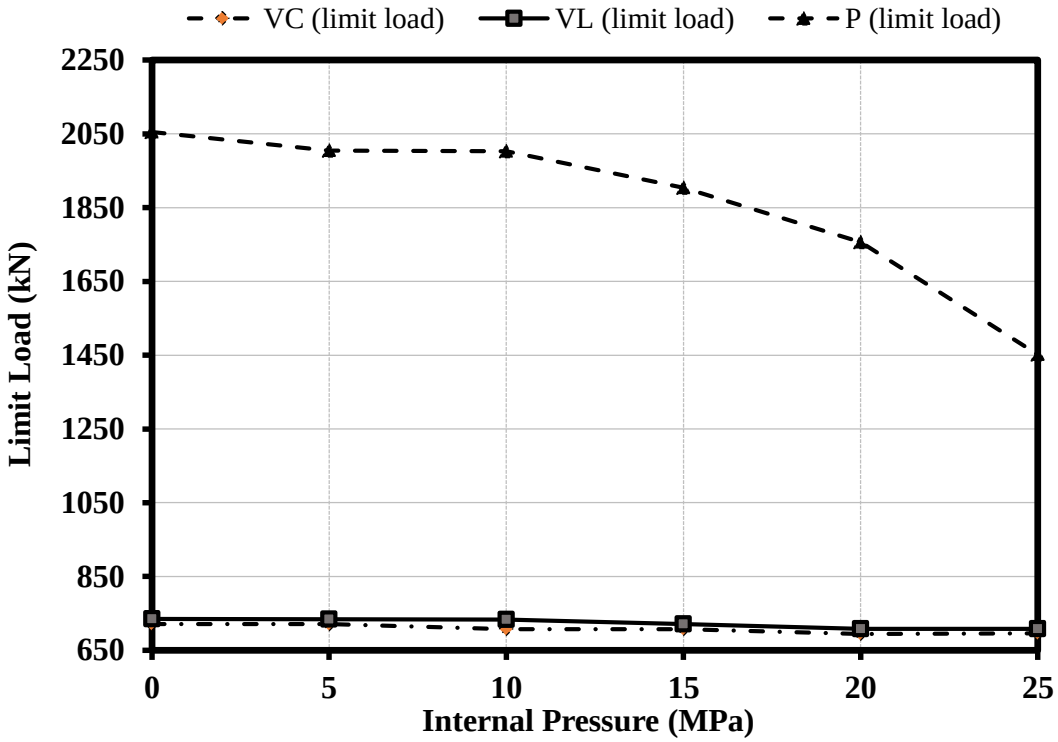

Figure 5. 6 Limit loads for changing external loads

It is clear the tensile force (P) applied in the Z direction according to the graph is much more dominant than the other loads. The increase in pressure of 25MPa in the system

leads to a 30% decrease in limit tensile force. In addition, the change in limit longitudinal and circumferential forces for the same rate of pressure increase is less than 2%. This is an indication that the limit load change is not affected by the pressure change when moment loads are present and it dominated by the pressure loading in the main.

As a result of this study, a comprehensive limit loading study was obtained for a nozzle-cylinder combination subjected to internal pressure and external loading conditions. First, the limit load calculations for the perfect cylinder were compared with the finite element limit analyses of the nozzle-cylinder junction under some parameters. In the obtained comparison analyses results, the limit load differences were less than 7%. This approach will allow researchers to have an idea about the problem and its results without waiting for modelling and FEA results in rapid engineering calculations. Finally, considering the limit load analysis for the combined load, the variation of the load parameters indicates the potential for overload carrying capacity when the load combinations act together with the internal pressure.

5.3. Full Elastic Plastic Analysis

The phenomenon of plasticity, with its simplest definition, is a permanent deformation given to a material under load. This means that the material cannot return to its original shape as a result of emptying a load on the structure. In pressure vessels, this may occur as a result of excessive pressure and cyclical loads. Under the influence of these forces, the container may collapse and even larger deformations may be caused in the event of an explosion. Considering these effects before manufacturing, design and analysis studies are carried out to avoid possible failure mechanisms. Practically, these studies are carried out in 3 stages: elastic stress analysis, limit loading (elastic - perfect plastic) analysis and plastic strain analysis after the loads on the container and damage modes are determined.

Since the plastic limit loads of the structure can be estimated thanks to full elastic-plastic analysis, this study has a great share in the predetermination of possible damages.

This section evaluates the elasto-plastic behaviour of the system for single and cyclic loading conditions at cylindrical pressure vessel-nozzle junctions under internal pressure. Firstly, a plastic internal pressure calculation is made for 5 different d/D ratios “by using TI and TES methods, which are widely used in the literature [40], [41], [42], [43], [44], [45] and frequently encountered. TES and TI method are two methods used to estimate the plastic limit load in the structure. Based on the load-deformation curve graph of the material in two applications. The method differences will be discussed in detail in the following sections. Finally, cyclic loading analysis are performed using the d/D and t/T parameters and the results are discussed.

5.3.1. Methodology - Determining Plastic Limit Load

Detection of plastic loads is of great importance in the design and analysis of pressure vessels. Especially for nozzle-connected pressure vessels, Twice Elastic Slope (TES) and Tangent Intersection (TI) Criteria are the main methods recommended for determining plastic limit loads. In this section, the application of these criteria are summarized.

The TES criterion is a characteristic load obtained from the load-deformation graph as a result of elastic-plastic analysis applied to the vessels. 2 times the angle of the elastic slop, Θ, represents the angle Φ and a line is drawn from there. This situation is formulated in **Equation 5. 3**. The TES criterion defines the point where this line intersects with the load-deformation curve as the limit burst load or the gross plastic load (P_{φ}). A representative illustration is given in the **Figure 5. 7**.

$$\varphi = tan^{-1}(2\,tan\,\theta)$$ **Equation 5. 3**

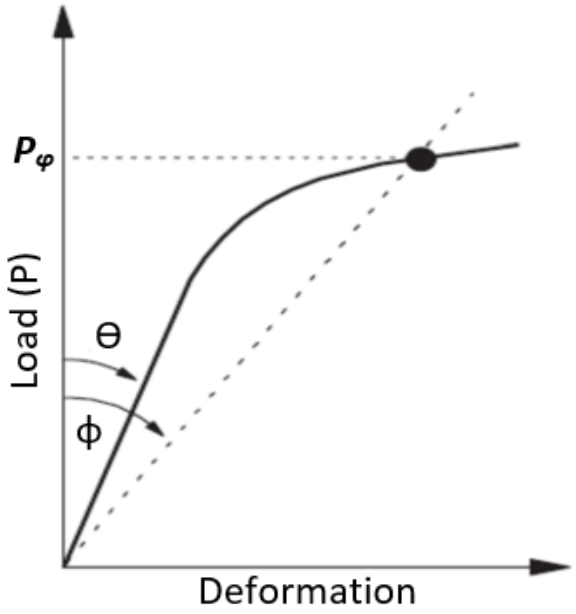

Figure 5. 7 Twice Elastic Slope (TES) Criterion

Tangent Intersection (TI) criterion is another widely used method to find plastic load. The TI criterion, like the TES criterion, defines the plastic load by using the load-deformation curve. A tangential line is drawn from the point where the maximum principal stress is 5 percent on the graph and intersects with the elongated elastic line. This intersection point is defined as the plastic load. A representative illustration is given in the **Figure 5. 8**. For more detailed information on the TI criteria application, the EN 13445 [4] draft standard can be consulted.

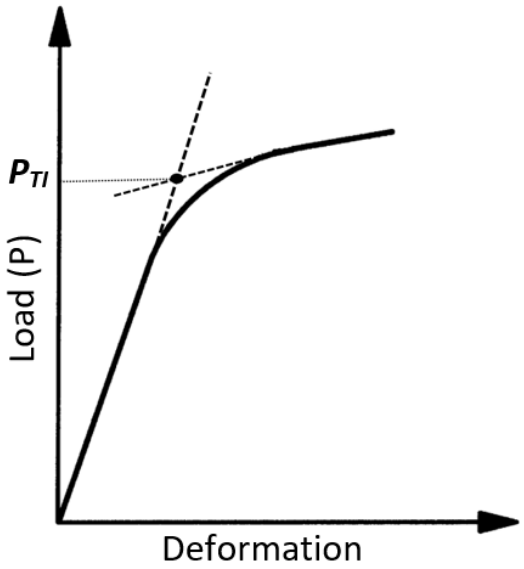

Figure 5. 8 Tangent Intersection (TI) Criterion

5.3.2. Stress-Strain Curve

For the two criteria (TES, TI) mentioned above, plastic load calculations can be made by using the load-deformation graphs. In order to estimate this graph, first of all, the stress-strain curve of the material and the strain values corresponding to each stress value must be determined. The material properties of the material to be used in this study are 260 MPa yield strength at the yield point and 485MPa ultimate strength at the ultimate point. Besides, Young modulus was determined as 200GPa and elongation 17.2%. Based on this information, with the Ramberg-Osgood approach [81], the total strain can be calculated as a function of the stress as seen in the **Equation 5. 4**.

$$\varepsilon = \frac{\sigma}{E} + 0.002\left(\frac{\sigma}{S_{ty}}\right)^{1/n} \qquad \textbf{Equation 5. 4}$$

where S_{ty} is the tensile yield strength of the material, n is the strain hardening exponent and e_f is the plastic strain at failure. The strain hardening exponent, n, is calculated as following **Equation 5. 5** the value of the n is 0.1403.

$$n = \frac{log(S_{tu}/S_{ty})}{log(e_f/0.002)}$$ **Equation 5. 5**

The strain values at the yield point are calculated with **Equation 5. 6**. below and its value is 0.0033. Here, a plastic strain value of 0.002 is also added to be consistent with the 0.2% offset method.

$$e_{yield} = \frac{S_{ty}}{E} + 0.002$$ **Equation 5. 6**

And finally, the strain value obtained at Ultimate Strength Points is calculated with the **Equation 5. 7** below and its value is 0.1724.

$$e_{ult} = \frac{S_{ty}}{E} + e_f$$ **Equation 5. 7**

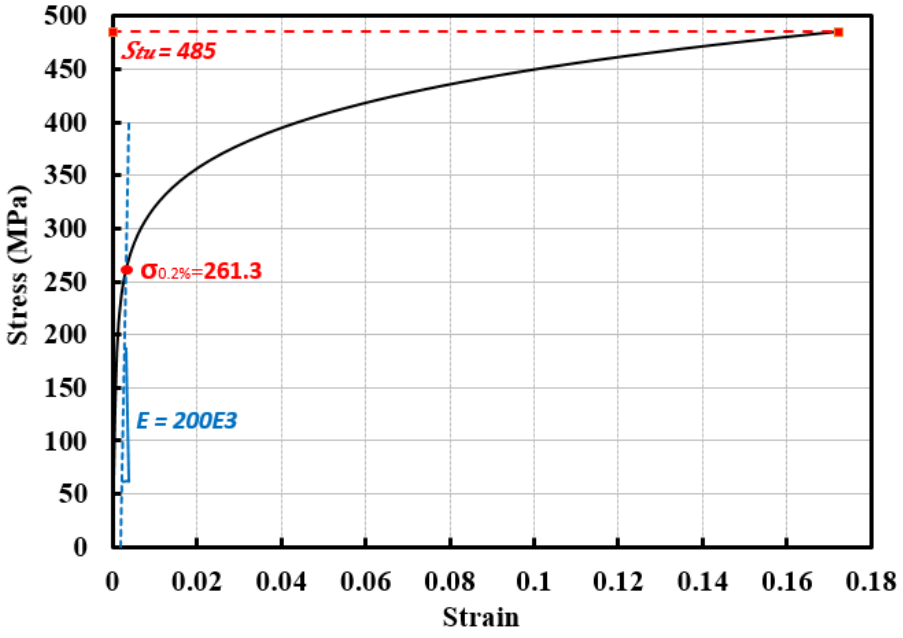

Figure 5. 9 Calculated Engineering Stress-Strain Curve

The engineering stress-strain curve obtained because of the calculations made with the Ramberg-Osgood equations is given in the **Figure 5. 9**.

5.3.3. TES and TI Criteria Implementation

In this section, a parametric study will be conducted in 3 different methods to determine the plastic load (internal pressure) values in an open-ended half-pressure vessel, whose front and side views are given in the **Figure 5. 10**. In modelling, the inner radius (Di) of the main cylinder is 500mm and the wall thickness (T) is fixed as 22.5mm and t/T is 1.0. Here, the inner diameter of the nozzle, in other words, the opening in the main cylinder will be increased at certain rates (di/Di = 0.05, 0.10, 0.15, 0.20, and 0.25) to obtain plastic load values.

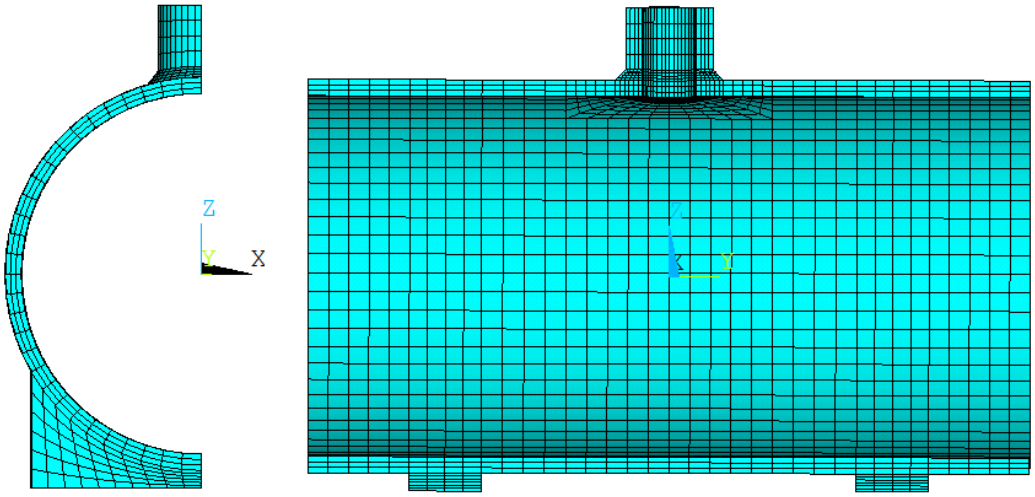

Figure 5. 10 Front and side views of the finite element model

In the previous section, the stress-strain diagram of the material was drawn with the Ramberg-Osgood approach. These stress-strain values were directly inputted in ANSYS, and Load-Strain graphics were obtained for each di/Di parameter with Multilinear Kinematic Hardening solutions.

For more detailed information about how the load-strain curves are obtained, the di/Di=0.25 case can be examined. First, points are selected at certain intervals from the

stress-strain graph of the material given in **Figure 5. 9**. For each of these points, there is a pressure value for the strain value corresponding to that point with the help of limit analysis in ANSYS. By using these obtained pressure values, load-strain graphs to be used in TES and TI methods are obtained. The pressure values obtained for 9 different strain values for the di/Di=0.25 condition are given in the **Table 5. 3**.

Table 5. 3 Determination of pressure values for Load-Strain graph drawing

Stress(MPa)	Strain(mm)	Load-Pressure(MPa)
0	0	0
260	0.0033	21.0
267.75	0.0037	21.64
286.92	0.0053	23.2
299.7	0.0068	24.3
363.6	0.0231	29.44
427.49	0.0705	34.61
459.44	0.1173	37.2
485.0	0.1724	39.317

After drawing the load-strain graph, the gross plastic load is found with the TES criterion firstly. As mentioned in Section 5.3.1. Methodology - Determining Plastic Limit Load, in this method, a line is drawn from 2 times the angle of the elastic slope, and the point where it intersects with the load-strain line is now the gross plastic load. The computed plastic loads are shown in **Figure 5. 11**.

As the second method, the plastic load will be detected with the TI criterion. In this method, a tangent is drawn from the 5 percent strain value. This tangential line is intersected with the extended elastic slope and the plastic load value is found. The plastic load values (P_{TI}) obtained for 5 different di/Di are shown in the **Figure 5. 12**.

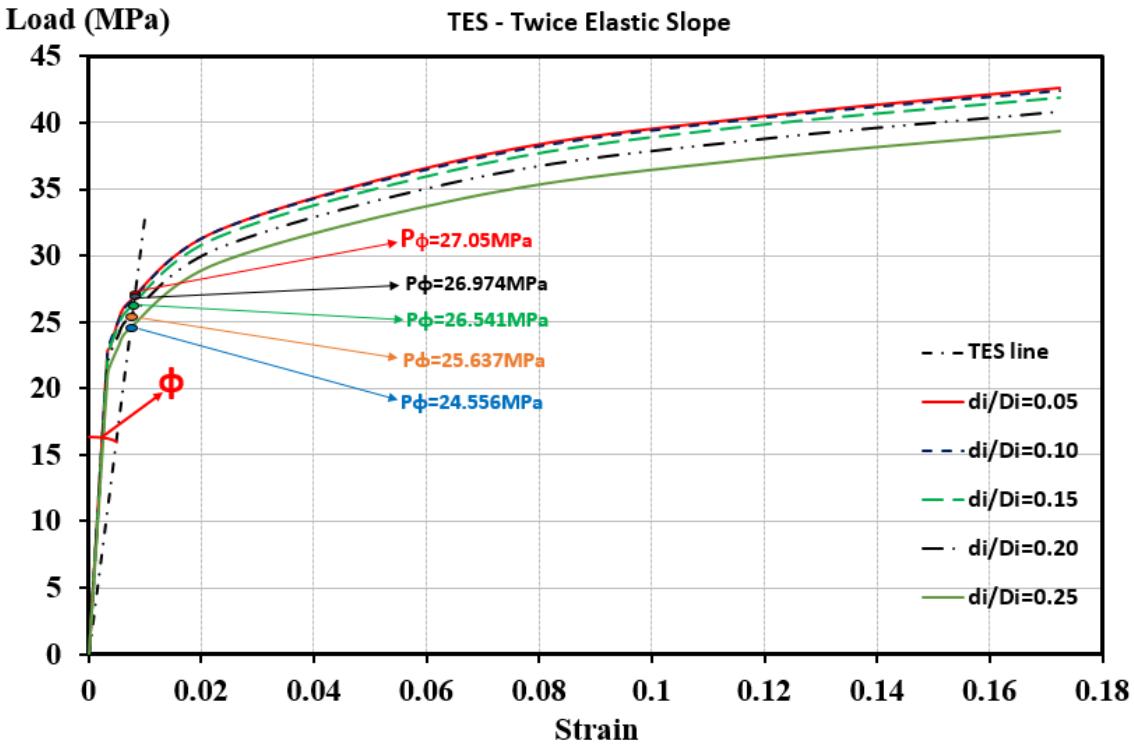

Figure 5. 11 Gross plastic loads according to TES criterion

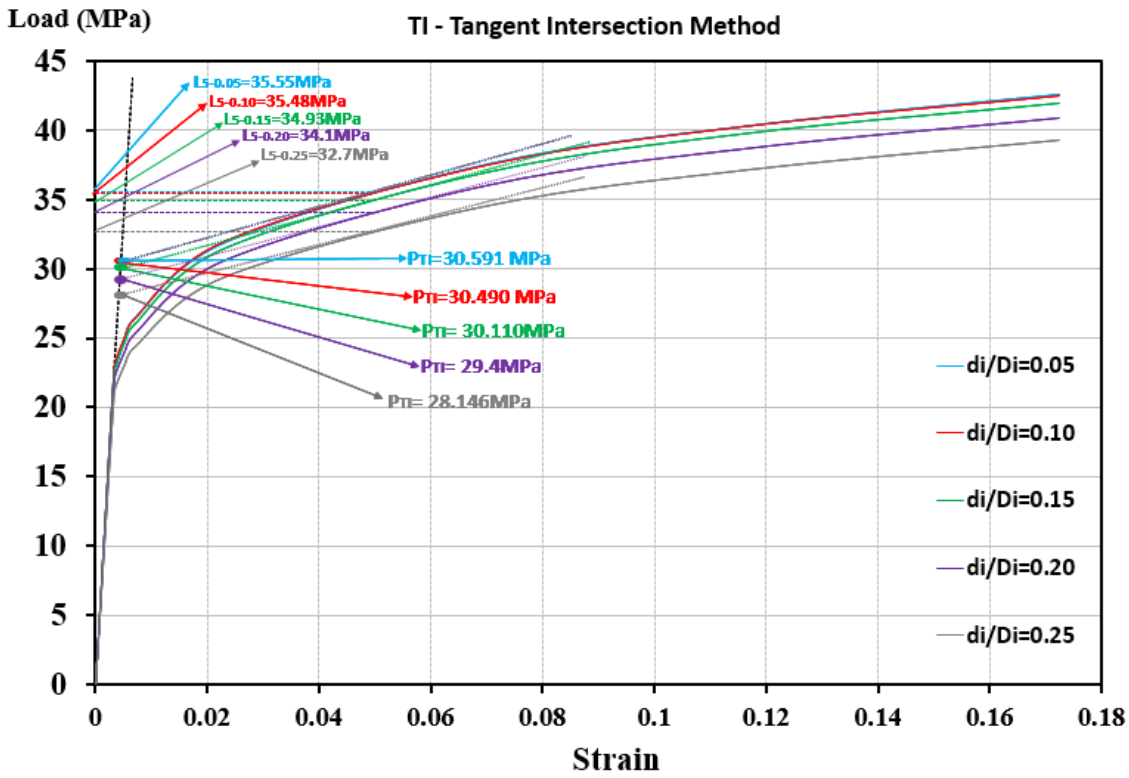

Figure 5. 12 Gross plastic loads according to TI criterion

5.5. Cyclic Loading Analysis

Plastic shakedown behaviour is one in which the steady state is a closed elastic-plastic loop, with no net accumulation of plastic deformation. Ratcheting behaviour is one in which the steady state is an open elastic-plastic loop, with the material accumulating a net strain during each cycle. For this reason, shakedown and ratcheting conditions should be examined since it is expected that a collapse will not occur at the end of possible cyclic loadings in designs. The highest load from which the shakedown is obtained is the deemed the shakedown load. If shakedown cannot be achieved, additional plastic strain is obtained after each cycle. This behaviour is called ratcheting. A representation of shakedown load and ratcheting behaviour in cyclic loads is given in **Figure 5. 13**.

Since shakedown loads are very difficult to determine, they are created for simple components only and are assumed to have perfect plastic behaviour in the material. Regarding nozzles and openings in pressure vessels, it is recommended that shakedown criteria be based on elastic strains. These assumptions are based on Leckie-Penny sphere/cylinder solutions [11].

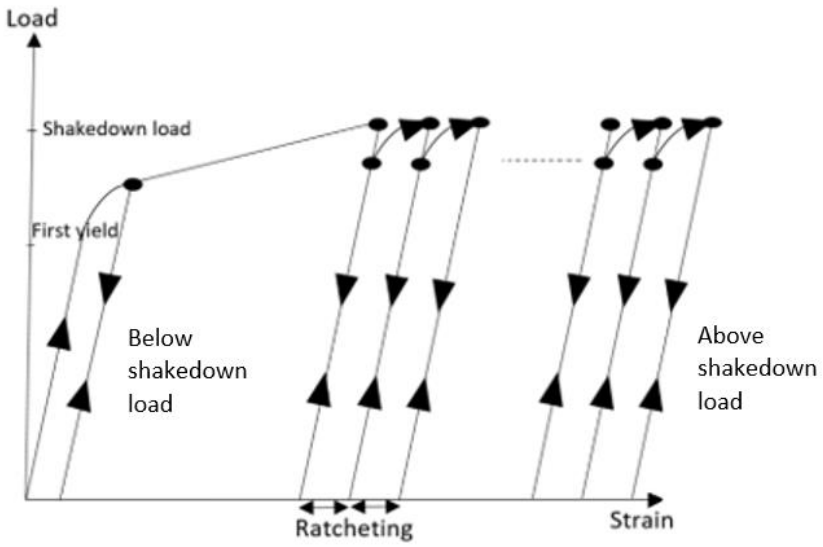

Figure 5. 13 The load-strain behaviour for cyclic loading

There are not many published experimental results for cyclic loading conditions in nozzle junctions. However, in a study conducted by Procter and Strong [82], studies were conducted on 6 different nozzles for cases with nozzle-vessel diameter ratio (d_m/D_m) 0.875, nozzle diameter - cylinder thickness ratio (d_m/T) 16, and nozzle - vessel thickness ratio (t/T) 0.373. In this study, the authors present a parameter study with test pressure and first yield pressure ratio. Here it is stated that the incremental strain drops to zero after 30 cycles for the case where the test pressure is $1.7*p_y$. In the case of $1.82*p_y$ they say that small incremental strains continue even after 45 cycles. In this way, they showed strain accumulations with increasing test pressure for the $p_y*1.6$ and $p_y*1.85$ ranges.

In this section, firstly, the analyses are repeated for $P_T/P_y = 1.7$ and $P_T/P_y = 1.82$ cases using the same parameters as the Procter & Strong approach. The results of the analyses performed in 100 cycles are given in **Figure 5. 14** and **Figure 5. 15**.

When the graphs are examined, as stated for the $P_T/P_y = 1.82$ case, small incremental strains continue even at the 100th cycle. However, it was observed that although Procter and Strong stated that the incremental strain dropped to zero after 30 cycles for the $P_T/P_y = 1.7$ situation, it continued even at the 100th cycle. For this purpose, for a more detailed analysis, solutions will be made with finite element analysis for different d_m/D_m ratios.

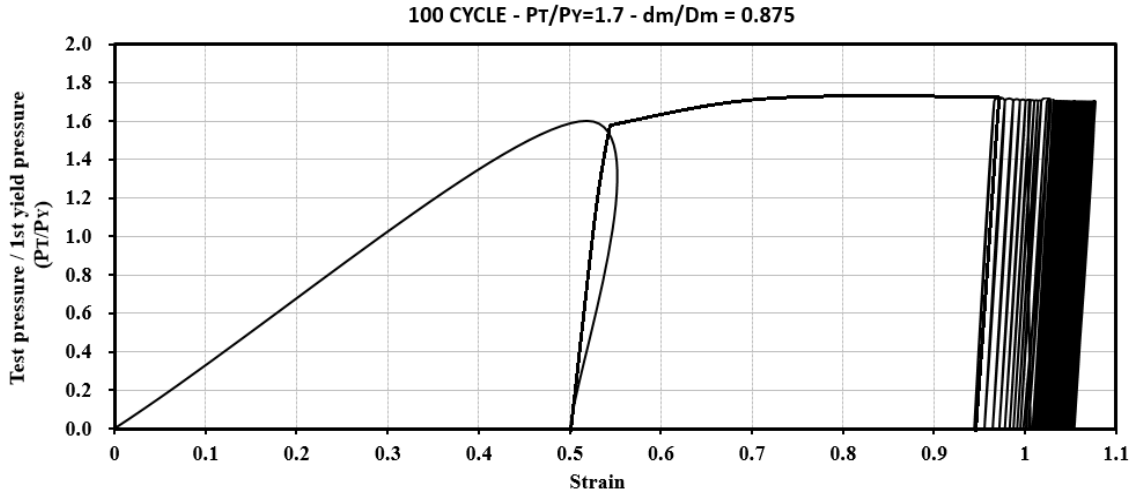

Figure 5. 14 Cyclic loading analysis results – 100 cycles, P_T/P_Y=1.7, dm/Dm=0.875

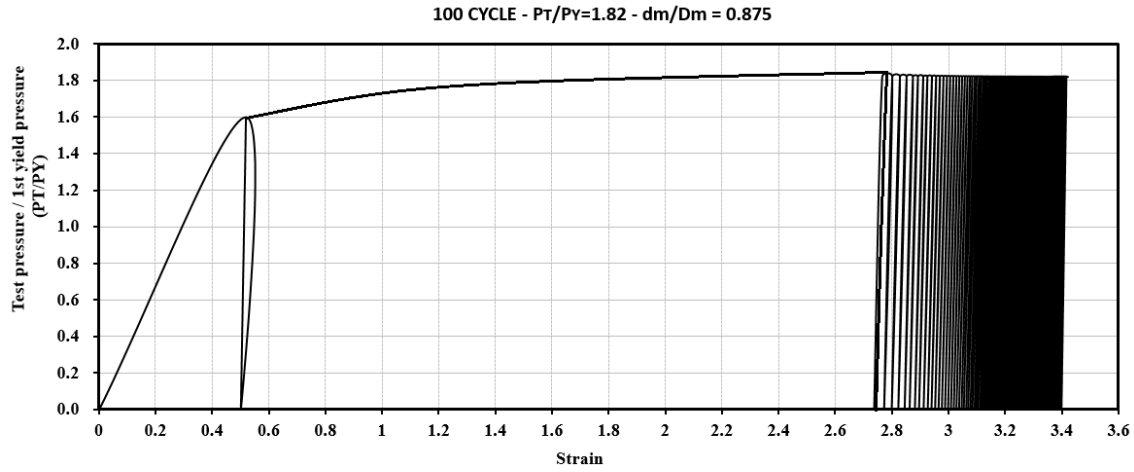

Figure 5. 15 Cyclic loading analysis results – 100 cycles, P_T/P_Y =1.82, dm/Dm=0.875

dm/Dm ratios will be determined by making changes only in the nozzle diameters so that the cylinder diameters remain the same. In the analyses, P_T/P_Y = 1.82 status will be examined first, and cyclic loading analyses were performed for 3 different d_m/D_m. The results are shown in **Figure 5. 16**, **Figure 5. 17**, and **Figure 5. 18**.

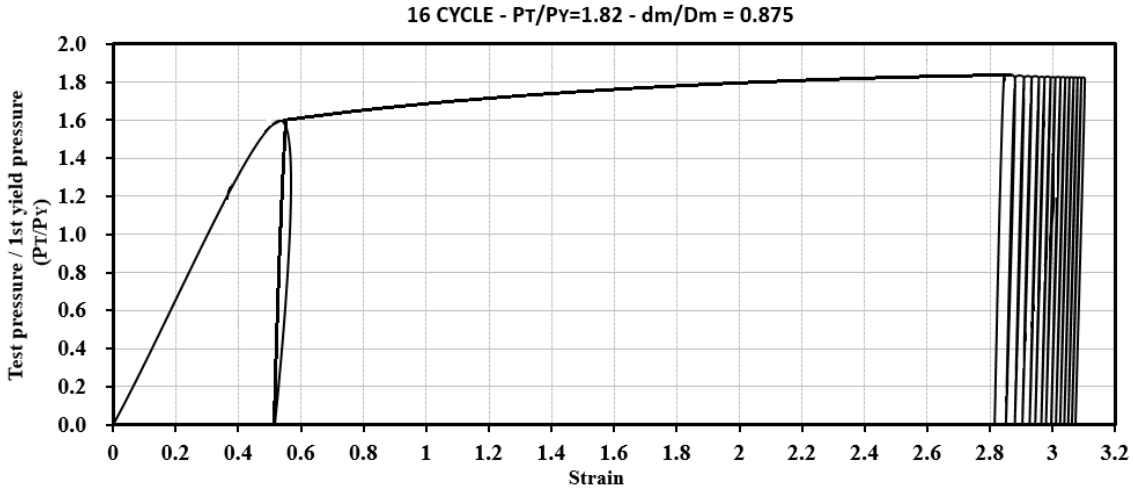

Figure 5. 16 Cyclic loading analysis results – 16 cycles, P_T/P_Y =1.82, dm/Dm=0.875

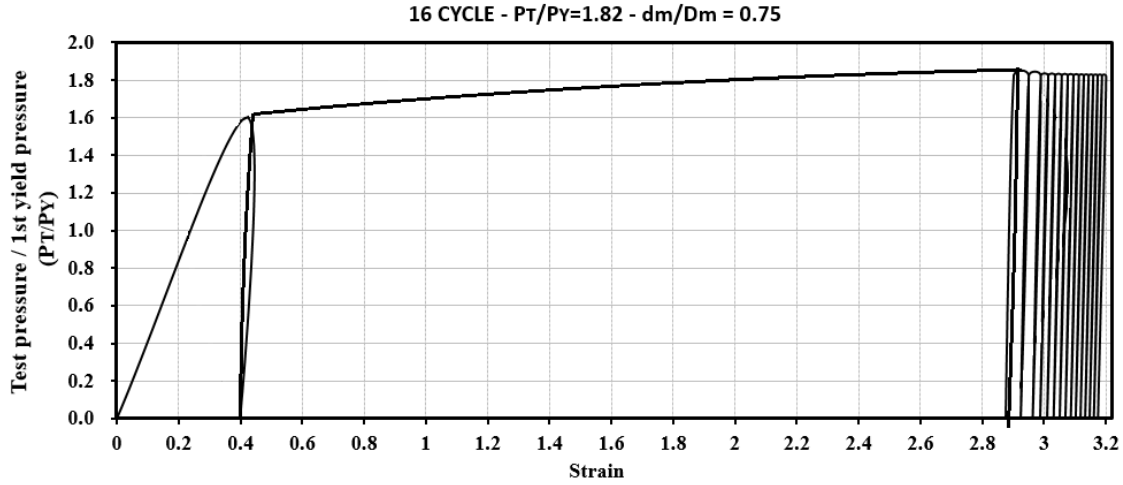

Figure 5. 17 Cyclic loading analysis results – 16 cycles, P_T/P_Y =1.82, dm/Dm=0.75

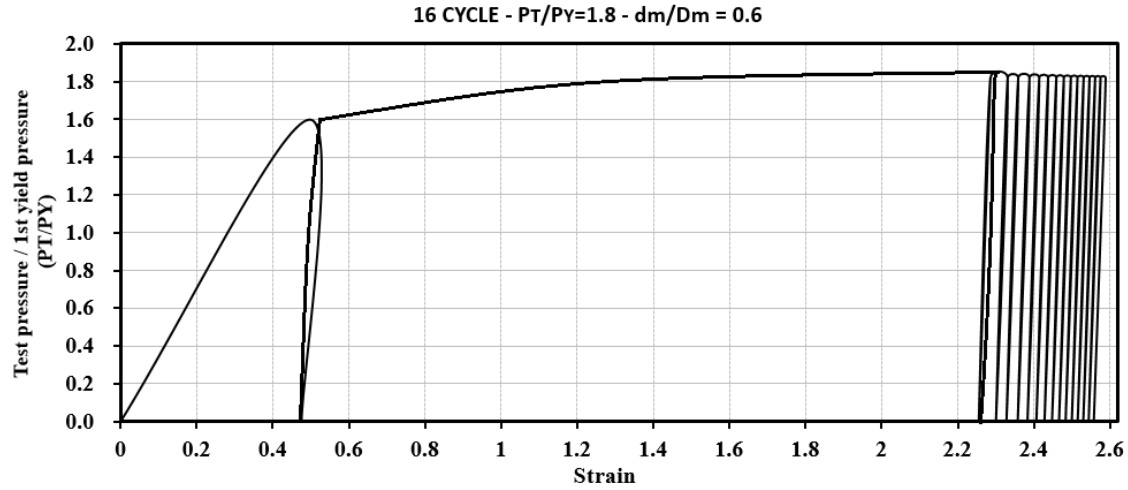

Figure 5. 18 Cyclic loading analysis results – 16 cycles, P_T/P_Y =1.80, dm/Dm=0.6

As can be seen from the graphs, as the d_m/D_m ratio decreases, the vessel reaches the burst pressure and therefore, FEA solution cannot be obtained in case of $P_T/P_y = 1.82$. In case $d_m/D_m = 0.6$, P_T/P_y value can be the highest 1.8 to obtain cyclic loading solutions. For this reason, the analyses were repeated in the case of 1.7 *p_y at the same d_m/D_m ratios. The results are shown in **Figure 5. 19**, **Figure 5. 20**, and **Figure 5. 21**.

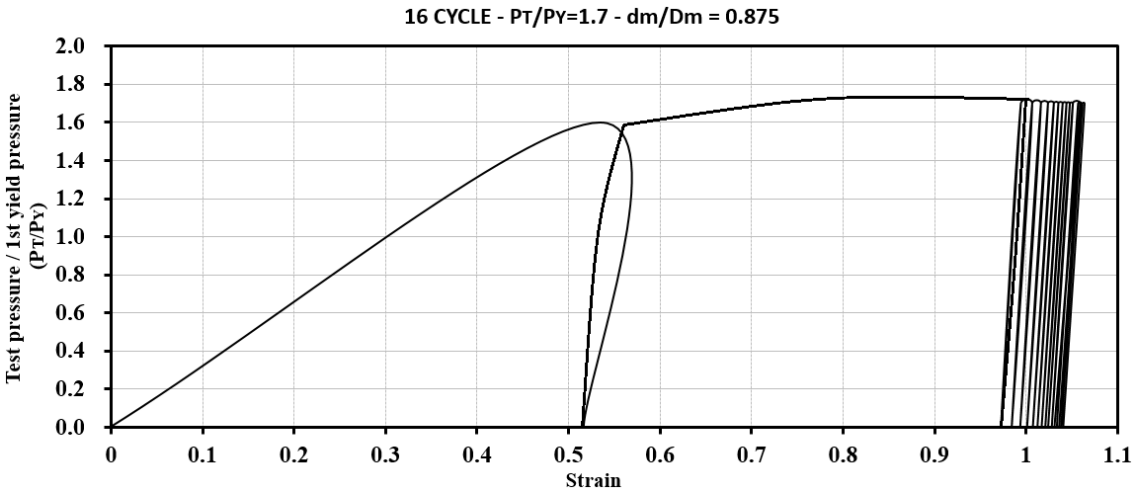

Figure 5. 19 Cyclic loading analysis results – 16 cycles, P_T/P_Y =1.7, dm/Dm=0.875

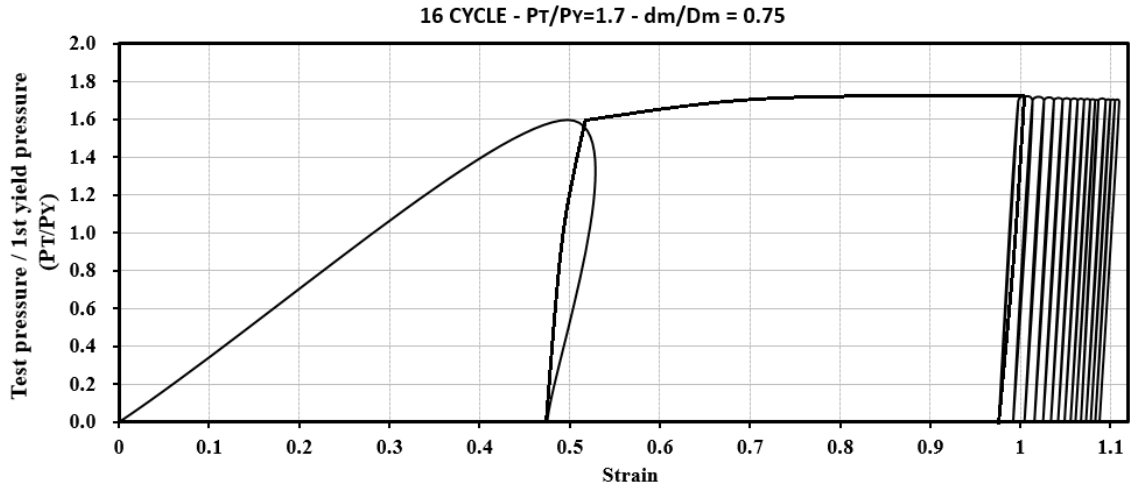

Figure 5. 20 Cyclic loading analysis results – 16 cycles, P_T/P_Y =1.7, dm/Dm=0.75

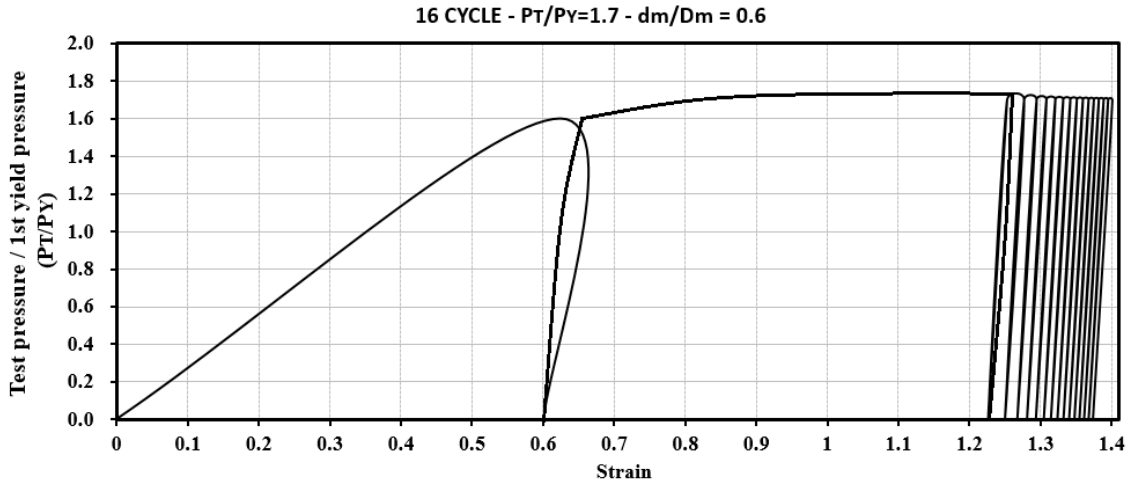

Figure 5. 21 Cyclic loading analysis results – 16 cycles, P_T/P_Y =1.7, dm/Dm=0.6

As can be seen from the graphs, as the d_m/D_m ratio decreases, the strain values increase for the same low cycle case. Because the nozzle diameter decreases, and this increases the resistance of the vessel to internal pressure. As the number of cycles increases, the additional plastic strain after each cycle decreases and tends to decrease in ratcheting value.

All these analyses obtained with the Procter & Strong approach show that it can be difficult to find the maximum test pressure value as the d_m/Dm ratio changes. Also, as it can be seen from the graphs, the maximum test pressure value will change as the nozzle diameter increases. In order to reveal a more localized and standard cyclic loading study on the yield pressure, a value of P_T/P_y =1.7 rather than 1.82 gave more accurate solutions to examine the total strain and ratcheting changes in low cycle analyses.

5.6. Concluding Remarks

In summary, in this section, studies were carried out on 3 different analysis methods. These are elastic – perfectly plastic (limit load) analyses, full elastic – plastic analyses and cyclic loading analyses. Firstly, limit analyses made for nozzle cylinder intersections and perfect cylinder limit load calculations without nozzle connection were compared.

For this comparison, only internal pressure is used since there cannot be an external load acting on the nozzle in the perfect cylinder. The close results obtained with differences of less than 8%, provided pressure vessel designers with a rapid engineering calculation approach without the need for modelling and FEA for nozzle connections. Then, it was concluded that this FE model is suitable for limit loadings and the internal pressure and external loading conditions of the model were examined under various dimension parameters. In this way, the load carrying capacity of the pressurized cabin was examined in detail according to the load conditions and size changes.

In the second part, full elastic plastic analyses were performed. In these analyses, TES and TI methods, which are frequently encountered, were used for the estimation of the plastic limit load. These methods were examined under various di/Di parameters and plastic limit load estimations were made.

Finally, cyclic loading analyses were performed for different dm/Dm parameters. As a result of the analyses made, examinations were made on the P_T/P_Y ratio recommended by Procter & Strong for test pressure, and it was seen that the P_T/P_Y=1,82 value was very high at some points and that the structure would undergo plastic collapse in a very short period of time with this value.

After all the elastic, limit load, plastic and cyclic load analyses carried out so far, it was decided to examine the breaking conditions of the structure. For this purpose, potential crack modelling and calculation of stress concentration factors for nozzle-cylinder intersections under different loading conditions will be presented in the next section.

CHAPTER 6- INVESTIGATION OF THE FRACTURE BEHAVIOUR ON PRESSURE VESSEL - NOZZLE JUNCTIONS

6.1. Description of the Fracture Mechanics and A General Overview

Cracks are found in many engineering structures, including machinery, buildings, and other structural members such as steel structures. Initial defects (micro cracks, inter granular spaces, corrosion, air bubbles formed during casting) in machinery and structural elements subjected to repeated loads may turn into crack propagation over time. These cracks can cause a massive damage in the form of breakage. Fracture mechanics studies damage that is determined almost entirely by fracture. The first successful work in this field was carried out by Griffith in 1920 [83]. In his study, Griffith observed the progression of brittle cracks in glass. In this work, Griffith formulated how a pre-existing crack would begin to propagate by introducing a simple energy balance. Elastic strain energy in a system tends to decrease as the crack progresses, and this energy is the energy required for fracture surfaces to occur.

The Griffith approach was also applied to the brittle fracture of metallic materials by Zener and Hollomon in 1944 [84]. Because it is not possible to include permanent deformation as a constant value specific to each material in Griffith's approach, this relation cannot be used directly for metals. In the 1950s, Irwin developed fracture principles for metallic materials based on the Griffith criteria [85]. Thus, he pioneered the development of Linear Elastic Fracture Mechanics (LEFM). In addition, as a result of the studies carried out with the stress intensity factor approach, the susceptibility of materials to subcritical cracking such as fatigue crack propagation or stress corrosion cracking has become predictable to some extent.

Since Linear Elastic Fracture Mechanics (LEFM) is applicable where plastic deformation in the crack tip region is limited, Elastic-Plastic Fracture Mechanics (EPFM) comes into play when significant plastic deformation occurs in the crack tip region. This work began in 1961 with Wells' work under the name of crack opening displacement (COD) [86].

After the Industrial Revolution, in the 19th century, there was a great increase in the use of metal in buildings. However, due to the damage to these structures, accidents that caused great loss of life and property were also seen. Although some of the accidents were due to design errors, over time it was understood that a much larger part of these damages occurred due to production errors due to the initiation of cracks in the materials and breakage of structural elements. With the development of fracture mechanics and crack propagation methods, better production methods have been used, and the damages caused by the prevention of defects in the material internal structures have been reduced to minimum levels. Today, efforts are still being made to develop these studies.

6.2. Methodology

Pressure vessels can be subjected to various external local forces and moments acting in combination with main internal pressure. As a result of the stress system set up, and in the presence of attachment welds, surface cracks can occur on the interior and exterior walls. If these cracks cannot be detected at an early stage, there is a real potential for the vessel to rupture with obvious dangerous consequences. The behaviour of fractured or geometric discontinuity structures can be investigated with linear elastic fracture mechanics (LEFM) parameters. The stress intensity factor (SIF) is the leading one, and with correct calculations, it can produce the stress intensity in the crack tip region. In cylinder-cylinder intersections subject to local loads, the maximum stress distribution

occurs in and around these opening areas and failure in the system usually occurs in this region.

Using this approach, the present study develops three-dimensional mixed mode stress intensity factor solutions on for external cracks on nozzle joints in cylindrical pressure vessels nozzle junctions for a variety of geometrical configurations. This was undertaken using a finite element approach and employing a bespoke software tool and solver, FCPAS - Fracture and Crack Propagation Analysis System — to create the finite element mesh and propagation characteristics. From this, a parameter study examining the influence of the crack shape, size and position was carried out with a fixed pressure vessel nozzle cylinder intersection geometry configuration and the appropriate stress intensity factors identified and reported. The FCPAS tool is shown to be an effective approach to modelling and characterizing cracks in pressure vessel nozzles.

6.3. FCPAS (Fracture and Crack Propagation Analysis System)

FCPAS (Fracture and Crack Propagation Analysis System) [74] is a finite element based software that can perform fracture and crack propagation analysis in three-dimensional problems. By using enriched elements along the crack tip, the FRAC3D program provides an efficient and accurate calculation of stress intensity factors (KI, KII and KIII) without the need for special meshing in the crack region and post-analysis requiring a very long post-processing.

In order to make these calculations, the creation of models, the creation of meshing, and the application of boundary conditions and loads are done using ANSYS. Then, the finite element model information, boundary conditions and load data from ANSYS are

converted to FCPAS format. Finally, the FCPAS Solver is run to solve the crack problem and determine the stress intensity factors for the problem of interest.

The chart below (**Figure 6. 1**)shows the general algorithm and file structure of the process.

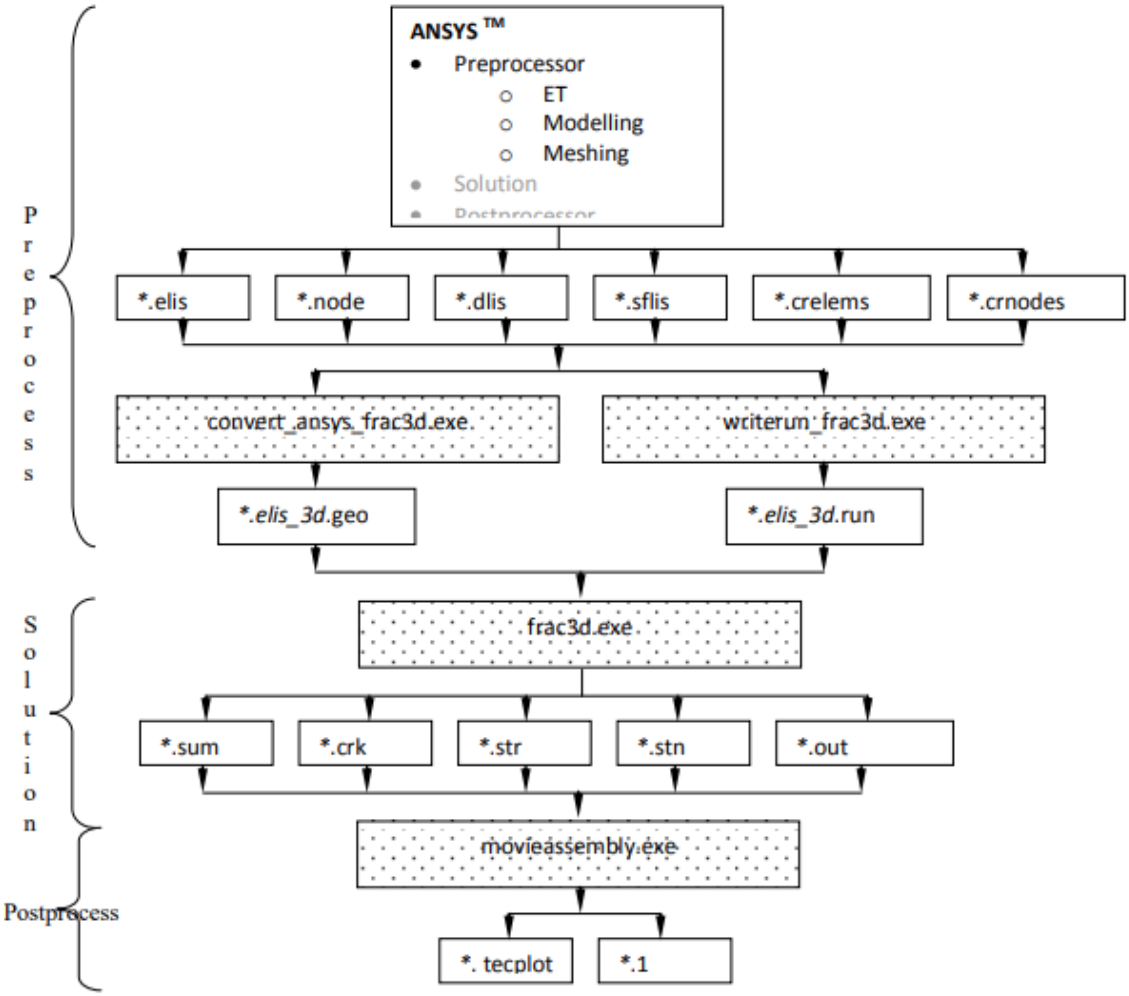

Figure 6. 1 General flow of the analysis process[74]

6.4. Statement of the Problem and Mixed Mode SIFs Calculation Method

In this section, mixed-mode stress intensity factors will be calculated for some potential crack profiles that may occur in the crotch corner and upper weld region of the nozzle cylinder joints. In 3D mixed mode crack propagation problems, the size and direction of

the crack changes with the magnitude and direction of the forces acting on the system. FCPAS (Fracture and Crack Propagation Analysis System) is used for mixed-mode 3D SIF calculations. This program provides efficient and accurate calculation of stress intensity factors (KI, KII and KIII) using enriched elements along the crack tip.

When nozzle connections in pressurised vessels are examined, the areas where the stress is maximum are located on the crotch corner on the inner surface (a) and on the weld joints on the outer surface (b). The stress level here is highest at the crotch corner and welding (shown in red) according to the loading condition, while the stress level decreases as you move away from this region. Maximum stress locations are shown in **Figure 6. 2**.

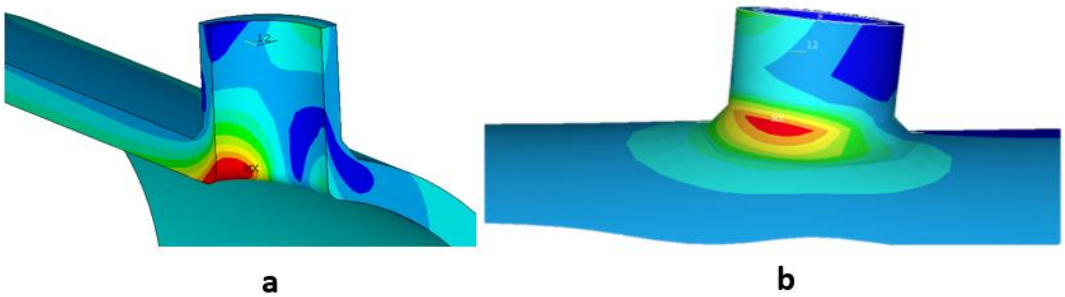

Figure 6. 2 Typical maximum Von Mises stress zones in cylinder - cylinder connections

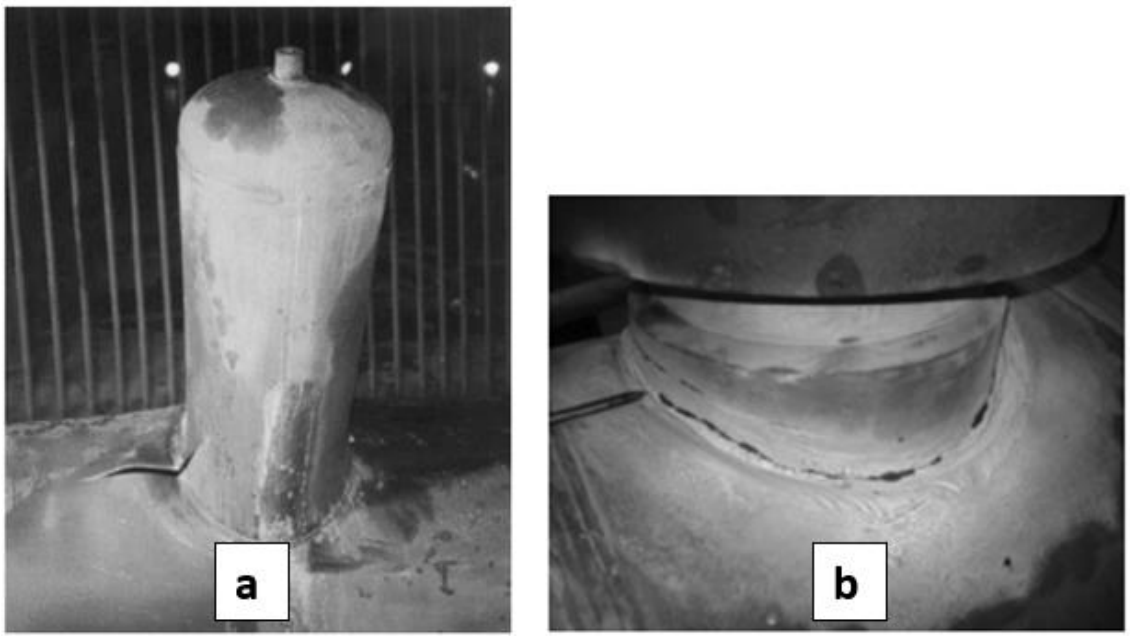

Figure 6. 3 a) perpendicular crack on nozzle -cylinder connections *[87]* **and b) transverse cracks on the weld on nozzle -cylinder connections** *[88]*

Two different situations supporting this information are shown in the **Figure 6. 3**. In **Figure 6. 3. a**, cracks are shown perpendicular to the nozzle, and in **Figure 6. 3. b**, along the weld path, cracks are shown. In Figure a, it usually starts with a small crack opening in the crotch corner, and then the container ruptures with crack progression. In Figure b, it cannot carry the loads on the welding zone, and it shows itself as a crack in the outer wall. For this reason, these two conditions are generally taken into consideration when modelling cracks in nozzle-cylinder junctions. In addition to this, all fracture problems start with a small crack and then breakage, tear or rupture occurs in the form of crack progression. It is also very difficult to predict the exact shape of the crack. For this reason, analyses should be performed with various crack length and crack diameter parameters during the modelling and analysis phase.

Figure 6. 4 shows a nozzle separated from the cylinder and a surface crack located over the weld zone, and **Figure 6. 5** shows a representative surface crack located on the crotch corner.

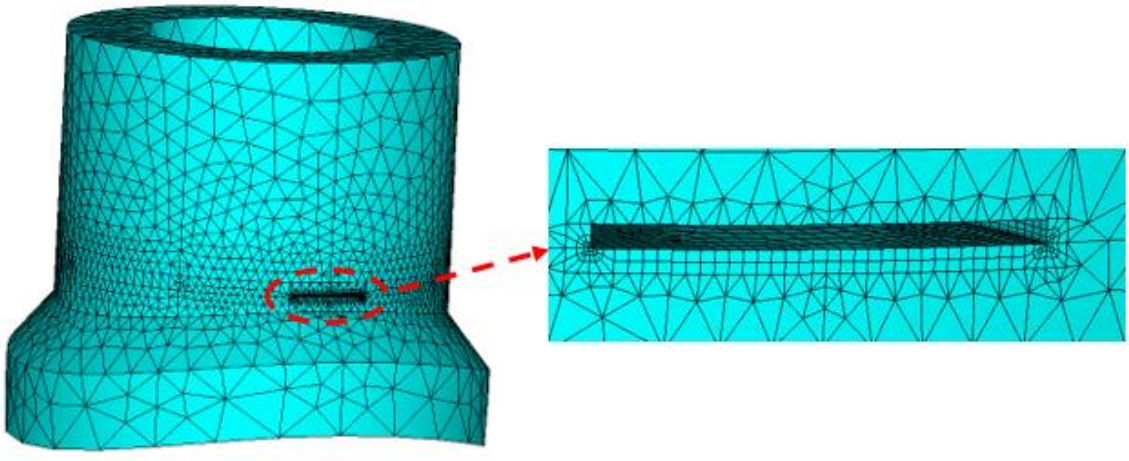

Figure 6. 4 Representation of outer wall crack location and modelling

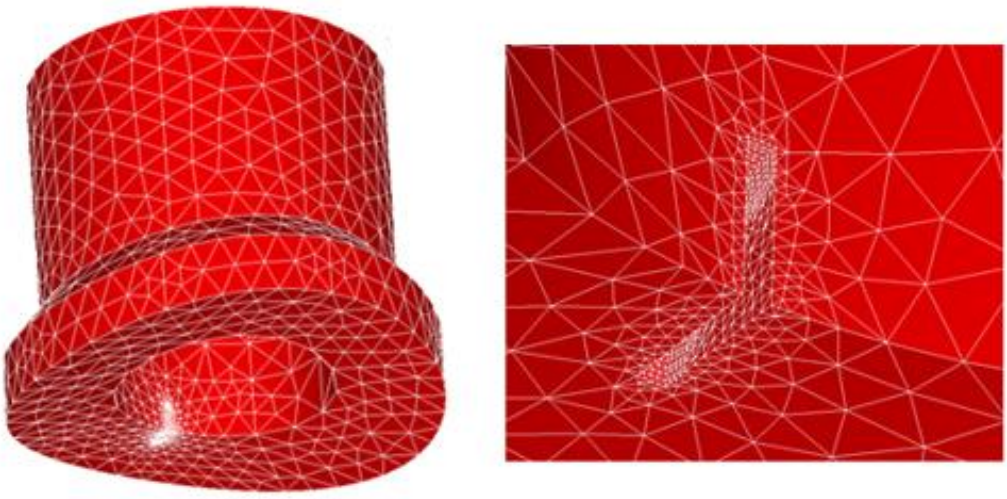

Figure 6. 5 Representation of inner wall crack location and modelling

In the finite FE model of the cracked model, the most important location is the crack opening region. For this reason, there are some improved methods when meshing in this region. One of them is the enriched element method. In this method, an element size of 0.01 is first assigned to the crack tip. An area mesh is created from the crack tip field and this mesh is swept along the crack path. For this reason, the cracked volumes have the appearance of brick mesh. As the remaining volumes have crack spaces, sweep mesh cannot be applied. For this reason, free mesh is applied to other volumes with tetrahedron elements.

In the finite element model with cracks, the elements touching the crack tip are defined as enriched elements and a representative image of the enriched elements is given in **Figure 6. 6**.

The elements shown in **Figure 6. 6** that directly touch the crack front are enriched elements and coloured in pink. The elements represented in orange colour are called transition elements and they act as a bridge with other regular finite elements moving along the crack path.

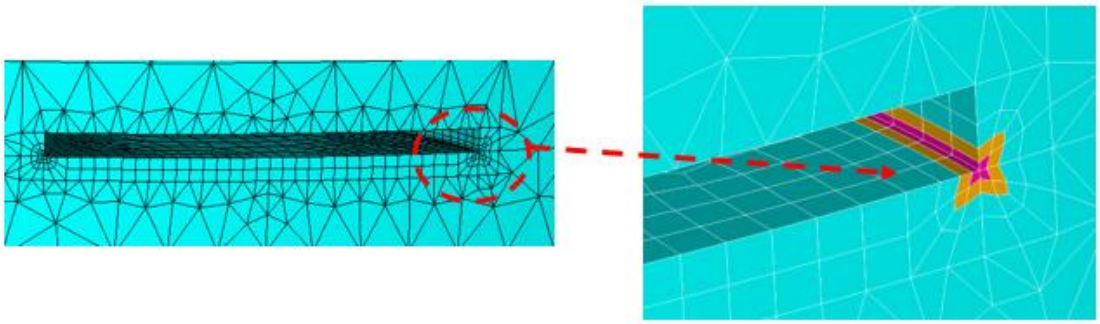

Figure 6. 6 A representative view of enriched and transition elements running along the crack

In addition to the conventional finite element formulation, these elements also contain the stress intensity factors located at the crack tip as unknown. For an integration point in ξ, η and ρ local coordinates in an enriched element, the u, v and w displacements are calculated with the equations [73] [89] given below.

$$u(\xi,\eta,\rho) = \sum_{j=i}^{m} N_j(\xi,\eta,\rho)u_j + Z_0(\xi,\eta,\rho)\big(f_u(\xi,\eta,\rho) - \sum_{j=i}^{m} N_j(\xi,\eta,\rho)f_{uj}\big)\big(\sum_{i=1}^{ntip} N_i(\Gamma)K_I^i\big) + Z_0(\xi,\eta,\rho)\big(g_u(\xi,\eta,\rho) - \sum_{j=i}^{m} N_j(\xi,\eta,\rho)g_{uj}\big)\big(\sum_{i=1}^{ntip} N_i(\Gamma)K_{II}^i\big) + Z_0(\xi,\eta,\rho)\big(h_u(\xi,\eta,\rho) - \sum_{j=i}^{m} N_j(\xi,\eta,\rho)h_{uj}\big)\big(\sum_{i=1}^{ntip} N_i(\Gamma)K_{III}^i\big)$$

$$v(\xi,\eta,\rho) = \sum_{j=i}^{m} N_j(\xi,\eta,\rho)v_j + Z_0(\xi,\eta,\rho)\big(f_v(\xi,\eta,\rho) - \sum_{j=i}^{m} N_j(\xi,\eta,\rho)f_{vj}\big)\big(\sum_{i=1}^{ntip} N_i(\Gamma)K_I^i\big) + Z_0(\xi,\eta,\rho)\big(g_v(\xi,\eta,\rho) - \sum_{j=i}^{m} N_j(\xi,\eta,\rho)g_{vj}\big)\big(\sum_{i=1}^{ntip} N_i(\Gamma)K_{II}^i\big) + Z_0(\xi,\eta,\rho)\big(h_v(\xi,\eta,\rho) - \sum_{j=i}^{m} N_j(\xi,\eta,\rho)h_{vj}\big)\big(\sum_{i=1}^{ntip} N_i(\Gamma)K_{III}^i\big)$$

$$w(\xi,\eta,\rho) = \sum_{j=i}^{m} N_j(\xi,\eta,\rho)w_j + Z_0(\xi,\eta,\rho)\big(f_w(\xi,\eta,\rho) - \sum_{j=i}^{m} N_j(\xi,\eta,\rho)f_{wj}\big)\big(\sum_{i=1}^{ntip} N_i(\Gamma)K_I^i\big) + Z_0(\xi,\eta,\rho)\big(g_w(\xi,\eta,\rho) - \sum_{j=i}^{m} N_j(\xi,\eta,\rho)g_{wj}\big)\big(\sum_{i=1}^{ntip} N_i(\Gamma)K_{II}^i\big) + Z_0(\xi,\eta,\rho)\big(h_w(\xi,\eta,\rho) - \sum_{j=i}^{m} N_j(\xi,\eta,\rho)h_{wj}\big)\big(\sum_{i=1}^{ntip} N_i(\Gamma)K_{III}^i\big)$$

In the above equations, Nj represents element shape functions for ξ, η, and ρ local coordinates. Z0 is the reset function that varies between 0 and 1. fu, gu, hu, fv, gv, hv, fw, gw and hw are derived from analytically known functions in asymptotic crack tip

displacement expressions and mod-I, mod-II and mod-III transferred from the local coordinate system to the global coordinate system. represent the displacement components. m takes the value 10 or 20 depending on the element type. The expression of $\left(\sum_{i=1}^{ntip} N_i(\Gamma) K_{I,II,III}^{i}\right)$ represents the change of stress intensity factors of edge elements touching the crack front. Γ is s the local isoparametric coordinate and takes values between -1 and 1 [73] [89].

6.5. Verification Studies

6.5.1. 1st Verification Example

In this study, the aim is to obtain 3-dimensional mixed-mode stress intensity factors of various crack profiles that may occur on the nozzle outer wall. The values of the stress intensity factors are obtained using FCPAS as previously stated. A validation study is undertaken in this section to show that the method achieves the correct results. Newman-Raju's work was used to show the accuracy of the method. In summary, Newman, and Raju [54] studied internal surface cracks in cylindrical pressure vessels in 1980. In their studies, stress intensity factors were determined by changing parameters such as crack length, crack depth, the wall thickness at certain rates. The study includes calculations in mode-I opening mode only. In this section, an elliptical crack was inserted into a cylindrical vessel, similar to Newman-Raju's approach. The model used by Newman-Raju and the resulting half finite element model is shown in detail in **Figure 6. 7** and **Figure 6. 8**, respectively.

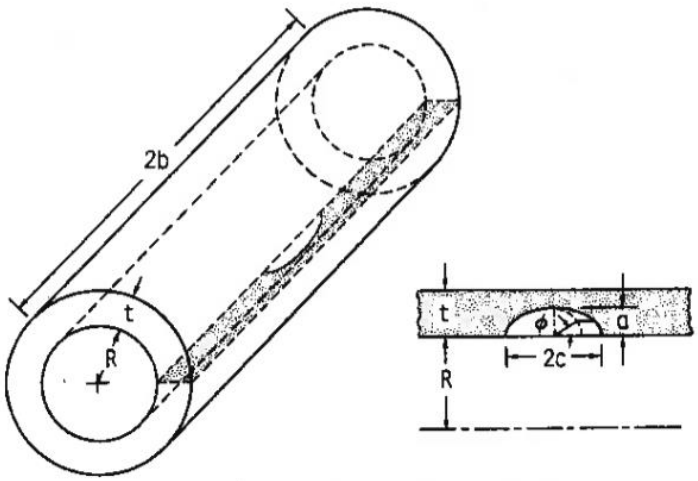

Figure 6. 7 Internal surface crack in a cylinder (Newman-Raju's model) *[54]*

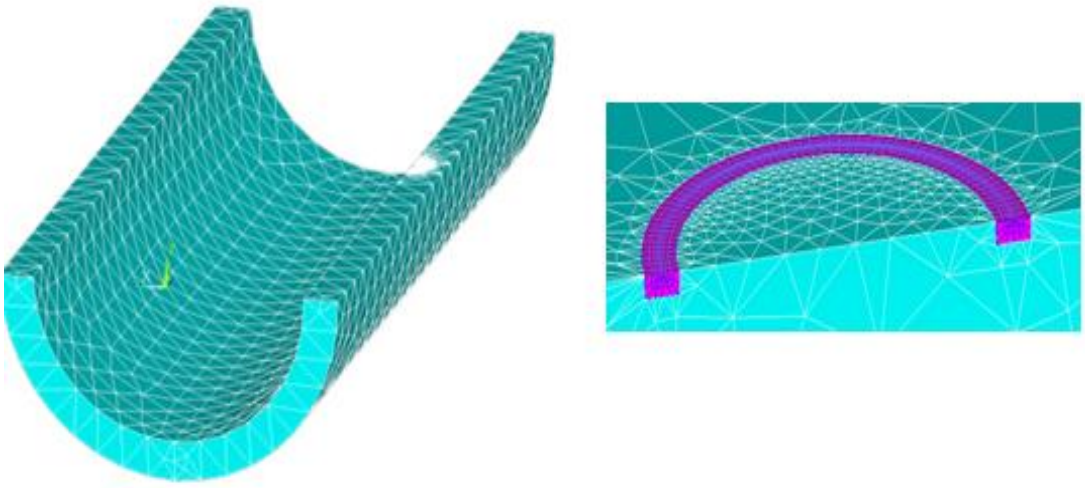

Figure 6. 8 Finite element modelling of Newman-Raju approach

Newman-Raju studies only include KI SIFs calculations, and these calculations are given in the following equations.

$$K_I = \frac{pR}{t}\sqrt{\pi\frac{a}{Q}}F\left(\frac{a}{c},\frac{a}{t},\frac{R}{t},\emptyset\right) \qquad \textbf{Equation 6. 1}$$

$$Q = 1 + 1.464(a/c)^{1.65} \qquad \textbf{Equation 6. 2}$$

$$F_i = \frac{t}{R}\left(\frac{R_o^2}{R_o^2 - R^2}\right)\left[2G_0 - 2\left(\frac{a}{R}\right)G_1 + 3\left(\frac{a}{R}\right)^2 G_2 - 4\left(\frac{a}{R}\right)^3 G_3\right] \qquad \textbf{Equation 6. 3}$$

In this equation, G_j values are taken from the tables in the current article in accordance with the parameters to be used. The inner diameter of the cylinder is determined as 250 mm. Also, the wall thickness is 25mm, the crack radius and depth are 12.5mm and the internal pressure to be applied is 10MPa. In line with this information, KI stress intensity factor.

In this equation, Gj values are taken from the tables in accordance with the parameters to be used [54]. The inner diameter of the cylinder is determined as 250 mm. Also, the wall thickness is 25mm, the crack radius and depth are 12.5mm and the internal pressure to be applied is 10MPa. The KI stress intensity factor values are then calculated at 9 different points from 0 degrees to 180 degrees with Newman-Raju approach. As a result of the calculations obtained, the comparison results are given in **Figure 6. 9**.

As can be seen from **Figure 6. 9**, the results obtained are very close to each other and differences of SIFs are nearly six per cent at the point where the difference is highest. There are some factors in making this difference. In the current study, there is a lack of information regarding boundary conditions and determination of cylinder length. For this reason, a cylindrical pressure vessel seated on 2 saddles was used in verification in order to be consistent with other analysis. In this way, all boundary conditions are applied under saddles and the cylinder is completely free to movement in all directions. In addition, KII and KIII values were ignored in the study. This difference is quite reasonable when these factors are taken into consideration.

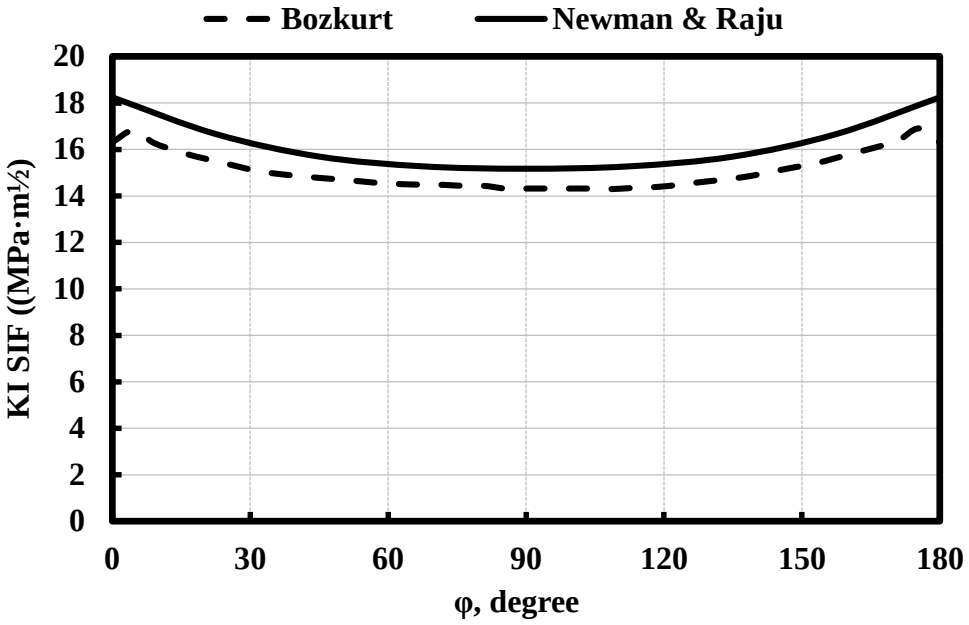

Figure 6. 9 Verification of Bozkurt solution with Newman & Raju approach

6.5.2. 2nd Verification Example

For the second verification, Sedighiani's study [90] was used. In this study, Sedighiani obtained normalized SIF values for the cracks occurring in the nozzle outer wall. The model used by Sedighiani is symbolized as follows in **Figure 6. 10**.

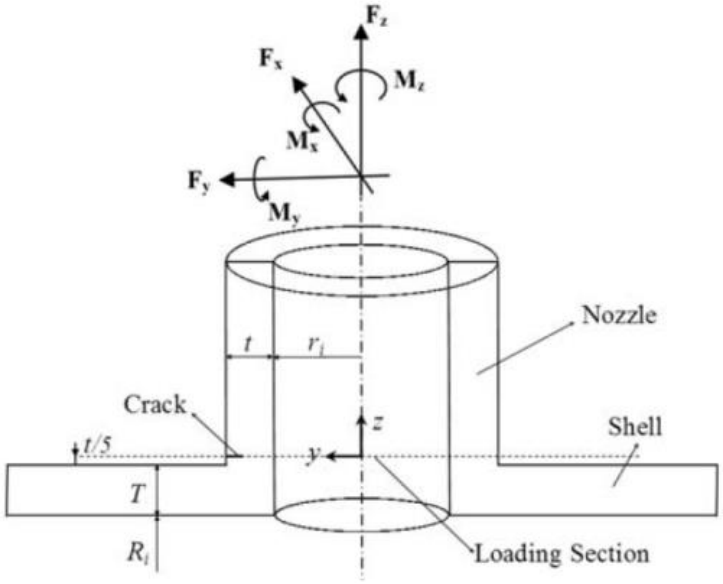

Figure 6. 10 Geometry and main parameters of nozzle - cylinder connections *[90]*

The parameters to be used in the verification study are as follows.

a/c = 0.3, a/t = 0.2, t/rm = 0.3, rm/Rm = 0.2, t/Ts = 1

As in the previous study, some assumptions have been made in addition to the existing parameters in the modelling phase since the boundary conditions and some measurements in the model are missing. The vessel is restricted the movement for all directions from the saddles sub-area, allowing the movement of the vessel in all directions.

During the calculation phase, YI, YII and YIII values are used to show the KI, KII and KIII to normalized. Equations are shown in **Equation 6. 4** - **Equation 6. 6**.

$$Y_I = \frac{K_I}{\sigma_0\sqrt{\pi a}} \qquad \textbf{Equation 6. 4}$$

$$Y_{II} = \frac{K_{II}}{\sigma_0\sqrt{\pi a}} \qquad \textbf{Equation 6. 5}$$

$$Y_{III} = \frac{K_{III}}{\sigma_0\sqrt{\pi a}} \qquad \textbf{Equation 6. 6}$$

Here YI, YII and YIII represent mode-I, mode-II, and mode-III. The following formulation **Equation 6. 7** is used for shear and axial load calculations.

$$\sigma_0 = \frac{F_j}{\pi\left(r_0^2 - r_i^2\right)} \qquad \textbf{Equation 6. 7}$$

In the analysis, the First step was to determine the nozzle length. Due to external loads are made from the centre of the nozzle, the length of the nozzle directly affects the stress intensity factors. For this purpose, the tensile load was applied in Z direction for 3 different nozzle lengths and the analyses were repeated. Results for YI values only are given in **Figure 6. 11**.

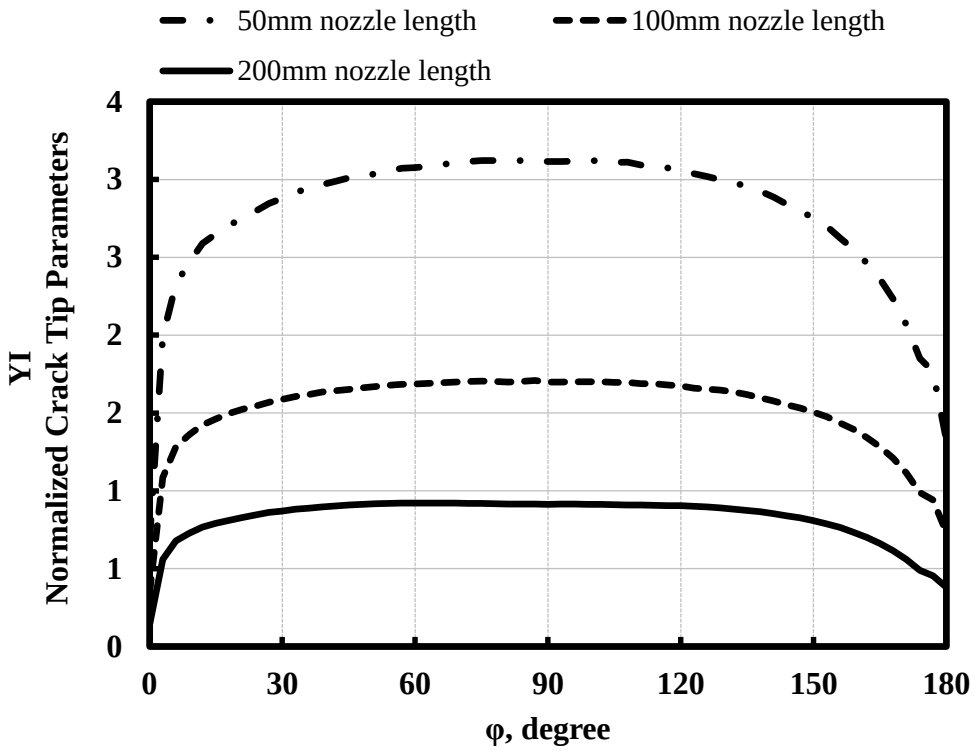

Figure 6. 11 YI normalized SIF distributions for determining the correct nozzle length

As seen in the figure, as the nozzle sizes increase, the stress intensity factors increase linearly. Since it is very difficult to detect the exact length for comparison, the 50mm long nozzle, which is the closest value, have been found suitable for comparison. The analysis with the above-mentioned parameters was repeated and the comparison results are given in **Figure 6. 12**.

When the results given above are examined, similar trends along the crack and very close results were obtained for YI and YIII values. For the YII case, more linear SIF values emerged throughout the crack, rather than the current study. The reason why these small differences occurred is because the boundary conditions are uncertain, as mentioned earlier. Also in this study, the link element method was used to apply the loading from the nozzle centre. In the Sedighiani's study, it was not stated how this loading was done centripetally. Finally, when the nozzle dimensions are determined exactly, it is clear that

the results are much closer. The computations obtained in the light of these results are consistent.

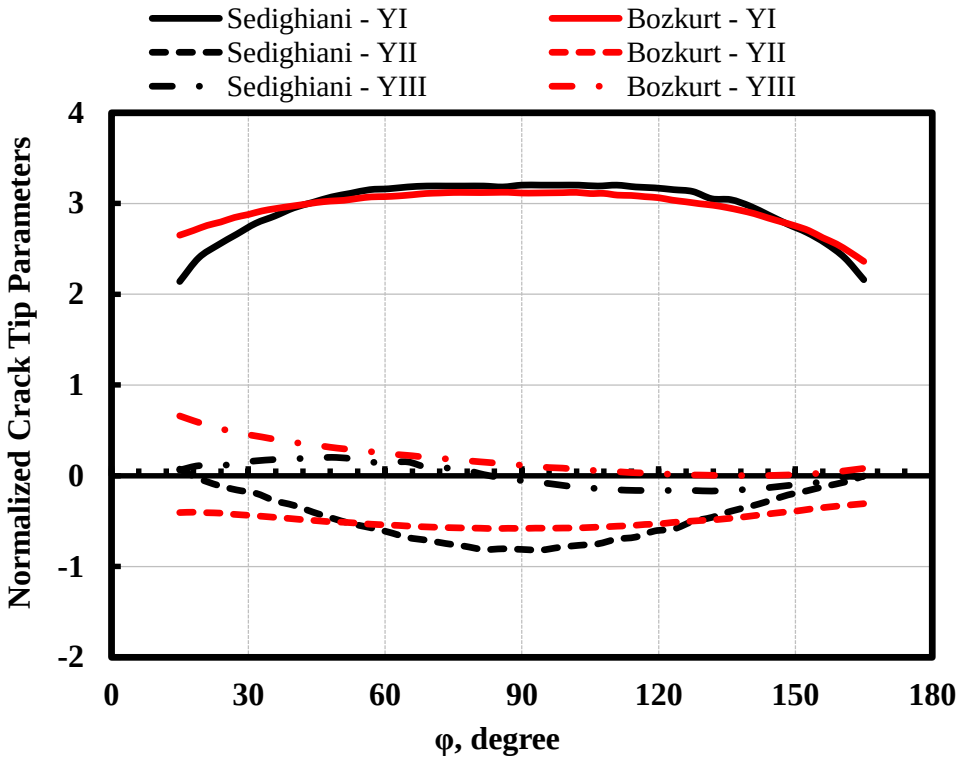

Figure 6. 12 Verification of the YI, YII and YIII normalized SIF distributions

6.6. Parameter Studies

6.6.1. Internal surface crack SIF computing on nozzle – cylinder junction

In this section, the SIF values of the cracks placed on the crotch corner under various loadings along the crack were calculated. Firstly, SIF values are obtained for 6 different crack depth and crack diameter ratios (a/c). Then, by keeping the crack radius (c) constant, the crack depth (a) is changed, and the values of the stress intensity factors are obtained. In the next step, the effect of the internal pressure change for a fixed a/c value is investigated. Stress intensity factors are obtained based on the different crack angles. Finally, external loading cases are examined. In external loading, firstly, forces are

applied to the X, Y and Z directions individually from nozzle centre. Thereafter, studies employing combinations of loadings are performed by means of a parameter study Stress Intensity Factor values are obtained using FCPAS (Fracture and Crack Propagation Analysis System).

6.6.1.1. Changing the ratio of crack depth and crack radius (a/c)

Here, crack modelling was undertaken by changing the ratios of crack depth to crack radius. Mixed mode SIF values were obtained along the crack for 7 different ratios. 40 elements were used throughout the crack in modelling. In the graphics obtained, point 0 represents crack start and point 1 represents the crack end. The elements placed between the points 0 and 1 are named as non-dimensional crack tip position in the graphic and are shown in **Figure 6. 13**.

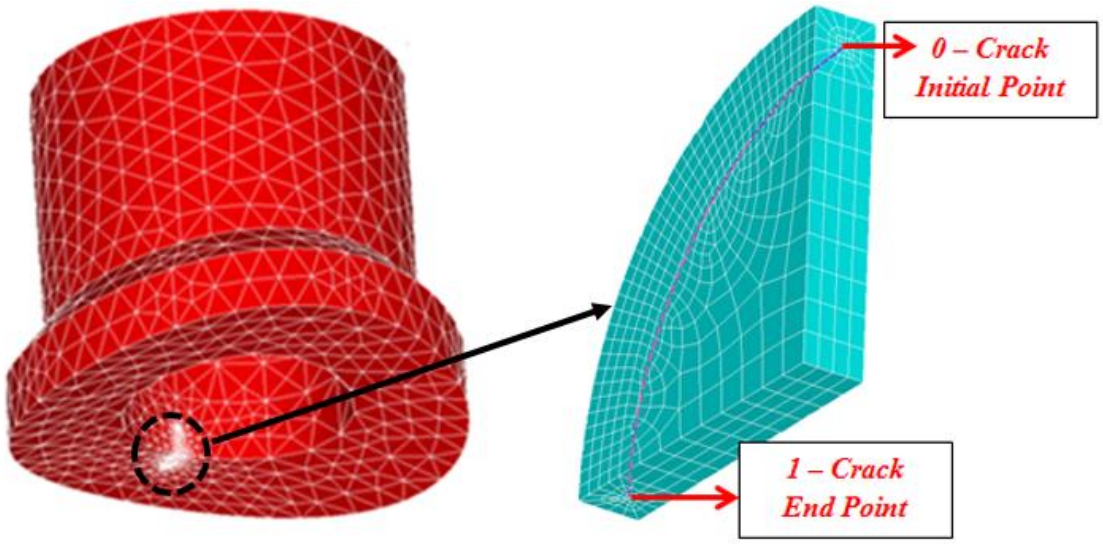

Figure 6. 13 Non-dimensional crack tip position

In the analysis performed, the crack depth (a) is 10mm and is constant for all ratios. In addition, 10MPa internal pressure acts on the pressure vessel inner surface. For a/c variation analysis, the crack is positioned at an angle of 90 degrees to the X-axis. For this

reason, crack opening acts like pure mode-I (opening) and there are no results for mode-II (sliding) and mode-III (tearing) effect. Von-Mises stress distributions for a/c=1,33 ratio is shown in **Figure 6. 14** and zoomed picture for crack opening is shown in **Figure 6. 15**.

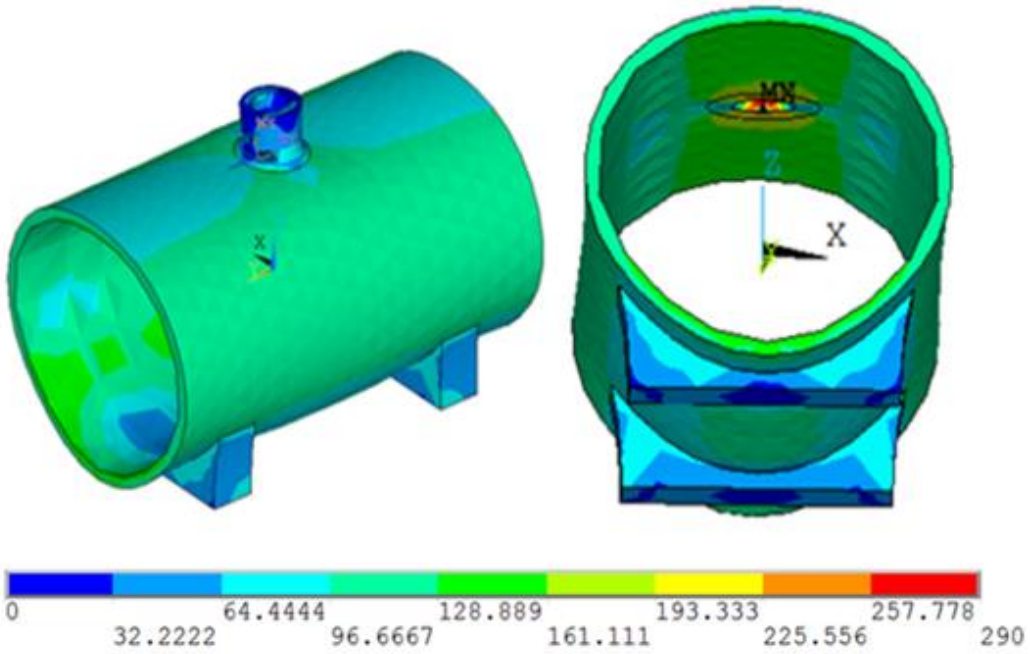

Figure 6. 14 Von-Mises stress distributions and crack opening

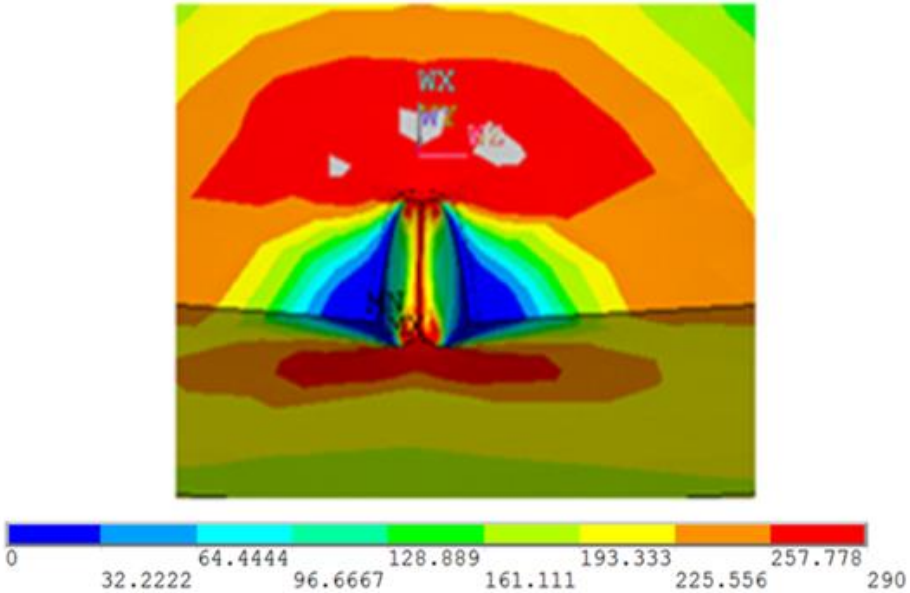

Figure 6. 15 Zoomed picture for crack opening

Also and Mixed Mode Stress Intensity Factor magnitudes obtained after the analysis is shown in **Figure 6. 16**.

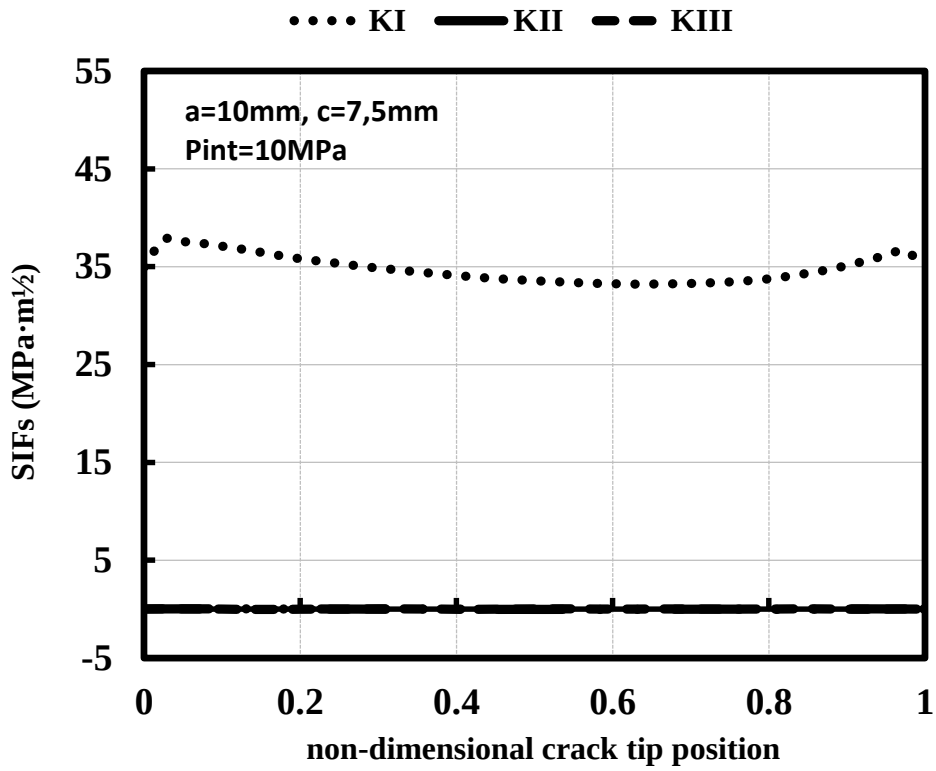

Figure 6. 16 Mixed mode Stress Intensity Factors distributions along the crack front for a/c=1,33

As it can be seen from the SIF values obtained, the mixed mode situation is not observed in cracks formed only by the effect of internal pressure and at an angle of 90degrees to the X-axes. Only pure mode I (opening) effect is present. Mode-I stress intensity factors are also given in **Figure 6. 17** for other cases analysed.

Figure 6. 17 presents SIF magnitudes extending along the crack in a/c ratio changes. As mentioned earlier, the crack depth (a) is 10mm and fixed in the analysis. A decrease in a/c value means an increase in crack radius (c). The graph clearly shows that as the crack diameter (c) increases, the stress intensity factor magnitudes also increase. Because increasing the crack diameter increases the crack opening in the nozzle, larger deformation occurs. Similarly, because the extension of the crack diameter enlarges the crack opening in the nozzle, larger deformation occurs.

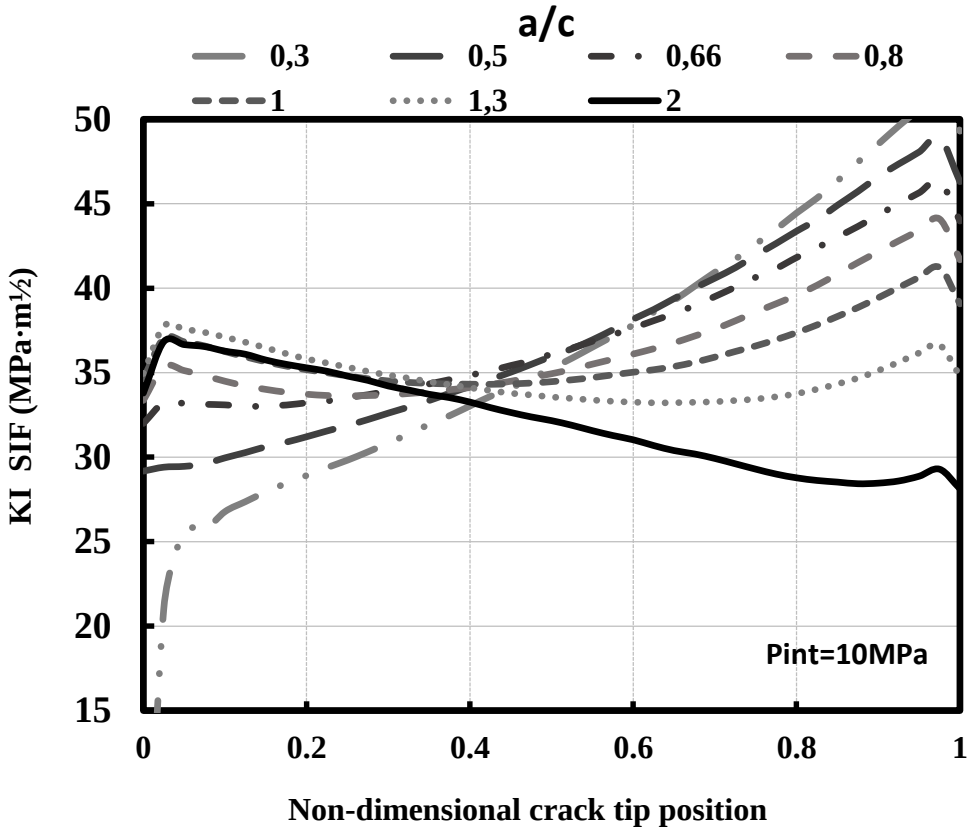

Figure 6. 17 Mode-I Stress Intensity Factors distributions for various a/c magnitudes

6.6.1.2. Changing the crack size for circular cracks

In this section, the effect of change in the size of circular cracks on SIF values is examined. In all analysis, the a/c ratio is taken to be 1. Analyses are undertaken for pressure vessels with a 2,5mm crack depth and continue with an increase of 2,5mm in each analysis and a 10MPa internal pressure is applied on the pressure vessel inner surface. The SIF values obtained are given in **Figure 6. 18**.

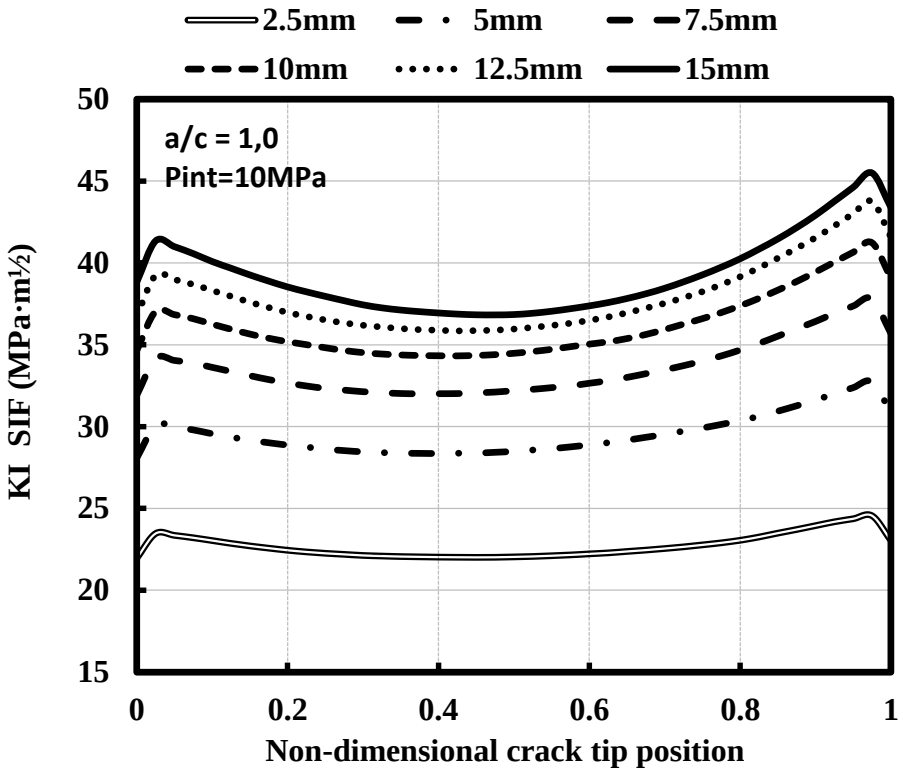

Figure 6. 18 Mode-I Stress Intensity Factors distributions in crack size change for a/c=1,0

Considering the **Equation 6. 8** below, the SIF values to be obtained with each increase of the value should increase in the square root ratio of the crack depth. As can be seen from the graph, the results are in accordance with the **Equation 6. 8**.

$$K_c = \sigma\sqrt{\pi a} \qquad \textbf{Equation 6. 8}$$

6.6.1.3. Changing internal pressure

In the previous section, SIF changes at a constant pressure value for circular cracks were examined. In this section, how the elliptical cracks are affected by the internal pressure change are considered. For this purpose, an elliptical crack with an a/c ratio of 2.0 was chosen. Analyses started with 1MPa internal pressure and were randomly increased until

they reached 10MPa. As the crack is positioned at an angle of 90 degrees as in other examples, only mode-I SIF values are considered. The SIF magnitudes obtained are given in the **Figure 6. 19**.

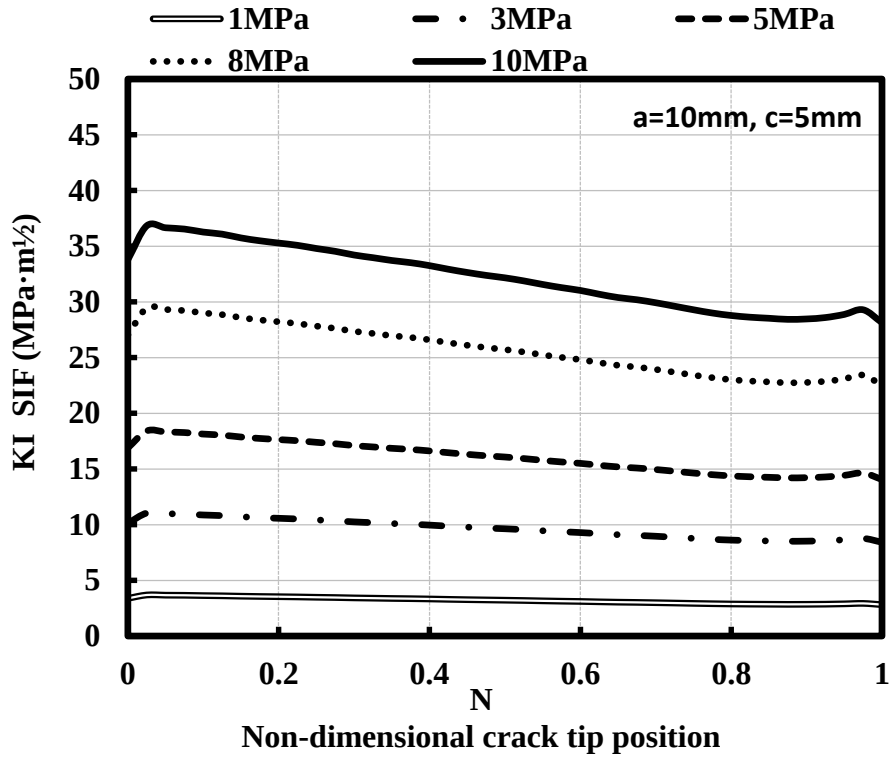

Figure 6. 19 Mode-I Stress Intensity Factors distributions for internal pressure change

As can be seen from **Figure 6. 19**, each pressure raise increases the SIF values linearly according to the ramping rate. The **Equation 6. *9*** taken in Newman & Raju's study [54] is given below. This equation applies to perfect cylinders and considers only the hoop stress. For cylinder-cylinder intersections, hoop stress can be obtained using Von-Mises and Tresca equations or the calculation methods in WRC297 [8]. Considering all these calculation methods, it is known that the increase in internal pressure (p) in complex structures increases the KI values linearly.

$$K_I = \frac{pR}{t}\sqrt{\pi\frac{a}{Q}}F\left(\frac{a}{c},\frac{a}{t},\frac{R}{t},\emptyset\right)$$ **Equation 6. 9**

Looking at the SIF values given in the graph, an increase is observed linearly. This situation is compatible with **Equation 6. *9***. Since the crack radius is half of the crack depth, there is much more stress accumulation at the crack initial point compared to the crack end. This accumulation becomes more evident as the internal pressure increases. As can be seen from the graph in **Figure 6. 19**, there is an almost linear SIF distribution throughout the crack in the crack problem with 1MPa internal pressure. However, when the pressure is increased 10 times, the stress intensity factor value that occurs at the crack initiation is about 20% higher.

6.6.1.4. Changing crack angle for various loading conditions

In the previous sections, only analyses related to opening mode-I were made and SIF values were examined. In this section, mixed mode SIF values are obtained by changing the crack angle (θ). Finite element modelling of the crack located angularly is given in **Figure 6. 20**.

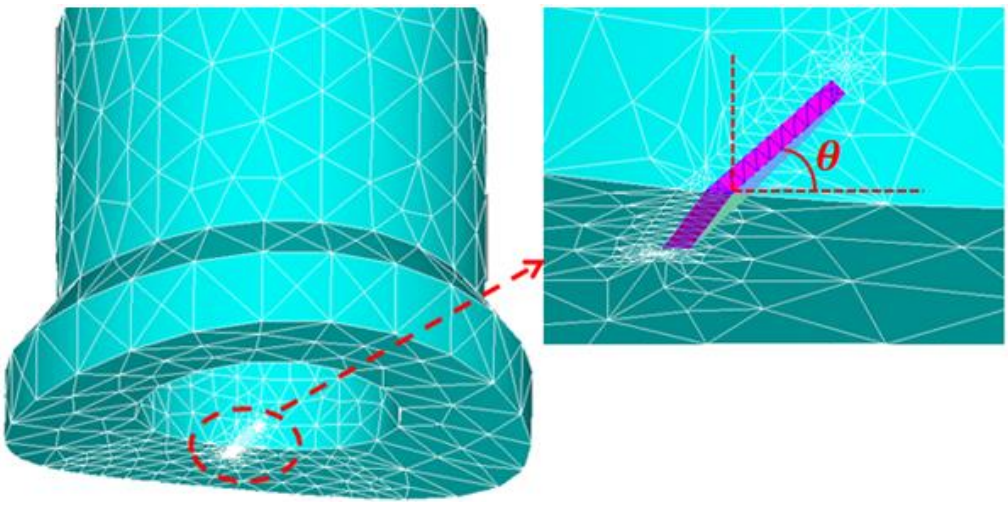

Figure 6. 20 Angular crack application on crotch corner

6.6.1.4.1. Internal pressure effect

In the analysis, only the internal pressure effect is examined first. Thereafter tensile, compressive, circumferential, and longitudinal forces affect the system separately from the centre of the nozzle and SIF values are computed. Finally, all these external loads are combined with various configurations and combined loadings are applied.

Firstly, a constant 10MPa internal pressure is applied to the system. The crack angle is increased by 15degrees in each analysis from 30degrees to 150degrees. In each case, the a/c ratio is 1. Since the effects of opening, sliding, and tearing in the system are observed at the same time, the SIF values obtained are given in **Figure 6. 21**, **Figure 6. 22**, and **Figure 6. 23** with 3 different graphs.

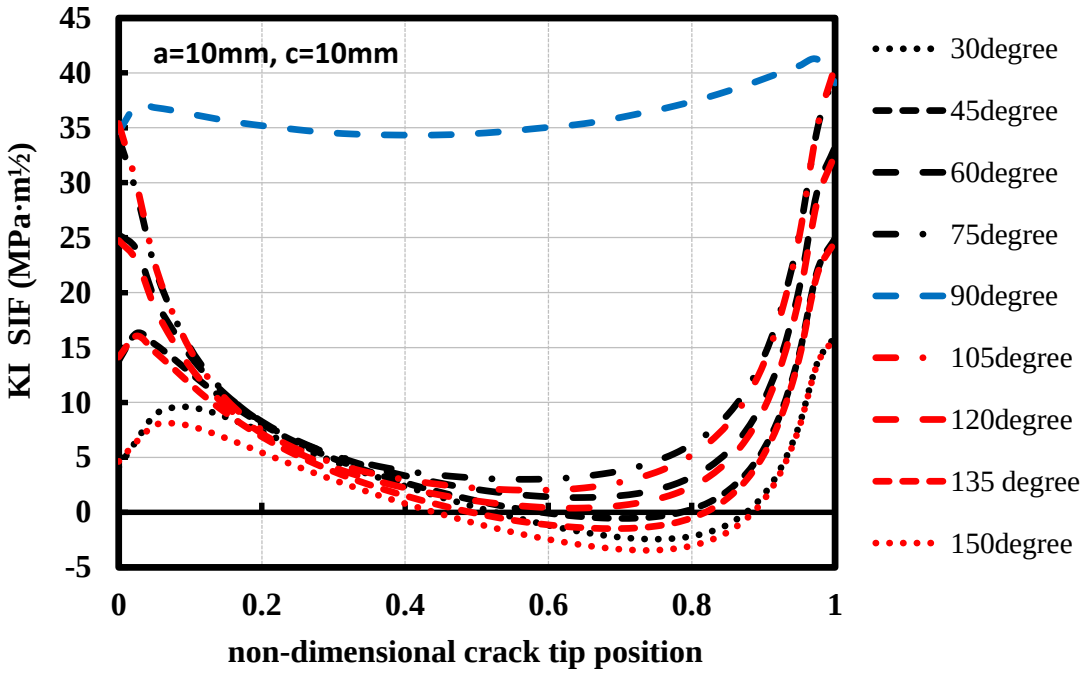

Figure 6. 21 Mode-I Stress Intensity Factors distributions for crack angle change

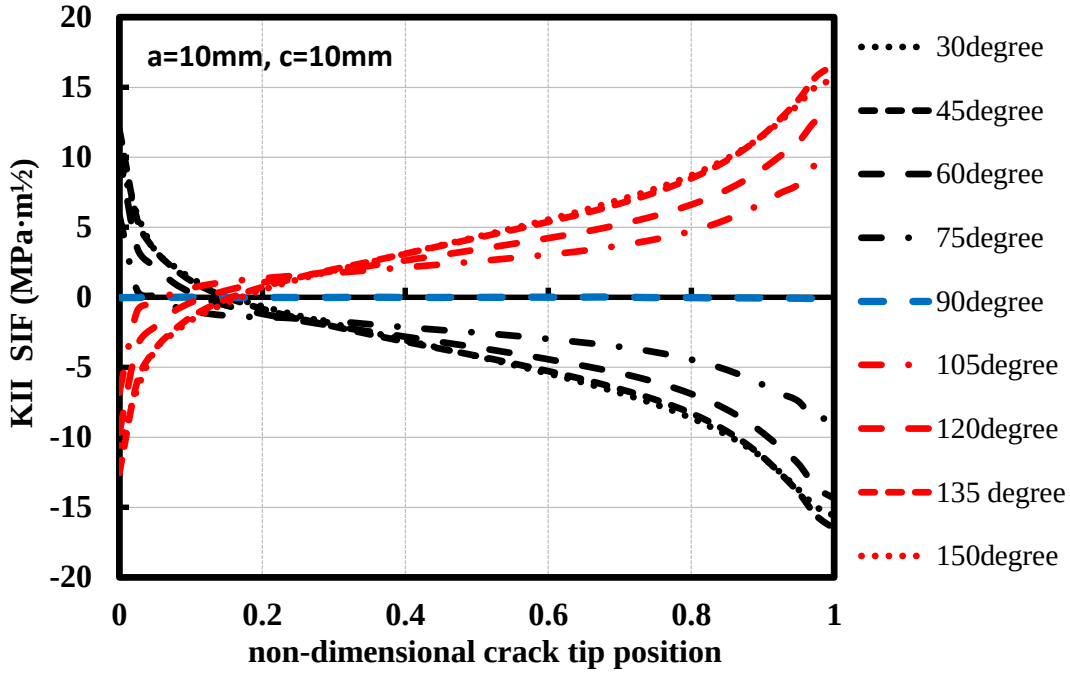

Figure 6. 22 Mode-II Stress Intensity Factors distributions for crack angle change

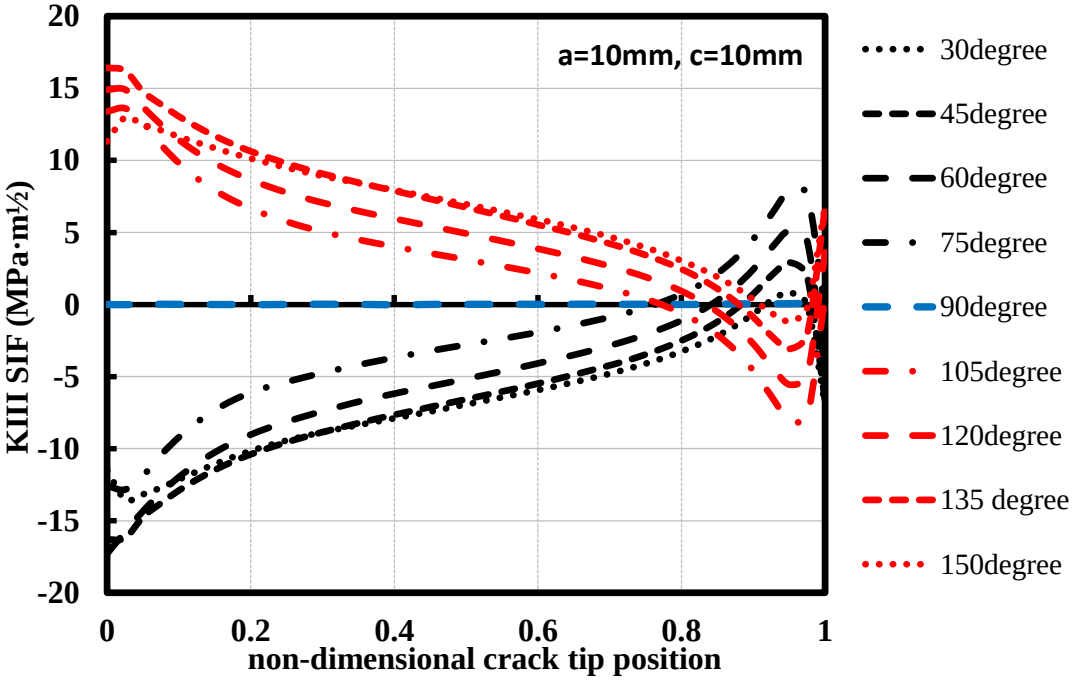

Figure 6. 23 Mode-III Stress Intensity Factors distributions for crack angle change

As can be seen from Figures, only mode-I effect is observed at 90degree crack angle. In all graphs, SIF values are the same for cracks at a distance equal to the angle of 90degrees (such as 45 and 135degrees). Only in the cases of mode-II and mode-III, the values change the sign (+, -) since the axis of sliding and tearing changes after 90 degrees.

If the 90degree crack is placed on the Y-axis in the FE Modelling, when all the graphs are examined, it is observed that as the angle made with the Y axis increases, the opening effect (mode-I) extending along the crack is replaced by sliding (mode-II) and tearing (mode- III). The biggest difference is observed undoubtedly on the mode-I effect. Because at 90degree crack angle, the same opening behaviour is observed throughout the crack, and this effect disappears as the crack angle increases. The opening effect is almost lost in the crack centre due to the mixed mode effect.

6.6.1.4.2. Tensile and compressive forces effect

Here, the tensile and compressive forces applied in the Z axis direction from the centre of the nozzle are examined. A 1000kN load is applied to the system in each analysis. The a/c ratio of 1,0 is chosen. The crack angle (θ) is increased from 30 degrees to 90 degrees with 15 degrees increasing in each step. First, SIF values are taken for tensile loads and the same process is repeated for compressive forces. Calculated SIF values are given in the **Figure 6. 24**, **Figure 6. 25**, and **Figure 6. 26** in 3 separate graphs for KI, KII and KIII.

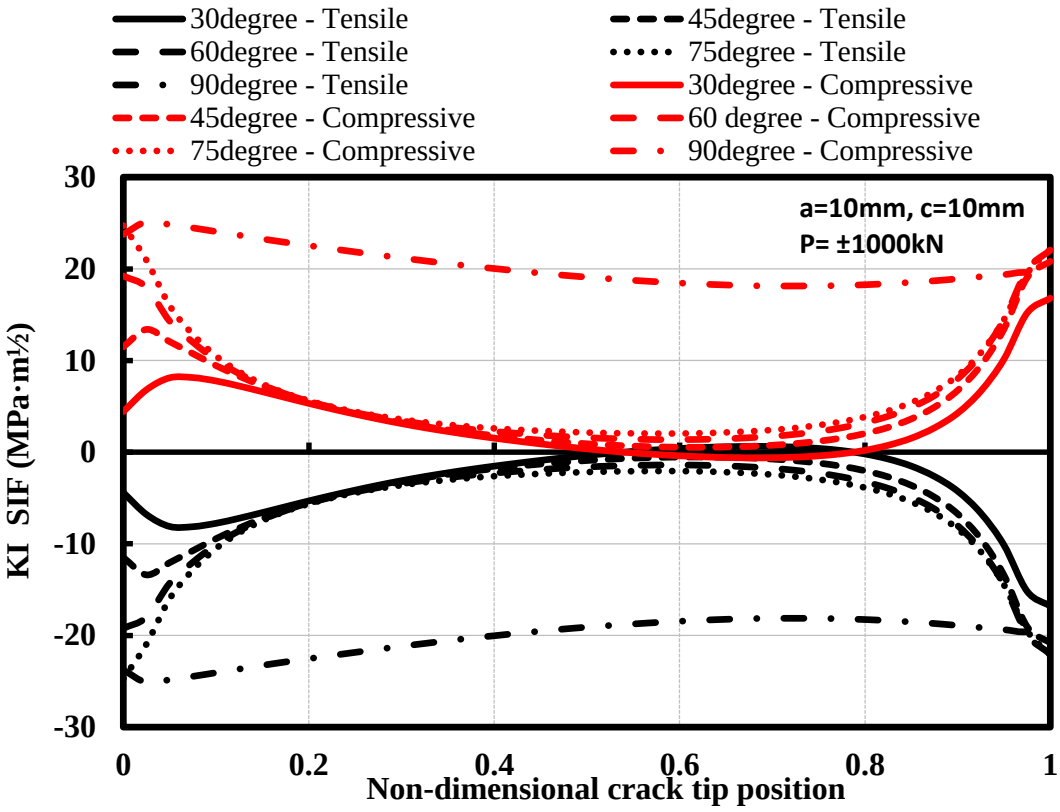

Figure 6. 24 Mode-I Stress Intensity Factors distributions for tensile and compressive forces

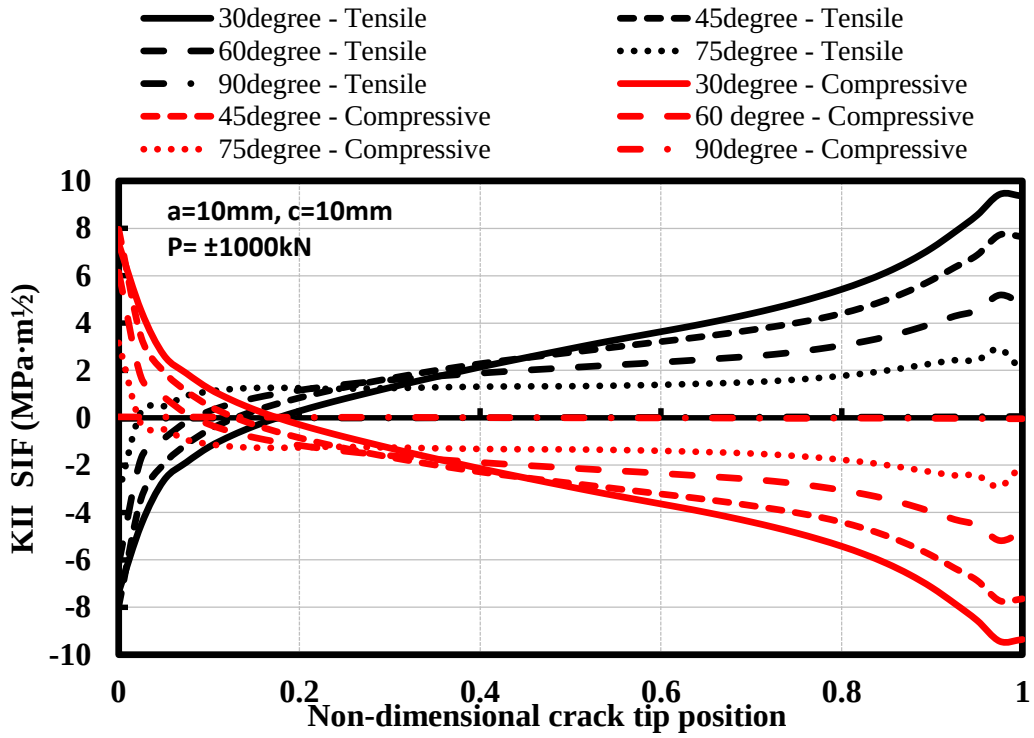

Figure 6. 25 Mode-II Stress Intensity Factors distributions for tensile and compressive forces

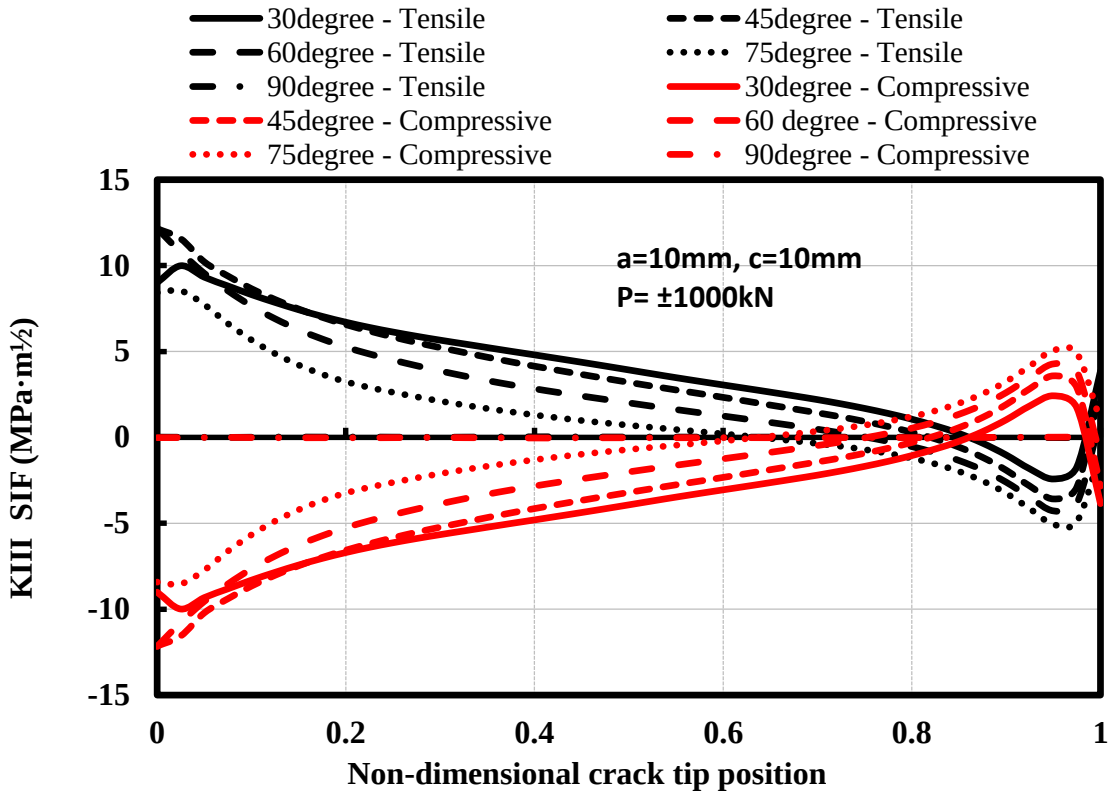

Figure 6. 26 Mode-III Stress Intensity Factors distributions for tensile and compressive forces

When the graphs are examined, the SIF values obtained in KI, KII and KIII states are the same for tensile and compressive forces. Since only the directions of the applied forces are opposite, the SIF values obtained are displaced both positively and negatively.

In all cases, maximum SIF values occur at the crack initiation and ending. In case of KI, as the crack angle decreases, the opening in the middle of the crack is replaced by sliding and tearing with the mixed mode loading effect. For this reason, as the dimensionless crack tip position approaches the point 0.5, KI values approach 0.

When the KII graph is examined, it is observed that the sliding at the 0.2-point changes direction. While the sliding effect decreases up to the point of 0.2, SIF values increase

until the end of the crack. In the case of KIII, the tearing effect continues up to 0.8 point with a decrease in SIF values.

6.6.1.4.3. Circumferential shear force effect (VX)

Here, external forces loaded from the centre of the nozzle are continued with the circumferential forces applied on the X axis. The only force acting on the system is VX named circumferential force and no internal pressure is applied to the system. Like the applied tensile force, the load magnitude is 1000kN and the crack angle is changed in each analysis. Mixed-mode K values computed are shown in **Figure 6. 27** - **Figure 6. 29**.

It is clearly observed that as the crack angle increases, KII and KIII values have also increased as can be seen from the graphs. Contrary to only internal pressure and tensile loading applications, pure mode-I condition is not observed when a circumferential force loading is applied in 90-degree crack angle. Moreover, the opening effect disappears completely at 90 degrees and the mode-II/III state is appeared. In other words, the situations that affect the crack are sliding and tearing modes.

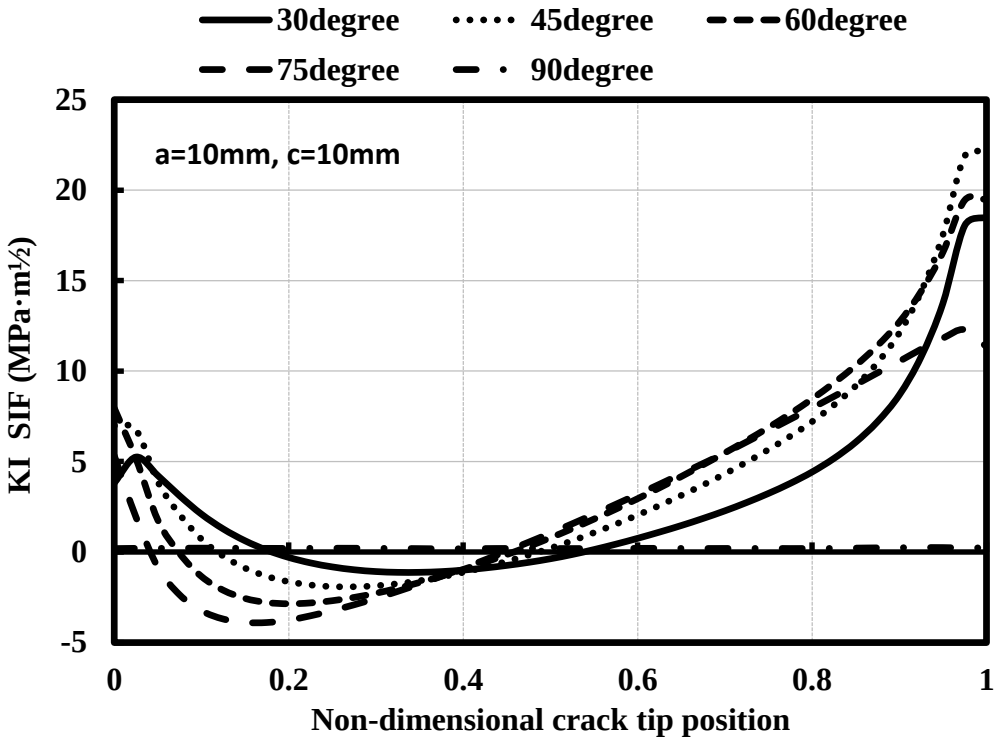

Figure 6. 27 Mode-I Stress Intensity Factors distributions for circumferential forces

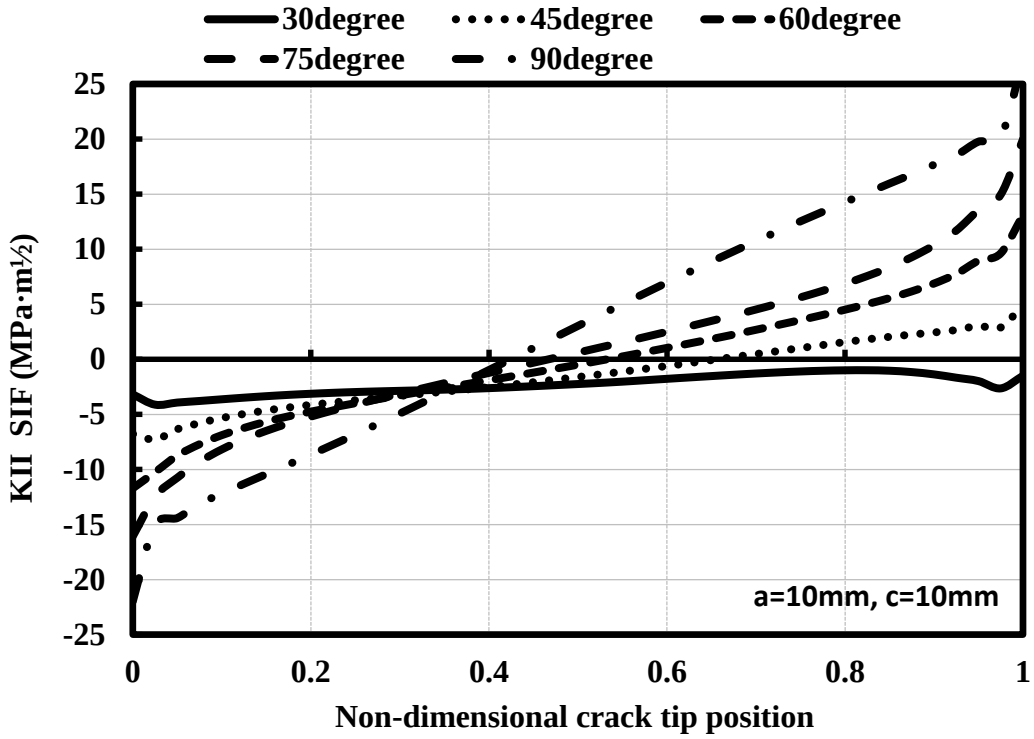

Figure 6. 28 Mode-II Stress Intensity Factors distributions for circumferential forces

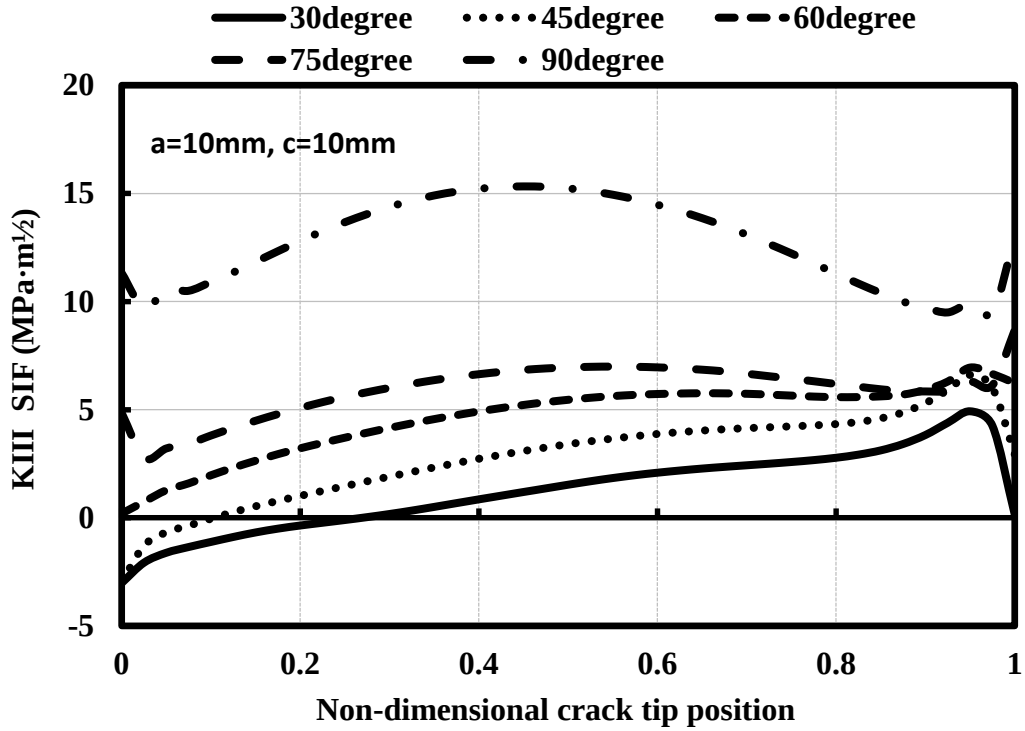

Figure 6. 29 Mode-III Stress Intensity Factors distributions for circumferential forces

6.6.1.4.4. Longitudinal shear force effect (VY)

In this section, mixed-mode stress intensity factors are calculated as a result of single longitudinal forces applied along the Y axis from the centre of the nozzle. As with other external force applications, there is no internal pressure affecting the system. The applied longitudinal shear force (VY) is 1000kN and the crack angle is increased by 15 degrees in a similar way in each analysis. The calculated stress intensity factors along the crack are given **Figure 6. 30**, **Figure 6. 31**, and **Figure 6. 32**.

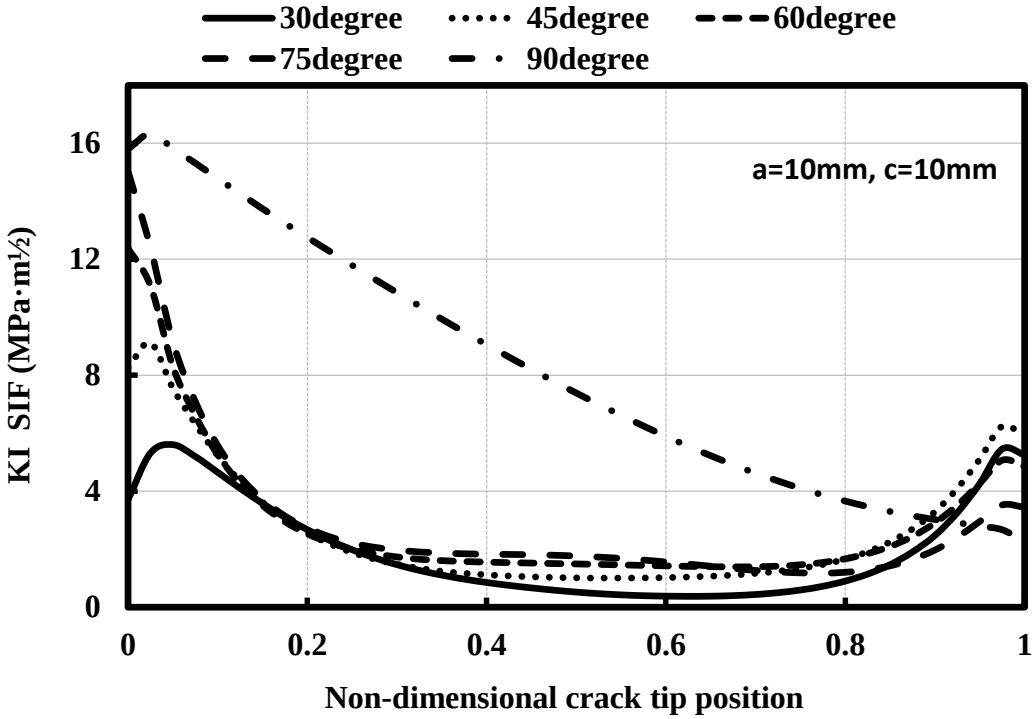

Figure 6. 30 Mode-I Stress Intensity Factors distributions for longitudinal shear forces

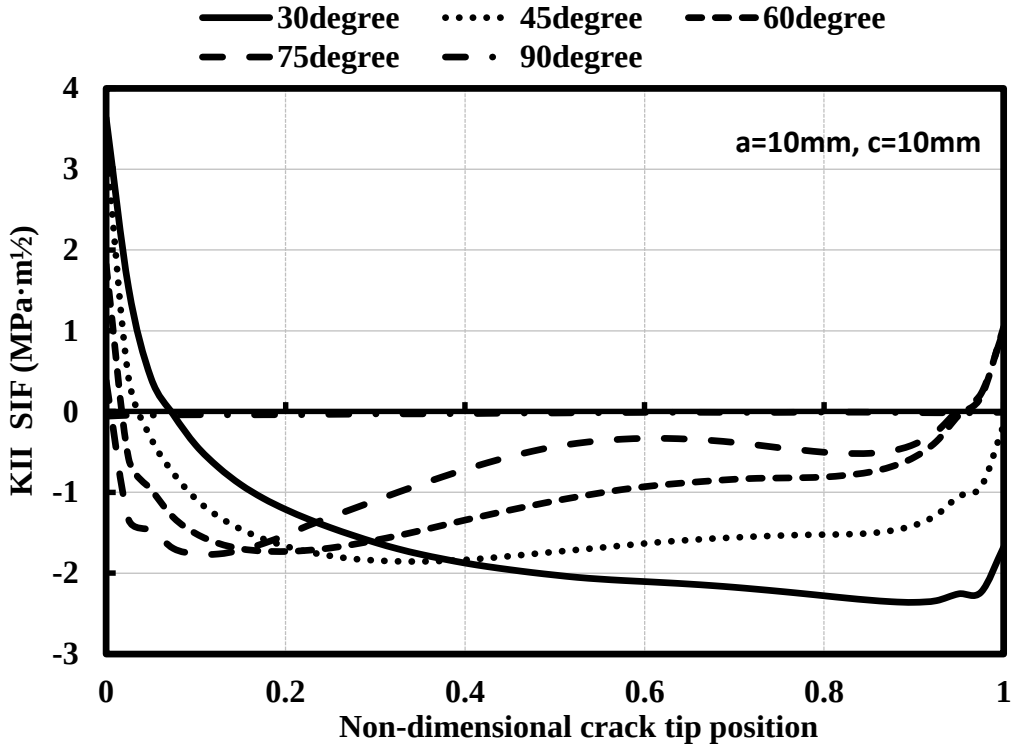

Figure 6. 31 Mode-II Stress Intensity Factors distributions for longitudinal shear forces

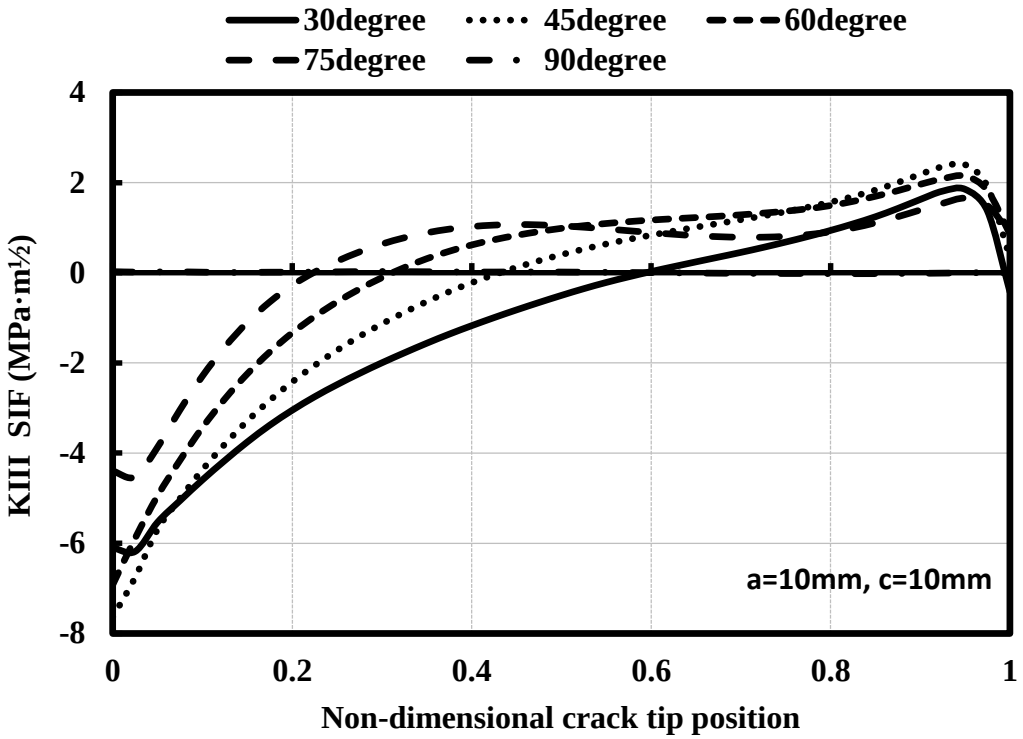

Figure 6. 32 Mode-III Stress Intensity Factors distributions for longitudinal shear forces

As seen in the graphs, pure mode-I opening is observed at 90degrees due to the direction of the applied shear force. Mixed mode effect has occurred as the crack angle decreases especially in the middle of the crack; Mode-II values increase as the angle value decreases. In Mode-III, the crack initiation at all angle values has maximum SIF values. Depending on the magnitude of the angle, Mode-III tearing changes direction. At 75degrees, this changing location is 0.2 units away from the beginning of the crack, while at 30degrees 0,6.

6.6.1.4.5. Combined external loading effect

In previous external loading cases, stress intensity factors that emerged as a result of individual loading were examined. Here, the various combined external loading situations are examined together. Circumferential shear force and tensile force in the first case, longitudinal shear force and tensile force in the second case,

longitudinal and circumferential shear forces in the third case, and finally circumferential shear force, longitudinal shear force and tensile force were applied to the system in combination. For these analyses, a circular crack with a 10mm crack radius and a 45degree angle was placed on the crotch corner. Then, the combine loads mentioned above were applied to the system. Each of the external loads is 500kN. The SIF values obtained are given in the **Figure 6. 33**, **Figure 6. 34**, and **Figure 6. 35**.

When the Mode-I graph is examined, the situation in which the opening is greatest occurred in the VX + VY case. In this case, it can be said that the tensile force has an adverse effect on the opening of the crack. In the case of Mode-II sliding, a linear decrease starting from the negative direction and a linear increase in the positive direction to the crack end is observed in all loads. The only difference is the locations in which the SIF values reach 0 on the crack line. In the case of Mode-III, in the absence of tensile loading, the SIF value starts at -5MPa.m½ and tears disappear after approximately 0.2 units at the beginning of the crack. Then, the tearing mode SIFs reaches up to 4 MPa.m½ by changing directions. When the tensile loading is applied to the system, the change of direction is almost lost, and all SIF values continue with positive direction and very little change throughout the crack. For this reason, it can be said that P (tensile) load has a balancing effect on SIF values coming on the crack.

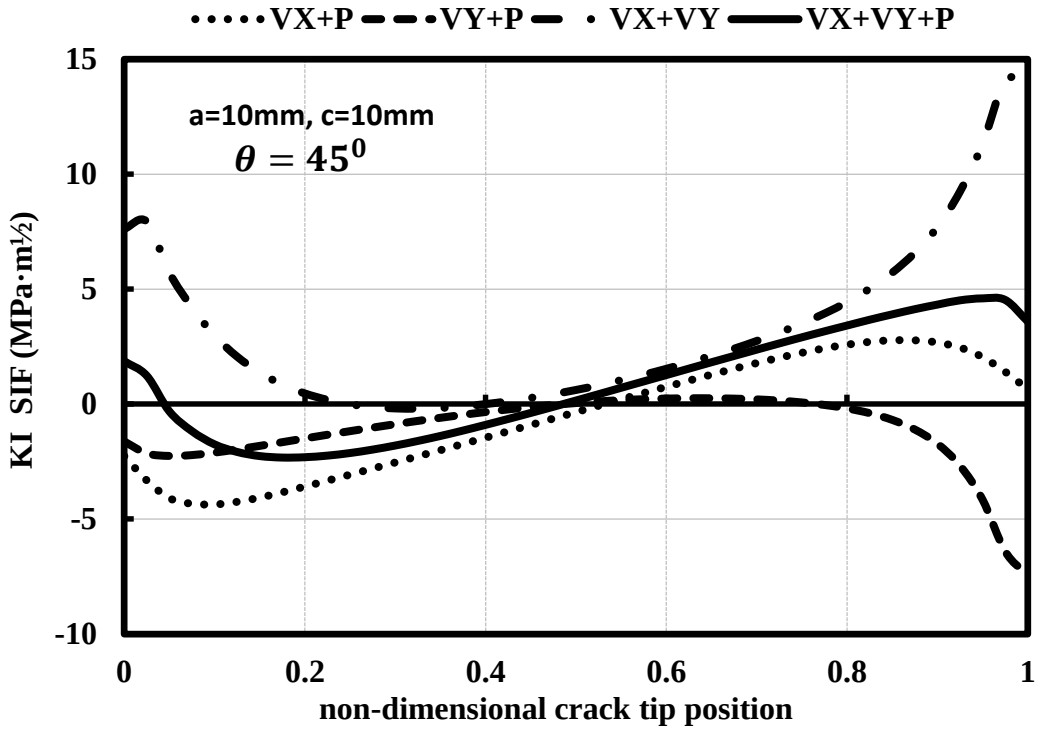

Figure 6. 33 Mode-I Stress Intensity Factors distributions for combine external loading

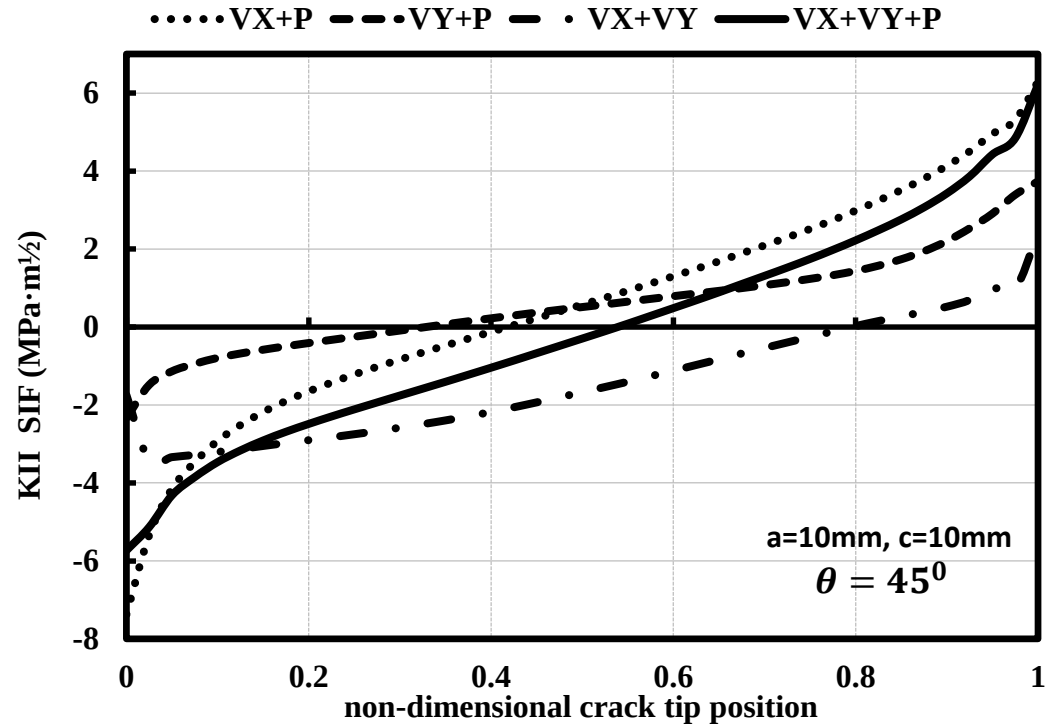

Figure 6. 34 Mode-II Stress Intensity Factors distributions for combine external loading

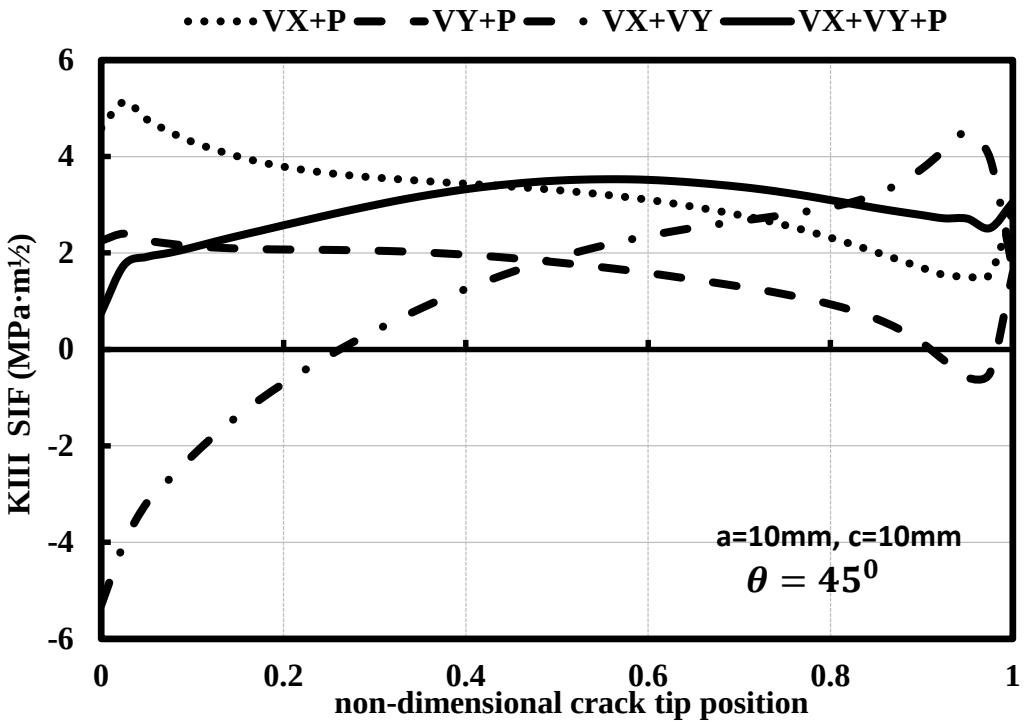

Figure 6. 35 Mode-III Stress Intensity Factors distributions for combine external loading

6.6.2. Outer surface crack SIF computing on nozzle – cylinder junction

In this section, the mixed-mode stress intensity factors extending along the crack line in modelled crack profiles (**Figure 6. 4**) with finite elements method under various parameters will be computed. In all analyses the cylinder dimensions will be fixed as Di = 500mm and T = 25mm. Changes will be based on nozzle and crack sizes. The parameter analysis to be made will take place in 4 stages. First, the mixed mode SIFs will be examined by obtaining elliptical crack profiles of different sizes by changing the ratio (a/c) of crack depth to crack radius under a constant internal pressure. Subsequently, the internal pressure changes will be examined, provided that they remain in the linear elastic zone in the vessel. Then, by changing the nozzle thickness, the effect of ro/ri change on SIFs will be figured out. Finally, the various local forces on the nozzle will be combined in 8 different ways and examined.

6.6.2.1. Changing crack depth magnitude (a/c ratio)

In this section, half elliptical surface crack profiles were modelled by keeping the crack radius (c) constant and only modifying the crack depth (a). A representative semi-elliptical profile showing the locations of the crack depth and crack diameter is shown in **Figure 6. 36**.

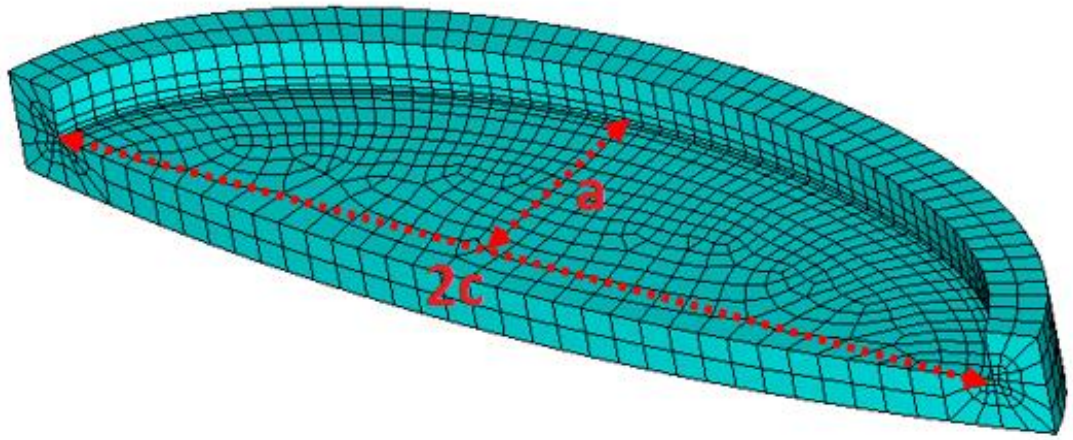

Figure 6. 36 A representative view of semi-elliptical crack profile

In each analysis c value is 12,5mm and constant. In addition, the crack depth was changed in each analysis and mixed mode SIF values were obtained for 7 different crack profiles from a/c = 0,3 to a/c = 1,8. The results obtained were grouped separately for mode-I (opening), Mode-II (sliding) and mode-III (tearing). KI Stress Intensity Factors results obtained for Mode-I status are shown in **Figure 6. 37**, KII Stress Intensity Factors results obtained for Mode-II status are shown in **Figure 6. 38**, and KIII Stress Intensity Factors results obtained for mode-III status are shown in **Figure 6. 39**.

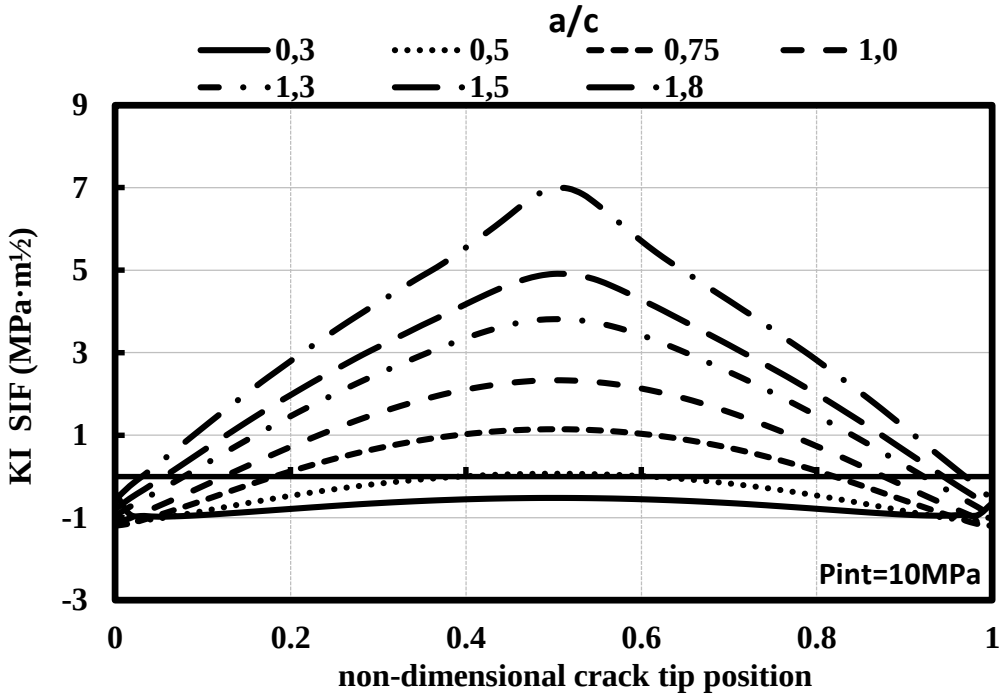

Figure 6. 37 Mode-I SIF distributions according to the change in crack depth (a) along the crack fronts c=6.25, Pint=10MPa

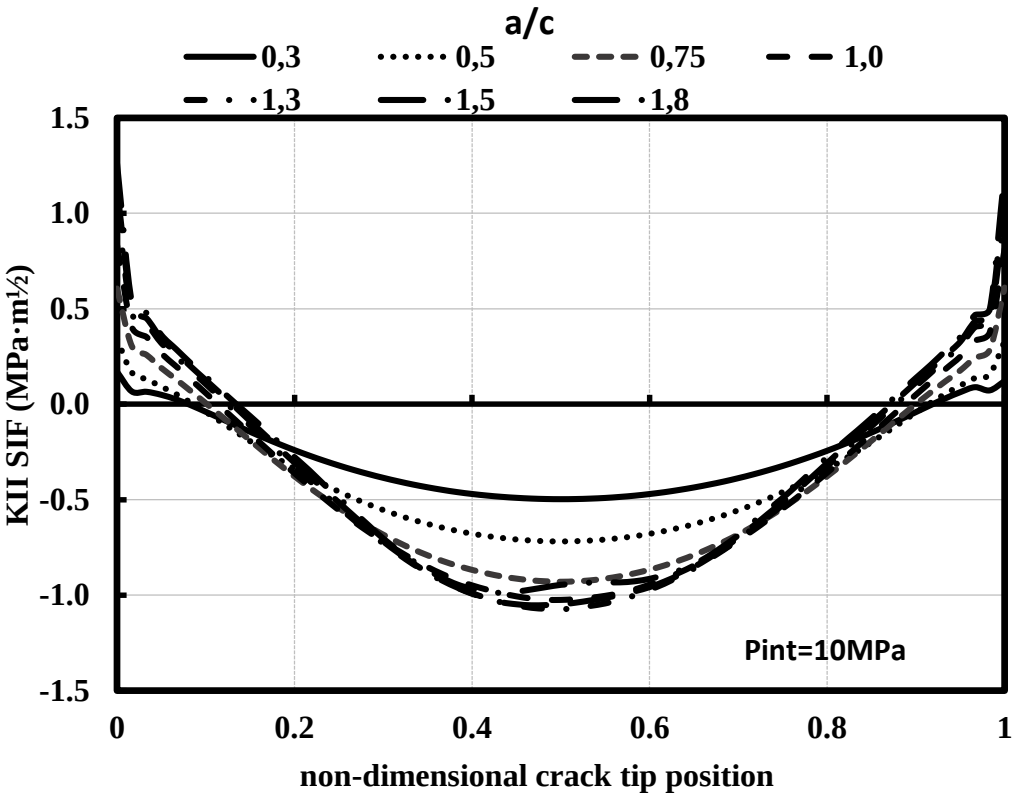

Figure 6. 38 Mode-II SIF distributions according to the change in crack depth (a) along the crack fronts c=6.25, Pint=10MPa

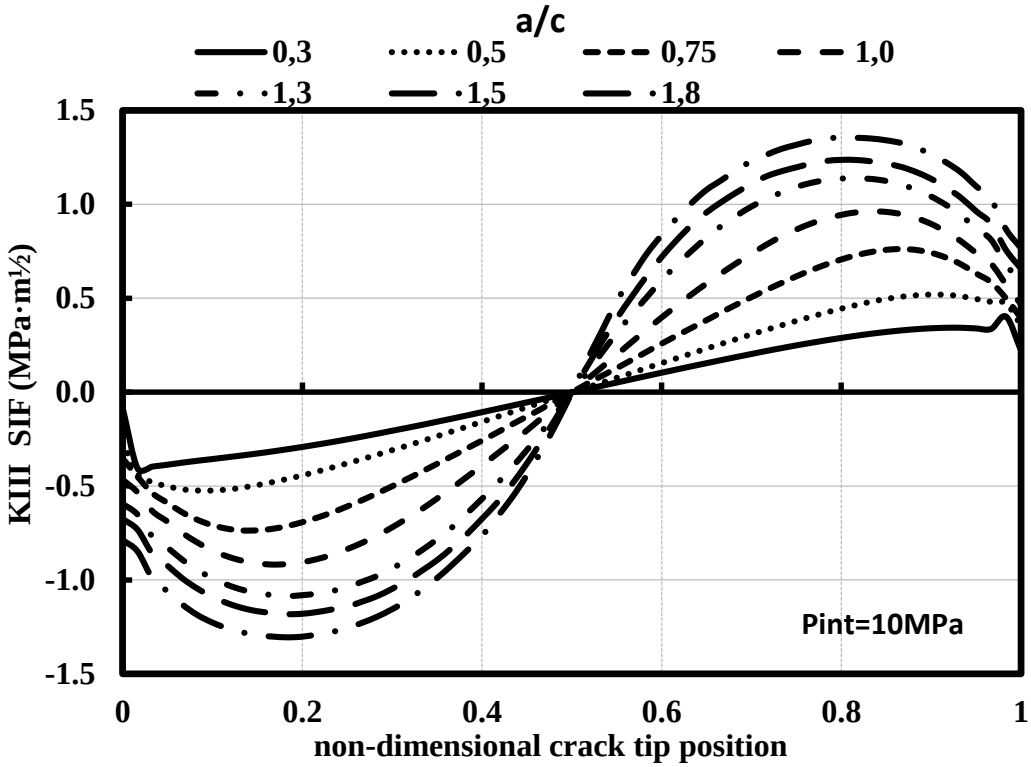

Figure 6. 39 Mode-III SIF distributions according to the change in crack depth (a) along the crack fronts c=6.25, Pint=10MPa

As it can be seen from the graphs, with the increase of the crack depth, the material approaches the fracture state more and especially the mode-I opening effect appears clearly. The same situation is observed in the case of mode-II and Mode-III, but it changes linearly from negative to a positive value along the crack line, especially in the case of mode-III. This is because under mod-III loading, crack surfaces tend to deform opposite each other around the crack tip centre point. Moreover, the sudden increase or decrease in the stress intensity factors at both crack tips is caused by the free-surface effect, and it is more obvious in the KII graph. This situation is ignored in the calculations.

6.6.2.2. Changing internal pressure (Pint)

In this section, a study has been done on how internal pressure variation affects SIF values. Considering the equations introduced by Newman-Raju, the internal pressure

increase is expected to increase the SIF values linearly as the internal pressure directly affects the hoop stress in the cylinder.

However, these equations were given for perfect cylinder internal surface cracks without nozzle connection and mode-I cases only. In this study, it was found important to examine these analyses because the cracks are located on the outer surface of the nozzle and the mixed-mode conditions are examined. In the analysis, the crack depth is half the radius of the crack (a/c = 0,5). In addition, analyses were carried out for 5 different internal pressure magnitudes and the SIF results are given in **Figure 6. 40**, **Figure 6. 41**, and **Figure 6. 42**.

The internal pressure to be applied during the analysis should not reach the limit load. Considering the Perfect Plasticity and Tresca criteria, the force and limit required for the initial yield to be realized can be calculated by the **Equation 5. 1** and **Equation 5. 2** [91]. Since the yield strength of the shell is smaller than the nozzle (260MPa for shell, 290MPa for nozzle), the calculations were made to obtain the limit load in the shell. As a result of these calculations, pressure values less than 24,7MPa should be applied to the container in order not to reach the yield point. For this reason, analyses with a maximum limiting value of 15MPa were undertaken.

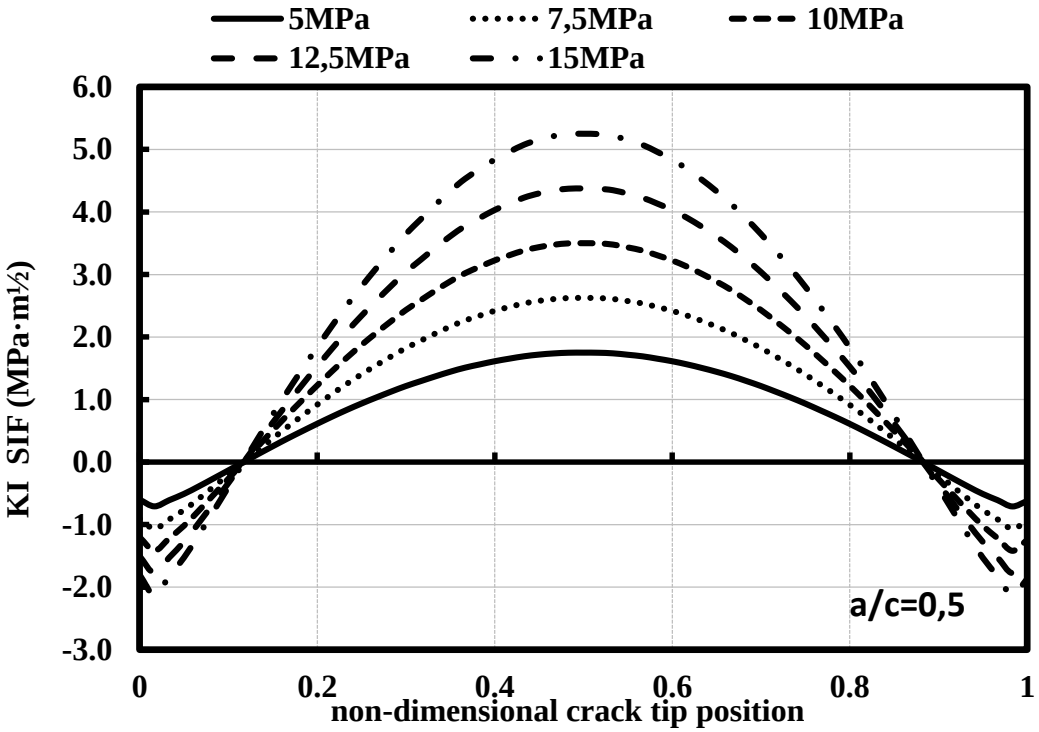

Figure 6. 40 Mod-I SIF distributions according to the change in internal pressure (Pint) along the crack fronts, a/c=0,5

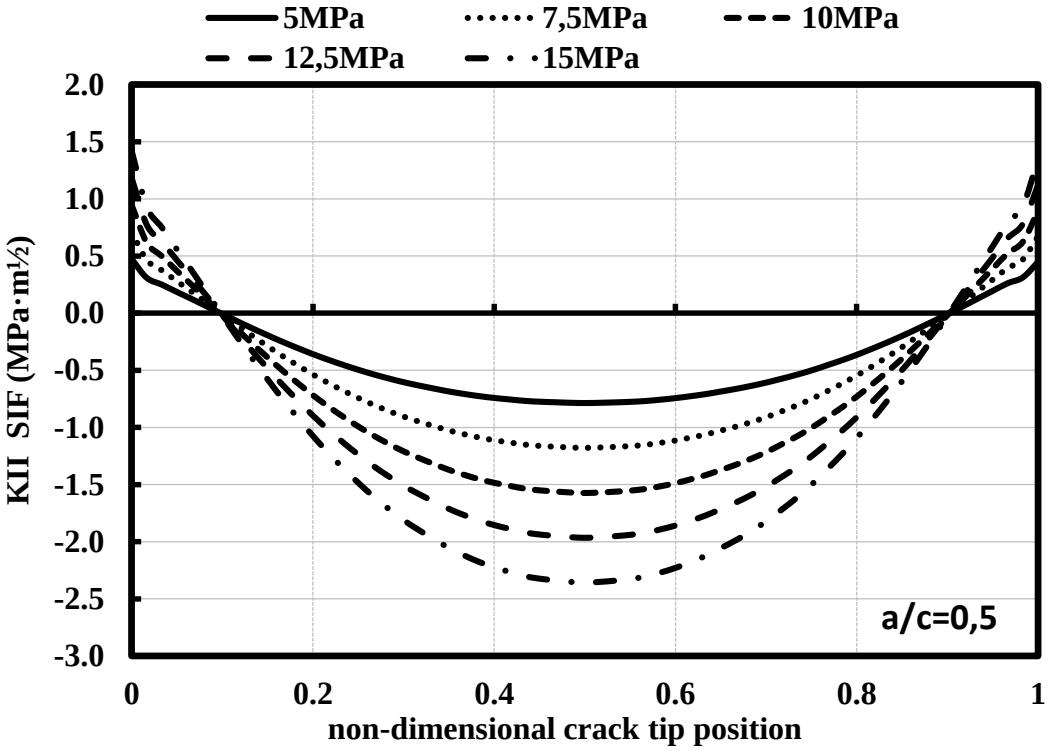

Figure 6. 41 Mod-II SIF distributions according to the change in internal pressure (Pint) along the crack fronts, a/c=0,5

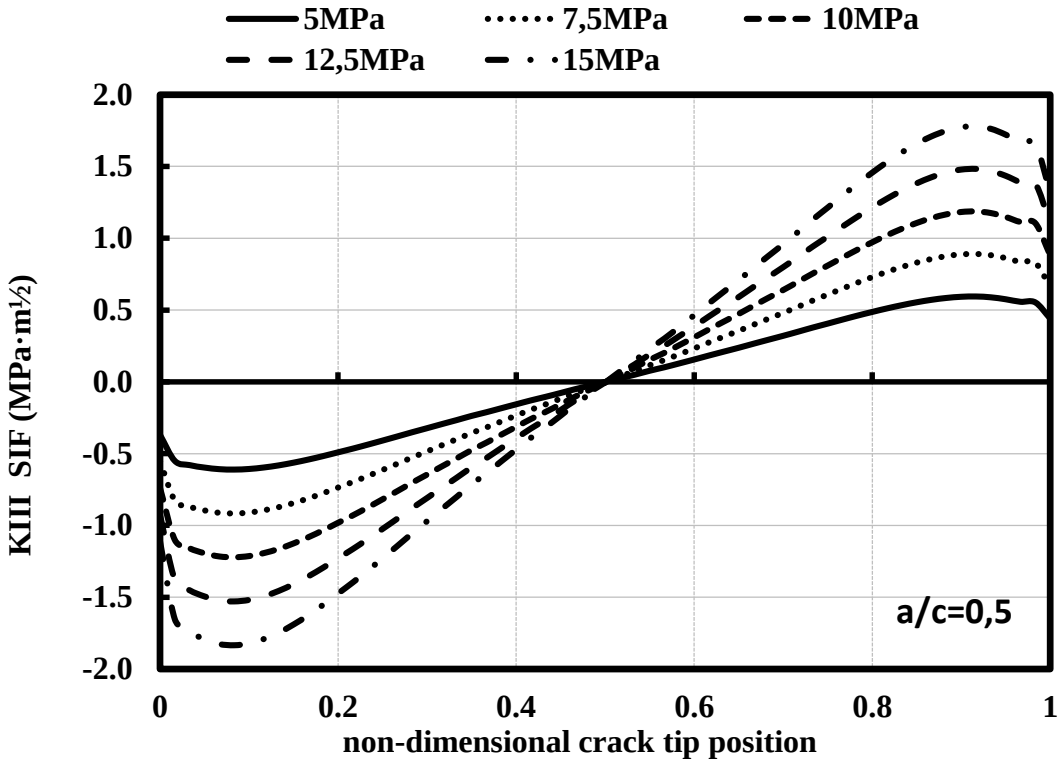

Figure 6. 42 Mod-I II SIF distributions according to the change in internal pressure (Pint) along the crack fronts, a/c=0,5

When the computed SIF values given in the graph are examined, a linear increase is seen in each crack point except the turning points. This situation is compatible with **Equation 6. 9**. In all cases the opening effect (mode I) is much more dominant than mode-II and mode-III effects. Since the crack depth is half the crack radius, there is much more stress build-up at the crack midpoint compared to the crack tip. This accumulation becomes more pronounced in Mode-I and mode-II as the internal pressure increases.

In summary, in this problem, the only force acting on the system is the internal pressure, and the stress shows a symmetrical distribution towards the outer walls. In Mode-I, a tensile stress normal to the crack plane occurs. For this reason, a full opening state occurs in the crack centre. In the mode-II state, the crack is in the in-plane shear state. That is, it is under a shear stress that acts parallel to the crack plane and perpendicular to the crack front. For this reason, the sliding effect in the crack centre is more pronounced than the

crack tip. Another important point in Mode-I and Mode-II cases is that the SIF values are 0 at the 0.1 and 0.9 positions. SIF values may be higher than expected in the calculations due to the fact that the crack tip and crack end are under the free surface effect. For this reason, excessive SIF spatters on the free surfaces can be neglected. The aforementioned 0.1 and 0.9 positions physically change the direction of crack opening in Mode-I and Mode-II. This numerically corresponds to 0 in SIF calculations.

On the other hand, in the case of Mode-III, the crack is in the out-of-plane shear state. In other words, there is a shear stress parallel to the crack plane and acting parallel to the crack front. For this reason, the tearing effect is zeroed in the centre and is more pronounced at the crack tip.

6.6.2.3. Changing nozzle diameter (do/di)

In this section, the outer diameter / inner diameter ratio (do/di) will be changed by keeping the nozzle inner diameter constant. In other words, SIF changes will be analysed using the change in nozzle thickness. In these analyses, the outer nozzle diameter is constant and 133,3mm. The a/c ratio is 0,5. The analyses were carried out in 5 steps for different do/di ratios and the results obtained are given in **Figure 6. 43**, **Figure 6. 44**, and **Figure 6. 45**.

The least nozzle thickness is the case where do/di = 1,2. At this rate, the crack depth has reached approximately 70% of the nozzle thickness. When do/di = 1,2, hoop stress is approximately 48% higher than do/di = 1,4. The difference between hoop stress at 1,6 and 1,4 do/di ratios are about 27%. On the other hand, SIF values increased by an average of 35% at this point as can be seen from the figures. Considering all these situations, this

increase is quite reasonable. In general, as expected, SIF values decrease with increasing nozzle thickness.

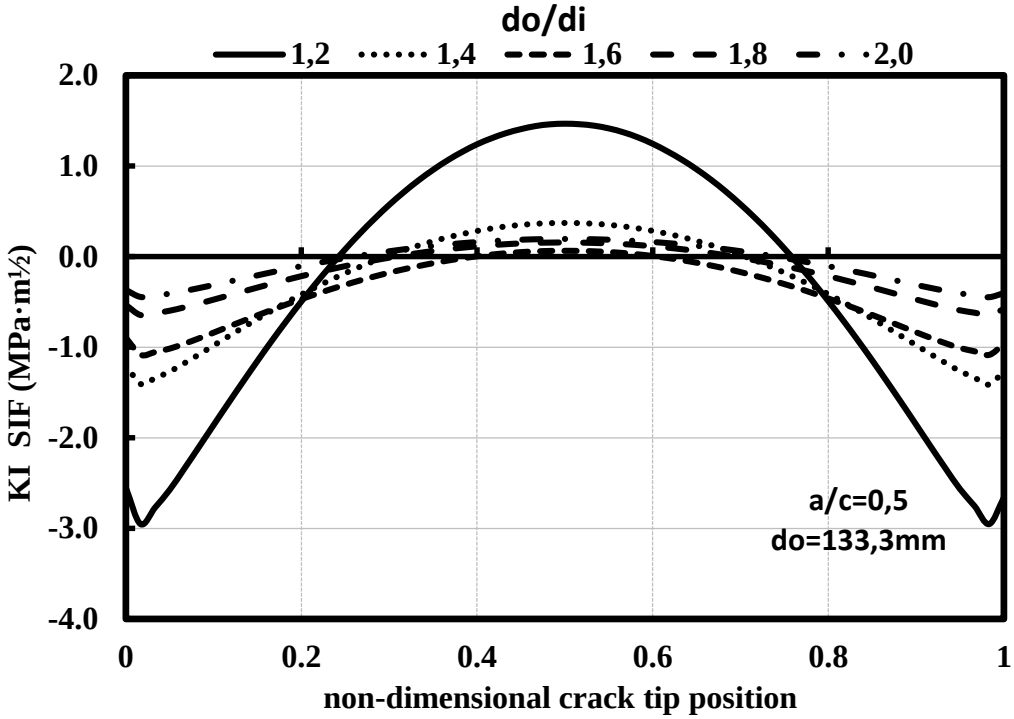

Figure 6. 43 Mode-I SIF distributions according to the change in do/di ratios along the crack fronts, a/c=0,5 - do=133,3mm

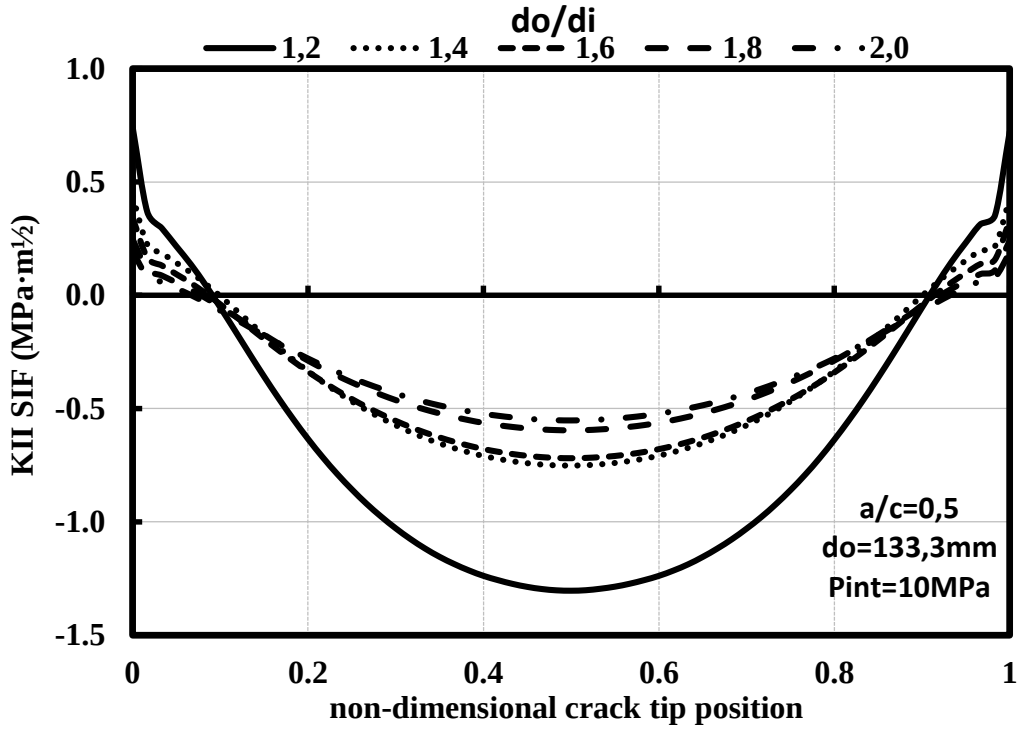

Figure 6. 44 Mode-II SIF distributions according to the change in do/di ratios along the crack fronts, a/c=0,5 - do=133,3mm

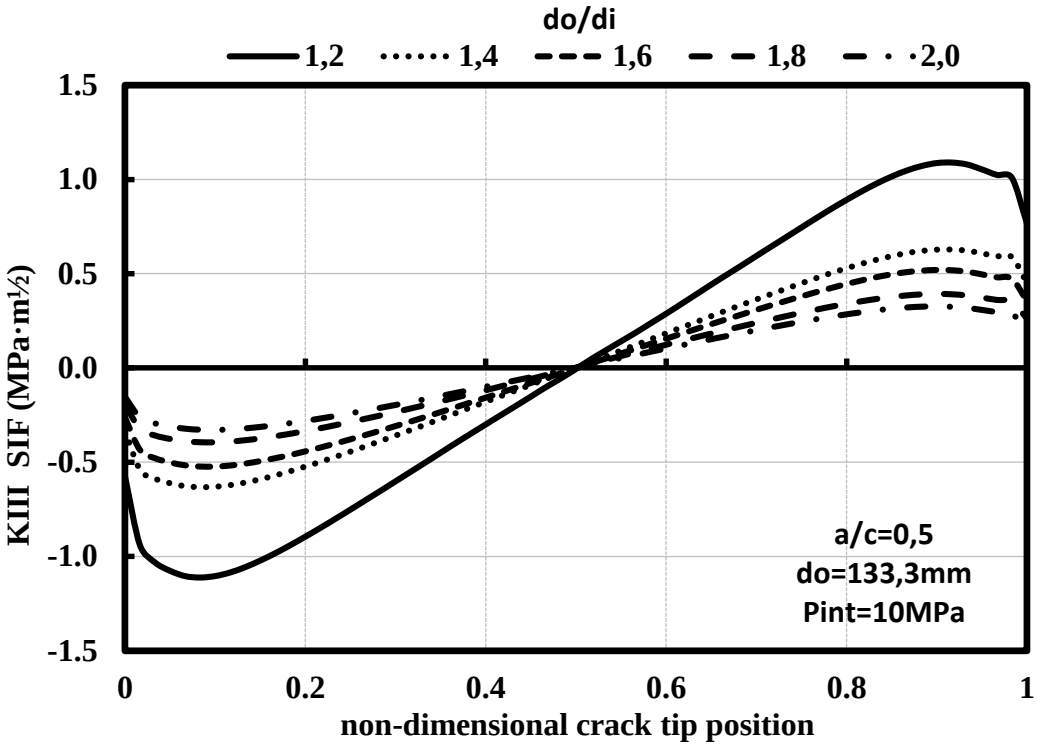

Figure 6. 45 Mode-III SIF distributions according to the change in do/di ratios along the crack fronts, a/c=0,5 - do=133,3mm

6.6.2.4. External Loading Applications

In this section, local loads on the system from the nozzle centre were examined in different combinations. First, the SIF values are calculated by analysing the tensile force (Vz), longitudinal force (Vy), and circumferential force (Vx) independently. Load conventions can be seen in **Figure 6. 46**.

Then, calculations are made for all variations in groups of 2, 3 and 4. Single axes loadings are represented by black colour, 2 axes loading variations with green colour, 3 axes loading combination with red and finally 3 axes loading with pressure loading combination with purple. The results obtained are shown in **Figure 6. 47**, **Figure 6. 48**, and **Figure 6. 49**.

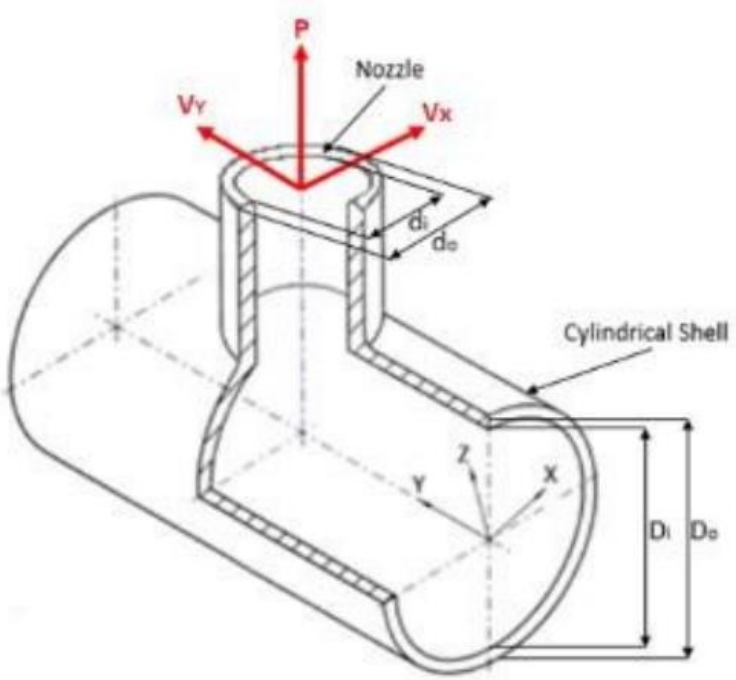

Figure 6. 46 Load conventions for the model

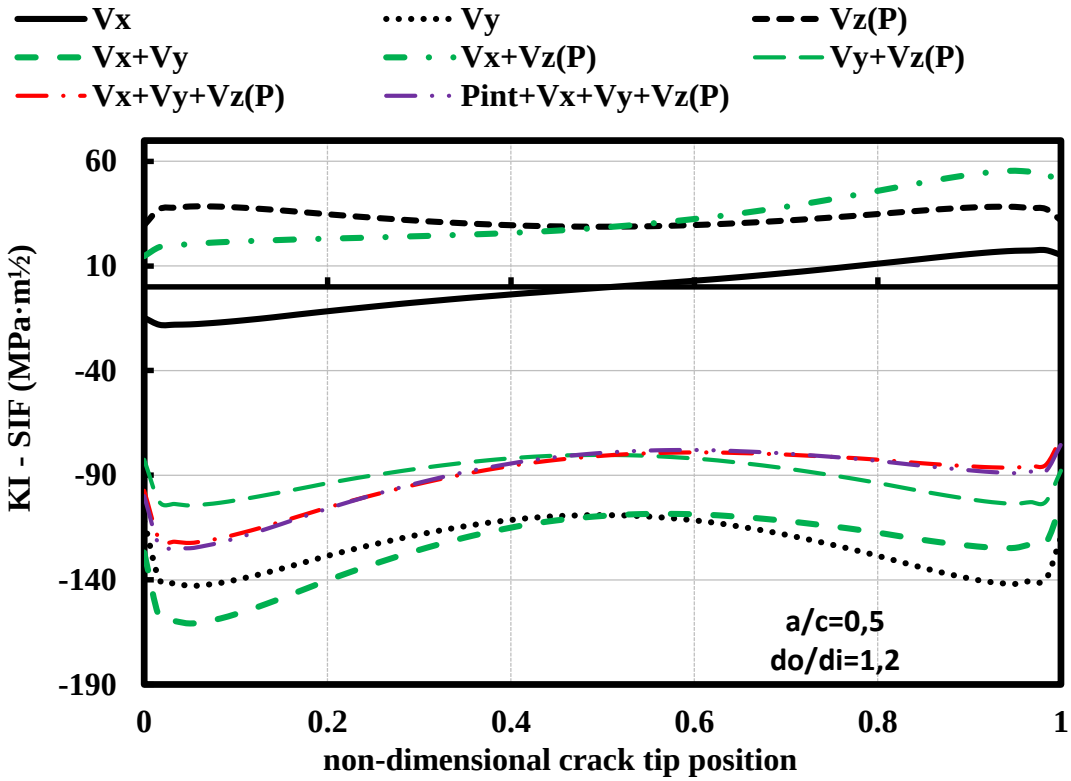

Figure 6. 47 Mode-I SIF distributions according to the change in combine external loadings along the crack fronts, a/c=0,5 - do/di=1,2

In these analyses, Vx, Vy and Vz are 1000kN for each case. Internal pressure is included in combined loading only in the last case and its value is 10MPa. As can be seen from the Mode I graph, the situation where the SIF values are the highest in the external loading situations are the cases with tensile loading (Vz). SIF values are the highest even when single Vz loading because the tensile force directly triggers the opening of the crack. In Mode-III case, Vz and Vy forces play the leading roles in tearing effect. Since the direction of the force changes in multiple loads, an SIF rise is not observed as dominant as singular loads in the opening, sliding, and tearing modes. The most interesting observation that can be said for the 3 graphs here alone is that the internal pressure has almost no effect on SIF changes.

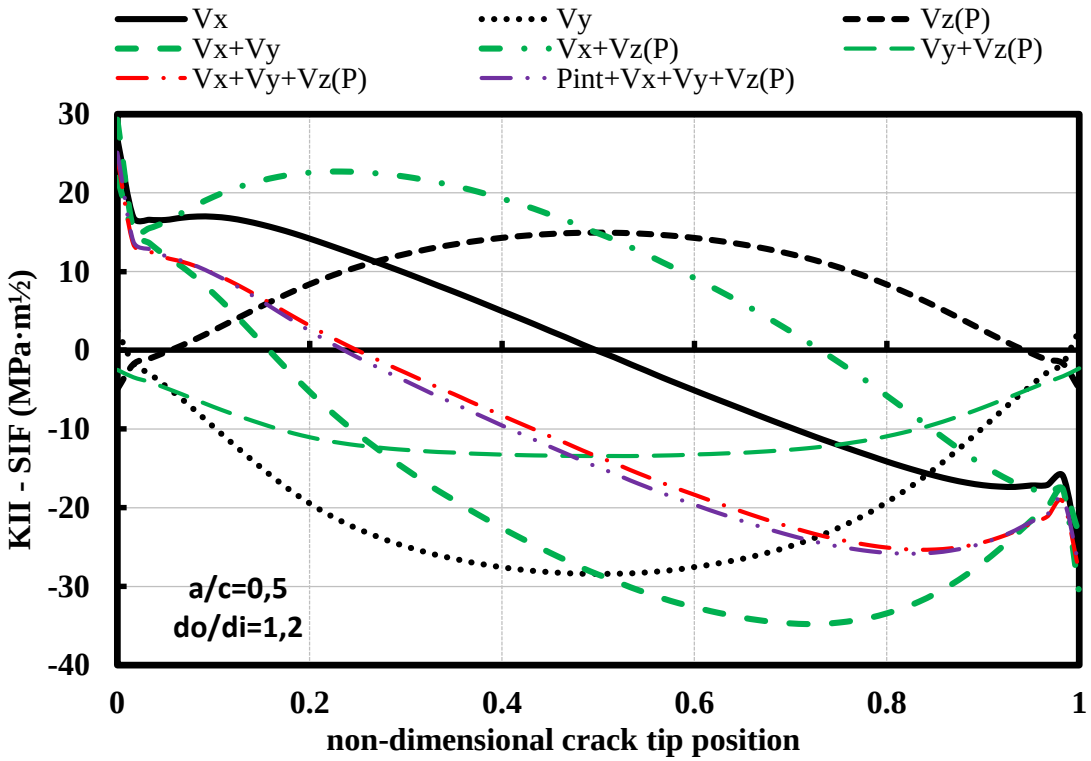

Figure 6. 48 Mode-II SIF distributions according to the change in combine external loadings along the crack fronts, a/c=0,5 - do/di=1,2

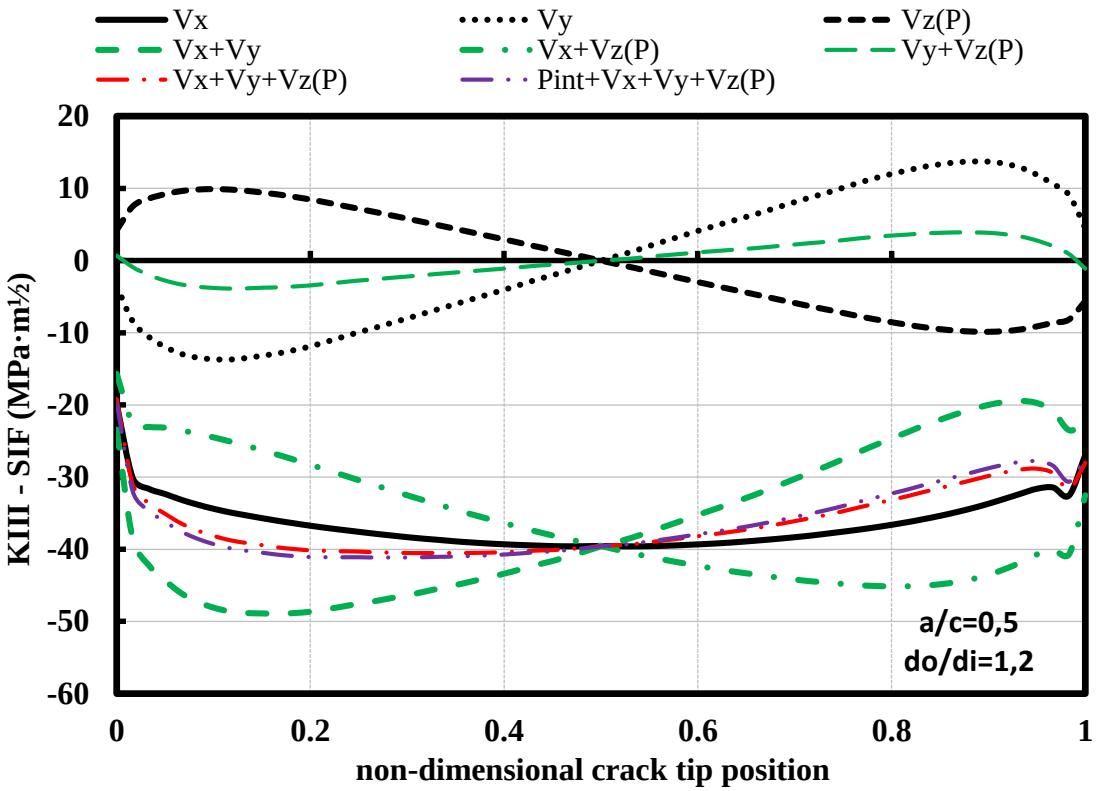

Figure 6. 49 Mode-III SIF distributions according to the change in combine external loadings along the crack fronts, a/c=0,5 - do/di=1,2

6.7. Concluding remarks

In pressure vessels, the nozzle region and the welded areas are the parts where the highest and most complex stress concentrations are experienced due to the available opening. When the system is only under internal pressure, the highest stress regions occur at nozzle-cylinder intersections, and these critical regions can change depending on the direction and magnitude of the force, especially in external local loads. Identifying these critical locations and possible failure mechanisms is crucial to avoid damaging such structures. There are some SIF calculation methods for cracks found on perfect cylinders in the literature, but these methods only provide calculations for the opening mode-I caused by hoop stress. On the other hand, although studies based on fracture mechanics related to nozzle-cylinder intersections have been made, there is no definitive solution for

calculating mixed mode stress intensity factors in possible cracks. For this reason, in this section, possible cracks that may occur in the nozzle-cylinder intersections under various loads, in the crotch corner and upper weld area, are modelled and stress intensity factor calculations are presented.

CHAPTER 7 - GENARATING DESIGN CURVES FOR STRESS CONCENTRATION FACTORS AND PROPOSING NEW APPROACH FOR ESTIMATING PLASTIC LOAD

7.1. Introductory Remarks

In this chapter, the results of the parametric analysis performed in the elastic and plastic regions will be re-discussed, and alternative improved approaches to the existing solutions presented. First of all, stress intensity factors (S.C.F.) are obtained with the maximum stresses calculated by finite element analysis for nozzle/cylinder connections under the influence of internal pressure and external local loads. Then, a wide range of design curves are presented for cylinder / cylinder connection problems by changing the basic dimensions on the geometry such as cylinder diameter, nozzle diameter, wall thicknesses with different parametric approaches and loading conditions.

Finally, a new approach will be presented as an alternative to TES and TI methods that help to estimate plastic load with the help of load-deformation curves.

7.2. Generating Design Curves for Nozzle-Cylinder Connection Problems

Analysing cylinder/cylinder geometry in pressure vessel problems is much more difficult than sphere/cylinder. Although a large number of suggestions are presented in theoretical solutions, none have been adopted in a design code to date, as implementations contain severely limiting assumptions. For example, when it is desired to obtain a suitable S.C.F for a nozzle in a cylindrical vessel, the calculation is made starting from a spherical vessel. In some implementations it uses a sphere/cylinder model where the sphere is twice the diameter of the actual cylindrical vessel, the goal here is to ensure that the remote membrane stress on the sphere is equal to the hoop stress in the cylindrical vessel. Another approach uses a sphere 1.5 times the radius of the cylindrical vessel. However, when

detailed stress distributions are obtained in cylinder/nozzle connection problems, it can be predicted that it will be different from the sphere/nozzle connection geometry. Therefore, there is a need for stress concentration factors (S.C.F.) design curves containing various geometric parameters that will directly guide designers in cylinder/cylinder problems.

7.2.1. Generating Design Curves Based on Stress Concentration Factors

The most important step in obtaining the stress concentration factors is the determination of the maximum stress. In nozzle / cylinder problems, as explained in the previous sections, the highest stresses occur at the crotch corner in internal pressure problems, while it varies depending on the direction and magnitude of the force in external loads. For this reason, in this part, the maximum stress magnitudes under internal pressure and external loads are calculated with finite element analysis solutions, regardless of the location where the stress occurs (crotch corner, welding, nozzle wall etc.). Results are given in terms of stress concentration factors defined as;

S.C.F.= (Maximum calculated Von Mises stress in cylinder) / (membrane stress).

Here, membrane stress is PD/T for internal pressure problems and V/2πrt for local loading (r is nozzle radius).

Initially, design curves will only be obtained for SCF results in nozzle-cylinder connections without pad reinforcement under internal pressure. Then the pad reinforcement effect will be examined. In the 3rd step, design curves are created for external local loads. All these S.C.F. data obtained are plotted with the aid of an appropriate attachment parameter - β.

7.2.1.1. Generating Design Curves for Nozzle-Cylinder Junctions Without Pad Reinforcement Under Internal Pressure

First, a fixed size cylinder is considered. That is, the wall thickness and diameter of the cylinder are constant throughout all analyses. Variables in the analysis are nozzle diameter and nozzle thickness.

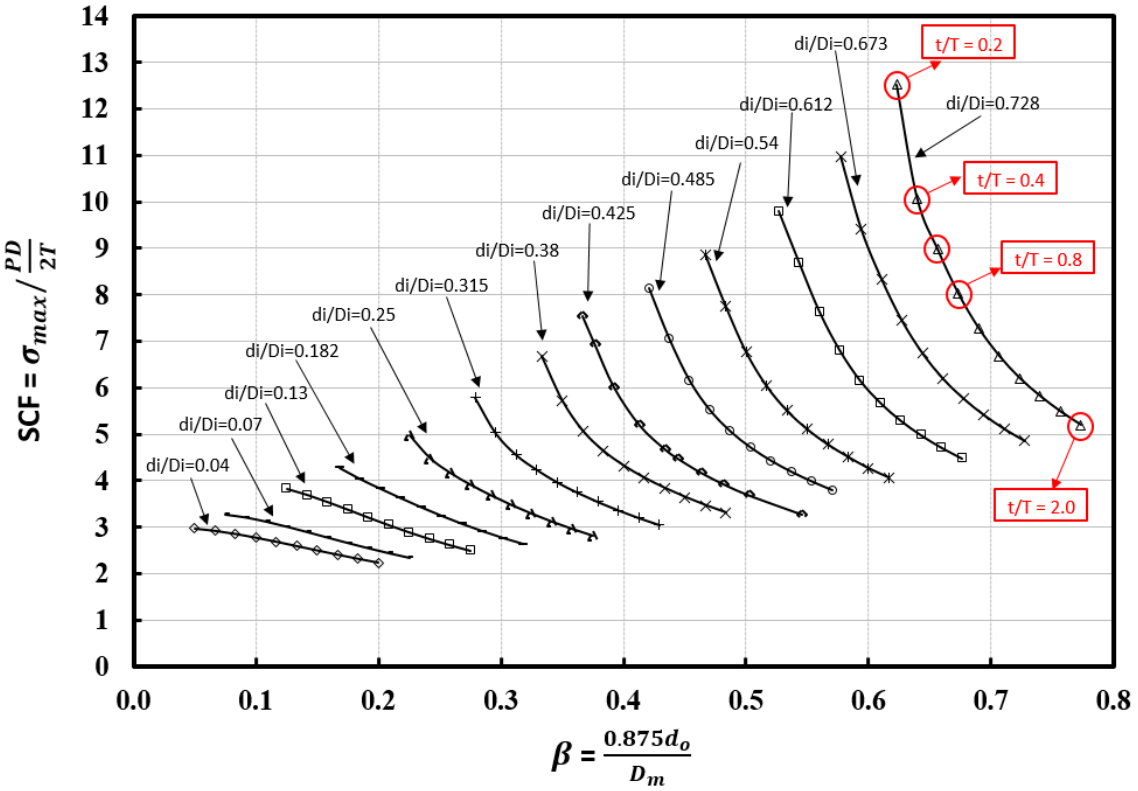

Figure 7. 1 Stress Concentration Factors for maximum stress in nozzle/cylinder junctions with no pad reinforcement subject to internal pressure

If **Figure 7. 1** is examined, curves are obtained for 13 different di/Di ratios. In each curve, there are SCF results for 10 different t/T. t/T ratios go from 0.2 to 2.0 with a constant increase. The point where SCF is highest is also the point where t/T is lowest. In t/T changes, some points are shown on the di/Di=0.728 curve as a representation. In addition, Attachment Parameter is expressed as in the equation since cylinder diameter is constant and nozzle diameter is variable.

$$\beta = \frac{0.875 d_o}{D_m}$$ Equation 7. 1

As seen in **Figure 7. 1** the increase in nozzle diameter for the same t/T ratios also causes an increase in S.C.F values. When the curves with the same di/Di ratio are examined, it is observed that there is a parabolic decrease in S.C.F values as t/T values increase. It is noteworthy that when the di/Di ratio falls below 0.25, the curve first tends to decrease linearly and the S.C.F variation decreases considerably.

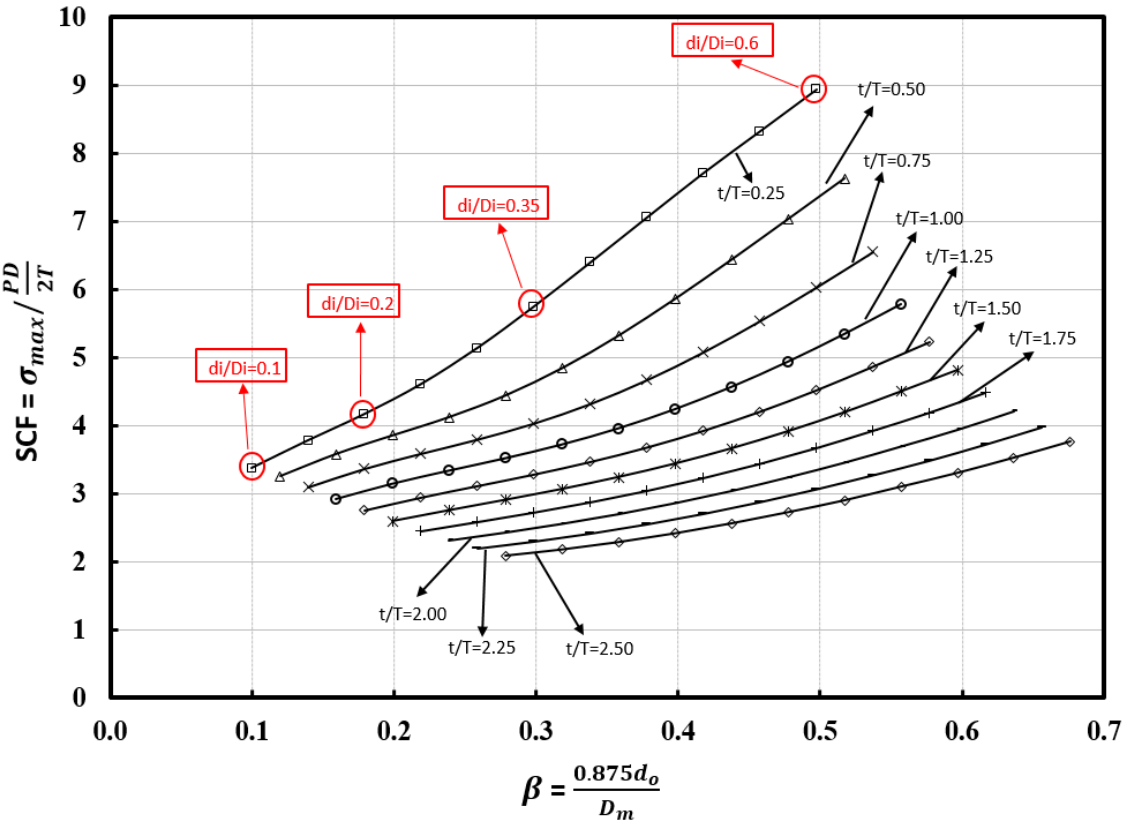

Figure 7. 2 Stress Concentration Factors for maximum stress in nozzle/cylinder junctions with no pad reinforcement subject to internal pressure

Another case studied is where the main variable is t/T. The curves to be obtained vary between t/T = 0.25 – 2.50 and progress with 0.25 increments for each curve. Here, Di and T values are fixed and each point on the curves represents the di/Di change. In total, S.C.F values were obtained for 11 different di/Di ratios in the generation of each curve, and the

increase in the ratios was 0.05 at each point. Generated curves are shown in the **Figure 7. 2**.

As can be seen from the **Figure 7. 2**, the di/Di ratio for each curve is 0.6 at the highest point of S.C.F and 0.1 at the lowest point. Considering that the shell diameter did not change, the increase in the nozzle diameter increased the S.C.F values for each curve. On the other hand, since the increase in nozzle wall thickness creates an effect increasing the strength, as t/T increases, S.C.F values drop.

In the third case, the t/T change will be handled with different parameters. dm/Dm and t/T are equal in all cases. In this problem, curves are obtained by changing t provided that T remains constant in all cases, and a total of 9 different t/T cases are examined. Each curve is drawn with the S.C.F results obtained from 5 different analyses. Each of these points is the case where D/T is 10, 20, 30, 40 and 50. The results are shown in **Figure 7. 3**.

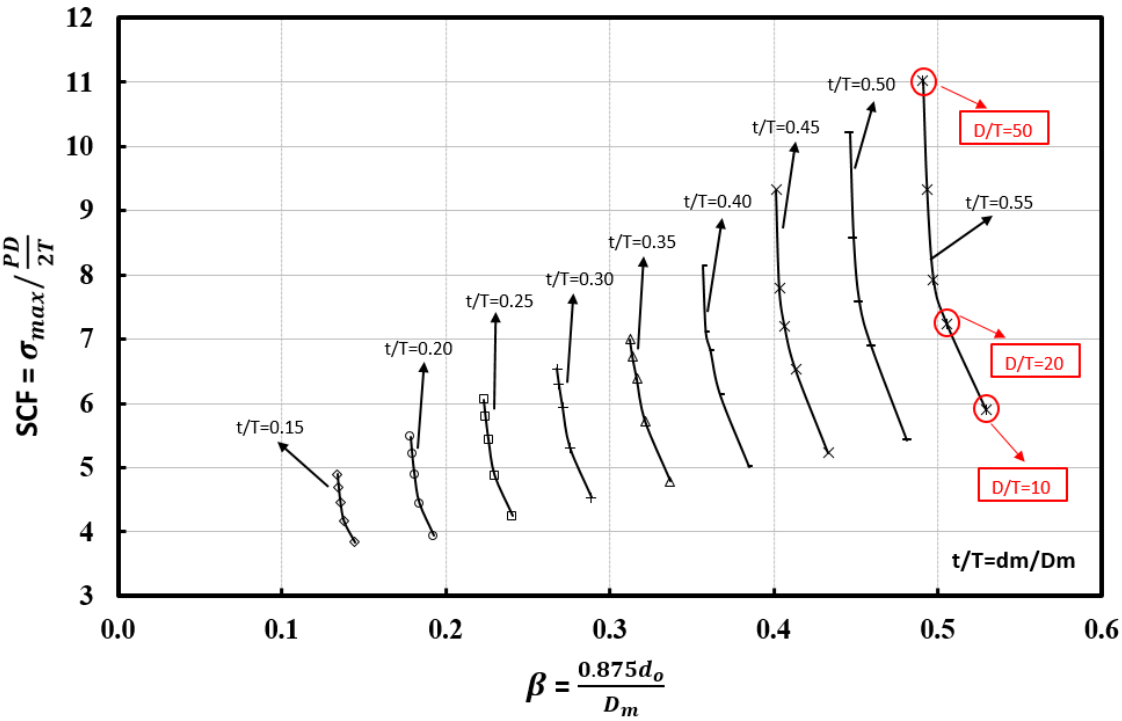

Figure 7. 3 Stress Concentration Factors for maximum stress in nozzle/cylinder junctions with no pad reinforcement subject to internal pressure

The trend of the S.C.F curves is the same for each case as shown in the **Figure 7. 3.** On the other hand, as t/T increases, dm/Dm will increase at the same rate, so the nozzle opening almost exceeds the half of the shell diameter. For this reason, since the maximum stress will increase, S.C.F values also tend to increase significantly.

In the case of t/T = 0.15, the difference between the S.C.F values obtained from D/T=10 and D/T=50 points are approximately 21%, while in the case of t/T = 0.55, this difference is approximately 47%. That is, an increase of approximately 3.5 times in t/T creates a 125% increase in S.C.F values at the maximum point.

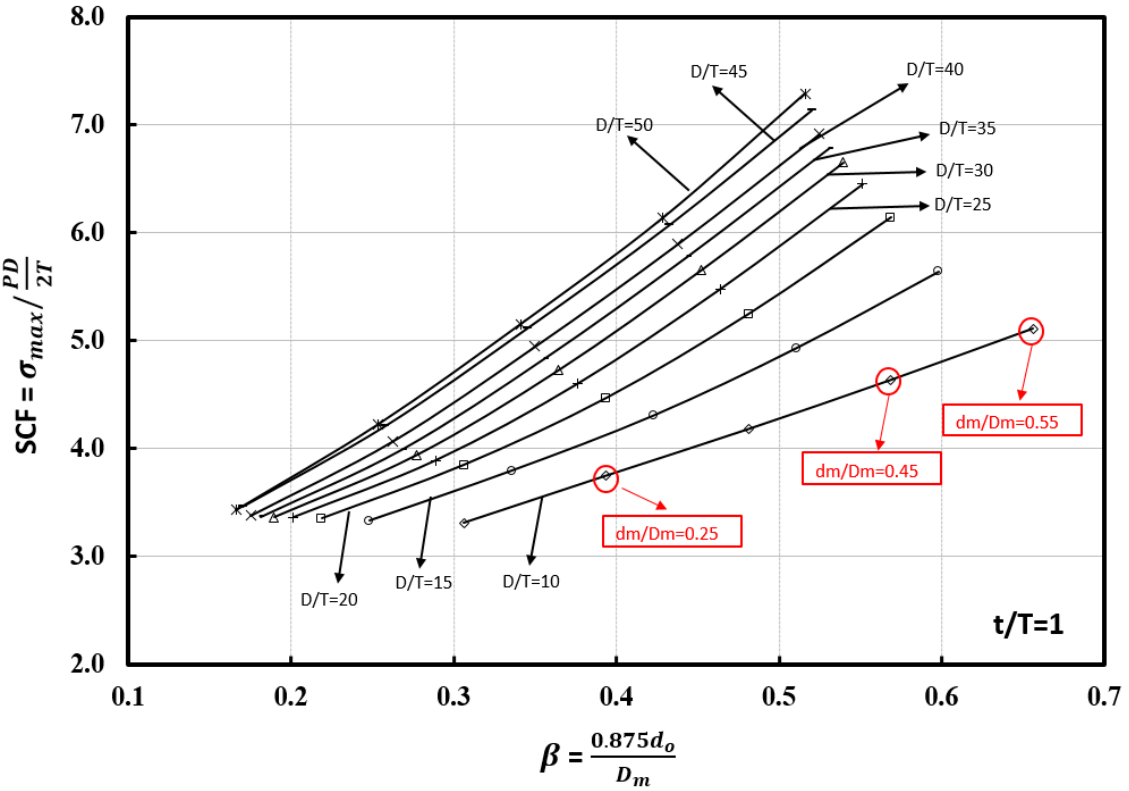

Figure 7. 4 Stress Concentration Factors for maximum stress in nozzle/cylinder junctions with no pad reinforcement subject to internal pressure

In case 4, curves for 9 different D/T values are obtained by increasing the shell diameter (D) at a fixed shell thickness (T). Here, the points on the curves are determined according to the dm/Dm parameter. For each curve, dm/Dm was determined as 0.15, 0.25, 0.35,

0.45 and 0.55. In all analyses, t/T=1. When the **Figure 7. 4** is examined under all these conditions, it is observed that although the nozzle diameter increases at the same rate as the shell diameter increases, the S.C.F does not remain constant and tends to increase. When this increase is dm/Dm=0.15, it is approximately 3% at the maximum point, and when dm/Dm=0.55, this difference increases to 30%. This shows that regardless of the shell diameter, the larger the nozzle diameter, that is, the opening, the more the S.C.F will increase due to the stress in the structure.

7.2.1.2. Generating Design Curves for Nozzle-Cylinder Junctions with Pad Reinforcement Under Internal Pressure

The application of reinforcement plate is one of the most effective methods to reduce the maximum stress values in pressure vessel problems. In this section, it is observed how S.C.F values change with pad reinforcement and design curves are created. Firstly, S.C.F changes are examined for a constant shell and nozzle thickness by increasing the pad thickness (Tp). Here t/T=1 and is constant. dm/Dm is determined as 0.11, 0.22, 0.33, 0.44, 0.55 and 0.66. Here, by changing the nozzle diameter and therefore the inner diameter of the pad, the maximum stress is changed. Generated curves are shown in the **Figure 7. 5.**

Another situation is that here the main variable is pad reinforcement, so the attachment parameter - β is recreated according to the pad diameter. The new expression is;

$$\boldsymbol{\beta = \frac{0.875 d_o}{D_p}} \qquad \textbf{Equation 7. 2}$$

As can be seen from the **Figure 7. 5**, pad reinforcement decreased S.C.F values by 4.21% at the maximum point while dm/Dm=0.11. This situation falls below 1% after dm/Dm=0.44. In this case, it can be said that pad reinforcement is a more effective method for smaller nozzles to reduce S.C.F.

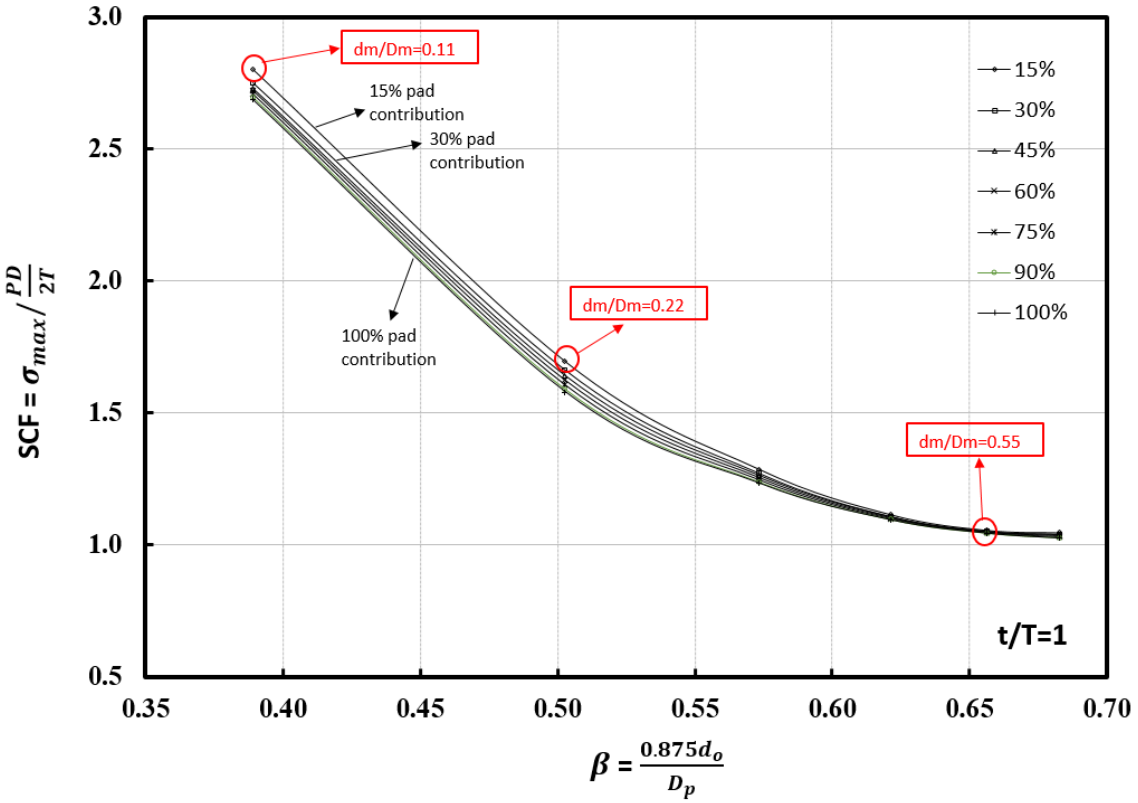

Figure 7. 5 Stress Concentration Factors for maximum stress in nozzle/cylinder junctions with pad reinforcement subject to internal pressure

In another study on the effect of pad contribution on S.C.F change, one of the main variables will be the increase in pad thickness in a similar way. The other variable is the change of the pad diameter (Dp). In order to observe this variable, 5 different Dp/dm ratios (1.25, 1.5, 1.75, 2.0, and 2.25) are determined for each curve generation. While determining this ratio, the nozzle diameter (dm) is kept constant in the analyzes and the pad diameter (Dp) is increased at constant intervals. Obtained results are shown in the **Figure 7. 6**.

Considering that the nozzle opening, and main cylinder dimensions do not change, changing the pad diameter plays a role that directly affects S.C.F. If Dp/dm = 1.25 is compared with Dp/dm = 2.25, approximately 2 times increase in pad diameter will result in an 80% decrease in S.C.F values. In addition to all these, the increase in pad thickness

plays a role in decreasing S.C.F values, similar to the previous graph. An 85% pad contribution will increase S.C.F by over 13% on average.

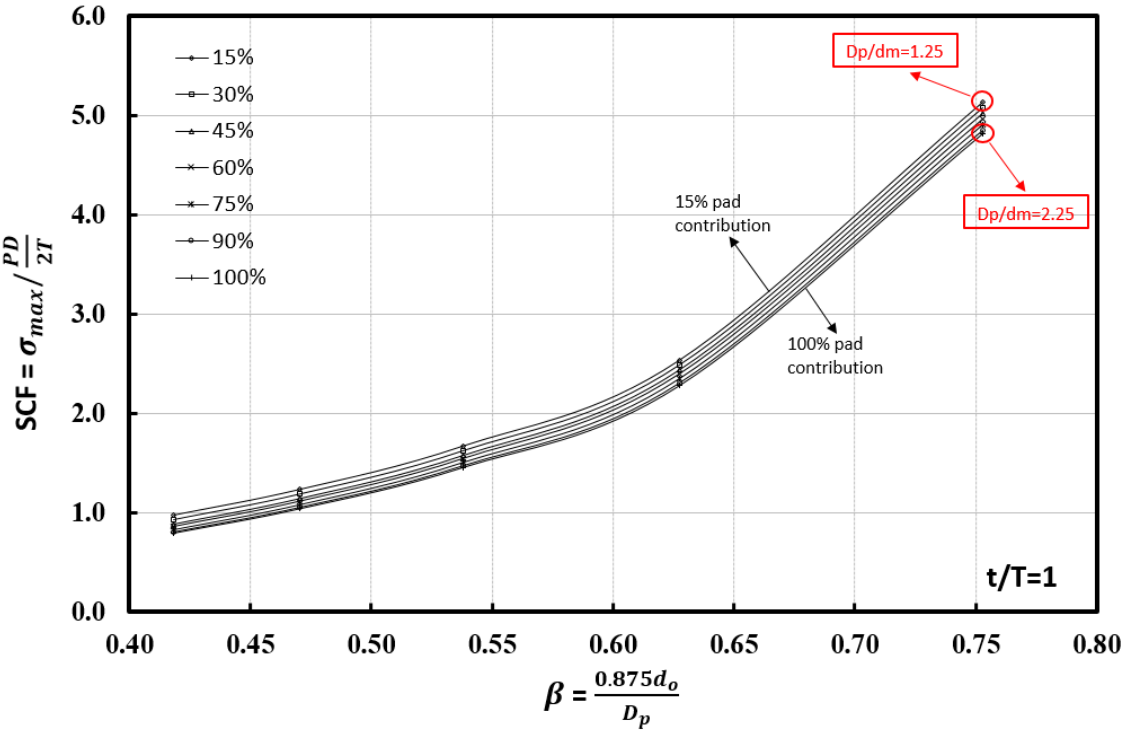

Figure 7. 6 Stress Concentration Factors for maximum stress in nozzle/cylinder junctions with pad reinforcement subject to internal pressure

Considering the design curves obtained from the pad reinforcement results, it is clear that the pad reinforcement and even the pad diameter applied have a positive reducing effect on S.C.F. Increasing the pad diameter together with the pad thickness will reduce the S.C.F, especially in cases where the nozzle opening is large (as the d/D value approaches 1.0).

7.2.1.3. Generating Design Curves for Nozzle-Cylinder Junctions Under External Local Loads

In this section, maximum stresses due to external local loadings will be determined and stress concentration factors related to this are obtained. Then, design curves related to external loads are obtained with a suitable attachment parameter. The location where the

maximum stresses occur in external loads varies according to the direction and magnitude of the force. That's why S.C.F. calculation is obtained with the following expression.

$$\mathbf{SCF} = \boldsymbol{\sigma_{max}} \Big/ \frac{\boldsymbol{Vi}}{\boldsymbol{2\pi Rt}}, \text{ (i = x, y, z)} \qquad \textbf{Equation 7. 3}$$

Here, Vx is the shearing force applied in the axial direction, Vy is the shearing force applied in the longitudinal direction, and Vz is the tensile force. The representation of these forces is given in the **Figure 7. 7**.

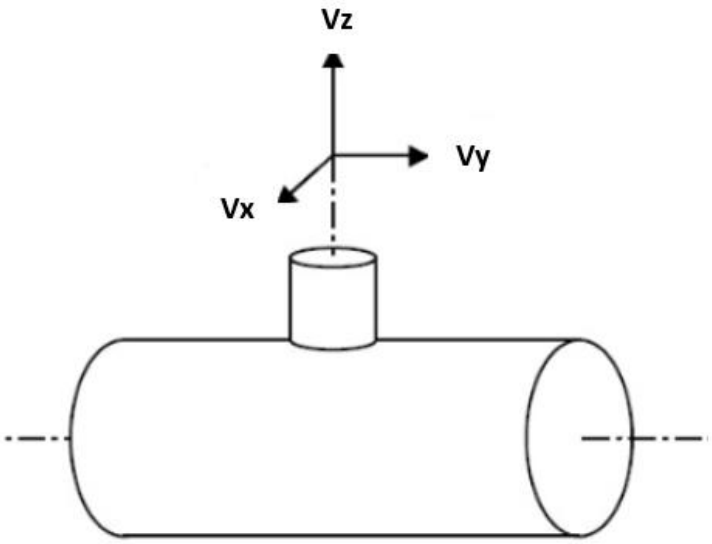

Figure 7. 7 Load conventions for nozzle / cylinder junctions

The same parameters will be applied for all external loading problems. The main variable in the analysis will be di/Di. In total, design curves are created for 11 different di/Di. Here, Di is always constant. In other words, the inner diameter of the nozzle (di) is widened at each step, and external forces act on the nozzle. Another variable forming the curves will be t/T. The t/T ratio, on the other hand, was increased with equal weights at 10 different points, starting from 0.2 to 2.0, to create a wide ranged examination area. The purpose of choosing these variables is to provide the opportunity to examine the

nozzle and cylinder diameters and their wall thicknesses, which directly affect the maximum stress on the structure, in the same design curve graph.

The design curves created under the aforementioned parameters for Vx, Vy and Vz are shown in the **Figure 7. 8**, **Figure 7. 9**, and **Figure 7. 10**.

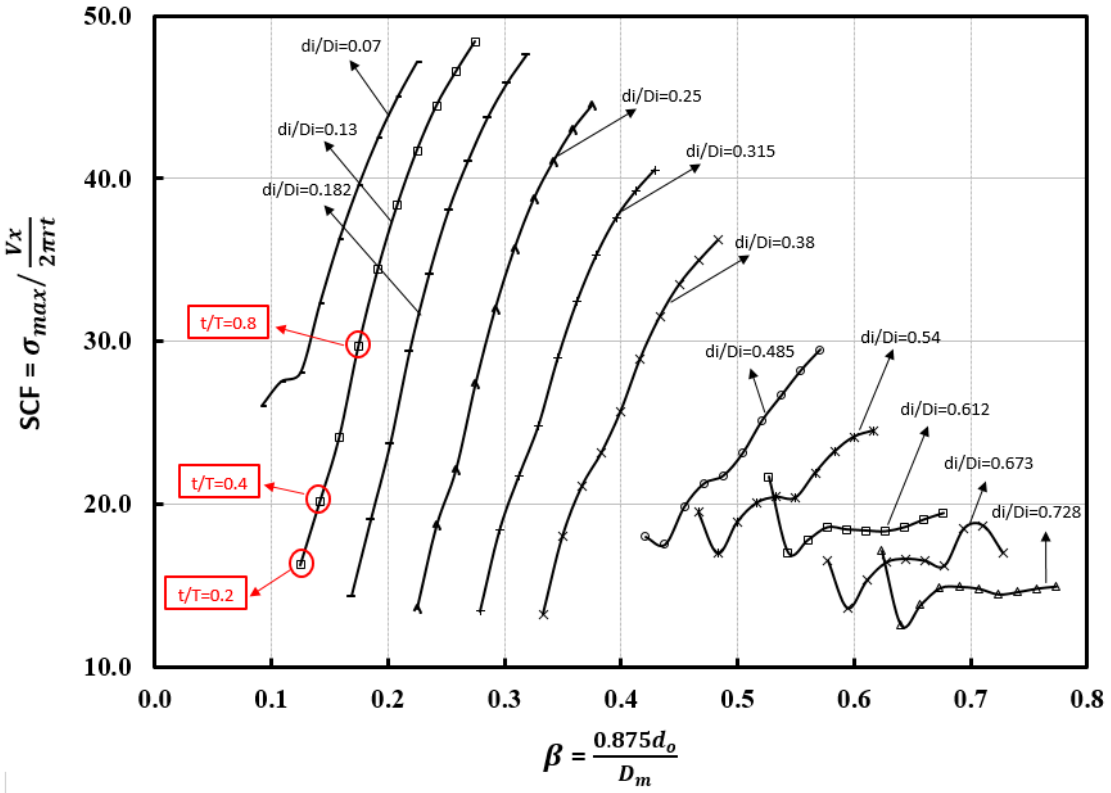

Figure 7. 8 Stress Concentration Factors for maximum stress in nozzle/cylinder junctions subject to External Loads (Vx)

When the Vx loading is examined in **Figure 7. 8**, the S.C.F values tend to decrease almost linearly as t increases up to the di/Di = 0.38 curve. However, when the nozzle diameter reaches almost half of the cylinder diameter (di/Di = 0.485), the S.C.F at t/T=0.2 is quite high. This is because the nozzle thickness (t) cannot meet the increasing maximum stress as di increases. This t/T=0.2 case is also one of the most striking points of the design curves. Another issue is that as the nozzle inner diameter increases, the maximum S.C.F obtained for the same t/T decreases and the wall thickness effect almost disappears.

Because as the di/Di value approaches 1, the clearance on the cylinder increases considerably and the maximum stress values that the vessel can withstand decrease. This means that SCF values decrease at the same rate. After di/Di=0.54, the nozzle opening exceeds half the vessel diameter. At this point, the stress in the system is much higher than the increase in nozzle thickness can afford. Therefore, as can be seen from the figure, the SCF-β relationship starts a linearization trend.

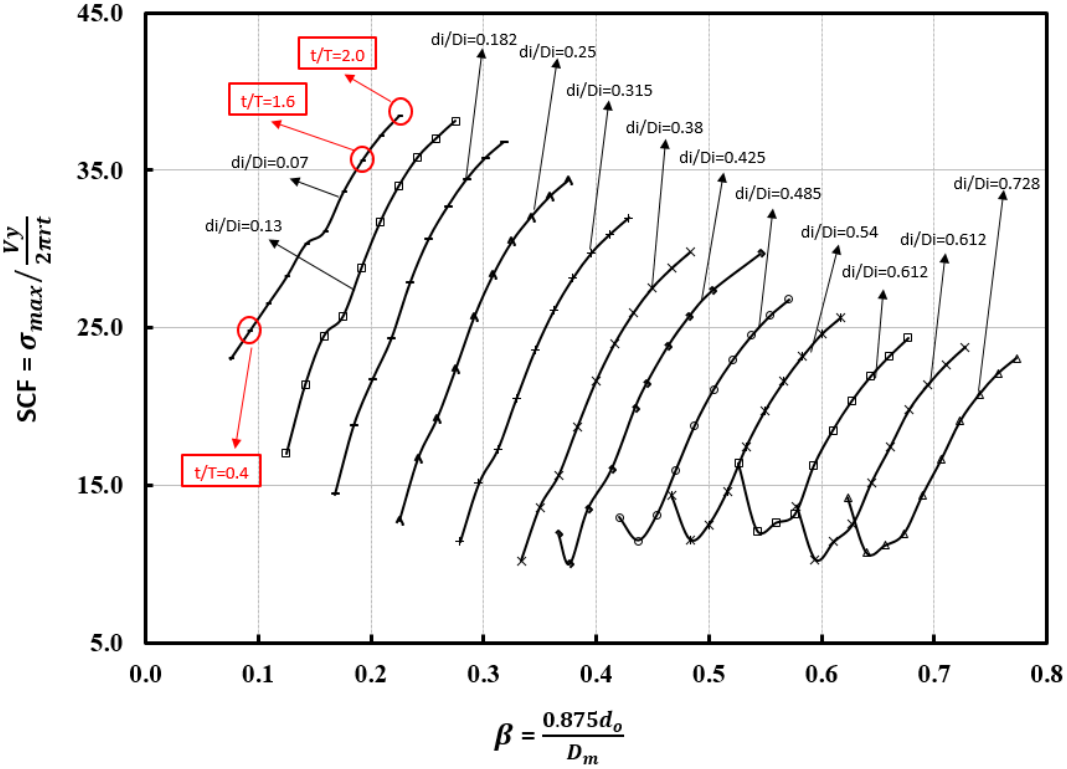

Figure 7. 9 Stress Concentration Factors for maximum stress in nozzle/cylinder junctions subject to External Loads (Vy)

If the **Figure 7. 9** on which the Vy force is applied is examined, the comments that can be made for Vx are mostly similar. However, a similar trending progression of the curves is remarkable, especially after the di/Di=0.425 curve. However, in case of t/T=0.2, the nozzle wall thickness cannot meet the loads on the structure and wall stresses are observed too much. Another striking point is that Vx loading produces an average of 15% more

S.C.F values than Vy. This shows that the axial loading applied in the X direction has a tendency to force the system more than that applied in the longitudinal direction.

The last case to be examined is the case of loading the tensile in the Z direction. The results are shown in the **Figure 7. 10**. If each curve is examined separately, it will be seen that an increase in t increases S.C.F as in other external loads.

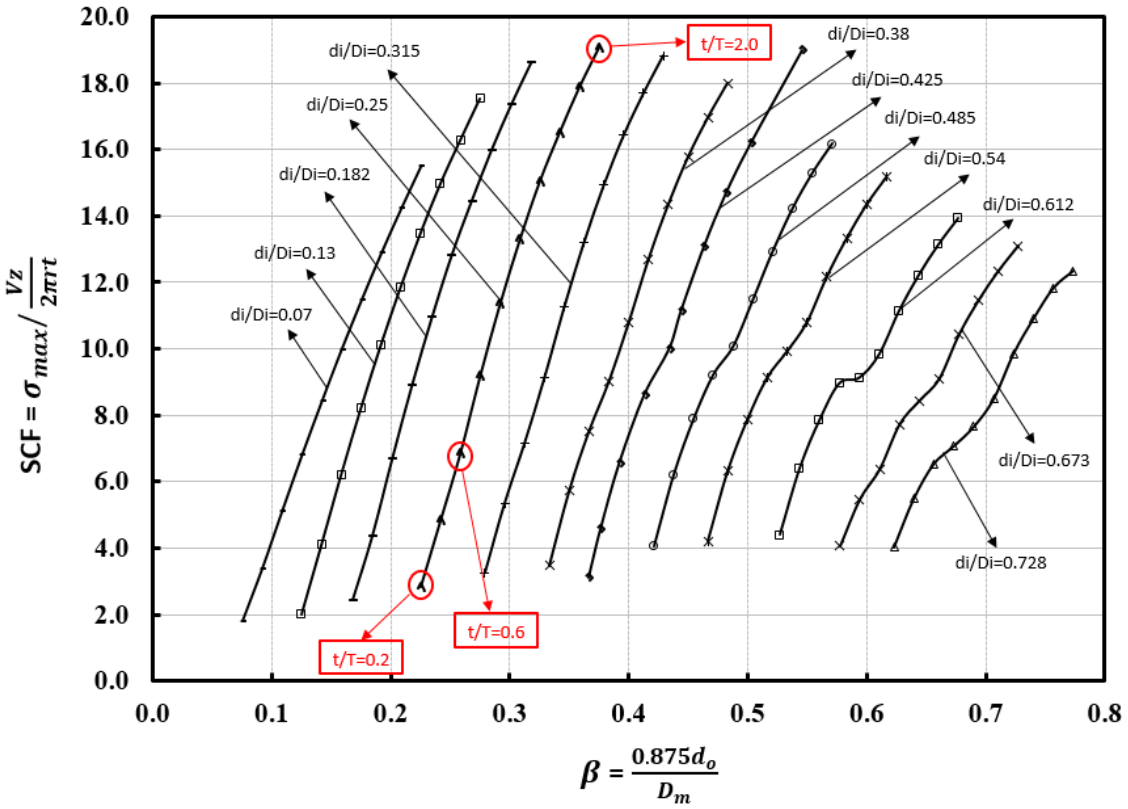

Figure 7. 10 Stress Concentration Factors for maximum stress in nozzle/cylinder junctions subject to External Loads (Vz)

In summary, all these obtained design curves show that pressure and external loads lead to a non-linear load-stress relationship. Another important point here is that the analysis made, and the curves obtained refer to loads in a certain direction (only tensile, only longitudinal, only axial directions etc.). As a result, this study is a guide for designers and researchers for various radius and wall thickness parameters in internal pressure and external loading conditions.

7.3. Multiple Plastic Slope (MPS) Method

As with all structural problems, the plastic failure mechanism in pressure vessels is a gradual process and it is very difficult to determine the certain plastic load precisely. Although most of researchers has been tried to determine the uncertain gross plastic loads by methods such as TES and TI criteria, new approaches or calculations must be established due to the obvious differences between the results of these methods.

When **Figure 7. 11** and **Figure 7. 12** are examined with these approaches, it will be seen that even for the same problem, there are differences of up to 15 percent in the determination of gross plastic load. In addition, when considering the Tangent Intersection Criterion, it is possible to obtain slightly different results depending on the ability of the person who constructs it, since the tangential drawing depends on a single point (5% strain point). In addition, since brittle materials that do not exceed 5% elongation do not comply with this rule, the tangent is drawn from the point where the maximum strain is in plastic deformations, and this is a big handicap. In addition, drawing load-deformation graphs for each problem causes great time losses in parametric studies. Considering all these, the Multiple Plastic Slope (MPS) method, which is an easier implementation, is proposed in this section.

In this method, the stress-strain diagram of the material is drawn first, again with the Ramberg-Osgood approach. Then, slopes (Li, Li+1, … Ln) are drawn from the 0.2% offset line, each of which reaches the ultimate strength (*Stu*), as seen in the **Figure 7. 13**. The strain values corresponding to the *Stu* values for each drawn slope are also read from the Stress-Strain diagram. To put it simply, in the first step, the stress-strain values up to the 0.2% offset line are taken directly from the diagram. Then, for each L line drawn, the strain value corresponding to the Stu value is read. All these stress-strain values are

entered in ANSYS for multilinear kinematic hardening analysis. As a result of the finite element analysis to be made, the maximum pressure values corresponding to each L line are found.

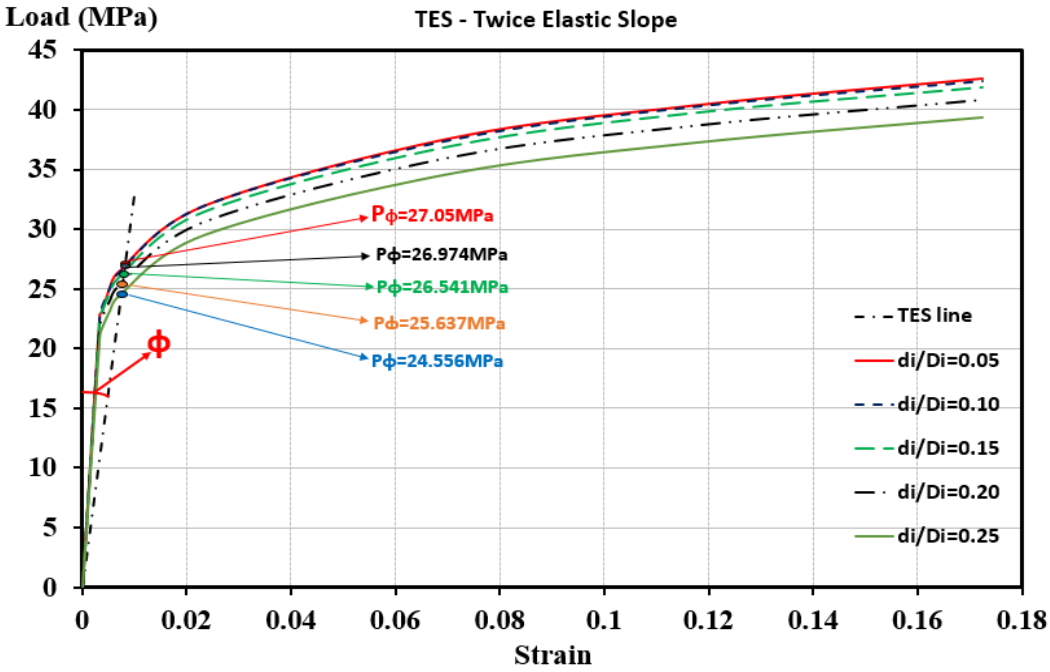

Figure 7. 11 Gross plastic loads according to TES criterion

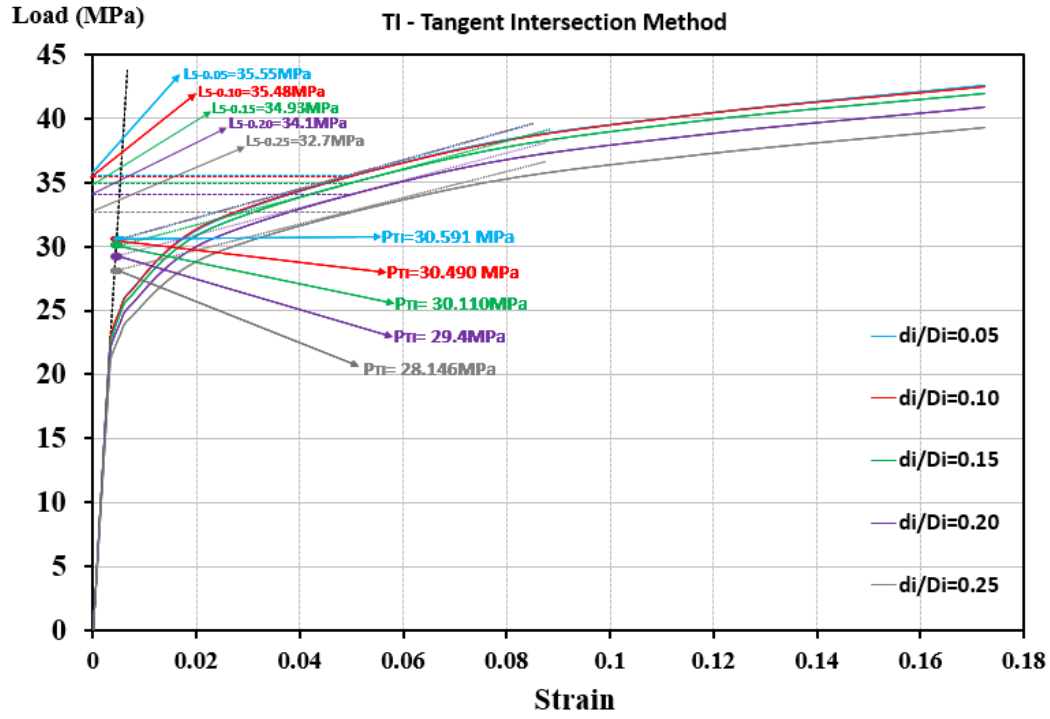

Figure 7. 12 Gross plastic loads according to TI criterion

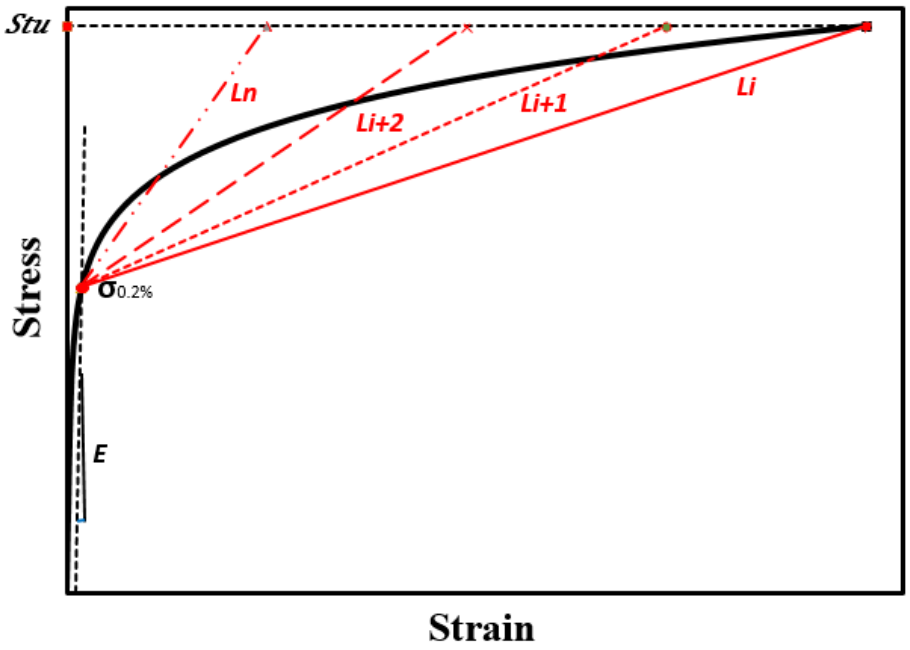

Figure 7. 13 Determination of stress - strain values for MPS method

Here, the point to be considered in the design and analysis phase of the nozzle-cylinder problem exposed to internal pressure should be to find a plastic pressure value to calculate the allowable static pressure. In other words, it is to approximate the pressure at which the plastic deformation is too high, rather than the collapse load. When ASME VIII Division 2 Appendix 4-136.5 is considered, it is stated that the loads determined in plastic analysis should not exceed two-thirds of the lower bound collapse load. With these expressions, the allowable pressure value (Pa) is

$$Pa = \frac{2}{3} Pp \qquad \textbf{Equation 7. 4}$$

where Pp is the internal collapse pressure obtained as a result of plastic analysis for this problem.

If an approximate allowable internal pressure expression is determined by the MPS method by integrating **Equation 7. 4**, Pa_{MPS} for n elastic slopes is

$$Pa_{MPS} = \frac{2}{3}\frac{\sum_{i=1}^{n}(P_{Li})}{n} \qquad \text{Equation 7. 5}$$

where P_{Li} is the collapse internal pressure value obtained for each L plastic slop.

Plastic load values obtained by the MPS method are calculated for 5 different di/Di parameters, as in the TES and TI methods. The compared results are shown in the **Figure 7. 14** below.

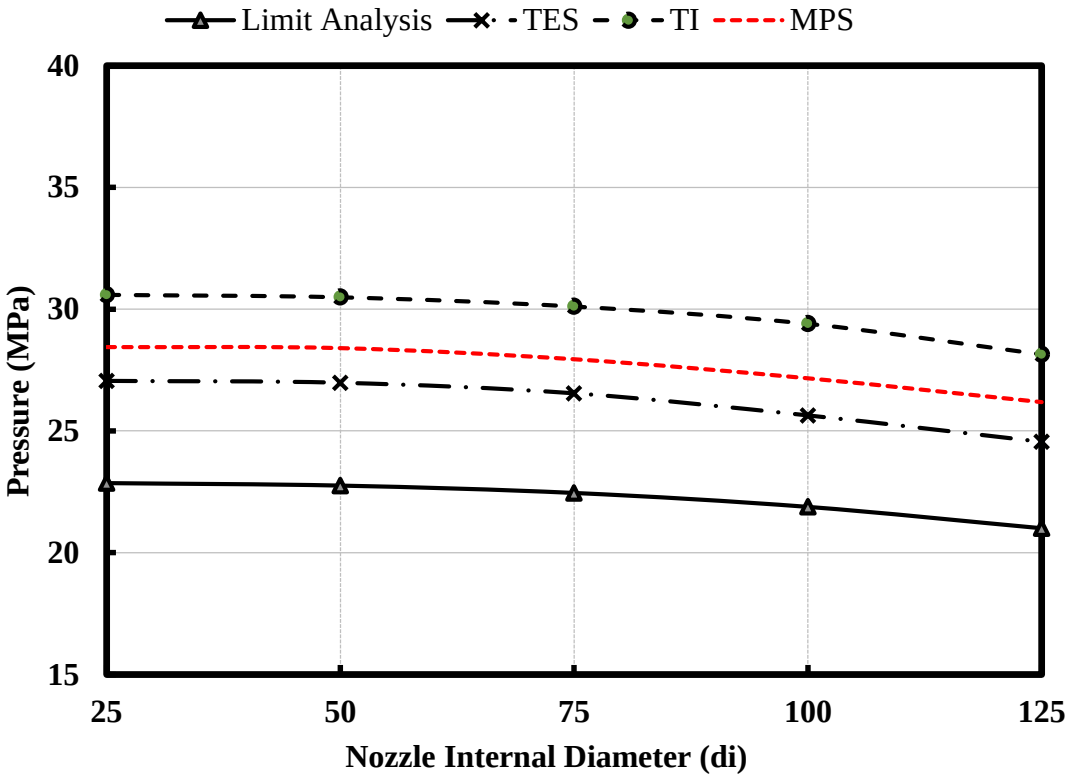

Figure 7. 14 Comparison of the plastic loads for TES, TI and MPS

As can be seen from the Figure, the plastic load value obtained by the MPS method is quite close to the values obtained by the TES and TI criteria. Besides, as can be predicted, plastic deformation occurs at lower pressures as the nozzle diameter increases. With an increase of 5 times the inside diameter of the nozzle (di), this value causes a decrease of approximately 8% in the plastic load for MPS, 9% in the TES criterion and 8% in the TI

criterion. This figure also shows that the values calculated using the load-strain graph in the TES and TI methods are similar to the load trends of the MPS method, which directly uses the results obtained with FEA results and **Equation 7. *5***.

7.4. Concluding remarks

In the earlier part of this work, stress concentration factor curves related to an attachment parameter were plotted for the nozzle-cylinder intersection under internal pressure and local loading. All these obtained design curves show that pressure and external loads lead to a non-linear load-stress relationship. Another important point here is that the analysis made, and the curves obtained refer to loads in a certain direction (only tensile, only longitudinal, only axial directions etc.). As a result, this study is a guide for designers and researchers to find SCF for various radius and wall thickness parameters in internal pressure and external loading conditions.

In the latter part of the work, an alternative method to TES and TI methods is proposed. In this method, called Multiple Plastic Slope (MPS), it can be said that plastic limit load is estimated by taking data from more than one point on the load - strain graph, and it can be said that it gives more reliable results, especially compared to the TES method. On the other hand, since the tangential line is drawn from a single point in the TI method, there is a slight possibility that the person drawing will make a mistake. For this reason, this proposed alternative method will be beneficial for the wider community and code writers

CHAPTER 8 – CONCLUSIONS AND RECOMMENDATIONS

The general objective of this study was to conduct a large-scale design-analysis study for nozzle-cylinder connections. For this purpose, high fidelity computational model was developed, and a wide ranging of parameter study presented, covering the elastic, elastic – perfectly plastic, full plastic, cyclic loading, and fracture behaviours of the structure. As a result, stress concentration factor design curves depending on a well-established attachment parameter were plotted for nozzle-cylinder connections and a new approach, the Multiple Plastic Slope (MPS) Method, which can predict plastic limit load, was presented.

8.1. Results and Conclusions

In chapter 2, a literature review on the design, analysis, and international design codes of pressure vessels in cylindrical vessels and nozzle connections were presented. These literature studies have shown that nozzle-vessel connection problems, elastic stress analysis, limit loading analysis, plastic load determination, fracture mechanics and international design codes have a wide research area in many subjects. Although the application of the finite element method has paved the way for these studies to be done more easily and accurately in the theoretical sense, the studies have shown that application differences can occur even in similar problem solutions in complex structures. For this reason, a high-fidelity finite element model should be created for answering all these analysis methods. Chapter 3 was written for this purpose.

In Chapter 3, a high-fidelity finite element model has been developed, which will be applied to all geometries used by the industry and will provide a universal approximation to local loads for nozzle-cylinder connections, as well as taking into account the

maximum stresses around the crotch corner. Because stress analysis of cylinder-cylinder connections is a very challenging engineering problem in finite element method applications, in order to ensure high sensitivity, first of all, mesh sensitivity analyses were completed, and the most appropriate element size and number were determined for the structure to be created. Since the maximum stress values in the model occur at the nozzle junction, these sensitivity analyses were made according to the number of elements extending along the nozzle thickness. As a result of these analyses, it has been revealed that the number of elements extending along the nozzle (provided that there is no single or 2 elements) does not have a great effect on the stress values. Then, material selection, loading conditions and boundary conditions were determined. Then, various validation studies were carried out for the finite element model created. Firstly, the obtained nozzle-cylinder model was compared with one of the existing models in Chandiramani's study [16] and validation analyses were performed on this model. The reason for choosing this study is that all model parameters are shared clearly and in detail in the article. In this way, it was possible to make comparisons in different size parameters. Secondly, validation studies were performed using WRC Bulletin 537 calculations for tensile force, longitudinal moment and circumferential moment loadings acting on the nozzle. In particular, the validation results under tensile force loading perfectly matched. There was a maximum stress difference of less than 5% in the Mc and ML results. Apart from this, 2 more validation studies were carried out for the fracture problems in Chapter 6. This part was not included in Chapter 3 in terms of subject integrity. In the validations obtained here, the results of the maximum stress intensity factor were also confirmed with a difference of less than 6%. The reason for this difference is explained in the relevant section, which is due to the free surface effect at the crack tip. All these validation studies

under very diverse conditions prove that the generated finite element model will respond to a wide range of nozzle – cylinder connection problems with high precision.

In the 4th chapter, finite element analyses in the elastic region for nozzle connections in pressure vessel problems with parametric studies were examined and the results were discussed. In addition, single and multiple nozzle connection problems, oblique nozzles, stress analysis and stress linearization approach were examined in detail. First, parameter studies were carried out for the effects of inner fillet and outer fillet on the validated model. Here the main aim was to reasonably reduce the stress values in the cylinder-nozzle connection. First, an inner radius of 5 mm was applied to the model mesh corner, resulting in a 10% reduction in stress values. These differences decreased by about 2 percent when the diameter of the cylinders was increased. These results showed that the outer weld fill and inner radius dimensions should be examined separately. In doing so, analyses were made on the change of welding dimensions. It was seen that the weld size is not very effective in reducing the stress in models with under internal pressure only. Following these analyses, inner radius dimensions were increased. As a result, the maximum stress values decreased by up to 10% and the most suitable welding dimensions and inner radius sizes were determined. In the next step, analyses were made for 5 different external loading situations. In the case of internal pressure, the maximum stress region was observed at the crotch corner, while in these analyses, as the external moment effect increased, the maximum stress region shifted to the outer wall, especially to the weld (see **Figure 4. 13**, **Figure 4. 14**, and **Figure 4. 15**). After that, torsional, circumferential, and longitudinal loading conditions were compared with WRC537 calculations. For the models where the external moment was applied, the differences were nearly 5 percent. The close results obtained once again demonstrate the correctness of the model. Whilst this gives confidence that WRC 537 was conservative

for the moment cases, it was over predicting the maximum stress which can have an influence when using these stresses for fatigue life evaluation.

Then, multiple nozzle combinations were examined. When considering multiple nozzle combinations, it can be seen the stress values decrease when the pitch between nozzles in axial direction is reduced. In addition, the stress values increase when pitched nozzles in the longitudinal direction are positioned close to each other. Therefore, if the nozzles get too close to each other radially or longitudinally, there is the potential for plastic collapse. Therefore, maintaining the die-out distance as shown by the code equation remains important even in limit load analysis. It is also noted that the maximum stresses in the multiple nozzle analyses occurred on the crotch corner in all cases when internal pressure is applied. Changes in the maximum stress magnitudes were observed when the pitch between the nozzles was changed. However, the stress magnitudes in the 1st nozzles, which are close to the thrust force, are greater in both longitudinal and axially positioned situations rather than at the 2nd nozzle position – hence showing the result of the combined interaction. These situations therefore need to be assessed on a case-by-case basis.

The last study of chapter 4 was pad reinforcement for oblique nozzles and standard nozzles. In this part, the research based on the stress linearization technique. Stress linearization is used to define constant and linear thickness FEA (Finite Element Analysis) stress distributions and membrane and membrane + bending stress distributions in Pressure Vessel Design by Analysis. In addition, the basis of this method is to correlate and determine the stress occurring along a path with the concept of limit load. As a result of this work, a comprehensive stress linearization study was carried out for a nozzle-cylinder combination that was subjected only to internal pressure. In the study, stress

distribution at critical locations determined on the nozzle and shell was investigated. According to the results, the tension is maximum in the paths chosen close to the opening zone in both the shell and the nozzle. Also, especially the increase in pad contribution significantly reduced the stresses obtained on the same paths. On the other hand, since the stress distribution on both sides of the sloping was not equal in oblique nozzles, the differences in stress magnitudes could be easily detected by this method. As a result, this study provides researchers an alternative stress analysis for critical locations in the intersection area in the design and analysis of cylinder nozzle connections.

Chapter 5 contains inelastic analysis. These are limit loading analysis, full elastic-plastic analysis, and cyclic loading analysis. The work in the limit loading situation was completed in 3 main stages. Firstly, the effect of nozzle diameter change was investigated. Here, it was observed that the limit load value decreased as the nozzle diameter increased. The reason why the limit pressure magnitude decreases as the nozzle diameter increases, is that the opening in the main shell increases and reduces the available material to support the load. Then, the effects of nozzle and shell thicknesses on the limit load conditions were examined. Finally, the limit loading conditions of external loading cases are examined. The thickness of the cylinder and nozzle were increased by 5mm in each analysis separately. As can be seen in the limit pressure calculations in pressure vessels, the most important variable is the inner and outer diameter ratio. As a result of this approach, when the thickness increases, the limit load increases linearly. In Case 3, the internal pressure values were increased by 5MPa in each analysis and limit loads were determined for external loading conditions. In the stress calculations of shear force, Bijlaard's [13] calculation approaches were shown in WRC537. According to this approach, the shear forces acting on the nozzle do not cause longitudinal and

circumferential stresses in the shell. Therefore, the increase in pressure inside the vessel reduces the shear limit forces to a very small extent (approx. 3%). As a result of this analysis, it was observed that the longitudinal (VL) and circumferential (VC) shear forces transfer the material to the plastic region at much lower values. On the Z axis, tensile loading (P) was involved. Tensile loading directly affects the longitudinal and circumferential stresses on the shell. For this reason, to transfer this material into the plastic zone, approximately 3 times more loads should be applied. Therefore, tensile limit load values tend to decrease as the internal pressure increases. These results were consistent with the current approach.

Then, full elastic plastic analyses were performed. First of all, TES, and TI methods, which are frequently used in estimating the limit plastic load, were introduced. By using these methods, limit plastic load estimations were made for 5 different di/Di ratios. These analyses formed the basis of comparison for the new plastic limit load estimation method (MPS) to be proposed in Chapter 7.

Finally, cyclic loading analyses were performed for different dm/Dm parameters. As a result of the analyses made, examinations were made on the PT/PY ratio recommended by Procter & Strong for test pressure, and it was seen that the PT/PY=1,82 value was very high at some points and that the structure would undergo plastic collapse in a very short period of time with this value.

In the 6th chapter, information is given about the outer wall cracks and the inner wall cracks in the nozzle-cylinder connections. Then, the finite element model was validated by Newman-Raju calculations [54] and Sedighiani's work [90]. There are some SIF calculation methods for cracks located on perfect cylinders in the literature, but these

methods only provide calculations for the opening mode-I caused by the hoop stress. On the other hand, although studies based on fracture mechanics related to nozzle-cylinder intersections have been made, there is no definitive solution for calculating mixed mode stress intensity factors in potential cracks that may occur. For this purpose, in this study, alternative solutions related to the calculation of stress intensity factors under internal pressure and various external local loads of elliptical cracks located at a location very close to the nozzle cylinder intersection (upper side of the welding) and inner wall crack located on the crotch corner were produced. As a result of the studies, it was observed that the SIF values increased in direct proportion to the magnitude of the loading and the size of the crack only in cracks under internal pressure. On the other hand, it was determined that the direction of the force is more effective than the magnitude of the force in external loads applications. For example, the single tensile force (Vz) of 1000kN applied from the nozzle center has a greater KI SIF value than the local forces applied in 3 different directions simultaneously (1000kN Vx + 1000kN Vy + 1000kN Vz) and the crack tends to open more.

In summary, this study discusses in detail the SIF calculations for surface cracks that may occur in the nozzle inner and outer wall in nozzle-cylinder connection problems and provides a wide parameter study.

In the 7th chapter, firstly, the maximum stresses calculated by finite element analysis and stress intensity factors (S.C.F.) were obtained for nozzle/cylinder connections under the influence of internal pressure and external local loads. Then, basic dimensions on geometry such as cylinder diameter, nozzle diameter, wall thickness were changed with different parametric approaches and loading conditions, and a wide range of design curves for cylinder/cylinder connection problems were presented. In summary, all these obtained

design curves shown that pressure and external loads lead to a non-linear load-stress relationship. As a result, this study is a guide for designers and researchers for various radius and wall thickness parameters in internal pressure and external loading conditions.

Finally, a new approach (MPS) was presented as an alternative to TES and TI methods that help to estimate plastic load with the help of load-deformation curves. This method was compared with TES and TI methods and the results were presented. It has been a good alternative method for researchers due to its ease of application, the fact that the researcher does not have the possibility of making mistakes while drawing tangent lines like the TI method, and because the TI method has hypothetical results for brittle materials (maximum strain is below 5%).

8.2. Recommendations

1. This study is basically based on finite element analysis. Especially in industrial containers, not every researcher has the opportunity to test the results due to the cost and size of the structure. Validation studies of these approaches can be carried out in special test centres or laboratories.

2. This work can be expanded with composite materials in order to provide more flexibility and strength to the structure.

3. Since the obtained design curves contain too many different parameters, it is very difficult to express them with a single formulation. For this reason, equations compatible with finite element analysis can be developed by combining appropriate parameters.

4. Although not very important in the United Kingdom, there is a high risk of earthquakes due to the mobility of fault lines in many parts of the rest of the world. For this reason, it will be useful to make seismic analyses of pressure vessels. Especially if the maximum stress areas can be followed by using the sensor technology with these study results, it can create a new study area for nozzle-cylinder connection problems.

REFERENCES

[1] J. Ellenberger, Pressure vessels: the ASME code simplified, McGraw-Hill Education, 2004.

[2] ASME Boiler and Pressure Vessel Code: Section VIII.

[3] B. S. PD5500, Specification for unfired fusion welded pressure vessel, British Standards Institution, 2000.

[4] E. 13445, Unfired Pressure Vessels, European Committee for Standardization-CEN, 2002.

[5] European Pressure Equipment Directive (PED) No. 97/23/EC, 1997.

[6] D. H. Nash, UK Rules for unfired pressure vessels, ASME, 2008.

[7] K. Wichman, A. G. Hopper and J. L. Mershon, Local Stresses in Spherical and Cylindrical Shells Due to External Loadings, New York: Welding Research Council Bulletin No. 107, 2002.

[8] J. Mershon, K. Mokhtarian, G. V. Ranjan and E. C. Rodabaugh, Local Stresses in Cylindrical Shells Due to External Loadings On Nozzles-Supplement to WRC Bulletin No. 107 (Revision I), Welding Research Council Bulletin No. 297, 1984.

[9] K. Wichman, A. G. Hopper and J. L. Mershon, Precision Equations and Enhanced Diagrams for Local Stresses in Spherical and Cylindrical Shells Due to External Loadings for Implementation of WRC Bulletin 107, Welding Research Council Bulletin No. 537, 2013.

[10] R. T. Rose, "Stress analysis of nozzles in thin walled cylindrical pressure vessels," *British Welding Journa,* vol. 12, no. 2, pp. 80-90, 1965.

[11] F. A. Leckie ve R. K. Penny, «Stress concentration factors for the stresses at nozzle intersections in pressure vessels.,» %1 içinde *Welding Research Council Bulletin 90*, 1963.

[12] H. A. Money, "Stress analysis of nozzles in thin walled cylindrical pressure vessels," Berkeley, Gloucestershire, 1966.

[13] P. P. Bijlaard, "On the Effect of Tangential Loads on Cylindrical and Spherical Shells,," Welding Research Council.

[14] T. L. Andrade, W. A. d. Paula and P. A. A. M. Junior, "Analysis of Stress in Nozzle/Shell of Cylindrical Pressure Vessel under Internal Pressure and External Loads in Nozzle," *Int. Journal of Engineering Research and Applications,* vol. 5, no. 9, pp. 84-91, 2015.

[15] C. J. Dekker and H. J. Bos, “Nozzles-on external loads and internal,” *International Journal of Pressure Vessels and Piping,* vol. 72, pp. 1-18, 1997.

[16] D. K. Chandiramani, S. Gopalakrishnan and A. Mathkar, “Effect of Nozzle Dimensions on the Stresses in Compensated Openings in Cylindrical Shells”

in *Proceedings of the ASME 2015 Pressure Vessels and Piping Conference PVP2015-45564*, Boston, Massachusetts, USA, 2015.

[17] M. R. Cheema, A. P. Niyamatullah and A. Aftab, “Analysis of Pad Reinforced Openings in Pressure Vessels,” *International Journal of Engineering Research & Technology (IJERT),* vol. 8, no. 08, 2019.

[18] L. R. Herrmann and D. M. Campbell, “A finite-element analysis for thin shells,” *AIAA Journal,* vol. 6, no. 10, pp. 1842-1847, 1968.

[19] F. M. Mukhtar and H. J. Al-Gahtani, “Finite Element Analysis and Development of Design Charts for Cylindrical Vessel–Nozzle Junctures Under Internal Pressure,” *Arabian Journal for Science and Engineering,* vol. 41, no. 10, pp. 4195-4206, 2016.

[20] C. D. Figueiredo and M. M. Neto, “Recommendation for linearization procedure in nuclear pressure vessel-nozzle intersections,” *Brazilian Journal of Radiation Sciences,* vol. 8, no. 3A, 2020.

[21] A. R. Kharat, S. J. Kadam and S. G. Bhosale, “Study of different type reinforcement in cylindrical pressure vessel,” *International Journal of Engineering Research and Technology,* vol. 02, no. 10, pp. 3178-3181, 2013.

[22] L. Xue, G. E. Widera and Z. F. Sang, “Influence of pad reinforcement on the limit and burst pressures of a cylinder-cylinder intersection,” *J. Pressure Vessel Technol.,* vol. 125, no. 2, pp. 182-187, 2003.

[23] J. Fang, Q. H. Tang and Z. F. Sang, “A comparative study of usefulness for pad reinforcement in cylindrical vessels under external load on nozzle,” *International Journal of Pressure Vessels and Piping,* vol. 86, no. 4, pp. 273-279, 2009.

[24] Y. J. Chao, B. C. Wu and M. A. Sutton, “Radial flexibility of welded-pad reinforced nozzles in ellipsoidal pressure vessel heads,” *International Journal of Pressure Vessels and Piping,* vol. 24, no. 3, pp. 189-207, 1986.

[25] D. H. Nash and J. Hitchen, “Effects of local reinforcement on nozzles in dished ends,” in *12th International Conference on Pressure Vessel Technology,* 2009.

[26] V. N. Skopinsky and A. B. Smetankin, “Parametric study of reinforcement of pressure vessel head with offset nozzle,” *International Journal of Pressure Vessels and Piping,* vol. 80, no. 5, pp. 333-343, 2003.

[27] A. L. Petrovic, M. M. Balac, A. Jovovic and A. Dedic, “Oblique nozzle loaded by the torque moment–stress state in the cylindrical shells on the pressure vessel,” *Proceedings of the Institution of Mechanical Engineers, Part C: Journal of Mechanical Engineering Science,* vol. 226, no. 3, pp. 567-575, 2012.

[28] E. Weiß, M. Rauth and J. Rudolph, “Fatigue behaviour of oblique nozzles on cylindrical shells submitted to internal pressure and axial forces,” *International Journal of Pressure Vessels and Piping,* vol. 75, no. 6, pp. 473-481, 1998.

[29] D. M. Patel ve B. Kumar, «Limit load estimation of cylindrical vessel with oblique nozzle,» *International Journal of Engineering Research and Technology,* cilt 2, no. 11, pp. 2421-2427, 2013.

[30] M. Robinson, A. Kirk and S. S. Gill, “An experimental investigation into the plastic behaviour of oblique flush nozzles in spherical pressure vessels,” *International Journal of Mechanical Sciences,* vol. 13, no. 1, pp. 41-46, 1971.

[31] Z. A. E. Sang, L. P. Xue, Y. J. Lin and G. E. O. Widera, “Limit and Burst Pressures for a Cylindrical Shell Intersections with Intermediate Diameter Ratio,” *International Journal of Pressure Vessels and Piping,* vol. 79, no. 5, pp. 341-349, 2002.

[32] C. Nadarajah, D. Mackenzie and J. T. Boyle, “Limit and shakedown analysis of nozzle/cylinder intersections under internal pressure and in-plane moment loading,” *International Journal of Pressure Vessels and Piping,* vol. 68, no. 3, pp. 261-272, 1996.

[33] C. J. Dekker and W. J. Stikvoort, “Pressure stress intensity at nozzles on cylindrical vessels: a comparison of calculation methods,” *International Journal of Pressure Vessels and Piping,* vol. 74, no. 2, pp. 121-128, 1997.

[34] D-Merkblatter, Taschenbuch Ausgabe, Essen (Germany): Verband der Technischen Uberwachungs- Vereine e.V.,, 1997.

[35] M. Muscat, D. Mackenzie and R. Hamilton, “A work criterion for plastic collapse,” *International Journal of Pressure Vessels and Piping,* vol. 80, no. 1, pp. 49-58, 2003.

[36] P. F. Liu, J. Y. Zheng, L. Ma, C. J. Miao and L. L. Wu, “Calculations of plastic collapse load of pressure vessel using FEA,” *Journal of Zhejiang University-SCIENCE A,* vol. 9, no. 7, pp. 900-906, 2008.

[37] A. M. Kulkarni and R. L. Wankhade, “Design by Analysis of Liquid Petroleum Gas Cylinder using Twice Elastic Slope Criteria to Calculate the Burst Pressure of Cylinder,” *International Journal of Engineering Research & Technology,* vol. 4, no. 01, pp. 561-568, 2015.

[38] S. Balakrishnan, A. R. Veerappan and S. Shanmugam, “Determination of ovality and wall thinning effects on B 2 stress indices for pipe bends under in-plane closing bending moment,” *Simulation,* vol. 95, no. 2, pp. 185-192, 2019.

[39] Y. C. Deng and G. Chen, “Elastic-Plastic Stress Analysis of Pressure Vessels.,” in *Pressure Vessels and Piping Conference,* 2012.

[40] D. G. Moffat, M. F. Hsieh and M. Lynch, “An assessment of ASME III and CEN TC54 methods of determining plastic and limit loads for pressure system components,” *The Journal of Strain Analysis for Engineering Design,* vol. 36, no. 3, pp. 301-312, 2001.

[41] B. H. Wu, Z. F. Sang and G. E. Widera, “Plastic analysis for cylindrical vessels under in-plane moment on the nozzle,” *Journal of Pressure Vessel Technology,* vol. 132, no. 6, 2010.

[42] A. Prakash, H. K. Raval, A. Gandhi and D. B. Pawar, “Plastic limit load analysis of cylindrical pressure vessels with different nozzle inclination,” *Journal of The Institution of Engineers (India): Series C,* vol. 97, no. 2, pp. 163-174, 2016.

[43] K. H. Lee, Y. J. Kim and C. Y. Park, “Plastic loads of pipe bends under combined pressure and out-of-plane bending,” *International Journal of Fracture,* vol. 149, no. 1, pp. 31-45, 2008.

[44] D. M. Patel and D. B. Kumar, “Pressure vessel limit load estimation by FEM and experimental method,” *Int. J. Innov. Res. Adv. Eng,,* vol. 1, no. 9, pp. 109-114, 2014.

[45] N. Li, Z. F. Sang and G. E. O. Widera, “Study of plastic limit load on pressurized cylinders with lateral nozzle,” *Journal of Pressure Vessel Technology,* vol. 130, no. 4, 2008.

[46] V. N. Skopinsky, N. A. Berkov and A. B. Smetankin, “Plastic limit load of ellipsoidal pressure vessel head with nozzle under internal pressure loading,” *International Journal of Applied Mechanics and Engineering,* vol. 18, no. 4, 2013.

[47] Y. Zeng, “True stress and shakedown analysis of pressure vessel under repeated internal pressure,” *Mechanics & Industry,* vol. 17, no. 4, p. 410, 2016.

[48] A. Kandil, “Analysis of thick-walled cylindrical pressure vessels under the effect of cyclic internal pressure and cyclic temperature,” *International Journal of Mechanical Sciences,* vol. 38, no. 12, pp. 1319-1332, 1996.

[49] H. F. Abdalla, “Shakedown limit load determination of a cylindrical vessel–nozzle intersection subjected to steady internal pressures and cyclic in-plane bending moments,” *Journal of Pressure Vessel Technology,* vol. 136, no. 5, 2014.

[50] A. K. Bakry, C. A. Saleh and M. M. Megahed, “Shakedown Limits for Hillside Nozzles in Cylindrical Vessels,” *Journal of Pressure Vessel Technology,* vol. 140, no. 3, 2018.

[51] L. G. Copley And J. J. Lyell Sanders, “A Longitudinal Crack in a Cylindrical Shell under Internal Pressure,” *International Journal of Fracture Mechanics,* vol. 5, 1969.

[52] F. Erdogan And M. Ratwani, “Fracture of Cylindrical and Spherical Shells containing a crack,” *Nuclear Engineering And Design,* vol. 20, no. 1, pp. 265-286, 1972.

[53] F. Erdogan and M. Ratwani, “A Circumferential Crack in a Cylindrical Shell under Torsion,” *International Journal of Fracture Mechanics,* vol. 8, no. 1, pp. 87-95, 1972.

[54] J. C. Newman Jr and I. S. Raju, “Stress-intensity factors for internal surface cracks in cylindrical pressure vessels,” *J. Pressure Vessel Technol.,* vol. 102, no. 4, 1980.

[55] R. Liu , M. Huang, Y. Peng, H. Wen, J. Huang and C. Ruan, “Analysis for crack growth regularities in the nozzle-cylinder intersection area of Reactor Pressure Vessel,” *Annals of Nuclear Energy,* vol. 112, pp. 779-793, 2018.

[56] U. T. Murtaza and M. J. Hyder, “The effects of thermal stresses on the elliptical surface cracks in PWR reactor pressure vessel,” *Theoretical and Applied Fracture Mechanics,* vol. 75, pp. 124-136, 2015.

[57] T. Jin, Z. Wang, Q. Wang, D. Wang, Y. Li and M. Zhou, “Weibull stress analysis for the corner crack in reactor pressure vessel nozzle,” *Advances in Mechanical Engineering,* vol. 11, no. 2, 2019.

[58] M. Susmikanti, R. Himawan, E. Hartini and R. Rokhmadi, “Analysis of 3D Semi-Elliptical Crack on Reactor Pressure Vessel Wall with Load Stress and Crack Ratio,” *Jurnal Teknologi Reaktor Nuklir Tri Dasa Mega,* vol. 21, no. 1, pp. 33-38, 2019.

[59] V. Akrami and S. Erfani, “An analytical and numerical study on the buckling of cracked cylindrical shells,” *Thin-Walled Structures,* vol. 119, pp. 457-469, 2017.

[60] H. E. Estekanchi and A. Vafai, “On the buckling of cylindrical shells with through cracks under axial load,” *Thin-walled structures,* vol. 35, no. 4, pp. 255-274, 1999.

[61] E. Alizadeh and M. Dehestani, “Analytical and numerical fracture analysis of pressure vessel containing wall crack and reinforcement with CFRP laminates,” *Thin-Walled Structures,* vol. 127, pp. 210-220, 2018.

[62] A. Subbaiah and R. Bollineni, “Stress Intensity Factor of Inclined Internal Edge Crack in Cylindrical Pressure Vessel.,” *Journal of Failure Analysis and Prevention,* vol. 20, no. 5, pp. 1524-1533, 2020.

[63] N. V. Challenger, R. Phaal and S. J. Garwood, “Fracture mechanics assessment of industrial pressure vessel failures,” *International journal of pressure vessels and piping,* vol. 61, no. 2-3, pp. 433-456, 1995.

[64] P. 1991, Guidance on methods for assessing the acceptability of flaws in fusion, London: British Standards Institution, 1991.

[65] P. K. Liaw, C. Y. Yang, S. S. Palusamy and W. Ren, “Fatigue crack initiation and propagation behavior of pressure vessel steels,” *Engineering fracture mechanics,* vol. 57, no. 1, pp. 85-104, 1997.

[66] G. Chai and K. Zhang, “Stress intensity factors for interaction of surface crack and embedded crack in a cylindrical pressure vessel,” *International Journal of Pressure Vessels and Piping,* vol. 77, pp. 539-548, 2000.

[67] A. Kiciak, G. Glinka and D. J. Burns, “Calculation of Stress Intensity Factors and Crack Opening Displacements for Cracks Subjected to Complex Stress Fields,” *Journal of Pressure Vessel Technology,* vol. 125, no. 3, pp. 260-266, 2003.

[68] A. T. Diamantoudis and G. N. Labeas, “Stress intensity factors of semi-elliptical surface cracks in pressure vessels by global-local finite element methodology,” *Engineering Fracture Mechanics,* vol. 72, no. 9, pp. 1299-1312, 2005.

[69] A. Saffih and S. Hariri, “Numerical study of elliptical cracks in cylinders with a thickness transition,” *International Journal of Pressure Vessel and Piping,* vol. 83, no. 1, pp. 35-41, 2006.

[70] A. Saffih and S. Hariri, “Comparison of semi-elliptical cracks in cylinders with a thickness transition and in a straight cylinders – Elastic–plastic behaviour,” *Engineering Fracture Mechanics,* vol. 73, pp. 2685-2697, 2006.

[71] K. J. Kirkhope, R. Bell and J. Kirkhope, “Stress intensity factors for single and multiple semi-elliptical surface cracks in pressurized thick-walled cylinders,” *International journal of pressure vessels and piping,* vol. 47, no. 2, pp. 247-257, 1991.

[72] B. E. K. Hachi, S. Rechak, Y. Belkacemi and G. Maurice, “Modelling of elliptical cracks in an infinite body and in a pressurized cylinder by a hybrid weight function approach,” *International Journal of Pressure Vessels and Piping* vol. 82, no. 12, pp. 917-924., 2005.

[73] A. O. Ayhan and H. F. Nied, “Stress intensity factors for three-dimensional surface cracks using enriched finite elements,” *International Journal for Numerical Methods in Engineering,* vol. 54, no. 6, pp. 899-921, 2002.

[74] A. O. Ayhan, “Simulation of three-dimensional fatigue crack propagation using enriched finite elements,” *Computers & Structures,* vol. 89, no. 9-10, pp. 801-812, 2011.

[75] M. Bozkurt, A. O. Ayhan, M. F. Yaren and S. Siriç, “Finite element modeling and experimental studies on mixed mode-I/III fracture specimens,” *Frattura ed Integrità Strutturale,* vol. 10, no. 35, pp. 350-359, 2016.

[76] E. Kurt and A. O. Ayhan, “Three-dimensional mixed-mode stress intensity factors for deflected internal surface cracks in thin and midsize-thick-walled spherical pressure vessels,” *International Journal of Pressure Vessels and Piping* , vol. 171, pp. 10-33, 2019.

[77] “Material properties for SA 516 Grade 70,” [Online]. Available: https://masteel.co.uk/asme-sa516-grade-70/. [Accessed 07 06 2021].

[78] “Material properties for ASTM A266 Grade 2 Carbon Steel,” [Online]. Available: https://www.makeitfrom.com/material-properties/ASTM-A266-Grade-2-Carbon-Steel. [Accessed 07 06 2021].

[79] A. M. A. Release, 15, ANSYS Mechanical APDL element reference., 2013.

[80] CEN, “Part 3. Unfired pressure vessels,” in *prEN 13445-3,* European Committee for Standardisation (CEN), 1999.

[81] W. Ramberg and W. R. Osgood, “Description of stress-strain curves by three parameters (No. NACA-TN-902),” 1943.

[82] E. Procter and J. T. Strong, “Pressure Tests on Flush Cylinder/cylinder Intersections: Elastic and Elastic/plastic Behaviour.,” Berkeley Nuclear Laboratories, Berkeley, Gloucestershire, UK, 1972.

[83] A. A. Griffith, “The phenomena of rupture and flow in solids.,” *Philosophical transactions of the royal society of london. Series A, containing papers of a mathematical or physical character,,* vol. 221, no. 582-593, pp. 163-198, 1921.

[84] C. Zener and J. H. Hollomon, “Effect of strain rate upon plastic flow of steel.,” *Journal of Applied physics,* vol. 15, no. 1, pp. 22-32, 1944.

[85] H. Tada, P. C. Paris and G. R. Irwin, The stress analysis of cracks., Handbook, Del Research Corporation, 1973.

[86] A. A. Wells, in *Crack Propagation Symposium,* Cranfield, 1961.

[87] M. BAalac, A. GrBovic and V. Popovic, “FEM analysis of pressure vessel with an investigation of crack growth on cylindrical surface,” *Eksploatacja i Niezawodność,* vol. 20, no. 3, 2018.

[88] L. S. de Schiara ve G. O. de Ribeiro, «Finite element mesh generation for fracture mechanics in 3D coupled with Ansys®: elliptical cracks and lack of fusion in nozzle welds,» *Journal of the Brazilian Society of Mechanical Sciences and Engineering,* cilt 38, no. 1, pp. 253-263, 2016.

[89] A. O. Ayhan, *Finite element analysis of nonlinear deformation mechanisms in semiconductor packages,* Lehigh University, 1999.

[90] K. Sedighiani, J. Mosayebnejad and M. Mafi, “Fracture analysis of a semi-elliptical crack in a nozzle–vessel junction under external loads.,” *Proceedings of the Institution of Mechanical Engineers, Part C: Journal of Mechanical Engineering Science,,* vol. 226, no. 4, pp. 871-886, 2012.

[91] J. Spence and A. S. Tooth, Pressure Vessel Design Concepts and Principles, CRC Press, 2012.

[92] D. R. Moss and M. Basic, “6-Special Design,” in *Pressure Vessel Design Manual (Fourth Edition),* 2013, pp. 393-434.

Appendix A - WRC 537 Local Stresses in Cylindrical Shells Due to External Loading – Solid Attachments

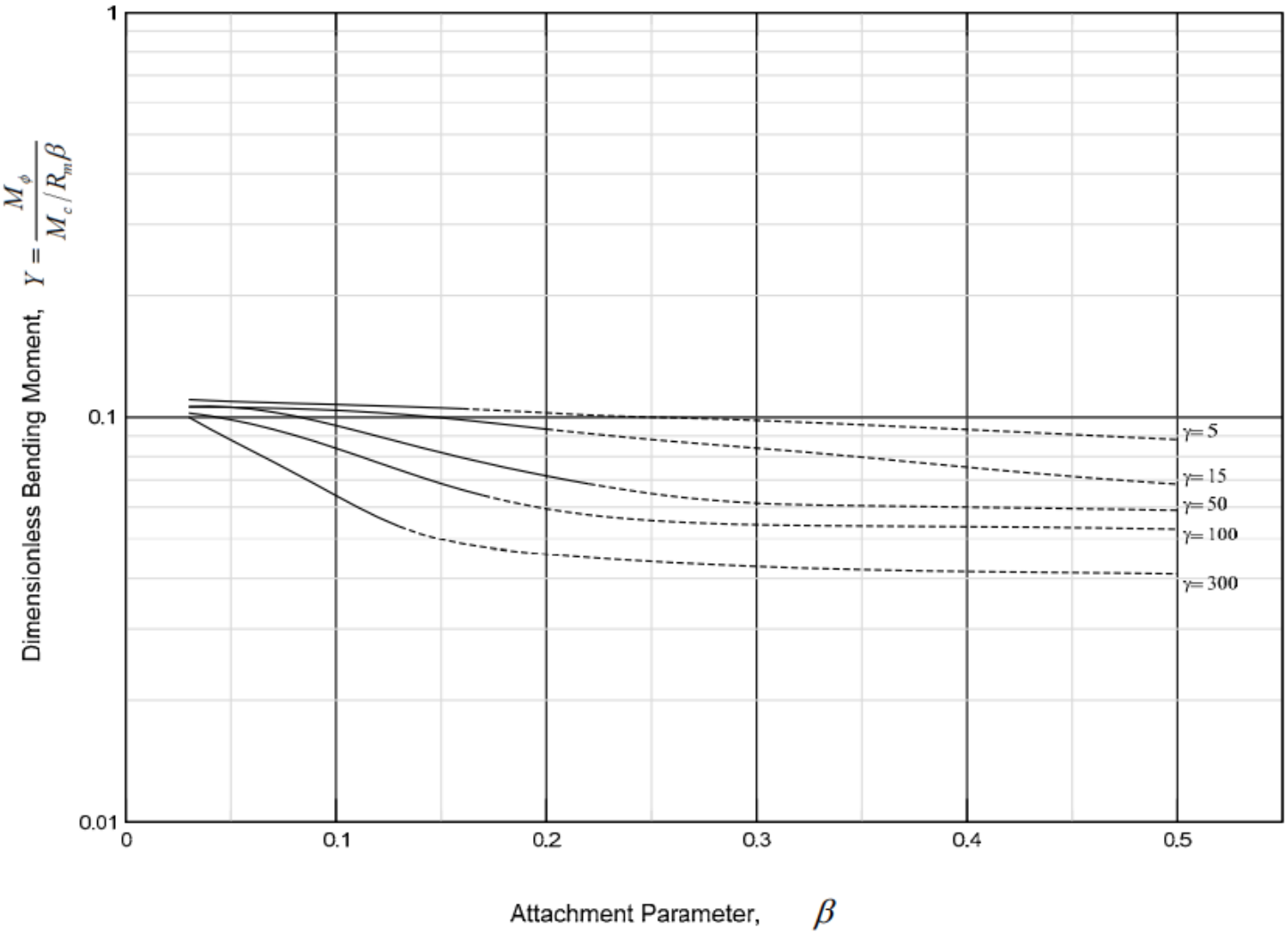

Figure A. 1 Moment $\left(\frac{M_\phi}{M_c/R_m\beta}\right)$ Due to an External Circumferential Moment M_c on a Circular Cylinder – Original

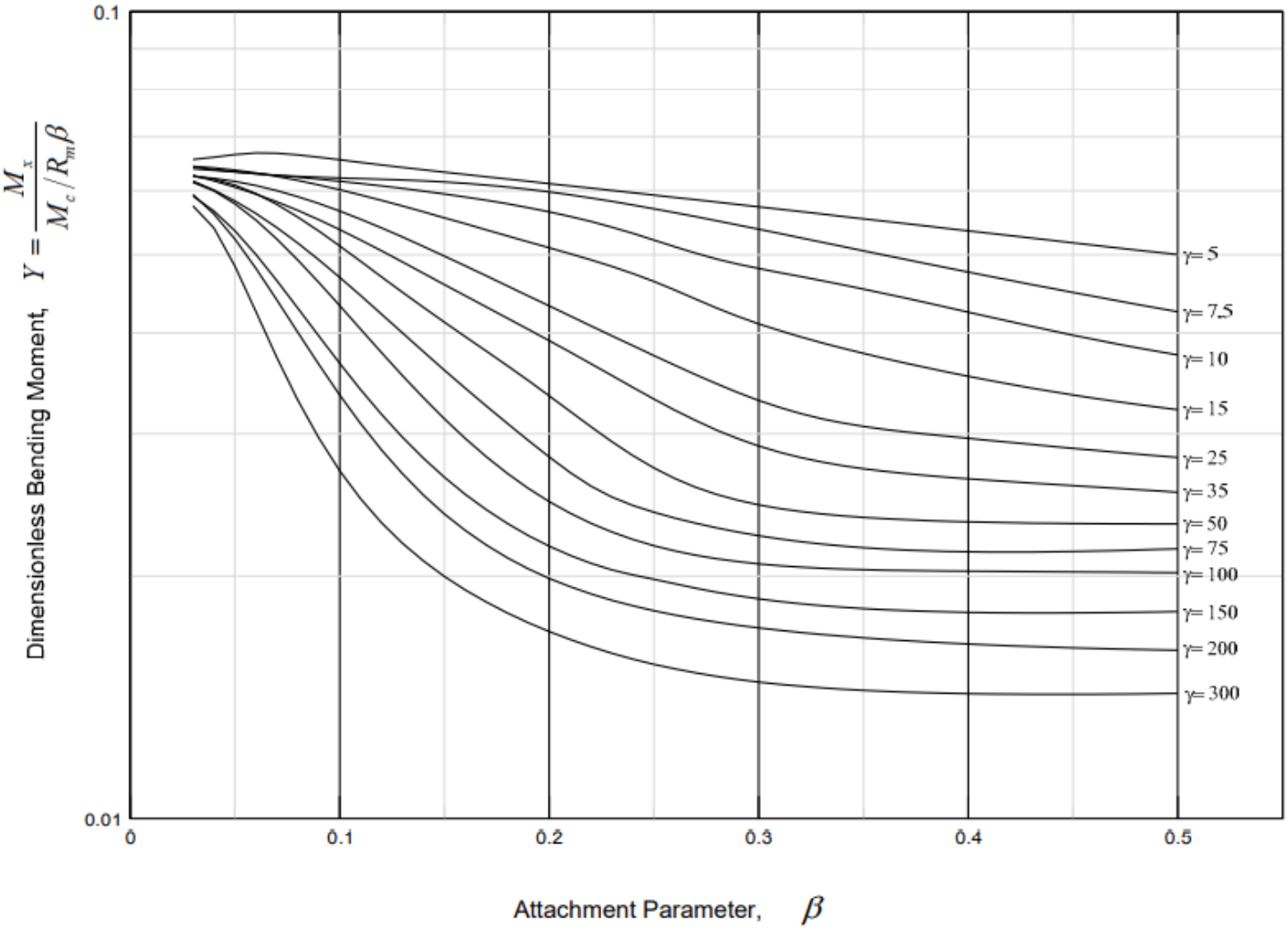

Figure A. 2 - Moment $\left(\frac{M_x}{M_c/R_m\beta}\right)$ Due to an External Circumferential Moment M_c on a Circular Cylinder – Extrapolated

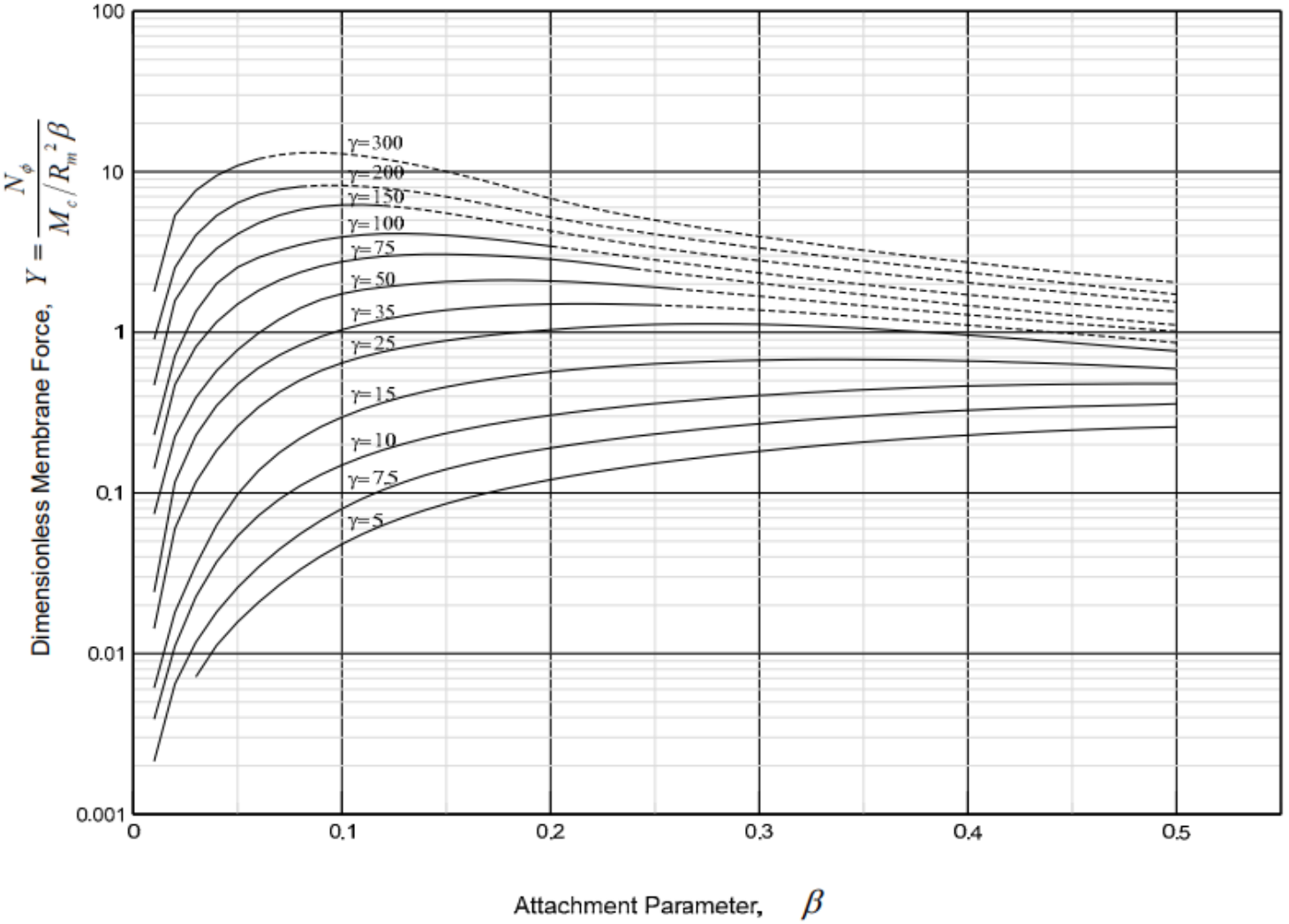

Figure A. 3 – ***Moment*** $\left(\frac{N_\phi}{M_c/R_m^2\beta}\right)$ ***Due to an External Circumferential Moment*** M_c ***on a Circular Cylinder – Extrapolated***

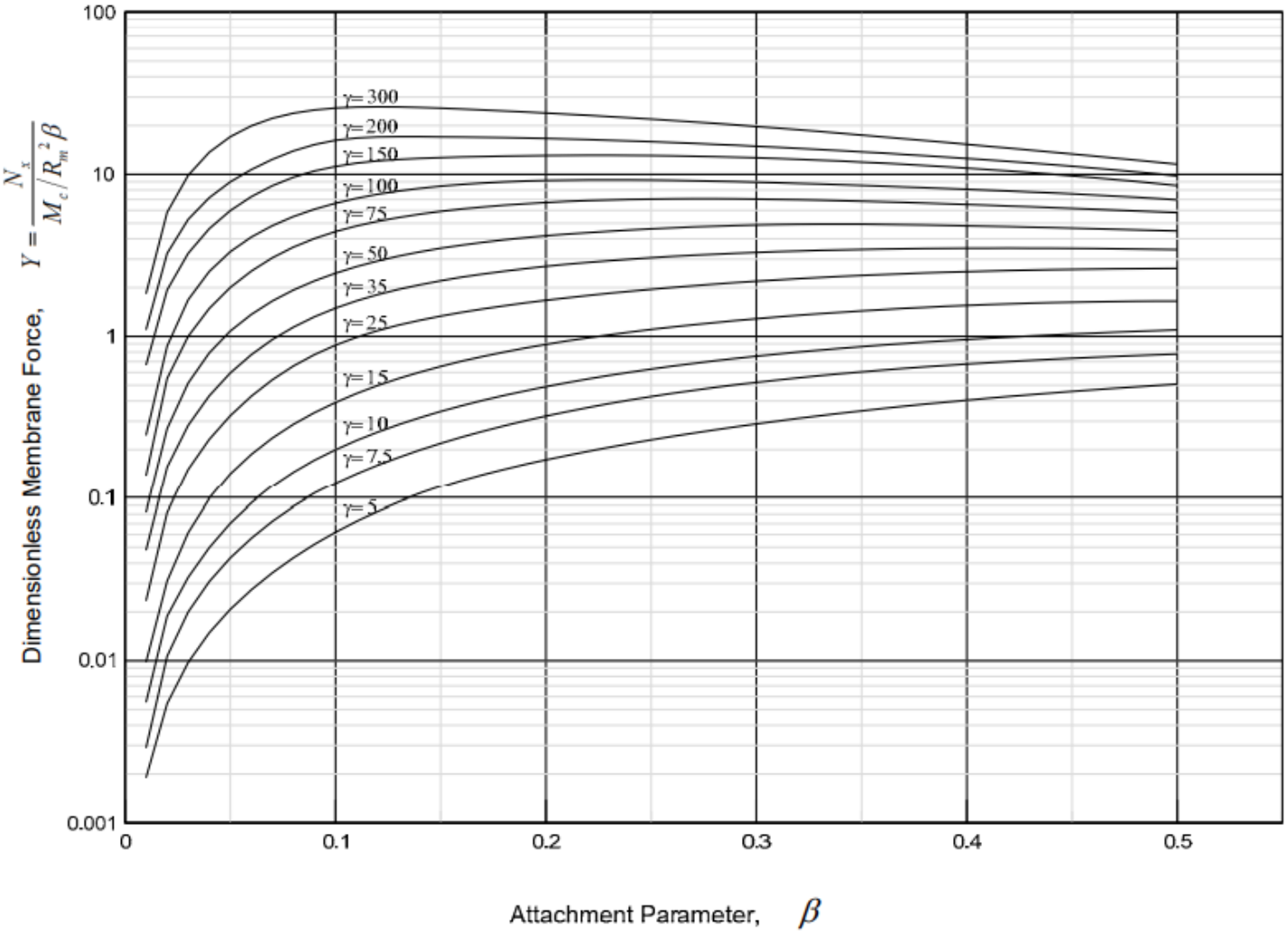

Figure A. 4 – ***Moment*** $\left(\frac{N_\phi}{M_c/R_m^2\beta}\right)$ ***Due to an External Circumferential Moment*** M_c ***on a Circular Cylinder – Original***

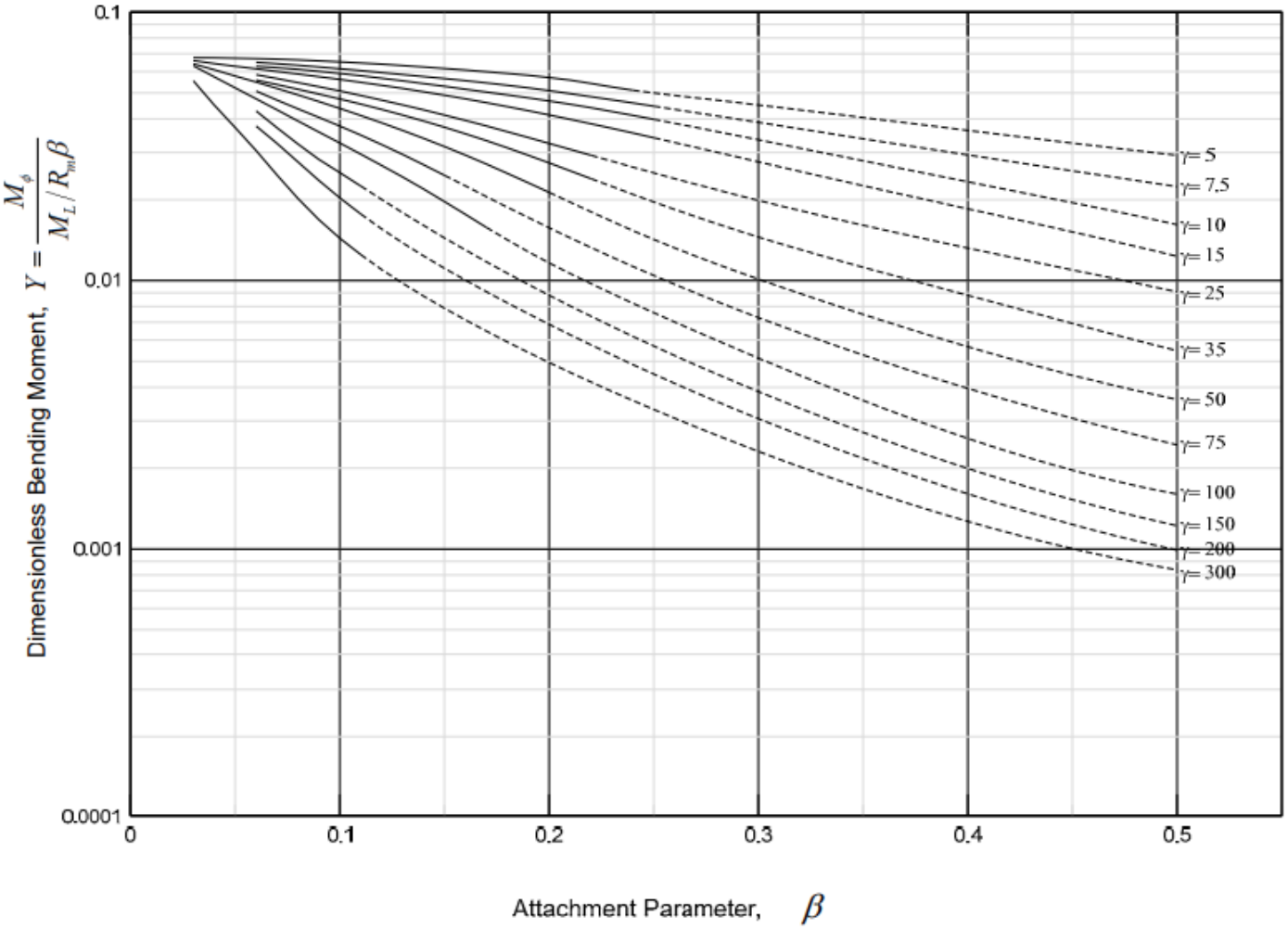

Figure A. 5 – ***Moment*** $\left(\frac{M_\phi}{M_L/R_m\beta}\right)$ ***Due to an External Longitudinal Moment*** M_L ***on a Circular Cylinder (Stress on the Longitudinal Plane of Symmetry) – Original***

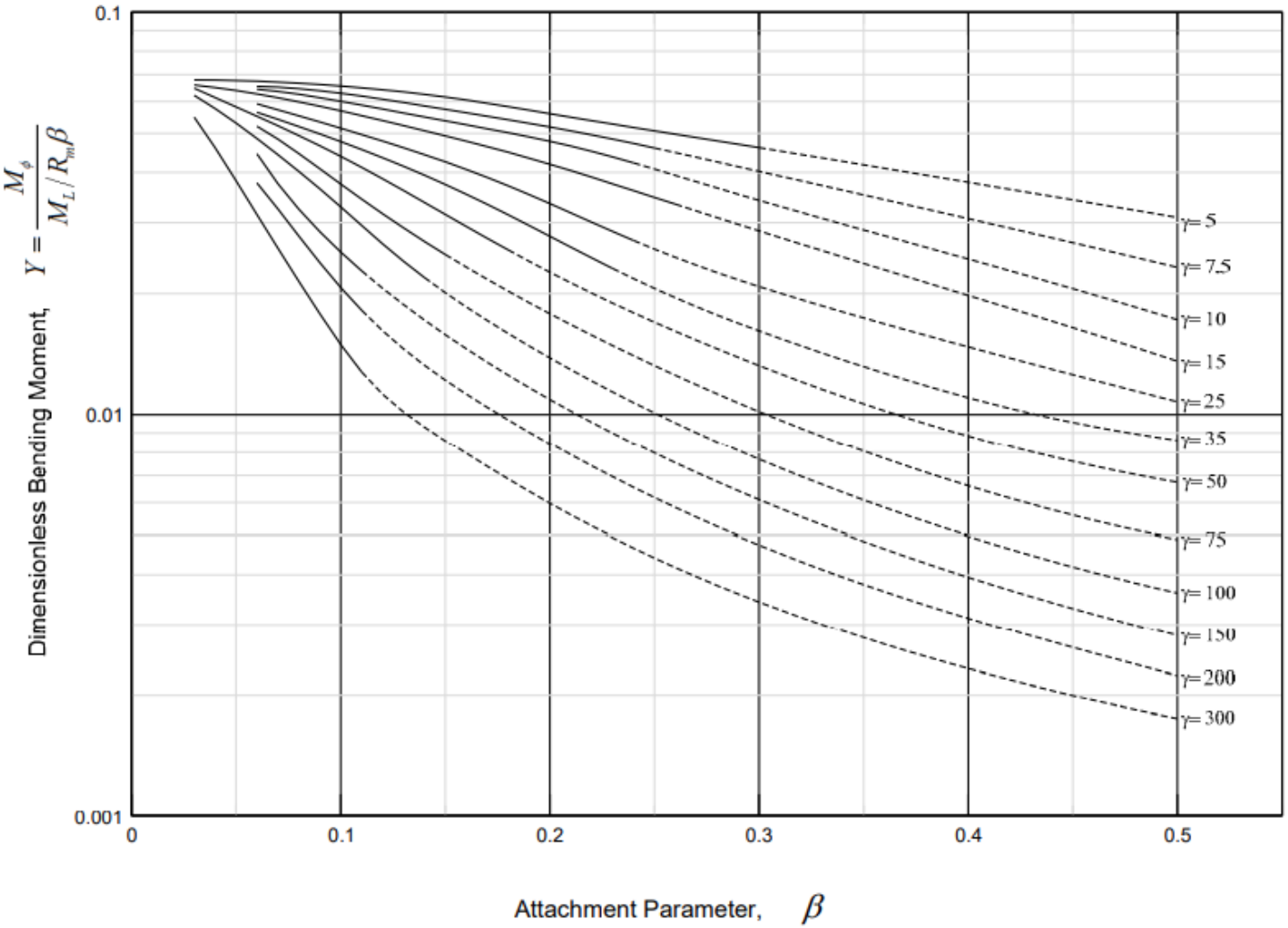

Figure A. 6 – ***Moment*** $\left(\frac{M_\phi}{M_L/R_m\beta}\right)$ ***Due to an External Longitudinal Moment*** M_L ***on a Circular Cylinder – Original***

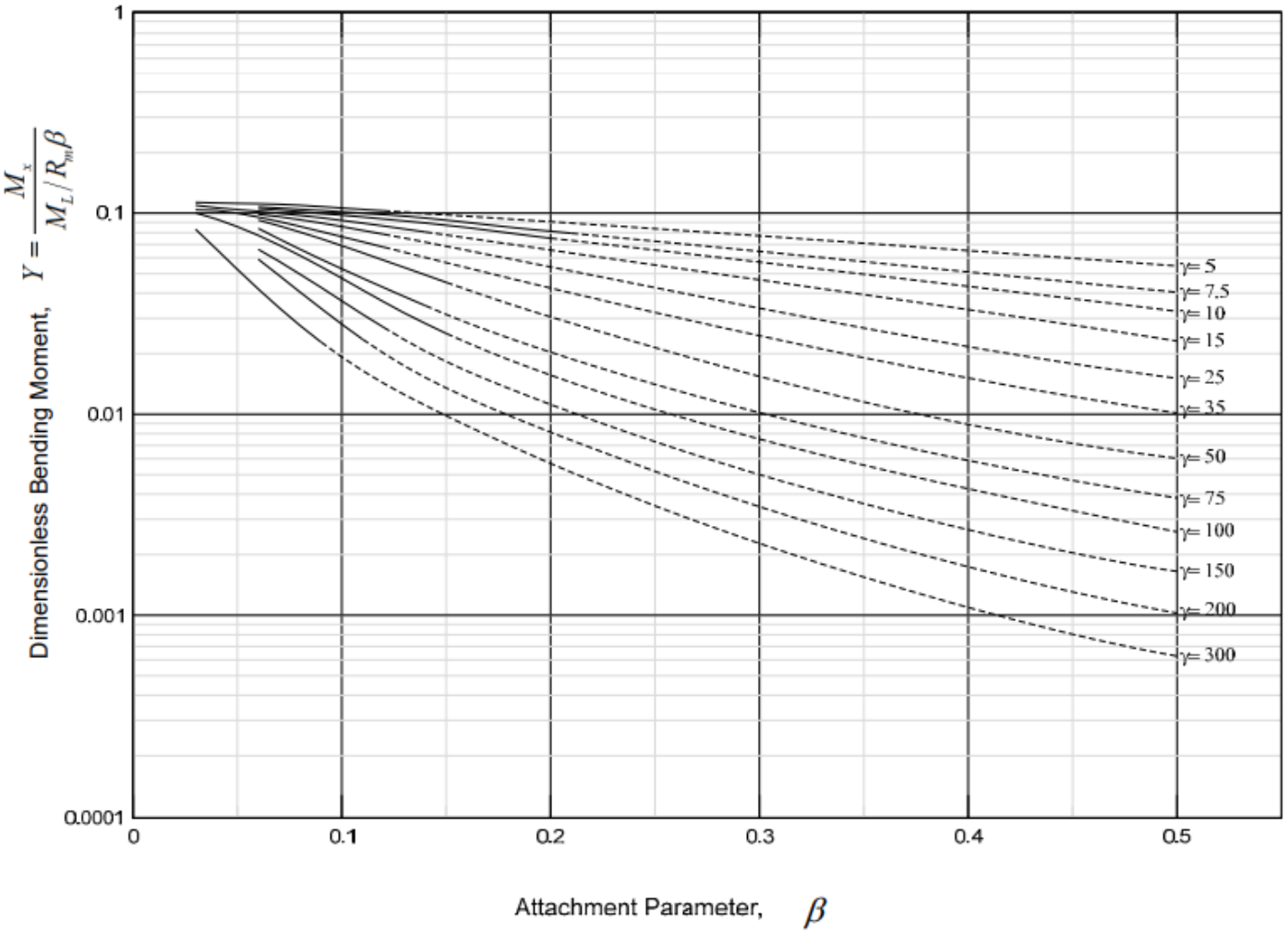

Figure A. 7 – ***Moment*** $\left(\frac{M_x}{M_L/R_m\beta}\right)$ ***Due to an External Longitudinal Moment*** M_L ***on a Circular Cylinder (Stress on the Longitudinal Plane of Symmetry) – Original***

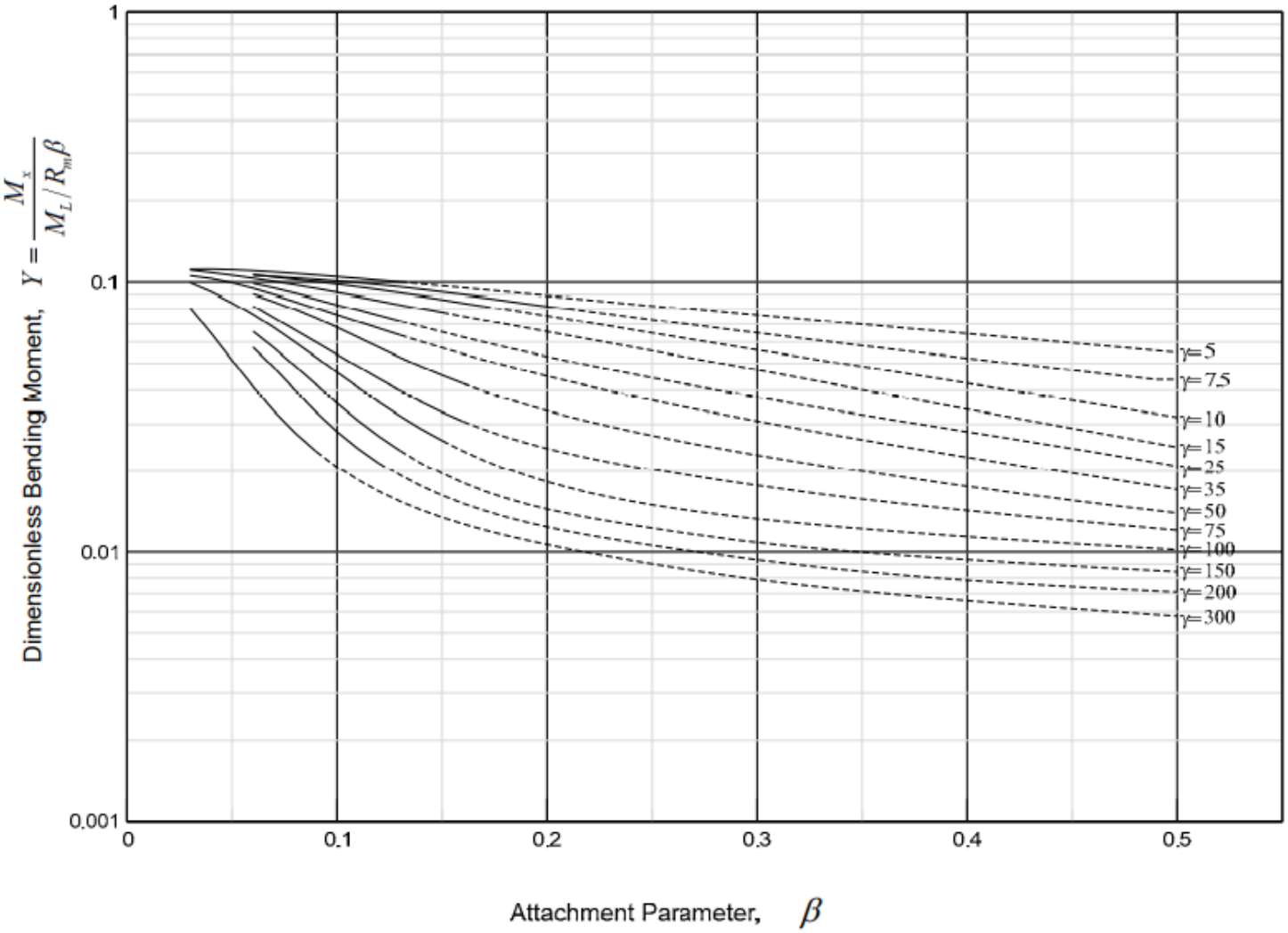

Figure A. 8 – ***Moment*** $\left(\frac{M_x}{M_L/R_m\beta}\right)$ ***Due to an External Longitudinal Moment*** M_L ***on a Circular Cylinder – Original***

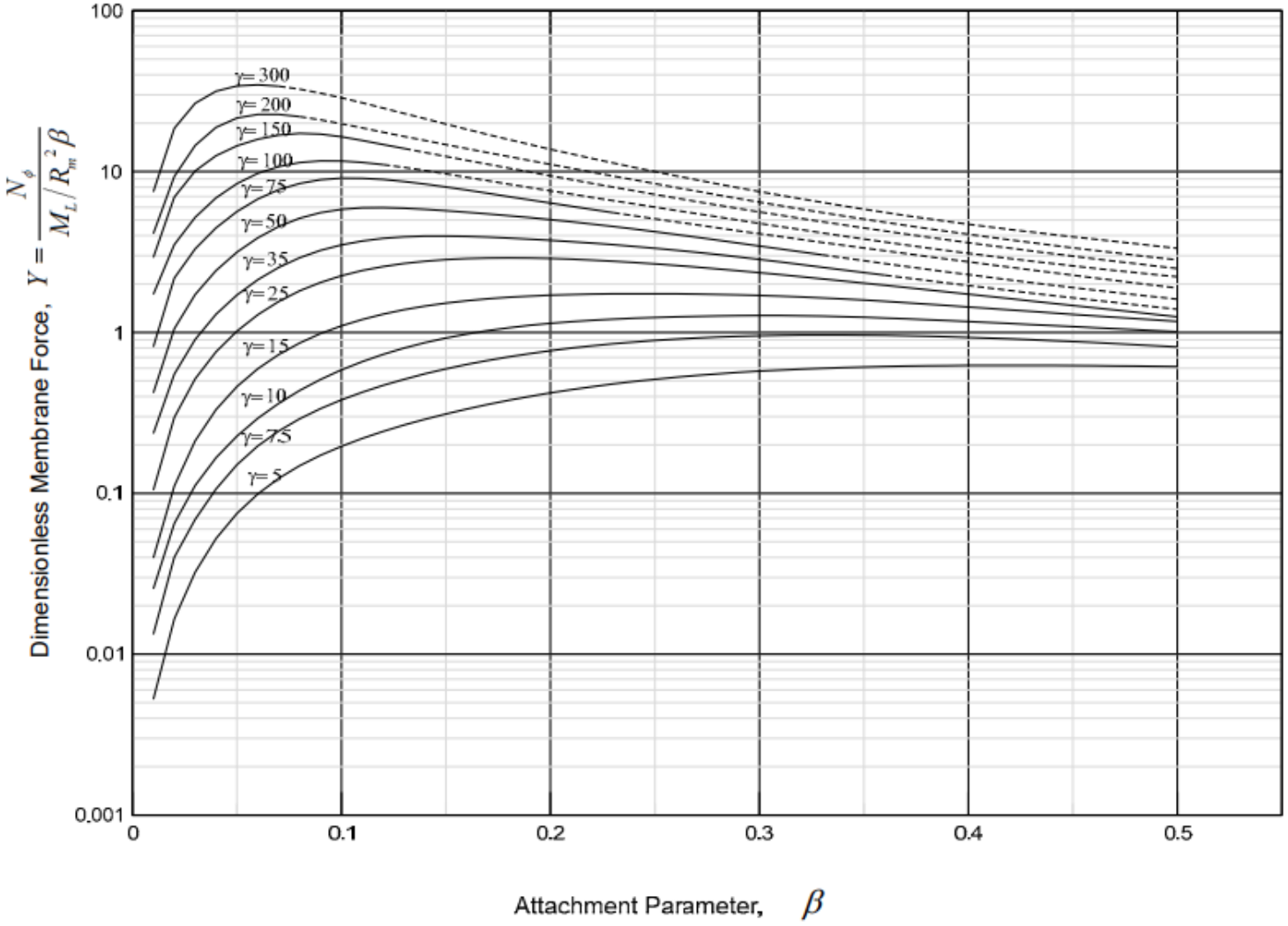

Figure A. 9 – ***Membrane Force*** $\left(\frac{N_\phi}{M_L/R_m^2\beta}\right)$ ***Due to an External Longitudinal Moment*** M_L ***on a Circular Cylinder – Original***

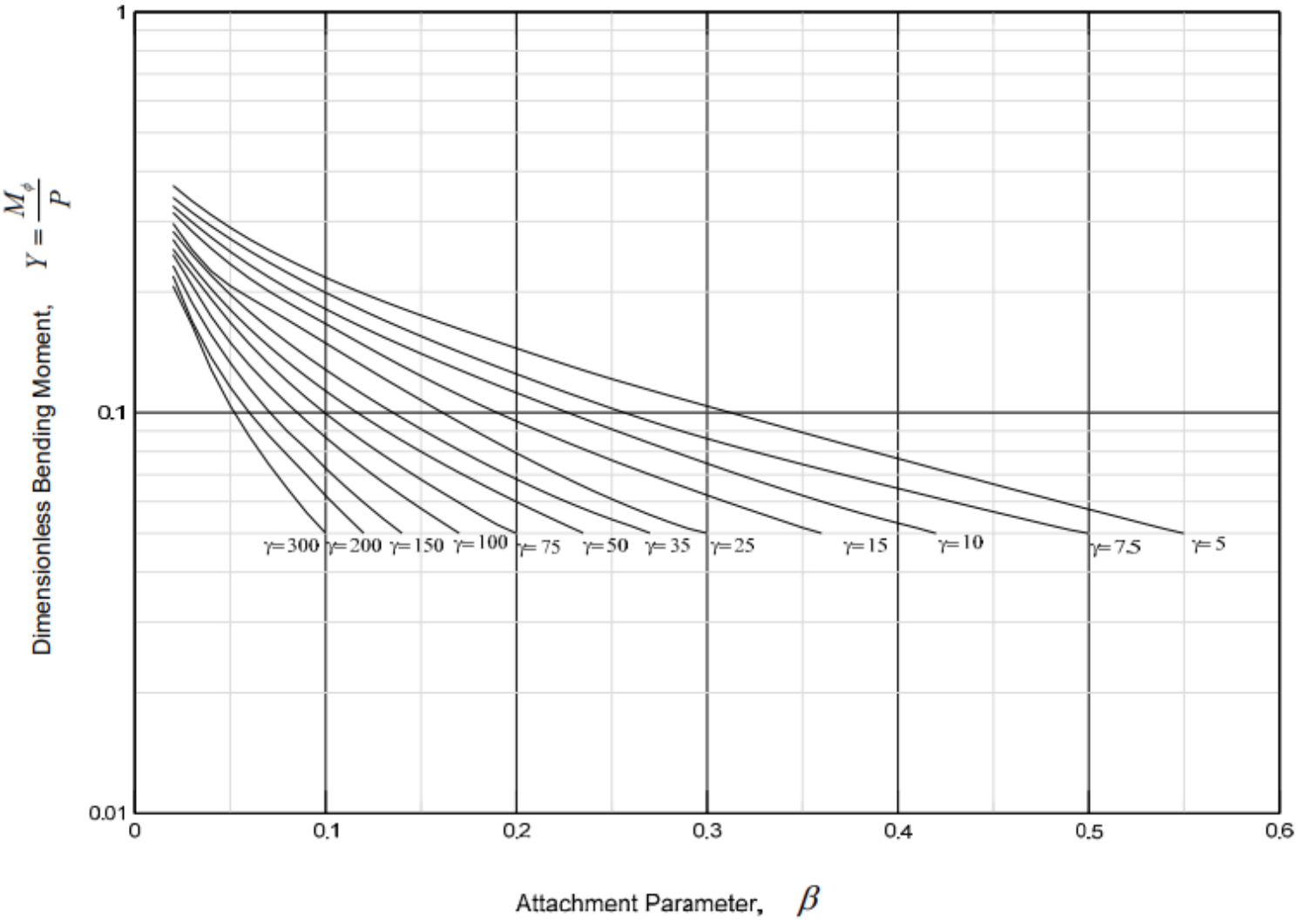

Figure A. 10 - Bending *Moment* $\frac{M_\phi}{P}$ *Due to an External Radial Load P on a Circular Cylinder (Transverse Axis) – Original*

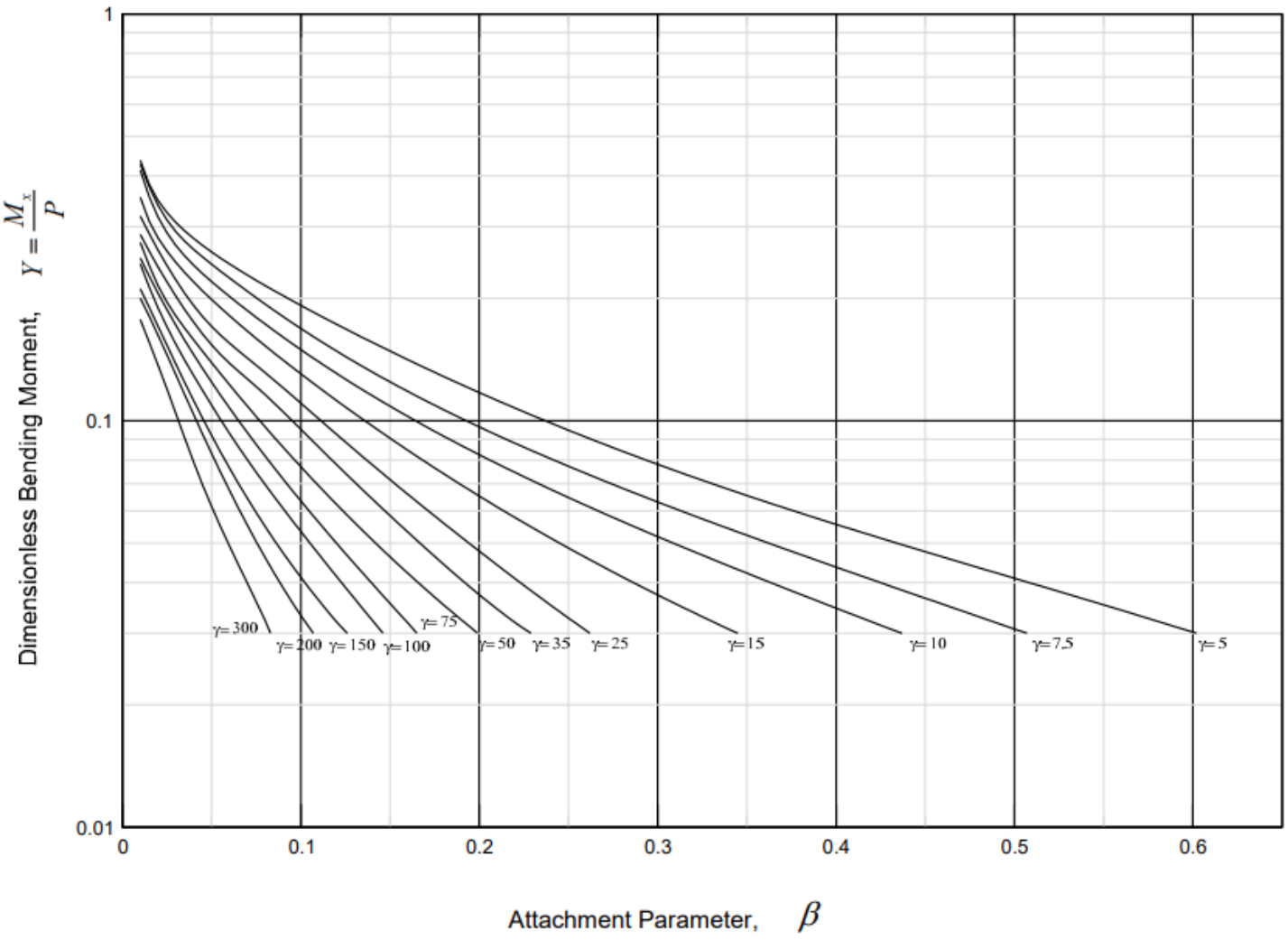

Figure A. 11 - Bending *Moment* $\frac{M_x}{P}$ *Due to an External Radial Load P on a Circular Cylinder (Transverse Axis) - Extrapolated*

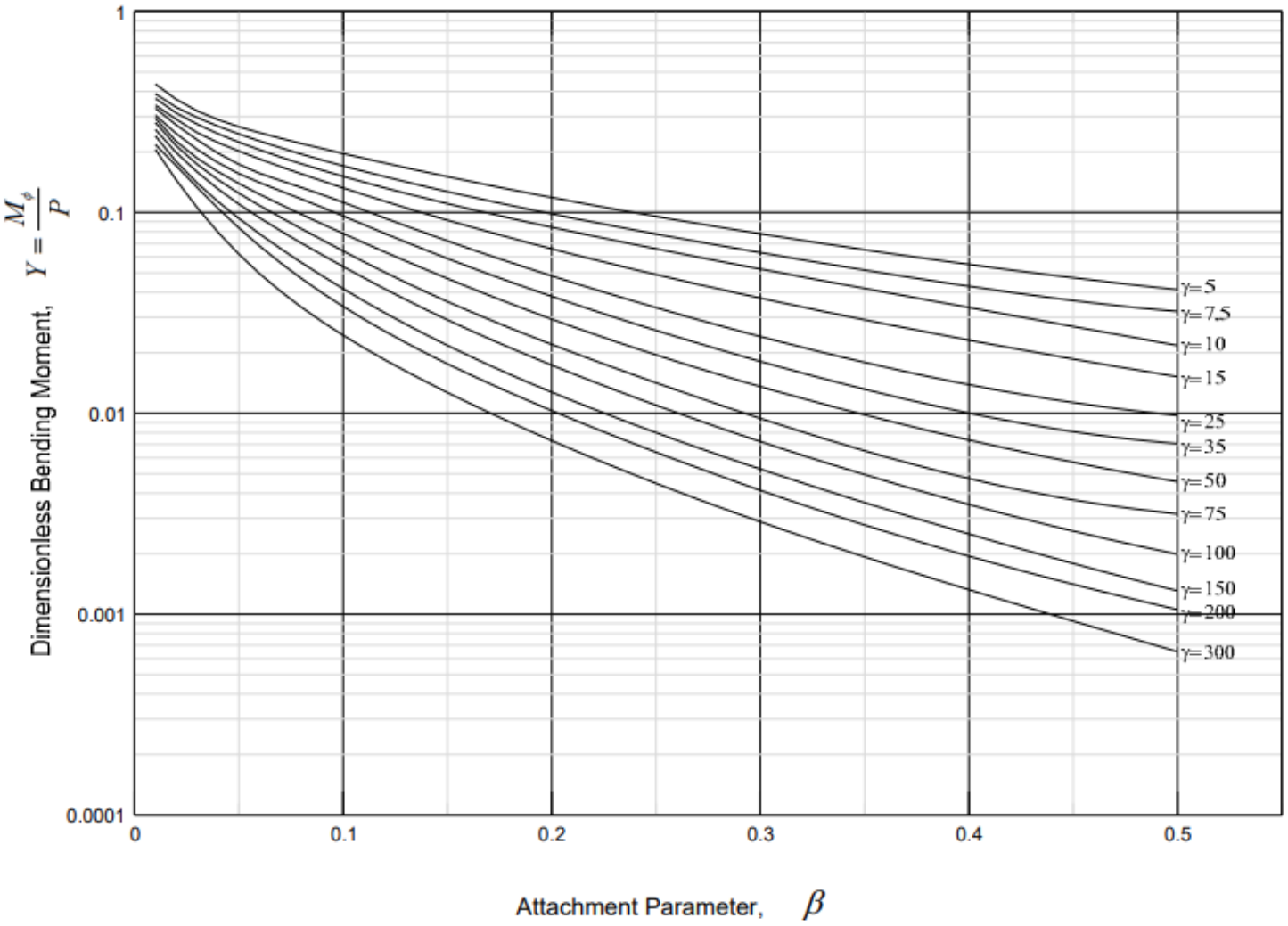

Figure A. 12 - Bending *Moment* $\frac{M_\phi}{P}$ *Due to an External Radial Load P on a Circular Cylinder (Longitudinal Axis) – Extrapolated*

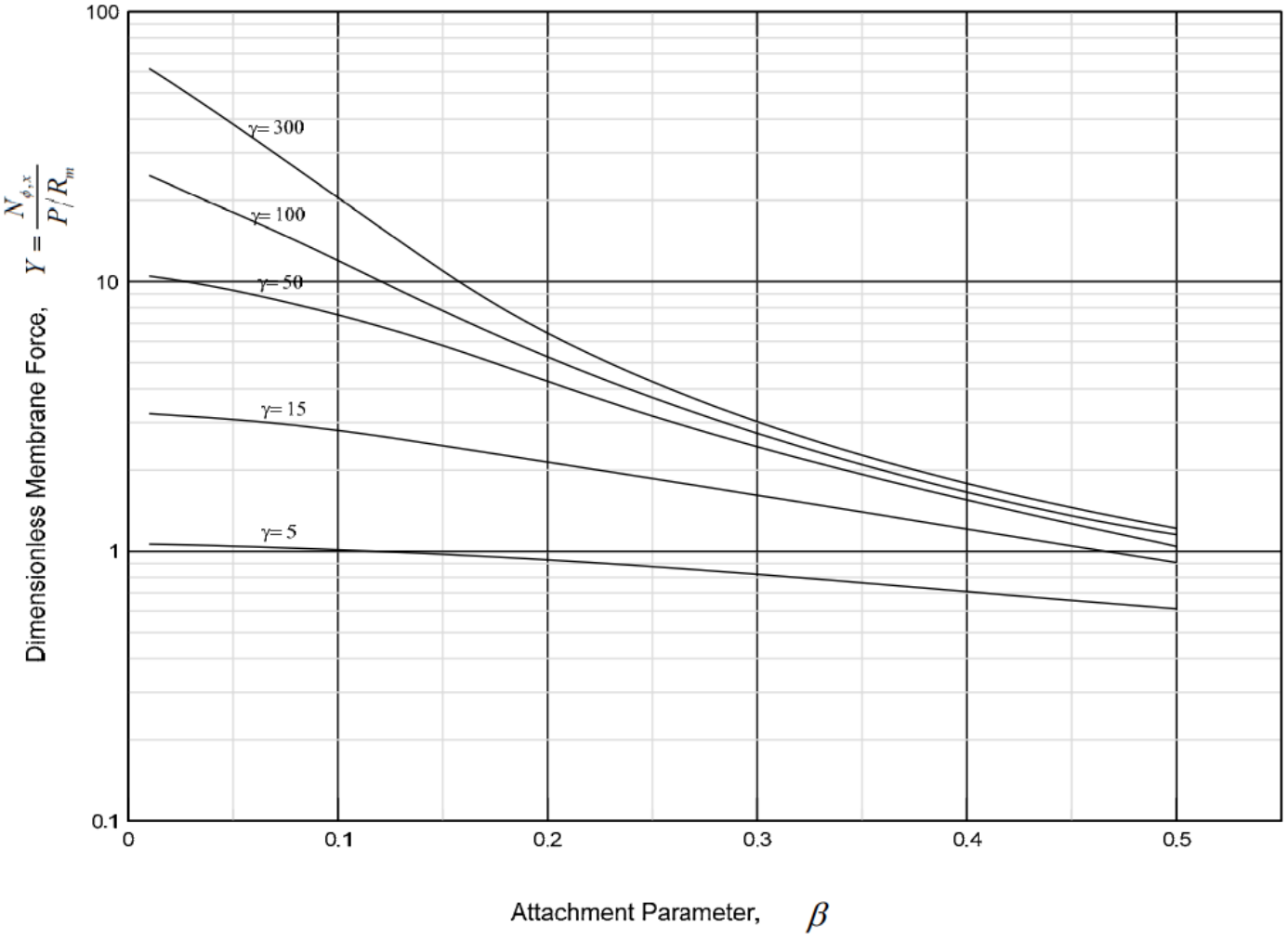

Figure A. 13 - Membrane *Force $N_\phi/(P/R_m)$ Due to an External Radial Load P on a Circular Cylinder (Transverse Axis) - Membrane Force $N_x/(P/R_m)$ Due to an External Radial Load P on a Circular Cylinder Longitudinal Axis) – Original*

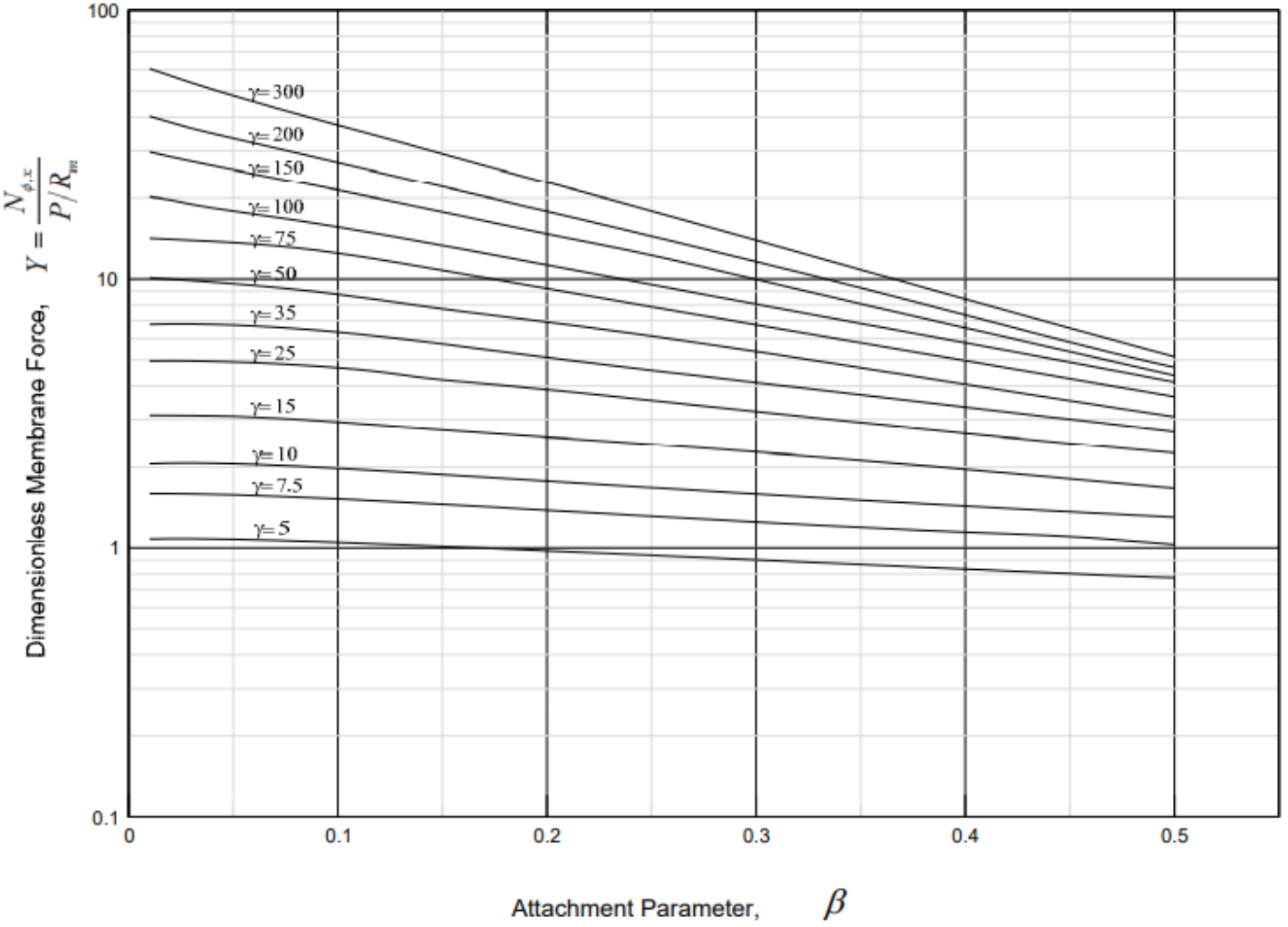

Figure A. 14 – Membrane Force $N_x/(P/R_m)$ Due to an External Radial Load P on a Circular Cylinder (Transverse Axis) - Membrane Force $N_\phi/(P/R_m)$ Due to an External Radial Load P on a Circular Cylinder Longitudinal Axis) – Extrapolate